VOLUME 79 APRIL 24, 1975 NUMBER 9

JPCHAx

THE JOURNAL OF PHYSICAL CHEMISTRY

PUBLISHED BIWEEKLY BY THE AMERICAN CHEMICAL SOCIETY

THE JOURNAL OF

PHYSICAL CHEMISTRY

AMERICAN CHEMICAL SOCIETY, *1155 Sixteenth St., N.W., Washington, D.C. 20036*

Books and Journals Division

JOHN K CRUM *Director*
VIRGINIA E. STEWART *Assistant to the Director*

CHARLES R. BERTSCH *Head, Editorial Processing Department*
D. H. MICHAEL BOWEN *Head, Journals Department*
BACIL GUILEY *Head, Graphics and Production Department*
SELDON W. TERRANT *Head, Research and Development Department*

 Published biweekly by the American Chemical Society at 20th and Northampton Sts., Easton, Pa. 18042. Second-class postage paid at Washington, D.C., and at additional mailing offices.

All manuscripts should be sent to *The Journal of Physical Chemistry*, Department of Chemistry, University of Minnesota, Minneapolis, Minn. 55455.

Additions and Corrections are published once yearly in the final issue. See Volume 78, Number 26 for the proper form.

Extensive or unusual alterations in an article after it has been set in type are made at the author's expense, and it is understood that by requesting such alterations the author agrees to defray the cost thereof.

The American Chemical Society and the Editor of *The Journal of Physical Chemistry* assume no responsibility for the statements and opinions advanced by contributors.

Correspondence regarding accepted copy, proofs, and reprints should be directed to Editorial Processing Department, American Chemical Society, 20th and Northampton Sts., Easton, Pa. 18042. Department Head: CHARLES R. BERTSCH. Associate Department Head: MARIANNE C. BROGAN. Assistant Editor: CELIA B. MCFARLAND. Editorial Assistant: JOSEPH E. YURVATI.

Advertising Office: Centcom, Ltd., 50 W. State St., Westport, Conn. 06880.

Business and Subscription Information

Send all new and renewal subscriptions *with payment* to: Office of the Controller, 1155 16th Street, N.W., Washington, D.C. 20036. Subscriptions should be renewed promptly to avoid a break in your series. All correspondence and telephone calls regarding changes of address, claims for missing issues, subscription service, the status of records, and accounts should be directed to Manager, Membership and Subscription Services, American Chemical Society, P.O. Box 3337, Columbus, Ohio 43210 Telephone (614) 421-7230. For microfiche service, contact ACS Journals Department, 1155 16th St. N.W., Washington, D.C. 20036. Telephone (202) 872-4444.

On changes of address, include both old and new addresses with ZIP code numbers, accompanied by mailing label from a recent issue. Allow four weeks for change to become effective.

Claims for missing numbers will not be allowed (1) if loss was due to failure of notice of change in address to be received before the date specified, (2) if received more than sixty days from date of issue plus time normally required for postal delivery of journal and claim, or (3) if the reason for the claim is "issue missing from files."

Subscription rates (hard copy or microfiche) in 1975: $20.00 for 1 year to ACS members; $80.00 to nonmembers. Extra postage $4.50 in Canada and PUAS, $5.00 other foreign. Supplementary material (on microfiche only) available on subscription basis, 1975 rates: $15.00 in U.S., $19.00 in Canada and PUAS, $20.00 elsewhere. All microfiche airmailed to non-U.S. addresses; air freight rates for hard-copy subscriptions available on request.

Single copies for current year: $4.00. Rates for back issues from Volume 56 to date are available from the Special Issues Sales Department, 1155 Sixteenth St., N.W., Washington, D.C. 20036.

Subscriptions to this and the other ACS periodical publications are available on microfilm. For information on microfilm write Special Issues Sales Department at the address above.

Notice to Authors last printed in the issue of January 16, 1975

THE JOURNAL OF
PHYSICAL CHEMISTRY

Volume 79, Number 9 April 24, 1975

JPCHAx 79(9) 859–950 (1975)

ISSN 0022-3654

There is no supplementary material for this issue.

* In papers with more than one author, the asterisk indicates the name of the author to whom inquiries about the paper should be addressed.

AUTHOR INDEX

ANNOUNCEMENT

On the last two pages of this issue you will find reproduced the table of contents of the April 1975 issue of the Journal of Chemical and Engineering Data.

THE JOURNAL OF
PHYSICAL CHEMISTRY

VOLUME 79, NUMBER 9 APRIL 24, 1975

Metastable Methane Ions. Temperature Dependence of the Translational Energy Release

B. H. Solka, J. H. Beynon, and R. G. Cooks*

Department of Chemistry, Purdue University, West Lafayette, Indiana 47907 *(Received August 5, 1974; Revised Manuscript Received January 27, 1975)*

Publication costs assisted by the National Science Foundation

The translational energy released in the unimolecular loss of H· from metastable methane ions has been examined and found to have a significant temperature dependence. Reaction mechanisms of the barrier traversal, tunnelling, and electronic predissociation types are all inconsistent with the observed temperature effect if centrifugal effects are neglected. The observed temperature dependence of the kinetic energy release correlates well with the variation in centrifugal barrier height with rotational energy derived from a simple form of Langevin collision theory. It is also in agreement with the more rigorous treatment of Klots which allows tunnelling through the centrifugal barrier.

Introduction

We wish to report the results of measurements of the translational energy released as a function of temperature and deuterium substitution in the metastable ion dissociation (I). Our objective was to obtain new types of experimental data which should prove of value to any future theoretical calculations on this system. We have also considered various possible mechanisms in the light of the present and earlier experimental data.

$$CH_4{\cdot}^+ \rightarrow CH_3^+ + H\cdot \qquad (I)$$

The occurrence (or nonoccurrence) and origin of the metastable peak in methane has been the subject of some interest, particularly as regards the applicability of quasi-equilibrium theory (QET). Rate constants calculated for reaction I by QET in both its original[1] and in a reformulated version[2] were found to be inconsistent with the experimentally observed metastable peaks if the classical barrier traversal mechanism was assumed. However, Hills et al.[1] were able to fit their calculations to the experimental data by modifying their treatment of the reaction coordinate while Klots[2] was able to reconcile the observed abundance of the metastable peak by postulating tunnelling[3] in his treatment.

Experimental Section

Translational energy releases were measured using the mass-analyzed ion kinetic energy spectrometer (MIKES) described previously.[4] Similar results are obtained using the Hitachi RMH-2 mass spectrometer modified as previously described[5] but reaction I is significantly enhanced by collision-induced dissociation[1,6] and the better differential pumping in the MIKES instrument permitted higher source pressures for a given field-free region pressure. Even at a pressure of 1×10^{-7} Torr in the field-free region, the contribution of the collision-induced dissociation to the metastable ion signal was ~50% of the total signal (Figure 1). This process is associated with the broad component of the observed composite peak. The translational energy release ($T_{50\%}$) was calculated from the measured half-width of the narrow component after correction both for the contribution of the collision-induced process (by resolving the composite metastable peak using a curve resolver) and for the energy spread in the parent ion beam (the corrected width was taken as the square root of the difference between the squares of the metastable peak width and of the fraction m_2/m_1 of the width of the beam of stable parent ions where the reaction in question is $m_1^+ \rightarrow m_2^+ + m_3$). The composite nature of the metastable peak precludes an accurate determination of the distribution of kinetic energy releases; however, it has been shown[7] that for gaussian shaped metastable peaks the value of the kinetic energy release calculated from the peak width at half-height is only one-half to one-third the average kinetic energy release.

Results and Discussion

The present kinetic energy release values may be compared to a value of $T_{50\%}$ of 5 meV obtained for CH_4 by Ottinger[6] and an estimation by Stockbauer[8] of the total energy release at the threshold for ion production of 140 ± 50

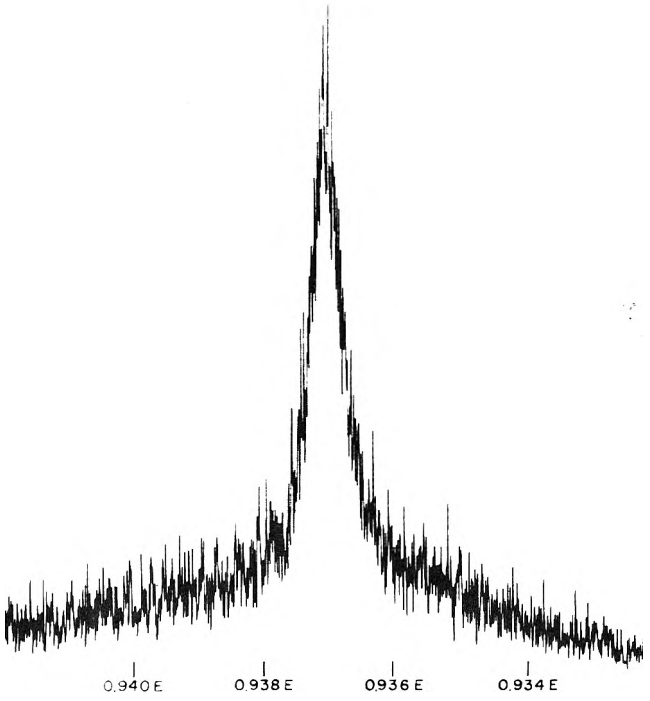

Figure 1. Metastable peak in the MIKE spectrum of CH_4 for the reaction $CH_4^{\cdot+} \rightarrow CH_3^+ + H\cdot$. E is the electric sector voltage necessary to transmit the stable $CH_4^{\cdot+}$ ion beam.

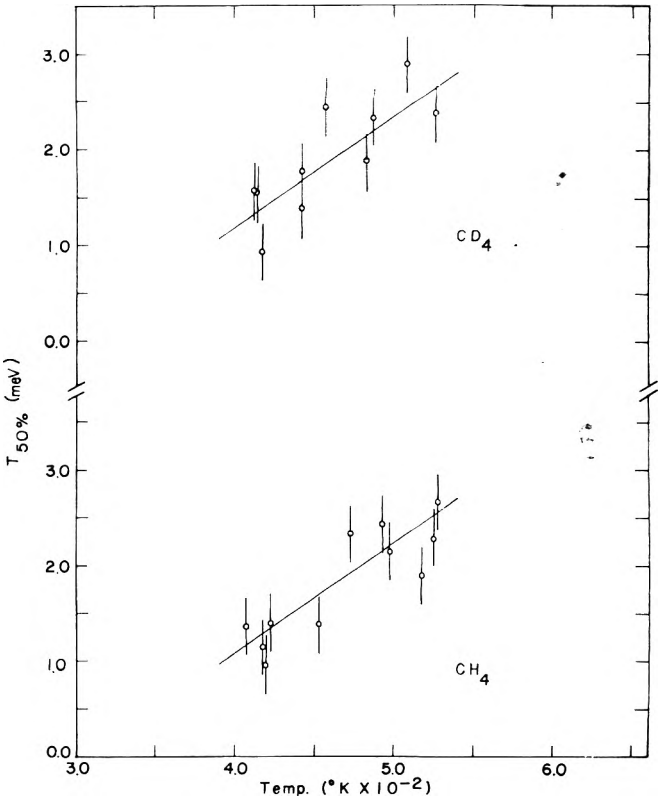

Figure 2. Measured kinetic energy release ($T_{50\%}$) for CH_4 and CD_4 as a function of ion source temperature.

and 90 ± 30 meV for CH_4 and CD_4, respectively. The $T_{50\%}$ value of Ottinger, at an ion source temperature of 150° and a resolution insufficient to distinguish the unimolecular and collision-induced dissociations, is in agreement with our data. Stockbauer's estimate, which is based on assumptions regarding the transmission of a mass analyzer as a function of ion kinetic energy, may reflect the energy release for ions dissociating from the same state(s) as those which give the collision-induced peak in our work.

Figure 2 illustrates the results obtained as a function of ion source temperature and deuterium substitution. Straight lines are drawn through the temperature dependence data but the limited temperature range accessible does not allow the exact form of the dependence to be established. Photoionization efficiency studies[9,10] have shown that rotational energy of neutral CH_4 is effective at threshold in the formation of CH_3^+. In the range covered in these experiments changes in the source temperature cause a much larger change in the rotational energy distribution of the neutral methane than in its vibrational energy distribution. Hence, assuming that the increased rotational energy of the neutral is largely retained in the ion (which will be true for not too drastic changes in geometry), the observed trend in $T_{50\%}$ with temperature probably reflects rotational effects.

One important feature of the metastable ion experiment must be contrasted with ion source studies. Since a limited and fixed range of ion lifetimes is sampled in the metastable time window, differences in the internal energy distributions of the reacting ions will only be transmitted in part to the population being sampled. This well-known feature of metastable ions[11] is useful in many studies in which differences in internal energies of ions are an undesirable complication. In experiments of the present type this feature may muffle any effect of temperature and the observed change in $T_{50\%}$ may underestimate the true change. This effect is considered in the discussion which follows.

The translational energy release observed for reaction I is rather small compared to values usually obtained when its origin is in the statistical partitioning of the nonfixed energy in the fragmenting ion. This may merely be a consequence of the small size of the ion but it does require that other types of mechanisms be given consideration. Three main possibilities exist: (i) reaction occurs on a single surface by surmounting an energy barrier, (ii) the reaction involves tunnelling or rotational predissociation, and (iii) the reaction occurs by a forbidden electronic predissociation. The calculations of Hills et al. and of Klots cover mechanisms i and ii, respectively. The electronic predissociation mechanism has not been previously suggested, but it deserves mention because such a mechanism has been postulated for several reactions which simultaneously show unusually small kinetic energy releases and unusual sensitivity to collision-induced dissociation.[12] The predissociation process might occur as follows: the $^2T_2$ ground state of tetrahedral $CH_4^{\cdot+}$ has a Jahn-Teller instability which results in a distortion to D_{2d} symmetry and a splitting of the $^2T_2$ state to ^2E and $^2B_2$ states.[13] If the rate of crossing between these surfaces happens to fall in the appropriate range, the metastable $CH_4^{\cdot+}$ ions could be those which are formed in the higher ^2E state with insufficient energy to fragment but then undergo a slow crossing to the $^2B_2$ ground state wherein they do have sufficient energy to fragment.

The magnitude of the translational energy release is in qualitative agreement with all three mechanisms. The QET calculations of Hills et al. predict metastable behavior for $CH_4^{\cdot+}$ ions with total internal energies on the order of 1 meV and those of Klots suggest that the ions fragmenting by the tunnelling mechanism could release only a quantity of energy less than or equal to the height of a small centrif-

ugal barrier in the reaction coordinate. The curve crossing process might also release very little kinetic energy as has been proposed[12] for other reactions.

In seeking a basis for selection of the mechanism the temperature dependence data of Figure 2 must be used. The arguments which follow can be summarized by noting that, if one makes the usual QET assumption of complete randomization of internal energy in the energized molecular ion, the barrier transversal mechanism requires an unrealistically small $k(\epsilon)$ slope to accommodate the observed temperature effect. Moreover, the predissociation mechanism is not expected to show a significant change in kinetic energy release with change in molecular ion energy distribution, and neither, in the absence of centrifugal effects, is the tunnelling process.

Both tunnelling and forbidden electronic predissociation may be characterized as unimolecular processes which have appreciable rate constants over only a narrow range of internal energies. This is in contrast to the well known form of the $k(\epsilon)$ vs. ϵ curves for over the barrier type reactions. Consequently, if the metastable ions are being formed by either tunnelling or slow predissociation only a relatively narrow range of molecular ion internal energies is being sampled. Therefore, changes in the molecular ion internal energy distribution which might be effected by ion source temperature should not cause any significant change in the energy distribution of ions sampled in the experiment.

In contrast to the situation for the other major mechanistic types, $k(\epsilon)$ for reaction by barrier transversal is not limited to a small range of internal energies and many of the ions sampled in the field-free region have rate constants (and hence internal energies) very different from those characterized by the reciprocal of the lifetime of ions fragmenting in this region.[14] In principle, therefore, this allows for a change in kinetic energy release with changes in ion source temperature. To determine to what extent a given shift in parent ion energy distribution might be reflected in the corresponding distribution of the metastable ions, model calculations were performed on the methane system. Internal energy distributions and $k(\epsilon)$ curves based on those of Hills et al. and Klots were used. It was found that no reasonable change in the assumed internal energy distribution for $CH_4{\cdot}^+$ could generate the observed change in translational energy release. That is, a change in a smooth parent ion energy distribution which might be induced by a 100° temperature change did not change the average metastable ion energy (and hence the translational energy release) by a detectable amount. The calculations do suggest that the observed change is only possible if the slope of the $k(\epsilon)$ curve is such that the internal energy window for metastable ions is considerably more than several tenths of a volt wide. This is inconsistent with the observed small kinetic energy release. While the transmission to metastable ions of internal energy changes made in the ion source is improved when the internal energy distribution contains pronounced maxima and minima the steep $k(\epsilon)$ curve suggested by other data[1,2] still does not accommodate the measured variation in energy release.

The foregoing arguments therefore require that the observed temperature effect be a result of centrifugal effects and in the remainder of this paper we show that the data can be rationalized in these terms.

Although tunnelling through a given barrier can be characterized by a set of rate constants (and internal energies) determined by the barrier height and width, the result of including centrifugal effects is to vary the height of the barrier relative to separated products as a function of molecular ion rotation.[2,15] Hence, if tunnelling is in fact the origin of the metastable ions, it follows that the rate of passage through at least some part of the barrier will generally fall in the metastable ion time scale. As the temperature is increased and the centrifugal barrier increases, some other portion of the barrier will transmit ions at the required rate and this position on the barrier will be at a higher energy relative to separated products. Thus, a metastable peak will again be observed and the associated translational energy release will increase.

Assuming that the rotational angular momentum of the methane molecular ion is approximately equal to that for the molecule (compare ref 9) a relationship can be derived between the rotational energy of the methane molecule and thus the ion source temperature on the one hand and the height of the centrifugal barrier for the reverse reaction and thus the kinetic energy release, on the other. The kinetic energy release so calculated will be the maximum possible neglecting any decrease due to tunnelling.

The rotational energy of methane, ϵ_{rot}, is

$$\epsilon_{rot} = L^2/2\mu r^2 \tag{1}$$

where L is the angular momentum, μ the reduced mass, and r the bond length of the quasi-diatomic CH_3–H rotor. Making the assumption noted above, the rotational angular momentum of the methane molecular ion is also L and, in the limit where all initial angular momentum of $CH_4{\cdot}^+$, appears as orbital angular momentum of the dissociating pair (i.e., the CH_3^+ product is taken as a point charge with no rotational motion), L may be expressed as

$$L = \mu r_c v \tag{2}$$

where v is the relative velocity of the separating pair and r_c equals the CH_3–H bond length in the $CH_4{\cdot}^+$ activated complex. The kinetic energy release is

$$\mathbf{T}_{max} = \tfrac{1}{2}\mu v^2 \tag{3}$$

From (1) and (2)

$$\epsilon_{rot} = \mu r_c^2 v^2/2r^2 \tag{4}$$

Substituting and rearranging

$$\mathbf{T}_{max} = \epsilon_{rot}(r^2/r_c^2) \tag{5}$$

If we make the usual assumption that an r^{-4} potential is appropriate for the reverse association reaction, an expression for the maximum impact parameter, b_{max}, consistent with a given velocity may be obtained from the Langevin treatment,[16] i.e.

$$b_{max} = (4\alpha e^2/\mu v^2)^{1/4} \tag{6}$$

where α is the polarizability of the neutral and e is the electronic charge. The maximum Langevin impact parameter is related[16] to the bond length in the activated complex, r_c, by

$$b_{max} = 2\sqrt{r_c} \tag{7}$$

Upon substitution of (6) and (7) in (5), the centrifugal barrier height ($\mathbf{T}_{max}$) is obtained.

$$\mathbf{T}_{max} = 2\epsilon_{rot}^2(r^4/2e^2\alpha) \tag{8}$$

Taking α_H as 6.67×10^{-25} cm^3 and r as 1.85 Å we find

$$\mathbf{T}_{max} = 1.22\ \epsilon_{rot}^2 \tag{9}$$

Or, with $\epsilon_{rot} = \frac{3}{2}kT$

$$T_{max} = 3.74(kT)^2 \quad (10)$$

Because of the lack of angular momentum restrictions on the reverse association reaction in this simple treatment the result represents the maximum temperature effect to be expected within the accuracy of the Langevin treatment. Recalling that the $T_{50\%}$ kinetic energy releases given in Figure 2 underestimate[7] the average kinetic energy releases by a factor of about 2.5, the data can be compared to the Langevin prediction by multiplying the $T_{50\%}$ values by 2.5 and plotting them as a function of $(kT)^2$. When this is done a least-squares slope of 4.0 is obtained. Considering the scatter in the data this agreement is satisfactory and the treatment does show that rotational energy is implicated in the reaction. It must also be noted that in his more elegant application of the Langevin treatment to unimolecular kinetics, Klots[2a] has predicted that the centrifugal barrier height for this reaction should vary as $1.5(kT)^2$. Furthermore, a referee has pointed out that this treatment[2] suggests that the mass dependence of tunnelling through polarization-centrifugal barriers should be negligible. The similar kinetic energy release behavior observed for CH_4 and CD_4 in the present study thus further substantiates the tunnelling mechanism.

In conclusion, the new experimental data presented here are compatible with the suggestion, first made by Rosenstock[3] and later expanded upon by Klots,[2] that the loss of H· from metastable $CH_4^{\cdot+}$ ions occurs via tunnelling. This reaction offers an interesting example of centrifugal effects on unimolecular reactions and its study has suggested one experimental approach to identifying cases in which such effects are dominant.

Acknowledgment. We thank Dr. K.C. Kim and a referee for valuable suggestions and the National Science Foundation for its support of this work.

References and Notes

(1) L. P. Hills, M. L. Vestal, and J. H. Futrell, *J. Chem. Phys.*, **54**, 3834 (1971).
(2) (a) C. E. Klots, *J. Phys. Chem.*, **75**, 1526 (1971); (b) *Chem. Phys. Lett.*, **10**, 422 (1971).
(3) Compare H. M. Rosenstock, *Adv. Mass Spectrom.*, **4**, 523 (1967).
(4) J. H. Beynon, R. G. Cooks, J. W. Amy, W. E. Baitinger, and T. Ridley, *Anal. Chem.*, **45**, 1023A (1973).
(5) (a) J. H. Beynon, W. E. Baitinger, J. W. Amy, and T. Komatsu, *Int. J. Mass Spectrom. Ion Phys.*, **3**, 47 (1969); (b) T. Ast, J. H. Beynon, and R. G. Cooks, *J. Am. Chem. Soc.*, **94**, 6611 (1972).
(6) C. Ottinger, *Z. Naturforsch. A*, **22**, 20 (1967).
(7) D. T. Terwilliger, J. H. Beynon, and R. G. Cooks, *Proc. Roy. Soc., (London), Ser. A*, **341**, 135 (1974).
(8) R. Stockbauer, *J. Chem. Phys.*, **58**, 3800 (1973).
(9) W. A. Chupka, *J. Chem. Phys.*, **48**, 2337 (1968).
(10) V. H. Dibeler and K. E. McCulloh, presented at Twenty-Second Annual Conference on Mass Spectrometry and Allied Topics, Philadelphia, Pa., May 1974.
(11) R. G. Cooks, J. H. Beynon, R. M. Caprioli, and G. R. Lester, "Metastable Ions," Elsevier, Amsterdam, 1973, p 99.
(12) R. G. Cooks, K. C. Kim, and J. H. Beynon, *Chem. Phys. Lett.*, **26**, 131 (1974).
(13) R. N. Dixon, *Mol. Phys.*, **20**, 113 (1971).
(14) W. A. Chupka, *J. Chem. Phys.*, **30**, 191 (1959).
(15) E. V. Waage and B. S. Rabinovitch, *Chem. Rev.*, **70**, 377 (1970).
(16) G. Gioumousis and D. P. Stevenson, *J. Chem. Phys.*, **29**, 294 (1958).
(17) C. E. Klots, *Z. Naturforsch. A*, **27**, 553 (1971).

Electron Exchange Reaction between Uranium(VI) and Tin(II) in Various *N*-Methylacetamide–Water Mixed Solvents

Richard T. Mayhew and Edward S. Amis*

Chemistry Department, University of Arkansas, Fayetteville, Arkansas 72701
(Received October 15, 1973; Revised Manuscript Received December 16, 1974)

The reduction of U(VI) with Sn(II) has been studied in 20, 40, 65, and 80 wt % *N*-methylacetamide–water solutions. The reaction rates were calculated using the second-order rate equation in 1, 2, 4, and 6 *M* HCl solutions in all the mixed solvents at 30, 40, and 50°. The change in rate constant with both change in solvent composition and HCl concentration was considered as possibly arising from the composition and charge (including sign) of the reacting complex ions, the macroscopic dielectric constants of the solvents, and the ionic strengths of the solutions. Certain limitations of the NMA–H_2O solvent systems for this reaction and these acidities were pointed out.

Introduction

The reaction

$$U(VI) + Sn(II) \longrightarrow U(IV) + Sn(IV)$$

has been studied in 100% water and in water–ethanol mixed solvents.[1,2] Water–*N*-methylacetamide (NMA) was chosen for further studies since the NMA would extend the dielectric constant range to 184.3.[3]

Experimental Section

Aldrich Chemical Co. 99+% pure NMA was distilled under vacuum and the center cut and the center cut of the first center cut were each distilled at about 5 Torr. The boiling point of the second center cut was observed to be 100 ± 10° at 5 Torr compared to the normal boiling point of 206°.[4]

The freezing point of the center cut of the last distilla-

TABLE I: Molar Extinction Coefficients for U(IV) in Mixed Solvent NMA-H_2O at 650 nm

	Wt % NMA				
2 *M* HCl	0	20	40	65	80
30°	54.2	58.1	56.7	60.7	45.8
40°	52.6	56.7	53.3	58.0	44.6
50°	50.8	54.8	51.9	53.4	41.6
	Wt % NMA				
40° Acid concn, *M*	0	20	40	65	80
1.00	52.4	57.1	*a*	*a*	*a*
2.00	52.6	56.7	53.3	57.9	44.6
4.00	54.0	55.4	48.7	65.2	56.1
6.00	51.2	49.7	44.9	57.0	*b*

[a] Tin precipitate. [b] $(NMA)_2$·HCl precipitate.

tion was 29°. Reported freezing points range from 28[5] to 30.56°.[6] This cut was used for mixed-solvent work.

The mixed solvents were prepared by weight and dried HCl gas was passed through the medium until the desired solvent acidity was obtained as determined by titrating an aliquote of the solution with standard sodium hydroxide using phenolphthalein as an indicator.

The procedures for making up stock solutions and runs have been described.[1,3] Table I shows the molar extinction coefficients taken at 650 nm for U(IV) in the NMA–water solvents at different temperatures and HCl concentrations. Precipitation data are included in the table. Temperatures of the runs were constant to within ±0.02°. All runs were 1.000 ± 0.002 *M* in Sn(II) and 0.0801 ± 0.0015 *M* in U(VI).

Results

The stoichiometry of the U(VI)–Sn(II) reaction is as represented in the Introduction. The reaction has been found to be first order with respect to both U(VI) and Sn(II).[7,8] We assumed the integrated form of the second-order rate equation

$$\log \frac{a_0(b_0 - x)}{b_0(a_0 - x)} = \frac{b_0 - a_0}{2.303} kt + \alpha$$

where k is the second-order rate constant, x is the concentration of product U(IV) at time t, a_0 is the initial concentration of A, and b_0 is the initial concentration of B. A plot of the log term vs. the time elapsed in the reaction should yield a straight line. The α term represents the nonzero intercepts observed in this work (see Figure 1). Other workers[9,10] have reported such intercepts. The large intercepts on the concentration ordinate indicate an initial reaction of a different rate which leveled off to a constant second-order rate. The initially different rate of reaction could have arisen from a combination of effects, including high local concentrations before complete mixing of the reactants; rapid reduction of the U(IV) by dissolved impurities;[9,10] a slow approach to steady-state concentration of intermediates; and the influence on the rate of products. The last effect mentioned would require, which is unlikely, a constant influence of the products with time, above a critical concentration of products even though the concentrations of products were increasing and the concentrations of reactants decreasing. This is so since the rate constant was

TABLE II: Rate Constants for Various NMA-H_2O Solvent Mixtures[a]

% NMA	|HCl|, *M*	Rate constant $\times 10^3$, M^{-1} hr^{-1};40°	Temp, °C	Rate constant, M^{-1} hr^{-1}; 2 *M* HCl
0	1	7.12	30	16.3
	2	43.5	40	43.5
	4	57.0	50	114
	6	125		
20	1	0.9	30	3.42
	2	8.06	40	8.06
	4	7.47	50	24.6
	6	24.7		
40	2	3.71	30	1.42
	4	5.41	40	3.71
	6	19.2	50	7.61
65	2	2.15	30	0.944
	4	0.868	40	2.15
	6	58.6	50	5.40
80	2	0.867	30	0.377
	4	1.71	40	0.867
			50	2.51

[a] U(VI) = 1.000 ± 0.002 *M*; Sn(II) = 0.0801 ± 0.0015 *M*.

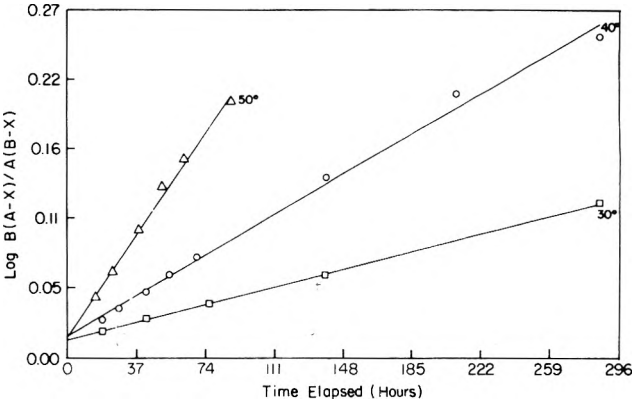

Figure 1. Second-order rate plot for 2.00 *M* HCl in 65 wt % NMA with 0.0802 *M* U(VI) and 1.00 *M* Sn(II).

constant throughout the measured change of concentrations for any run.

As to dissolved impurities, oxygen is ruled out since the initial rate was here to fast in opposition to the effect of the oxidation by oxygen of U(IV) to U(VI). The tin salt was purified[2] and should have been free of reducing impurities. Errors due to mixing of runs are minimized by the long times over which the reactions were measured. Thus the slow approach to steady-state intermediates which decreased the concentrations of reacting simpler ions, or which became prominent or even dominant and reacted, but at a different rate, than did the simpler ions to produce U(IV), seems the most plausible explanation of the intercepts.

Second-order plots, as in Figure 1, gave straight lines for different weight percent solvent mixtures and for 1, 2, 4, and 6 *M* HCl to 40–70% completion, consistent with a second-order rate constant even though it is unlikely that the reaction is a simple one-step collision mechanism. Table II lists the observed second-order rate constants determined over periods of time from 2 to 42 days. The rate of change

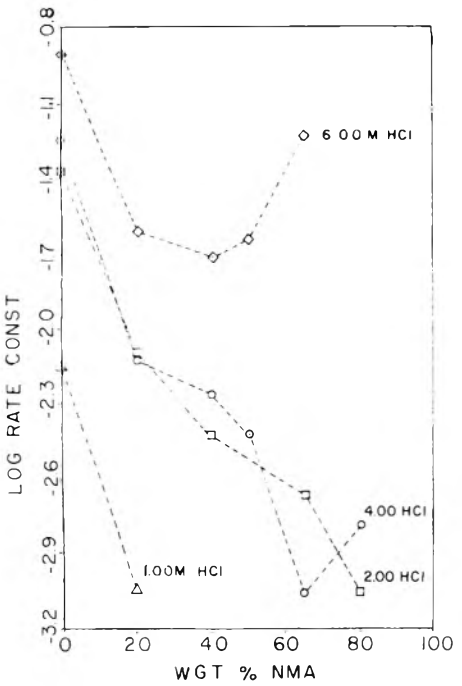

Figure 2. Change in log of the rate constant for 1, 2, 4, and 6 *M* HCl solutions as the weight percent of NMA is increased.

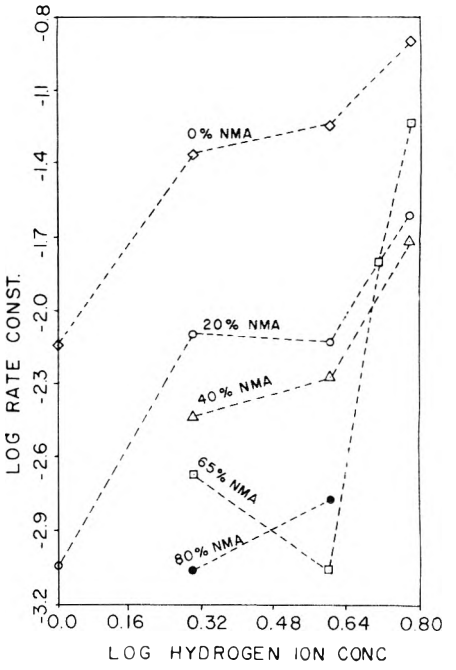

Figure 3. Change in log of the rate constant for 0, 20, 40, 65, and 80 wt % NMA as the log hydrogen ion concentration increased.

in U(IV) concentration with time was so slow, that attempts to get consistent data within the first 5–15 hr were not too successful for the slower runs, though 1–2-hr initial readings were often made on the runs of 2 days. In every case the reactions were at least duplicated and, in all cases, were repeated until the error limit among the runs was less than 7% except for the data in 6 *M* HCl, where the error limit among the runs was less than 10%. The symbols, as drawn, cover about 5% on either side of the point, so that the errors among the runs, the average of which run values are represented by a point, are well within the dimensions of the symbol for the point.

Some difficulties arose using NMA as a solvent. The first was the precipitation of a tin complex in solutions of less than 2 *M* HCl. Even for the 20% NMA–1 *M* HCl solvent, the reaction was terminated after 30 hr because of the accumulation of tin precipitate in the flask. Hence, the rate constant of $0.9 \times 10^{-3}\ M^{-1}\ hr^{-1}$ may be in doubt although it does reflect the initial rate for the 1.0 *M* HCl–20% NMA solvent.

In the NMA rich solvent system, another problem developed. Around 80% NMA, the system could not handle the large amounts of HCl being forced into it. As the 80% NMA approached 6 *M* in acid, long crystals formed when the solution remained undisturbed for several hours. A cloudy gel-like mass of crystals formed in a stirred solution. In both cases, the crystals were removed, washed with benzene and ether in a sintered glass crucible, and dissolved in water from which a AgCl precipitate was taken. The experimentally determined percents of Cl were 19.73, 19.81, and 19.74. The crystals were *N*-methylacetamide hydrochloride, $(NMA)_2 \cdot HCl$, whose theoretical Cl content is 19.41%. We obtained a melting point of 88.0 ± 0.5° compared to a literature value of 87–89°.[11] This compound was first reported by D'Alelio and Reid[5] and later by Dawson et al.[4,12]

Because of the formation of (NMA) · HCl, no kinetic data could be taken above 80% NMA. At higher NMA concentrations, even small amounts of HCl precipitated the salt. From the NMA mixed solvent work up to 80%, the following trends may be noted.

Figure 2 shows the change in the log of the second-order rate constant with increase of NMA. For each acid strength there is a sharp initial decrease in the rate with the introduction of small amounts of NMA. This marked but somewhat solvent dependent decrease in rate continues for 2 *M* HCl to 80% NMA.

The rapid decrease and abrupt increase in the rates at 4 and 6 *M* HCl suggest that the solvent may be favoring the formation of complexes which discourage or encourage the reaction rate.

For example, it is agreed that both Sn(II) and U(VI) form chloride complexes in acid solutions.[13-17] However, there is little data in the literature on the dissociation constants for these complexes and those data are for limiting cases of zero or very low ionic strengths.

The peculiar variations of the rate constants with solvent composition and with HCl molarity (see Figure 3) are perhaps due to very complicated relationships between the stabilities and charges (including signs) of chloro and solvo complexes, the reactivities of pertinent complexes toward each other, and the dielectric constants of the system which influence electrostatic forces between reactants. Ionic strength change with changing HCl molarity may have contributed to the results on concentration studies.

It is improbable that the formation of $(NMA)_2 \cdot HCl$ influenced the results except perhaps as a solvent component, since similar trends were observed in the water–ethanol solvent system.[2]

References and Notes

(1) R. T. Mayhew and E. S. Amis, *J. Inorg. Nucl. Chem.*, **35**, 4245 (1973).
(2) Z. C. Ho Tan and E. S. Amis, *J. Inorg. Nucl. Chem.*, **28**, 2889 (1966).
(3) O. D. Bonner and C. B. Woolsey, *J. Phys. Chem.*, **75**, 2879 (1971).
(4) L. R. Dawson, J. E. Berger, J. W. Vaughn, and H. C. Eckstrom, *J. Phys. Chem.*, **67**, 281 (1963).
(5) G. F. D'Alelio and E. Reid, *J. Am. Chem. Soc.*, **59**, 109 (1937).

(6) R. W. Kreis and R. H. Wood, *J. Chem. Thermodyn.*, **1**, 523 (1969).
(7) D. M. Mathews, J. D. Hefley, and E. S. Amis, *J. Phys. Chem.*, **63**, 1236 (1959).
(8) R. L. Moore, *J. Am. Chem. Soc.*, **77**, 1504 (1954).
(9) J. C. Sullivan, A. J. Zielen, and J. C. Hindman, *J. Am. Chem. Soc.*, **82**, 5288 (1960).
(10) A. C. Harkness and J. Halpern, *J. Am. Chem. Soc.*, **81**, 3526 (1959).
(11) F. F. Blicke and J. H. Burckhalter, *J. Am. Chem. Soc.*, **64**, 451 (1942).
(12) L. R. Dawson, R. C. Sheridan, and H. C. Eckstrom, *J. Phys. Chem.*, **65**, 1829 (1961).
(13) J. N. Donaldson, W. Moser, and W. B. Simpson, *J. Chem. Soc.*, 1727 (1963).
(14) C. E. Vandergee and D. E. Rhodes, *J. Am. Chem. Soc.*, **74**, 3552 (1952).
(15) C. I. Browne, R. P. Craig, and N. Davidson, *J. Am. Chem. Soc.*, **73**, 1946 (1951).
(16) J. D. Hefley and E. S. Amis, *J. Phys. Chem.*, **64**, 870 (1960).
(17) S. W. Rabideau and R. H. Moore, *J. Phys. Chem.*, **65**, 371 (1961).

One-Electron Oxidation of Odd-Valent Metal Ions in Solution

P. S. Rao and E. Hayon*

Pioneering Research Laboratory, U.S. Army Natick Laboratories, Natick, Massachusetts 01760 *(Received September 3, 1974)*

Publication costs assisted by U. S. Army Natick Laboratories

The fast-reaction technique of pulse radiolysis and kinetic absorption spectrophotometry was used to generate odd-valent metal ions in neutral aqueous solution, and study their one-electron oxidation reactions. Using the sulfate and perchlorate salts, the M^{2+} ions were reduced to the M^+ ions by e_{aq}^-. The Zn^+, Co^+, Cd^+, Pb^+, Ni^+, as well as Cr^{2+} and Tl^0, odd-valent metal ions were produced. The one-electron oxidation of these odd-valent metal ions was studied in the presence of various electron acceptors A (including phenones, dyes, and quinones) whose two-electron redox potentials E^{01} (V, at pH 7.0, 25°) are known. The percentage efficiency of the electron transfer reaction $M^+ + A \rightarrow M^{2+} + \cdot A^-$ was found to be dependent upon the E^{01} values of the acceptors. Titration-type curves are obtained, and from the midpoint (50% electron transfer) kinetic potentials for the $M^+|M^{2+}$ redox couples were derived. These potentials are not the thermodynamic values since the electron transfer processes followed were found to be irreversible, under the experimental conditions used. The results show that the reducing power of the odd-valent metal ions decreases in the order $Zn^+ \geq Co^+ \geq Cd^+ > Tl^0 > Pb^+ > Ni^+ > Cr^{2+}$.

Introduction

Most divalent transition metal ions react with e_{aq}^- with high rate constants[1] in aqueous solution. The products of the reaction with e_{aq}^- are the monovalent ions in their ground states (reaction 1). The formation of Co^+, Zn^+,

$$M^{2+} + e_{aq}^- \rightarrow M^+ \quad (1)$$

Cd^+, and Ni^+ have been shown based on their uv absorption spectra.[2] The ESR of some of these odd-valent metal ions were also observed in frozen solutions.[3] These reduced species have been found to react with various oxidants, including O_2, N_2O, H_2O_2, NO_2^-, NO_3^-, alkyl halides, etc. (see ref 1, p 122). It was shown[4] that Zn^+ is more reactive than Cd^+, and that both species are much more reactive than Ni^+. Explanations for some of these observations have been suggested,[1-4] based on the configuration of the metal ions and the type of electron transfer (inner sphere vs. outer sphere) mechanism.

We have recently developed a method,[5] using the pulse radiolysis technique, for determining the *kinetic* (not thermodynamic) potentials of free radicals in aqueous solutions. This method is based on the one-electron redox properties of the free radicals, $\cdot RH$, in the presence of electron acceptors, A, whose two-electron redox potentials (E^{01}, pH 7.0, ~25°) in water are known:

$$\cdot RH + A \rightarrow R + \cdot A^- + H^+ \quad (2)$$

The rate constants of reaction 2 and the efficiencies of formation of $\cdot A^-$ were shown to be dependent on the E^{01} values of the acceptors used. A plot of the percentage efficiency for electron transfer vs. E^{01} of the acceptors gave "titration-type" curves, and from the midpoint (50%) the kinetic potentials of the radicals, E_k^{01}, were derived.

This method has been used to obtain the kinetic potentials of odd-valent metal ions in water. The results obtained for the following redox couples are presented below: $Zn^+|Zn^{2+}$, $Co^+|Co^{2+}$, $Cd^+|Cd^{2+}$, $Tl^0|Tl^+$, $Pb^+|Pb^{2+}$, $Ni^+|Ni^{2+}$, and $Cr^{2+}|Cr^{3+}$.

Experimental Section

The pulse radiolysis and kinetic absorption spectrophotometry experimental set-up used have been described.[6,7] Single pulses of ~2.3 MeV electrons and ~30-nsec duration were provided from a Febetron 705 machine (Field Emission Corp.).

The radiation chemistry of water produces

$$H_2O \rightsquigarrow e_{aq}^- (2.8), OH (2.8), \text{and } H (0.6)$$

where the numbers in parentheses are the G values (number of free radicals formed per 100 eV of energy absorbed by the water). The experimental condition used to generate the odd-valent metal ions in water was a one-electron reduction of Zn^{2+}, Co^{2+}, Cd^{2+}, Tl^+, Pb^{2+}, Ni^{2+}, and Cr^{3+} salts by e_{aq}^-, reaction 1. These experiments were carried out using 5 mM concentration of the salts in the presence of ~1.0 M *tert*-butyl alcohol to scavenge[6] the OH radicals.

The sulfate salts were used for all metal ions, except for lead and chromic when the perchlorate salts were used.

The experimental conditions used to study the one-electron oxidation of these odd-valent metal ions in the presence of electron acceptors were described in detail.[5] The concentration of the acceptors A was 5×10^{-5} M, except for dyes when $2.0–2.5 \times 10^{-5}$ M concentrations were used. Under all conditions, all the e_{aq}^- reacted with the metal ions, none with the acceptors, and the $[A]/[M^+] \geq 15$. Relatively low concentrations of e_{aq}^- were used, ~1–2 μM. Table I lists the acceptors employed in this work. Their redox potentials were obtained from the literature,[9] and the values are for two-electron changes.

The 100% efficiency level for formation of $\cdot A^-$ radicals, or for "bleaching" of the dyes, was established in each case from the reaction of the acceptors with e_{aq}^- in the absence of the metal ions (eq 3). The wavelengths used to monitor

$$A + e_{aq}^- \rightarrow \cdot A^- \quad (3)$$

the formation of $\cdot A^-$, or the bleaching of the dye, are given in ref 5 and 8.

Chemicals were the highest research grade commercially available and were purchased from Baker and Adamson, J. T. Baker, Mallinckrodt, Aldrich, and Eastman Chemicals. Solutions were buffered at pH 7.0 with ~1 mM phosphates.

Results and Discussion

All the metal ions examined react with e_{aq}^- at diffusion-controlled rates[1] in water at pH 7.0. Under the experimental conditions used, the odd-valent metal ions are produced in $\leq 10^{-8}$ sec. The nature of the aquo–metal complex of these species present in sulfate (or perchlorate) solutions at pH 7.0 are not known or assumed in this work. For convenience, the odd-valent ions are represented as M^+ (for Zn^+, Co^+, Cd^+, Pb^+, and Ni^+), M^{2+} (for Cr^{2+}), and M^0 (for Tl^0). In the case of Tl^0, the actual species present[10] in these solutions may be Tl_2^+, produced from the reaction $Tl^0 + Tl^+ \rightarrow Tl_2^+$.

The lifetimes and decay characteristics of these odd-valent metal ions are known[1-4] only in general terms. It was assumed (as was found to be the case) that their reaction with the acceptors would occur in a time scale significantly shorter than their natural lifetimes, under the experimental conditions used.

Oxidation of Zn^+, Co^+, and Cd^+ Ions. The reaction of, for example, Co^+ with menaquinone (MQ) has already been shown[11] to form the $MQ\cdot^-$ radical anion, whose transient spectrum and extinction coefficient is in complete agreement with literature data on the spectral properties of $MQ\cdot^-$. The dependence of the percentage efficiencies for the one-electron oxidation of these ions, reaction 4, upon

$$M^+ + A \rightarrow M^{2+} + \cdot A^- \quad (4)$$

the redox potential of the acceptors used are shown in Figure 1. A rapid change can be observed with acceptors whose E^{01} values are in the range −1.1 to −1.0 V. Small, but experimentally distinguishable, differences were observed for Zn^+, Co^+, and Cd^+.

The presence of the β-hydroxyl alkyl radical produced from *tert*-butyl alcohol (present in solution to scavenge the OH radicals) was found not to interfere with the results observed. This was established as follows: (a) the percentage of $\cdot BP^-$ (BP = benzophenone) formed from the reaction of Co^+ and Zn^+ with BP was 80–84%, in solutions containing 5 mM $CoSO_4$ or $ZnSO_4$, pH 7.0, in the presence of either 1.0 M t-BuOH, 1.0 M i-PrOH, or 1.0 M HCO_2^- used to scavenge the OH radicals. The t-BuOH radical and the $(CH_3)_2\dot{C}OH$ and CO_2^- radicals formed did not react with Zn^+ or Co^+, Zn^{2+} or Co^{2+}, or with BP. The latter was already established;[5] (b) in 5 mM solutions of $NiSO_4$, 5×10^{-5} M anthraquinone 2,6-disulfonate (AQ), pH 7.0, 1 atm of argon, ~100% formation of $\cdot AQ^-$ was found in 1.0 M t-BuOH (Figure 1). An almost doubling in the yield of $\cdot AQ^-$ was observed in the presence of 1.0 M i-PrOH or 1.0 M HCO_2^-. This is explained on the basis of reactions 5 and 6. These reactions have already been established.[5]

$$(CH_3)_2\dot{C}OH + AQ \rightarrow \cdot AQ^- - CH_3COCH_3 + H^+ \quad (5)$$

$$CO_2^- + AQ \rightarrow \cdot AQ^- + CO_2 \quad (6)$$

Under the experimental conditions used, reaction 4 was found to be irreversible. This was concluded on the basis of an absence of a dependence on the formation (both rate of formation and efficiency) of $\cdot A^-$ upon $[M^{2+}]$, over the range up to 5×10^{-2} M. The decay kinetics of $\cdot A^-$ was also not affected by the concentration of M^{2+} ions. Hence thermodynamic redox potentials cannot be derived from these results. The potentials are referred to as *kinetic* potentials.[5b]

TABLE I: List of Electron Acceptors Used

	E^{01}, V[a]
1. 4,4¹-Dimethoxybenzophenone	−1.120
2. p-Chlorobenzophenone	−1.050
3. Benzophenone	−1.00
4. p-Cyanobenzophenone	−0.80
5. 3-Benzoylpyridine	−0.75
6. Fluorenone	−0.68
7. Rhodamine B	−0.54
8. Eosin Y	−0.50
9. Crystal Violet	−0.357
10. Safranine T	−0.289
11. Phenosafranine	−0.254
12. Anthraquinone 2,6-disulfonate	−0.184
13. Indigodisulfonate	−0.125
14. Menaquinone	+0.002

[a] See ref 9, 5, and 8.

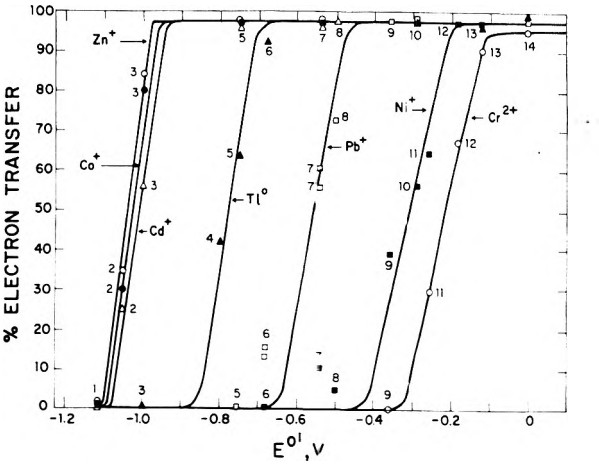

Figure 1. Dependence of the percentage efficiency for the one-electron oxidation of odd-valent metal ions upon the redox potential (E^{01}, V at pH 7.0 and ~25°) of the electron acceptors A. Experiments carried out in aqueous solutions using 5×10^{-3} M of the metal sulfates (except for Pb^{2+} and Cr^{3+} perchlorates) at pH 7.0, in the presence of $2.5–5 \times 10^{-5}$ M concentration of the acceptors. See text for further experimental details and Table I for the list of electron acceptors used.

TABLE II: Kinetic Potential of Odd-Valent Metal Ions in Water at pH 7.0, 25°

System	Redox couple[a]	E_k^{01}, V[b]
$ZnSO_4$	$Zn^+ \mid Zn^{2+}$	−1.04
$CoSO_4$	$Co^+ \mid Co^{2+}$	−1.02
$CdSO_4$	$Cd^+ \mid Cd^{2+}$	−1.01
Tl_2SO_4	"Tl^0" $\mid Tl^+$	−0.78
$Pb(ClO_4)_2$	$Pb^+ \mid Pb^{2+}$	−0.56
$NiSO_4$	$Ni^+ \mid Ni^{2+}$	−0.31
$Cr(ClO_4)_3$	$Cr^{2+} \mid Cr^{3+}$	−0.21

[a] The redox couple studied is for the one-electron oxidation of the lower valent ion to the higher valent ion (see text). [b] Values are derived from the midpoints (50% electron transfer) of the curves in Figure 1; values are good to ±0.03 V; the signs are given for the reduction process, in agreement with convention (i.e., the kinetic *oxidation* potential for the $Zn^+ \mid Zn^{2+}$ couple is +1.04 V).

From the midpoint (50% electron transfer) of the curves given in Figure 1, the kinetic potentials, E_k^{01}, of these odd-valent metal ions can be derived and are given in Table II. The results indicate that these monovalent ions are powerful reducing agents, capable of reducing molecules with E^{01} values greater than ~−1.0 V. A recent study[12a] of Co(I) complexes containing unsaturated macrocyclic ligands gave a $E_k^{01} = -0.88$ V for the Co^I (4,11-diene-N_4) species.

The thermodynamic redox potentials for the $Zn^+ \mid Zn^{2+}$ and $Cd^+ \mid Cd^{2+}$ couples have recently been calculated.[12b] Values of −2.0 ± 0.4 and −1.8 ± 0.4 V, respectively, were derived. On the basis of Marcus' theory[13] for electron transfer reactions, the redox potentials for the couples $Zn^+ \mid Zn^{2+}$ and $Cd^+ \mid Cd^{2+}$ were estimated[14,12b] as −1.0 and ≤−0.5 V, respectively. The E_k^{01} values of ~−1.0 *V* for these couples appear to be closer to the E^{01} values calculated on the basis of Marcus' theory. It should be pointed out, however, that while thermodynamic redox potentials provide information as to whether a reaction is energetically feasible, the kinetic potentials provide information on the occurrence and rate constants of the reaction. Neither method, however, provides any information on the mechanism of the electron transfer reaction.

Oxidation of Pb^+ and Ni^+ Ions. The results obtained are presented in Figure 1 and the E_k^{01} values derived are given in Table II.

Ionization constant values ranging from 7.1 to 8.8 have been obtained[15] for the hydrolysis of Pb^{2+} ions. Hence there is uncertainty on the nature of the Pb^+ species present at pH 7.0. A E_k^{01} value of −0.57 V is obtained for the $Pb^+ \mid Pb^{2+}$ couple making this metal ion a poorer reducing agent compared to Zn^+, Co^+, and Cd^+.

Ni^+ is an even poorer reducing agent, with E_k^{01} of −0.31 *V*. E^{01} value of −0.7 ± 0.4 V have been derived[12b] for the $Ni^+ \mid Ni^{2+}$ couple, while the value estimated from thermodynamic data[16] is −2.7 V. A value of −0.7 V was derived[14] based on Marcus' theory.

The Ni(I) complexes of unsaturated macrocyclic ligands have been studied[17] and their kinetic potentials determined.

Oxidation of Cr^{2+} Ions. The Cr^{2+} ions were produced from the reaction of e_{aq}^- with chromic perchlorate at pH 7.0. The oxidation of Cr^{2+} to Cr^{3+} was found to have a E_k^{01} value of −0.21 V; see Figure 1 and Table II.

In perchloric acid solutions at pH 3.4, the one-electron oxidation of the Cr^{2+} species to Cr^{3+} occurred at a much higher (i.e., more positive) potential. A E_k^{01} value of ~+0.35 V was found, making the Cr^{2+} species at pH 3.0 a poorer reducing agent than at pH 7.0. A pK_a for the hydrolysis of Cr^{3+} of ~4.0 has been reported.[15] The redox potential for the Cr^{3+} couple in 1.5×10^{-3} *M* H_2SO_4 was reported[18] to be −0.41 V. This is a clear example where the pH and the nature of the aquo–metal complex ion can considerably affect the redox properties of the ions.

Oxidation of Tl^0. As mentioned above, the form and nature of the species present at pH 7.0 are uncertain. Figure 1 and Table II show the results obtained.

The one-electron of the "Tl^0" species shows this ion to be a relatively strong reducing agent, with $E_k^{01} = -0.77$ V. The redox potential for the $Tl^+ \mid Tl^0$ couple is reported[18] to be −0.336 V. This is considerably different from the E_k^{01} value found for the reverse process. Among other reasons which may account for this difference is the nature of the "Tl^0" species present in solutions which is oxidized to Tl^+.

Oxidation of Ag^0 and Cu^+ Ions. Some preliminary experiments with $Ag(SO_4)_2$ and $CuSO_4$ were carried out at pH 3.0. Considerable irreproducibility was observed with these ions at pH 7.0 and also at pH 3.0.

It appears that the "Ag^0" species present at pH 3.0 is a poor reducing agent with E_k^{01} ~+0.5 V for the $Ag^0 \mid Ag^+$ couple. Similarly, the oxidation of "Cu^+" at pH 3.0 is equally difficult, with $E_k^{01} > +0.4$ V for the $Cu^+ \mid Cu^{2+}$ couple. Due to the observed irreproducibility of these systems, the E_k^{01} values given above are probably not significant.

TABLE III: Reaction Rate Constants of Odd-Valent Metal Ions with Electron Acceptors in Aqueous Solution, pH 7.0

System	Odd-valent ion	Acceptor[a]	k, M^{-1} sec^{-1}[b]
$ZnSO_4$	Zn^+	*p*-Benzoquinone (+0.293)	4.8×10^9
		Menaquinone (+0.002)	3.8×10^9
		Benzophenone (−1.00)	2.5×10^9
$CoSO_4$	Co^+	*p*-Benzoquinone (+0.293)	4.8×10^9
		Menaquinone (+0.002)	4.0×10^9
		Benzophenone (−1.00)	2.5×10^9
$CdSO_4$	Cd^+	*p*-Benzoquinone (+0.293)	4.4×10^9
		Menaquinone (+0.002)	4.6×10^9
		Benzophenone (−1.00)	1.0×10^9
Tl_2SO_4	"Tl^0"	*p*-Benzoquinone (+0.293)	2.8×10^9
$Pb(ClO_4)_2$	Pb^+	Menaquinone (+0.002)	3.7×10^9
$NiSO_4$	Ni^+	Menaquinone (+0.002)	2.4×10^9
$Cr(ClO_4)_3$	Cr^{2+}	*p*-Benzoquinone (+0.293)	3.5×10^9
		Anthraquinone 2,6-disulfonate (−0.184)	2.8×10^9

[a] Numbers in parentheses are the redox potentials of the acceptors. [b] Determined by monitoring the formation kinetics of ·A radicals at appropriate wavelengths. $M^{n+} + A \rightarrow M^{(n+1)+} + \cdot A^-$ (see text).

Conclusions

The kinetic potentials for the $Zn^+ \mid Zn^{2+}$, $Co^+ \mid Co^{2+}$, $Cd^+ \mid Cd^{2+}$, $Pb^+ \mid Pb^{2+}$, $Ni^+ \mid Ni^{2+}$, $Cr^{2+} \mid Cr^{3+}$, and $Tl^0 \mid Tl^+$ couples in water at pH 7.0 were derived. For most of these one-electron redox couples, no calculated thermodynamic redox potentials are known. The results obtained here appear to be relevant to the chemical reactivity of these odd-valent metal ions in water.

The reaction rate constants of these ions with a number of the acceptors used are given in Table III. These values

are close to diffusion-controlled rates for acceptors which have higher (more positive) potentials than the oxidation potentials of the $M^+|M^{2+}$ couples.

References and Notes

(1) E. J. Hart and M. Anbar, "The Hydrated Electron", Wiley-Interscience, New York, N.Y., 1970.
(2) J. H. Baxendale, E. M. Fielden, and J. P. Keene, *Proc. R. Soc., Ser. A*, **286**, 320 (1965); D. M. Brown and F. S. Dainton, *Trans. Faraday Soc.*, **62**, 1139 (1966).
(3) P. N. Moorthy and J. J. Weiss, *Adv. Chem. Ser.*, **No. 50**, 180 (1965); T. Feldmann, A. Treinin, and V. Volterra, *J. Chem. Phys.*, **42**, 3366 (1965).
(4) D. Meyerstein and W. A. Mulac, *J. Phys. Chem.*, **72**, 784 (1968); *Trans Faraday Soc.*, **65**, 1818 (1969).
(5) (a) P. S. Rao and E. Hayon, *J. Am. Chem. Soc.*, **96**, 1287 (1974); (b) in press.
(6) M. Simic, P. Neta, and E. Hayon, *J. Phys. Chem.*, **73**, 3794 (1969).
(7) J. P. Keene, E. D. Black, and E. Hayon, *Rev. Sci. Instrum.*, **40**, 1199 (1969).
(8) P. S. Rao and E. Hayon, *J. Am. Chem. Soc.*, **96**, 1295 (1974).
(9) "Handbook of Biochemistry", Chemical Rubber Publishing Co., Cleveland, Ohio, 1970, p J-33; W. M. Clark, "Oxidation Reduction Potentials of Organic Systems", Williams and Wilkins, Baltimore, Md., 1960; L. Meites, "Polarographic Techniques", Interscience, New York, N.Y., 1967; I. M. Kolthoff and J. J. Lingane, "Polarography", Interscience, New York, N.Y., 1958.
(10) B. Cercek, M. Ebert, and A. J. Swallow, *J. Chem. Soc. A*, 612 (1966).
(11) P. S. Rao and E. Hayon, *Biochim. Biophys. Acta*, **292**, 516 (1973).
(12) (a) A. M. Tait, M. Z. Hoffman, and E. Hayon, *J. Am. Chem. Soc.*, submitted for publication; (b) G. Navon and D. Meyerstein, *J. Phys. Chem.*, **74**, 4067 (1970).
(13) R. A. Marcus, *J. Chem. Phys.*, **43**, 3477 (1965); *Adv. Chem. Ser.*, **No. 50**, 138 (1965).
(14) M. Anbar, *Quart. Rev.*, **22**, 578 (1968).
(15) D. D. Perrin, "Dissociation Constants of Inorganic Acids and Bases in Aqueous Solutions", Butterworths, London, 1969.
(16) J. H. Baxendale and R. S. Dixon, *Z. Phys. Chem. (Frankfurt am Main)*, **43**, 161 (1964).
(17) A. M. Tait, M. Z. Hoffman, and E. Hayon, to be submitted for publication.
(18) G. Charlot, "Oxidation-Reduction Potentials of Inorganic Substances in Aqueous Solution", Butterworths, London, 1971.

Radiolysis of H_2O and D_2O between 0 and 300° [1]

K. N. Jha, T. G. Ryan, and G. R. Freeman*

Chemistry Department, University of Alberta, Edmonton, Alberta, Canada T6G 2G2

(*Received August 12, 1974*)

The γ radiolysis yield of fluoride ion from millimolar solutions of sulfur hexafluoride at 23° was $G(F^-)$ = 16.0 ± 0.6 in H_2O and 18.6 ± 0.6 in D_2O. One scavenged electron ultimately gave rise to six fluoride ions, so the above values correspond to $G(e_{solv}^-)_{fl}$ = 2.7 ± 0.1 in H_2O and 3.1 ± 0.1 in D_2O. The scavenging yield increased with increase in temperature up to 300° and values obtained in D_2O were persistently about 0.5 G units larger than those in H_2O. At 300°, $G(F^-)/6$ = 4.8 ± 0.2 in H_2O and 5.3 ± 0.2 in D_2O. Similar results were obtained at 23° with nitrous oxide, and the difference in the scavenging yields in D_2O and H_2O persisted up to high scavenger concentrations. The larger yields in D_2O were tentatively attributed to an isotope effect in the total ionization yield, in addition to the previously suggested isotope effect on the ranges of the secondary electrons. Absorption coefficients are reported for sulfur hexafluoride in H_2O and D_2O at temperatures up to 300°.

Introduction

It has been noted that the free ion yields in perdeuterio water,[2,3] ammonia,[4] and dimethyl sulfoxide[5] are larger than those in the corresponding perprotio liquids. The isotope effect amounts to ~10% in water and ammonia and to about 30% in dimethyl sulfoxide. The (D/H) isotope effects in the total ionization yields of gaseous ethylene and *n*-butane, ionized by energy transfer from metastable Ne* and Ar*, were only 1%.[6] The large magnitudes of the effects in the polar liquids are difficult to understand.

In an attempt to learn more about the isotope effect, the radiolysis of solutions of sulfur hexafluoride in H_2O and D_2O have been studied at temperatures between 0 and 300°. The competing processes that lead to an isotope effect may be temperature sensitive. Furthermore, nitrogen yields from nitrous oxide solutions were measured over a wide concentration range in H_2O and D_2O.

Experimental Section

The H_2O was purified as reported previously.[7] The D_2O was distilled once from alkaline permanganate, then once without additive, just prior to use. The salts used as solutes were reagent grade. The other solutes were the purest available grade and were purified by standard techniques.[8,9]

Nitrous oxide and sulfur hexafluoride solutions were prepared by standard vacuum techniques.[7] The latter solutions were irradiated at pH ≈7, adjusted with Na_2HPO_4 and KH_2PO_4 buffer, to avoid competition between sulfur hexafluoride and the product hydrofluoric acid for electrons.

Nitrogen yields were measured by standard vacuum techniques.[7]

The fluoride ion yields were measured with an Orion fluoride ion specific electrode Model 94-09A in conjunction with an Orion double junction reference electrode Model 90-02-00. The electrode potentials were measured at pH 5–7 by an Orion Model 801 digital pH/mV meter, using microsample dishes. The electrodes were calibrated with standard sodium fluoride solutions before, during and after sample measurements. The accuracy of the analytical technique was ±1%. The ionic strength of the sample and calibrating solutions was adjusted to 1.0 *M*.

TABLE I: Bunsen Absorption Coefficient of SF_6

T, °C	α H_2O	α D_2O
20	7.0×10^{-3}[a]	
23		5.1×10^{-3}
146	7.1×10^{-3}	
300	12×10^{-3}	9.9×10^{-3}

[a] Earlier value $\alpha = 6.4 \times 10^{-3}$ interpolated from data in H. L. Friedman, *J. Am. Chem. Soc.*, 76, 3294 (1954).

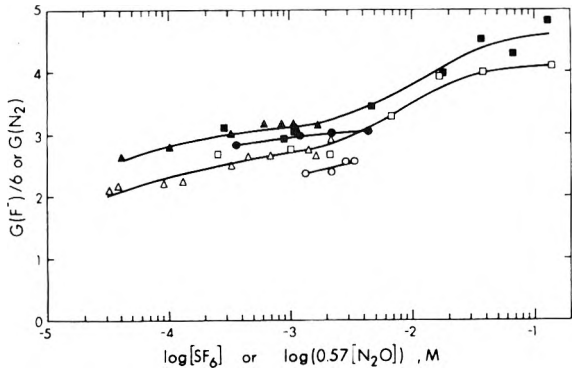

Figure 1. Yields of fluoride ions from solutions of sulfur hexafluoride and of nitrogen from nitrous oxide solutions: SF_6 ○, ●, 0°; △, ▲, 23°; N_2O □, ■, 23°. The N_2O concentrations were normalized to the same reactivity as that of SF_6 by multiplying them by $k(e_s^- + N_2O)/k(e_s^- + SF_6) = 0.57$. Open points are for H_2O and dark points for D_2O.

The concentrations of N_2O in samples at 23° were calculated with the aid of the Bunsen coefficient $\alpha = 0.63$.[10]

Several solutions of SF_6 at a given concentration and temperature were irradiated at doses in the range from 1 to 4×10^{17} eV/g, both in H_2O and D_2O. The solubility coefficient of SF_6 was determined from the point at which the slope of the linear yield of fluoride ions vs. dose plot suddenly decreased to a small value. The sudden decrease in slope was due to the complete consumption of sulfur hexafluoride in the bulk solution, and the residual yield was due mainly to diffusion of sulfur hexafluoride into the liquid from the gas above it. Values of α thus estimated are listed in Table I.

The high temperature apparatus has been described previously.[11] The only differences were that water was used as the pressurizing fluid and a copper gasket was used instead of lead in the steel autoclave (bomb).

Irradiations were done in a ^{60}Co Gammacell-220 from Atomic Energy of Canada Ltd. The dose rate was 2×10^{17} eV/g min.

Results and Discussion

Sulfur hexafluoride produces six fluoride ions for every electron scavenged,[12] so the yields were plotted as $G(F^-)/6$.

Yield vs. concentration curves for H_2O and D_2O at 0 and 23° are presented in Figure 1. Results for 220 and 300° in H_2O and 200 and 300° in D_2O are in Figure 2. The yield of fluoride ions increases with increasing temperature over the entire range both in H_2O and D_2O. The yields obtained in D_2O are higher than those in H_2O at all temperatures by approximately 0.5 units of $G(F^-)/6$ (Table II).

Thus the isotope effect persists up to high temperatures.

TABLE II: The Yields $G(F^-)/6$ and $G(N_2)$ from 1 m*M* Solutions of SF_6 or N_2O in H_2O and D_2O

T, °C	$G(F^-)/6$ H_2O	$G(F^-)/6$ D_2O	$G(N_2)$ H_2O	$G(N_2)$ D_2O
0	2.5	3.0		
23	2.7	3.1	2.7	3.1
81			3.2	3.9
106	3.2	3.7		
200		4.3		
220	3.7			
300	4.8	5.3		

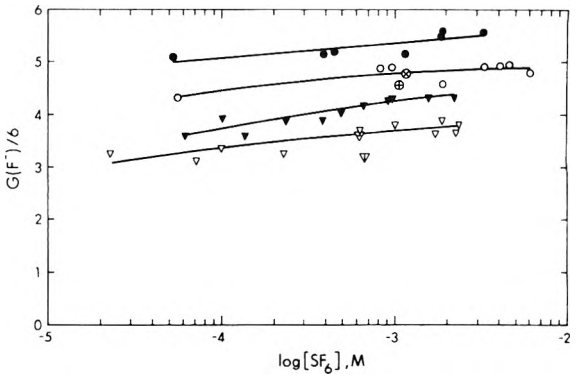

Figure 2. Yields of fluoride ions from solutions of sulfur hexafluoride in H_2O and D_2O. H_2O: (▽) 220°; (▼) 0.1 *M* methanol at 220°; (⊽) saturated with *n*-hexane at 220°; (○) 300°; (⊗) 0.1 *M* methanol at 300°; (⊕) saturated with *n*-hexane at 300°. D_2O (▼) 200°; (●) 300°.

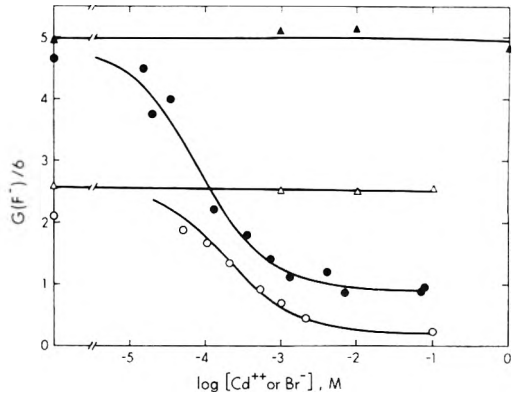

Figure 3. Effects of cadmium chloride in unbuffered H_2O and potassium bromide in buffered H_2O on the fluoride ion yield from sulfur hexafluoride solutions. $CdCl_2$: (○) 23°, 0.8 m*M* SF_6; (●) 300°, 2.2 m*M* SF_6. KBr: (△) 23°, 0.7 m*M* SF_6; (▲) 300°, 5.0 m*M* SF_6. The yields in unbuffered water in the absence of Cd^{2+} are slightly low due to acid resulting from electron scavenging by SF_6.

It decreases as a percentage of the measured yield with increasing temperature.

Addition of cadmium chloride, an efficient electron scavenger, to solutions containing millimolar sulfur hexafluoride in unbuffered H_2O decreases the fluoride ion yield at 23 and 300° (Figure 3).

Potassium bromide was added as a hydroxyl radical scavenger at 23 and 300°. The yield of fluoride ions was independent of bromide ion concentration up to 0.1 *M* (Figure 3). In solutions saturated with *n*-hexane, a hydrogen atom and hydroxyl radical scavenger, the yield of fluoride ions remained unaffected at 220 and 300° (Figure 2). Fur-

thermore, addition of up to 0.1 M of methanol had no appreciable effect on the yield (Figure 2).

The above scavenger competition results seem to imply that the observed fluoride ion yields were due exclusively to solvated electron reactions. The lack of effect of hydrogen atom scavengers argues against reaction of hydrogen atoms with sulfur hexafluoride although one cannot rule out the possibility that both hydrogen atoms and the organic radicals produced by (1) react with sulfur hexafluoride at high temperatures to produce fluoride ions.

$$H + RH \longrightarrow H_2 + R \qquad (1)$$

The solubility of nitrous oxide in water is greater than that of sulfur hexafluoride, so studies could be made to higher concentrations with the former. At low concentrations $G(N_2)$ from the nitrous oxide solutions equals $G(F^-)/6$ from the sulfur hexafluoride solutions (Figure 1). The larger scavenging yield in D_2O persists up to high nitrous oxide concentrations, where scavenging occurs in the spurs as well as in the bulk liquid.[7] This seems to imply that the total ionization yield in liquid D_2O is larger than that in liquid H_2O, by somewhat more than 0.5 G units.

The free-ion yield in liquid H_2O is nearly double that in $(CH_3)_2SO$; the values at 23° are 2.7 ± 0.1 and 1.5 ± 0.3,[5] respectively. It is therefore curious that the differences between the free-ion yields in the deuterio and protio compounds should be the same in these very different liquids: $G_{fi}^D - G_{fi}^H = 0.4$–$0.5$ in both water (Table II) and dimethyl sulfoxide.[5] The magnitude of the difference in ammonia at −15° is $G_{fi}^D - G_{fi}^H = 3.6 - 3.3 = 0.3$,[4] similar to that in the other two liquids. It has been suggested that the isotope effect may be due to a wider initial distribution of electrons in spurs.[2a,5] However, the persistence of the difference between the product yields in D_2O and H_2O, up to high temperatures and high scavenger concentrations, seems to imply that there is also an isotope effect on the total ionization yield in an irradiated liquid.

References and Notes

(1) Assisted by the Defence Research Board of Canada.
(2) (a) D. A. Armstrong, E. Collinson, and F. S. Dainton, *Trans. Faraday Soc.*, **55**, 1375 (1959); (b) E. M. Fielden and E. J. Hart, *Radiat. Res.*, **33**, 426 (1968).
(3) K.-D. Asmus and J. H. Fendler, *J. Phys. Chem.*, **73**, 1583 (1969).
(4) W. A. Seddon, J. W. Fletcher, J. Jevcak, and F. C. Sopchyshyn, *Can. J. Chem.*, **51**, 3653 (1973).
(5) T. K. Cooper, D. C. Walker, H. A. Gillis, and N. V. Klassen, *Can. J. Chem.*, **51**, 2195 (1973).
(6) W. P. Jesse and R. L. Platzman, *Nature (London)*, **195**, 790 (1962).
(7) J. C. Russell and G. R. Freeman, *J. Chem. Phys.*, **48**, 90 (1968).
(8) K. N. Jha and G. R. Freeman, *J. Chem. Phys.*, **48**, 5480 (1968).
(9) J.-P. Dodelet, K. Shinsaka, U. Kortsch, and G. R. Freeman, *J. Chem. Phys.*, **59**, 2376 (1973).
(10) W. F. Linke, "Solubilities: Inorganic and Metal-Organic Compounds", Vol. II, 4th ed, American Chemical Society, Washington, D.C., 1965, p 902.
(11) J. C. Russell and G. R. Freeman, *J. Phys. Chem.*, **72**, 808 (1968).
(12) K.-D. Asmus and J. H. Fendler, *J. Phys. Chem.*, **72**, 4285 (1968).

Reaction Products and Stored Energy Released from Irradiated Sodium Chloride by Dissolution and by Heating[1]

G. H. Jenks,*[2] E. Sonder, C. D. Bopp, J. R. Walton

Oak Ridge National Laboratory, Oak Ridge, Tennessee 37830

and S. Lindenbaum

Pharmaceutical Chemistry Department, University of Kansas, Lawrence, Kansas 66045 *(Received September 3, 1974)*

Publication costs assisted by Oak Ridge National Laboratory

As a part of a study of energy stored in irradiated NaCl, we found that heats evolved upon aqueous dissolution of irradiated samples were consistently about 50% lower than the stored energy released during heating of the samples. It seemed likely that these differences could be explained in terms of the reactions that take place during dissolution; therefore, we conducted a combination of measurements to help identify such reactions. Parameters determined included heat release upon thermal bleaching and upon dissolution of irradiated samples, identity and quantity of gases evolved during aqueous dissolution, and concentrations of hypochlorite ion in solutions of irradiated salt. Analyses of our experimental data and of other information indicated that during dissolution a reaction occurs between irradiation-activated NaCl molecules and H_2O, in which the principal solution products are OCl^-, HOCl, and H_2 in addition to Na^+ and Cl^-. The results indicated that the energy per radiation-activated molecule of NaCl is approximately equal to the heat of formation of NaCl from the elements. The results of this work confirm that heat-of-solution as well as drop calorimetry can be used to measure stored energy in irradiated NaCl and, probably, other solids. However, it is essential that the species formed by dissolution of the displaced atoms be known in order to interpret the solution calorimeter data correctly.

I. Introduction

It has been known for some time that the aqueous dissolution of sodium chloride may be affected by previous γ-ray irradiation of the salt. In particular, the escape of H_2 has been observed during dissolution of irradiated salt.[3,4] Also, oxidation of solutes such as I^- and Fe^{2+} and reduction of solutes such as O_2 have been noted when irradiated salt is dissolved in a solution containing such solutes. Normally, when unirradiated NaCl is dissolved in water, the NaCl simply goes into solution, forming Na^+ and Cl^- ions and absorbing about 16 cal/g of salt. Our interest in the identities of dissolution products which are formed after the salt has been irradiated stemmed from a study of stored energy in irradiated salt in which it was found that heats evolved upon aqueous dissolution of irradiated samples were consistently about 50% lower than the stored energy released during heating of the samples. It seemed likely that these differences could be explained in terms of the reactions which take place during dissolution; therefore, we conducted a combination of measurements to identify the reaction and verify this thesis. Parameters determined included heat release upon warming and upon dissolution of irradiated samples, identity and quantity of gases evolved during aqueous dissolution, and concentrations of OCl^- in solutions of irradiated salt.

Previous workers[5] recognized that the formation of dissolution products other than Na^+ and Cl^- would affect values of stored energy obtained by solution calorimetry techniques. They limited their consideration to the species OCl^- and H_2, and were uncertain about the reactions that might lead to these species. In the present work, we studied all the reactions which we thought to be of possible significance involving product species OCl^-, H_2, ClO_3^-, H_2O_2, O_2, H^+, and OH^-, in addition to Na^+ and Cl^-.

II. Experimental Section

The amount of heat released from irradiated salt during thermal bleaching was determined using a heat-flow calorimeter of a type developed by Calvet[6] and Roux.[7] Irradiated samples weighing 50–200 mg, and at about 100°, were dropped into a quartz tube within a furnace which was at a temperature (≥465°) above that at which release of stored energy takes place rapidly. The heat release was deduced from the differences in the temperature–time behavior of this quartz furnace tube when the irradiated and subsequently the annealed samples were dropped into it. This method will be referred to as the drop calorimeter method. A more detailed description of our calorimeter and its use is given elsewhere.[8]

Differences between heats of solution of irradiated and unirradiated salt samples were determined using a heat-of-solution calorimeter which has been described previously.[9] In this method, approximately 200 mg of salt was dissolved in 500 g of distilled water within the calorimeter cell, and temperature changes resulting from the dissolution were measured.

Gas evolution analyses were accomplished with a mass spectrometer which was calibrated for relative peak-height sensitivity to H_2, O_2, and Ne. A solution cell which could be cooled to 77°K was attached to the inlet of the mass spectrometer. In practice, 1.5 ml of distilled water (pH ~5.4) and 10–130 mg of salt were placed in the cell. Before these components were mixed, the cell was cooled and evacuated to remove dissolved gases from the water. Then the water was warmed to melting, a measured volume of Ne gas was allowed to enter the cell, and the salt was dissolved. The dissolution time was approximately 1 hr except in the case of the most heavily irradiated sample, which was crushed prior to dissolution. For that case, the sample dissolved in a

few seconds. The cell was subsequently recooled to 77°K to lower the H_2O vapor pressure; the remaining gases, at a pressure less than 0.2 Torr, were allowed to bleed into the mass spectrometer. Since the vapor pressures of H_2, O_2, and Ne are all above 100 Torr at this temperature, no difficulty was encountered in measuring the relative concentrations of these constituents. However, species such as H_2O, Cl_2, and HCl did not enter the mass spectrometer.

Analyses for hypochlorite ion content in salt solutions were made with a Cary 14 spectrophotometer and a pair of 10-cm quartz sample cells. Irradiated salt samples weighing from about 60 to 500 mg were dissolved in distilled water to prepare solutions, 0.7–1.3 M in NaCl, which simulated those used in the gas evolution measurements. These solutions were then diluted to about 0.05 M NaCl to permit filling the sample cells, and enough NaOH was added to adjust the pH to about 9.0. The OCl^- absorption peak at 290 nm was subsequently recorded, and the concentration of OCl^- was calculated using the reported[10] molar extinction coefficient of 350 for the peak of the 290-nm band.

Salt samples used in this work were Harshaw synthetic crystals. They had been irradiated in a cobalt source at 1.1 $\times 10^7$ rads/hr and at a salt temperature of either 95 ± 5 or 126 ± 3°.

III. Experimental Results

Results of the heat release measurements with the drop and solution calorimeters are plotted in Figure 1. The points obtained by the two methods vary with dose, D, according to a simple exponential expression

$$E = A[1 - \exp(-\beta D)]$$

Both sets of data can be fitted with the same parameter β, as shown by the curves drawn through the points. The factors, A, for the two curves are in the ratio of 1:0.51. In other words, at all doses the stored energy measured by the solution method is approximately 0.51 times as great as the heat measured by drop calorimetry.

Figure 2 shows how the values for gas release and OCl^- ion concentration compare and also how they vary with radiation dose. The numbers of moles of hydrogen gas released and of OCl^- in solution are comparable for most doses. Moreover, except for the three points near a dose of 2.7×10^{10} rads, both the quantity of hydrogen released and the OCl^- concentration increase with dose in a manner similar to the stored energy. In order to display this relationship between hydrogen gas release and OCl^- ion on the one hand and stored energy on the other more clearly, the stored-energy curve of Figure 1 was fitted to the data points of Figure 2 simply by scaling the ordinate (see the right ordinate of Figure 2). This scaling implies that 1 μmol of reaction product corresponds to 5.5×10^{18} eV of stored energy. A more convenient form of this correspondence, which will be used later, can be given as the ratio $E/2AM = 4.6$, where E is the stored energy in eV/g, M is the number of moles of reaction product per gram, and A is Avogadro's number.

Let us now discuss the three results of OCl^- determinations that fall significantly below the curve. The salt temperature for these samples during irradiation was 126° whereas it was 95° for the samples used for the hydrogen evolution experiments and the stored energy measurements shown in Figure 1. It is possible that the deviation may have been related to the higher irradiation temperature, particularly since the OCl^- determination on a sample irradiated heavily at 95° (see diamond-shaped point in Figure 2) indicated a smaller deviation. The inset in Figure 2 shows that for doses above about 2×10^{10} rads the values for energy stored in samples irradiated at 126° seem to scatter and fall significantly below the 95° curve. Thus, for irradiation at 126°, it appears that both the stored energy and the OCl^- concentration increase more slowly with dose at doses above approximately 2×10^{10} rads.

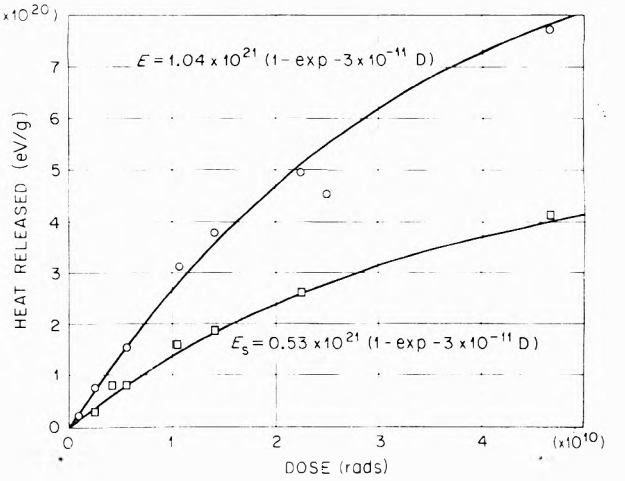

Figure 1. Energy released from NaCl irradiated to various doses at 95°. The circled points were obtained by the drop calorimeter method, the squares by solution calorimetry. The symbol D in the equations for the solid curves refers to the dose in rads.

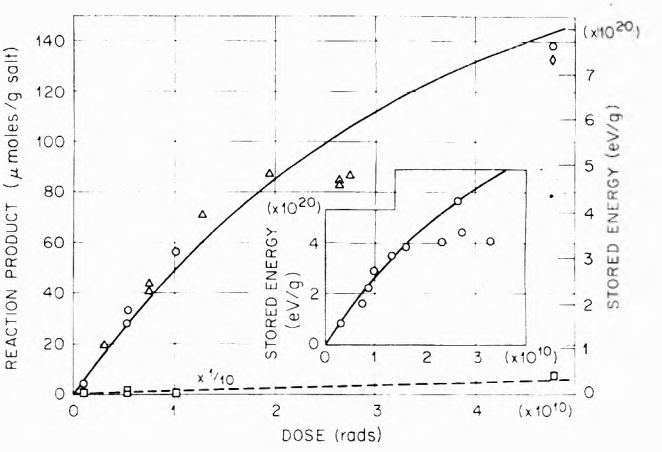

Figure 2. Reaction products of dissolution of irradiated salt. The circles refer to hydrogen gas evolved from samples irradiated to various doses; the squares are drawn to show ten times the amount of oxygen evolved; the triangles and the diamond-shaped point refer to OCl^- ion concentration in solutions. The solid curve has been drawn identically with the upper curve of Figure 1 (right ordinate scale). All gas-evolution samples and the diamond-shaped OCl^- sample were irradiated at 95 ± 5°. The other samples were irradiated at 126 ± 3°. The inset, which gives stored energy data obtained from samples irradiated at 126°, is discussed in the text.

As can be seen from Figures 1 and 2, there is a rather large amount of scatter in the data. It was impractical to try to determine the relative importance of errors in the various measurements that are being compared, particularly since these measurements were performed in a variety of places over a period of more than 1 year. However, a few comments can be made. During irradiation, the temperatures of the samples fluctuated by a few degrees even though heaters and cooling water were used to control temperature. Power interruptions occurred on several occa-

sions, and the samples were removed from the cobalt sources and were allowed to cool to room temperature. Small temperature differences probably also existed between samples that varied with regard to size and position within the γ source. These differences were the result of the different ratios of γ heating to surface heat loss.

Another uncertainty arises from the fact that the various measurements were performed independently of each other. This gave rise to differences in solution conditions, particularly concentrations, during the determinations for heat of solution, hydrogen gas, and OCl^- ions. As stated above, most of the hydrogen gas measurements were made on solutions containing approximately 0.1 g of salt in 1.5 ml of water. For the most part, the same conditions were used for OCl^- ion determinations; however, the solutions had to be diluted to 40 ml to permit filling of the absorption cell. Even greater dilutions occurred during the solution calorimetry measurements, in which approximately 0.2 g of salt was dissolved in 500 ml of water. We made several measurements of OCl^- concentration in samples that had been diluted as in the calorimeter; the results of these indicated less OCl^- than found when the same amount of the sample material was dissolved in smaller amounts of water. Apparently, when irradiated salt was dissolved in large amounts of water the observed OCl^- concentration decreased faster than would be expected simply on the basis of the dilution. Because of this it is possible that, with the low concentrations of irradiated salt used in the solution calorimetry measurements, as much as 30% of the radiation-activated sites may not have produced OCl^- ions but may have dissolved via another reaction.

It was not possible to make a comparable study of hydrogen evolution vs. concentration.

IV. Chemistry and Energetics of Dissolution of Irradiated NaCl

(a) Dissolution Reactions. Irradiation of solid NaCl is known to produce F centers[11] or so-called "colloidal" centers[12] and interstitial chlorine aggregates.[13] The F centers are electrons in negative ion vacancies, i.e., electrons in a volume of the crystal that is sodium rich. Thus, the effects of radiation can be described in terms of a reduction of the Na^+ and an oxidation of the Cl^-, i.e., as a removal of electrons from Cl^- ions and their trapping by the Na^+ species.[14] Table I lists the reactions that oxidized and reduced species can undergo upon dissolution of the irradiated salt in oxygen-free and in aerated water.[15] Reactions 1 and 2 describe two possible reactions of the trapped electron species. Reactions 3–6 describe what the oxidized species (trapped hole) might do. Finally, reaction 0 describes an overall redox reaction that produces only sodium and chloride ions in solution, as occurs with unirradiated salt.

(b) Interpretation of Hydrogen Gas Release and of Results of OCl^- Measurements. When an irradiated NaCl sample is dissolved, one or more of the reactions involving Na^+e^- (reactions 1, 2, or 0) as well as one or more of the reactions involving Cl^-e^+ (reactions 3–6 or 0) occur. The results summarized in Figure 2 show that reaction 1, the only one by which H_2 gas is produced, took place in the gas release experiments and that no significant number of trapped holes underwent reaction 6, by which O_2 is evolved. The results in Figure 2 also show that a number of trapped holes underwent reaction 4 and that this number corresponded to the number of trapped electrons undergoing reaction 1. We thus conclude that the primary dissolution reactions that occur in addition to reaction 0, at least under the conditions prevailing in the gas release and OCl^- experiments, are reactions 1 and 4.

It should be pointed out that different reactions may occur according to the conditions of dissolution. In particu-

TABLE I: Possible Aqueous Dissolution Reactions[15] of Trapped Electrons and Holes[a]

$Na^+e^- + (Cl^-)^+ \longrightarrow Na^+ + Cl^-$	(0)
$Na^+e^- + H_2O \longrightarrow {}^1/_2H_2 + Na^+ + OH^-$	(1)
Reaction 1 might occur via the following partial reactions:	
$Na^+e^- \longrightarrow Na^0$	(1a)
$Na^0 \xrightarrow{H_2O} e_{aq}^- + Na^+$	(1b)
or	
$Na^+e^- \xrightarrow{H_2O} e_{aq}^- + Na^+$	(1c)
$2e_{aq}^- + 2H_2O \longrightarrow H_2 + 2OH^-$	(1d)
$Na^+e^- + {}^1/_2O_2 + H^+ \longrightarrow {}^1/_2H_2O_2 + Na^+$	(2)
Reaction 2 might occur via some partial reactions given above and the following:	
$e_{aq}^- + O_2 \longrightarrow O_2^-$	(2a)
$HO_2 \rightleftharpoons H^+ + O_2^- \quad (K_{2b} = 1.3 \times 10^{-5})$	(2b)
$O_2^- + HO_2 \longrightarrow O_2 + HO_2^-(HO_2^- + H^+ \rightleftharpoons H_2O_2)$	(2c)
$(Cl^-)^+ + H_2O \longrightarrow H^+ + Cl^- + {}^1/_2H_2O_2$	(3)
Reaction 3 might occur via the following partial reactions:	
$(Cl^-)^+ + H_2O \longrightarrow H_2O^+ + Cl^-$	(3a)[b]
$H_2O^+ + H_2O \longrightarrow OH + H_3O^+$	(3b)
$OH + OH \longrightarrow H_2O_2$	(3c)
$(Cl^-)^+ + {}^1/_2H_2O \longrightarrow {}^1/_2Cl^- + {}^1/_2H^+ + {}^1/_2HOCl$	(4)
$HOCl \rightleftharpoons H^+ + OCl^- \quad (K = 3 \times 10^{-8})$	
Reaction 4 might occur via the following partial reactions:	
$(Cl^-)^+ \longrightarrow Cl^0$	(4a)
$Cl^0 + Cl^0 \longrightarrow Cl_2$	(4b)
$Cl_2 + H_2O \longrightarrow Cl^- + H^+ + HOCl$	(4c)
$(Cl^-)^+ + {}^1/_2H_2O \longrightarrow H^+ + (5/6)Cl^- + (1/6)ClO_3^-$	(5)
Reaction 5 might occur via some partial reactions given above and the following:	
$Cl^0 + HOCl \longrightarrow H^+ + Cl^- + ClO^0$	(5a)[c]
$ClO^0 + ClO^0 \longrightarrow Cl_2O_2$	(5b)[d]
$Cl_2O_2 + H_2O \longrightarrow ClO^- + ClO_2^- + 2H^+$	(5c)[d]
$Cl_2O_2 + ClO_2 \longrightarrow ClO_3^- + Cl_2O(\xrightarrow{H_2O} 2ClO^- + 2H^+)$	(5d)[d]
$(Cl^-)^+ + {}^1/_2H_2O \longrightarrow H^+ + Cl^- + {}^1/_4O_2$	(6)
Reaction 6 might occur via some partial reactions given above and the following:	
$ClO^0 + HOCl \longrightarrow H^+ + Cl^0 + Cl^- + O_2$	(6a)[c]

[a] Cl^0 and Cl^- interact rapidly to form Cl_2 (ref 16). Accordingly, when Cl^0 is written in this table, it may also represent Cl_2 (with reactions appropriately altered). [b] Reference 4. [c] Reference 17. [d] Reference 18.

lar, as pointed out earlier, the salt concentrations in the solution calorimetry experiments were lower than in the reaction product determinations. Moreover, many of the solution calorimetry experiments were performed with normal laboratory distilled water, which may have contained some dissolved oxygen. In contrast, gas evolution experiments were performed with water that had been frozen and pumped, while OCl^- ion determinations were performed with water that had been boiled. Thus, the possibility of contributions from reactions other than 0, 1, and 4 in the solution calorimeter may not be ruled out.

(c) Analysis of Reaction Energies. Let us first consider the energy, E, measured in the drop calorimeter. We will assume that E represents the energy released upon re-formation of crystalline NaCl from radiation-activated molecules. If N is the total number of activated molecules per gram of NaCl, then E/N represents the stored energy per activated molecule. It can be shown that E is related to heats of aqueous dissolution by

$$E = N(\Delta H_0 - \Delta H_s) \quad (1)$$

where ΔH_0 is the heat of reaction in eV per molecule of radiation-activated species going from the postirradiation solid state ($Na^+e^- + Cl^-e^+$) to $Na^+ + Cl^-$ *in solution*, and ΔH_s is the heat of solution of unirradiated NaCl. The energy, E_s, measured by solution calorimetry can similarly be written in terms of heats of reaction. The measured heat upon dissolution of an unirradiated sample is $N_0\Delta H_s$, where N_0 is the number of NaCl molecules per gram. For an irradiated sample, if n_{ij} molecules per gram react according to reactions i,j (i = 1 or 2 and j = 3, 4, 5, or 6; see Table I), and n_0 molecules react to form Na^+ and Cl^- in solution (reaction 0), the measured heat upon dissolution, E_m, is

$$E_m = \sum n_{ij}\Delta H_{ij} + n_0\Delta H_0 + (N_0 - n_{ij} - n_0)\Delta H_s \quad (2)$$

The stored energy as measured by solution calorimetry, E_s, is the difference between E_m and the heat of solution of an unirradiated sample, $N_0\Delta H_s$, so that

$$E_s = \sum_{ij}(n_{ij}(\Delta H_{ij} - \Delta H_s) + n_0(\Delta H_0 - \Delta H_s)) \quad (3)$$

Since all radiation-activated species dissolve via reactions ij or 0, $N = \sum n_{ij} + n_0$ and the terms in ΔH_s cancel in the expression for the difference between E and E_s:

$$E - E_s = N\Delta H_0 - \sum_{ij} n_{ij}\Delta H_{ij} - n_0\Delta H_0 = \sum n_{ij}(\Delta H_0 - \overline{\Delta H_{ij}}) \quad (4)$$

where

$$\overline{\Delta H_{ij}} = \sum(n_{ij}\Delta H_{ij})/\sum n_{ij}$$

This equation can be rewritten in the form

$$(E/\sum n_{ij})(1 - E_s/E) = \Delta H_0 - \overline{\Delta H_{ij}} \quad (5)$$

It should be noted that only those radiation-activated molecules ($\sum n_{ij}$) that dissolve to produce end products other than Na^+ and Cl^- in solution enter in eq 5. For ease of discussion, let us define the ratios F_c, F_g, and F_o, respectively, for the solution calorimeter, gas release cell, and optical cell, as follows:

$$F = n_0/(n_0 + \sum n_{ij})$$

In words, F is the fraction of radiation-activated molecules that dissolves to produce only Na^+ and Cl^- under the conditions of the particular-type experiment. If we assume for the moment that $F_c = F_g$ (or F_o), then it is possible to replace $\sum n_{ij}$ in eq 5 by $2AM$, i.e., by twice the number of hydrogen molecules (or OCl^- ions) measured by the gas release (or OCl^- solution) experiment. This permits a comparison to be made between experimentally determined ratios (left side of eq 5) and calculated values of heats of solution (right side of eq 5). The experimentally determined ratios have been given earlier as $E_s/E = 0.51$ and $E/2AM = 4.6$ eV/reaction so that $(E/2AM)(1 - E_s/E) = 2.2$. Quantities for $\Delta H_0 - \Delta H_{ij}$ can be calculated for each of the specific reactions, ij, using literature values[19] for heats of formation of the chemical species involved. Since these calculations are for *differences* of heats of solution, the values do not depend on knowledge of the chemical nature or energy states of the radiation defects within the salt. Table II lists the results of such calculations and indicates how these values were obtained.

Comparison of the values given in Table II with the 2.2 eV/reaction obtained from the experimental results (and the assumption that the dissolution reactions were the same in the calorimeter and reaction-product experiments) leads us to believe that reactions 1,3 and 1,4 are favored over the others. A 20% composite error in the three measurements (drop calorimetry, solution calorimetry, and reaction products) would bring the 2.2 eV/reaction down to the 1.78–1.95 range.[20] Such an error is, in our judgment, very likely.

We have considered the effect of allowing F_c and F_g (or F_o) to differ. For that case, $\sum n_{ij}$ would be replaced by $2MA(1 - F_c)/(1 - F_o)$. The left side of eq 5 would then be decreased if $F_o > F_c$. The OCl^- measurements performed on dilute solutions suggested that, for the dilute conditions of the solution calorimeter, it was possible that the OCl^- concentrations per gram of irradiated salt were less than for the more concentrated solutions. If some of the trapped holes that produce OCl^- in more concentrated solutions dissolve in the solution calorimeter via reaction 0, then $F_c > F_o$, which would increase (not decrease) the left side of eq 5, thereby making agreement with any of the considered reactions unlikely. Thus, we conclude that the fraction of irradiation-activated molecules dissolving via reaction 0 is not greater in the solution calorimeter than in the gas release and OCl^- experiments, and, if there is a change of reaction type as suggested by the OCl^- vs. salt concentration measurements, then it is a replacement of reaction 1,4 by a different reaction of comparable thermal effects as the solution becomes more dilute. The values of $\Delta H_0 - \Delta H_{ij}$ in Table II indicate that reaction 1,3 or 1,5 could be the replacement reaction. We did not confirm the occurrence of either of these reactions since it was not feasible for us to make the analyses for H_2O_2 and/or ClO_3^- in the ClO^- solutions, which would be required for confirmation.

(d) Energy Stored per Activated Molecules. These experiments do not yield a direct value for the parameter E/N since the n_0 radiation-activated molecules that dissolve via reaction 0 do not contribute to the difference $E - E_s$. However, it is possible to estimate upper and lower limits. The trapped electrons undergo either reaction 1 or 0 during the gas release experiments. Their total number, N, may be greater than that for reaction 1 (releasing H_2) by the factor $1/(1 - F_g)$. From the expression

$$E/N = E(1 - F_g)/2MA \quad (6)$$

it is then clearly seen that E/N can be no larger than $E/2MA$. The latter has been given earlier as 4.6 eV per one-half hydrogen molecule. Approximately the same value re-

TABLE II: Calculated Values of the Difference between the Heats of Reaction 0 and Other Possible Reactions Given in Table I[a]

Parameter	Relationship between heats of formation[b]	Value, eV/reaction
$\Delta H_0 - \Delta H_{1,3}$	$f^0H_2O - 0.5f^0H_2O_2 - 0.5f^0H_2$	−1.95
$\Delta H_0 - \Delta H_{1,4}$	$0.5f^0Cl^- + \left[1 - \frac{T}{a} - \frac{T'}{a} - \frac{0.5K}{K + (H^+)}\right]f^0H_2O + \frac{T}{a}f^0H^+ + \frac{T'}{a}f^0CO_2 - 0.5f^0H_2 - \left[\frac{0.5K}{K + (H^+)}\right]f^0OCl^- - \left[\frac{0.5(H^+)}{K + (H^+)}\right]f^0HOCl - \frac{T'}{a}f^0HCO_3^- - \left[0.5 - \frac{0.5K}{K + (H^+)} - \frac{T}{a} - \frac{T'}{a}\right]f^0OH^-$[c]	−1.76 to −1.81[d]
$\Delta H_0 - \Delta H_{1,5}$	$0.5f^0H_2O + 0.167f^0Cl^- - 0.5f^0H_2 - 0.167f^0ClO_3^-$	−1.58
$\Delta H_0 - \Delta H_{2,3}$	$f^0H_2O + 0.5f^0O_2 - f^0H_2O_2$	−1.04
$\Delta H_0 - \Delta H_{2,4}$	$\Delta H_0 - \Delta H_{1,4} + 0.5f^0O_2 + 0.5f^0H_2 - 0.5f^0H_2O_2$[c]	−0.85 to −0.90[d]
$\Delta H_0 - \Delta H_{2,5}$	$0.5f^0H_2O + 0.5f^0O_2 + 0.167f^0Cl^- - 0.5f^0H_2O_2 - 0.167f^0ClO_3^-$	−0.67

[a] The second column of the table indicates how the various heats of formation enter in the calculations. [b] The symbol f^0H_2O represents the heat of formation of liquid water. The other symbols, f^0Cl^-, etc., represent the dilute-solution heat of formation of the chemical species. [c] K is the acid ionization constant of HOCl, a is the number (mole/liter) of electron–hole pairs introduced into solution and undergoing reaction 1,4 (or reaction 2,4). T is the initial concentration of hydrogen ions in the solvent water, T' is the amount (mole/liter) of initially undissociated CO_2 which reacts with OH^- produced in reaction 1,4 (or reaction 2,4), and (H^+) is the final hydrogen ion concentration, which is calculated from the relationship $K_w/a(H^+) = 0.5 - [0.5K/(K + (H^+))] - [T/a] - [T'/a]$. [d] These values were calculated for a equal to 1.2×10^{-5} to 11.33×10^{-5} M; for T equal to 10^{-6} M; and for T' equal to either 0 or 2.3×10^{-6} M. The pH of the distilled water used in the calorimeter was about 6.

sults from use of the OCl^- data, indicating that 4.5 eV is the maximum energy per radiation-activated molecule of NaCl.

A minimum value can be estimated by extrapolating the data in Figure 1 to obtain a saturation energy storage near 1×10^{21} eV/g. It is generally assumed that the maximum concentration of radiation defects that can be formed is 5–10% of the total number of lattice sites.[21] This gives a minimum of 1–2 eV/molecule.

The energy of formation of NaCl from sodium metal and chlorine gas is 4.3 eV/molecule. This value falls into the range just discussed and is consistent with the hypothesis that the radiation defects in our salt samples are Na colloids and Cl_2 and/or Cl_2^- aggregates. It is also consistent with results from other work on irradiated alkali halides.[12,13] Furthermore, the close agreement between the value 4.3 and the upper limit, 4.6, suggests that the factor $1 - F_g$ in eq 6 is near 1, indicating that most or all of the radiation-activated molecules dissolve via reaction 1,4 (or to some extent, 1,3 or 1,5) and that very few dissolve via reaction 0.

V. Conclusions

Analyses of our experimental results and of other available information showed that the observed differences between the amount of heat evolved upon heating and upon dissolving irradiated NaCl resulted from a reaction between irradiation-activated NaCl molecules and H_2O in which the principal products were OCl^-, HOCl, and H_2 in addition to Na^+ and Cl^- (reaction 1,4, Table I). Contributions of a number of other reactions in the very dilute calorimeter solutions cannot be ruled out, but they appear to total less than about 30%. Additionally, the results indicated that the stored energy per radiation-activated molecule of NaCl is approximately equal to the heat of formation of NaCl from the elements.

References and Notes

(1) Research sponsored by the U.S. Atomic Energy Commission under contract with the Union Carbide Corporation.
(2) Author to whom correspondence should be addressed.
(3) W. G. Burns and T. F. Williams, *Nature (London)*, **175**, 1043 (1955).
(4) C. Gopinathan, P. S. Damle, and E. J. Hart, *J. Phys. Chem.*, **76**, 3694 (1972).
(5) T. Phelps, Jr., and E. Pearlstein, *Phys. Rev.*, **128**, 1575 (1962).
(6) E. Calvet, *C. R. Acad. Sci.*, **22**, 1702 (1948).
(7) A. Roux, Thesis, Faculte des Sciences, University of Lyons, 1969.
(8) A. L. Boch et al., USAEC Report No. ORNL-4824, Oak Ridge National Laboratory, pp 201–208, Dec 1972.
(9) S. Lindenbaum and G. E. Boyd, *J. Phys. Chem.*, **69**, 2374 (1965).
(10) J. Carrol Morris, *J. Phys. Chem.*, **70**, 3798 (1966).
(11) E. Sonder and W. A. Sibley, "Point Defects in Solids", J. H. Crawford and L. F. Slifkin, Ed., Plenum Press, New York, N.Y., 1972.
(12) L. Przibram and J. E. Caffyn, "Irradiation Colours and Luminescence", Pergamon Press, London, 1956, pp 148–152; S. V. Pappu and K. A. McCarthy, *J. Phys. Chem. Solids*, **32**, 1287 (1971).
(13) L. W. Hobbs, A. E. Hughes, and D. Pooley, *Proc. Roy. Soc., Ser. A*, **332**, 167 (1973).
(14) The exact nature of the energy storage sites is not known. We will describe them herein in a general way as trapped electrons (Na^+e^-) and trapped holes [$(Cl^-)^+$] or irradiation-activated molecules (M). N = number of Na^+e^- = number of $(Cl^-)^+$.
(15) Reactions not otherwise referenced are discussed by G. H. Jenks, Oak Ridge National Laboratory, Technical Memo, ORNL-TM-3717, March 1972.
(16) G. G. Jayson and B. J. Parsons, *J. Chem. Soc., Faraday Trans. 1*, **69**, 1597 (1973).
(17) K. W. Young and A. J. Allmand, *Can. J. Res.*, **27B**, 318 (1949).
(18) G. V. Buxton and M. S. Subhani, *J. Chem. Soc., Faraday Trans. 1*, **68**, 947 (1972).
(19) D. D. Wagman, W. H. Evans, V. B. Parker, I. Halow, S. M. Bailey, and R. H. Schumm, *Natl. Bur. Stand., Tech. Note* **No. 270-3** (Jan 1968).
(20) Since E enters twice in eq 5, a systematic error as small as +10% in the value of E would lower the 2.2 to 1.8.
(21) G. H. Kinchin and R. S. Pease, *Rep. Prog. Phys.*, **18**, 1–51 (1955).

An Electron Impact Investigation of 1,1,2,2-Tetrafluorocyclobutane

A. R. Ravishankara and Robert J. Hanrahan*

Department of Chemistry, University of Florida, Gainesville, Florida 32611

(Received May 30, 1974; Revised Manuscript Received December 26, 1974)

Publication costs assisted by the U. S. Atomic Energy Commission

An investigation has been made of the fragmentation of 1,1,2,2-tetrafluorocyclobutane under electron bombardment in a Bendix time-of-flight mass spectrometer. Using the Fox retarding potential difference technique, measurements were made of the appearance potentials of major ionic fragments including $C_2H_2F_2^+$ (12.15 V), $C_2F_4^+$ (12.60 V), $C_2H_4^+$ (13.15 V), and $C_3H_4F^+$ (12.85 V). From these results it is found that $\Delta H_f°$ for the $C_3H_4F^+$ ion is $\leq +207$ kcal/mol and $\Delta H_f°$ for parent c-$C_4H_4F_4$ is ≥ -202 kcal/mol with good agreement between three independent routes of calculation. For the c-$C_4H_4F_3^+$ ion an approximate appearance potential of 13.5 V is found; a reasonable interpretation of this result requires that the conjugate product is F^- rather than the neutral atom. A rather detailed argument suggests that the symmetrical rupture of the molecule into $C_2H_2F_2^+$ plus $C_2H_2F_2$ is a sequential process with the sum of the energy of breaking two nonequivalent C–C bonds (between two CF_2 and two CH_2 groups) equal to 126 kcal/mol, while the nonsymmetrical rupture into $C_2H_4^+$ and C_2F_4 is concerted, and the energy of breaking each of two equivalent C–C bonds between CF_2 and CH_2 groups is 61 kcal/mol.

Introduction

It has been proposed that the 1,1,2,2-tetrafluorocyclobutane ion (subsequently referred to as c-$C_4H_4F_4$)

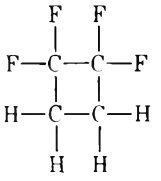

constitutes the transition complex in ion–molecule reactions of $C_2H_2F_2^+$ with $C_2H_2F_2$ and $C_2F_4^+/C_2H_4^+$ with C_2H_4/C_2F_4.[1,2] It was postulated that the complex is very short lived and during its existence maintains its cyclic structure. Accordingly, a study of the fragmentation of this compound under electron impact is an obvious experiment to shed light on whether the predictions of the model are right and the assumptions plausible.

In the present work, the appearance potentials of $C_2F_4^+$, $C_2H_4^+$, $C_2H_2F_2^+$, and $C_3H_4F^+$ from c-$C_4H_4F_4$ were measured. From this data we can calculate some of the bond dissociation energies in this compound and estimate some others. The experiments were done on a time-of-flight mass spectrometer using standard retarding potential difference (RPD) techniques.[3,4]

Experimental Section

The mass spectral cracking pattern of c-$C_4H_4F_4$ was obtained on the Bendix time-of-flight mass spectrometer at 70 eV. The RPD experiments were also done on the Bendix, as described by Melton and Hamill[4] with some minor changes. Potentials on the five-grid electron gun were as follows: No. 1 grid (electron control grid, nearest to the filament), −6 V with a +12 V pulse of 3 μsec duration repeated at a frequency of 10 kHz; No. 2 grid, +0.01 V; No. 3 grid (Fox retarding potential difference grid), −1.000 V with an intermittent ΔV of −0.200 V; No. 4 grid, +0.01 V; and No. 5 grid was grounded to the ion source structure (and therefore to the frame of the instrument). Potentials on grids 1–4 are referenced to the electron filament, and hence their absolute value relative to ground varies along with the filament. The choice of −1.000 V for the Fox grid and −0.200 as ΔV was made after preliminary optimization experiments, to obtain the best compromise of ion current I and its variation ΔI in response to ΔV applied to the RPD grid. The purpose of the RPD procedure is to measure an amount of ion current ΔI attributable to electrons in a narrow voltage range ΔV taken as a "slice" out of the much broader thermal electron energy distribution from the filament.

The ion focus pulse was triggered 0.7 μsec after the control grid pulse; we found this measure essential to obtaining reliable results. (It is possible to use the "time-lag-focusing" control for this purpose, on Bendix instruments so equipped.) The potential on the electron collecting trap was reduced to +8 V to minimize extraneous additional ionization of the experimental compound in the target region. Several minor modifications to the control electronics of the Bendix were made as recommended by Melton and Hamill.[4]

The ion current signal from the electrometer circuit in the "scanner" unit was fed to a potentiometric chart recorder through a potential divider. The compound under study was contained in a 5-l. vessel and was leaked into the ionization chamber through a gold leak. The pressures in the ionization chamber could be changed by changing the pressure in the 5-l. vessel. The usual operating pressure in the ionization chamber was 6–8 × 10^{-6} Torr. The normal trap current was 5 μA and the change in trap current was less than 5%. (The trap current was not regulated.)

The electron beam accelerating potential, which was applied to the filament, was generated by standard circuitry in the Bendix and monitored on the 40-V scale of a Digitec Model Z-204-B digital volt meter (resolution 0.005 V, accuracy 0.01 V). However, due to contact potentials, surface charges, etc., it can not be assumed that the effective accelerating potential of the electron gun is identical with that measured externally. Accordingly an RPD curve was measured for Ar^+ ion from argon gas and the apparent appear-

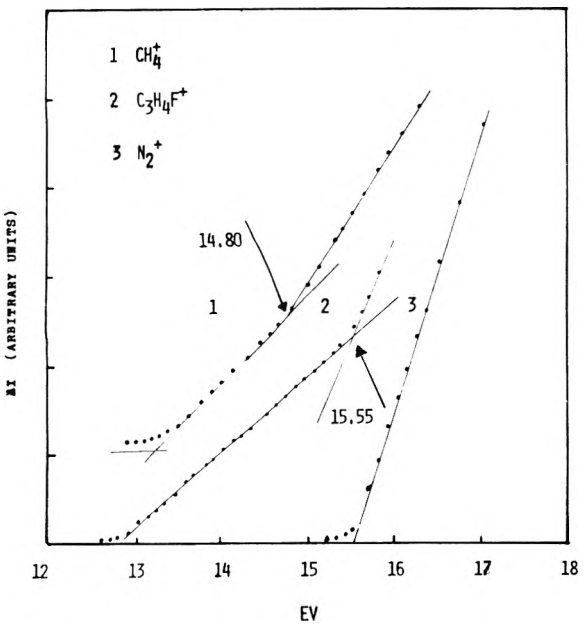

Figure 1. RPD curves for CH_4^+ from CH_4, N_2^+ from N_2, and $C_3H_4F^+$ from c-$C_4H_4F_4$, measured on a Bendix TOF mass spectrometer.

ance potential of Ar^+ (corresponding to the first break) was determined from a graph made against the experimental voltage scale. The difference between the measured value and the accepted literature value gave the necessary correction for the displacement of the voltage scale. Using the scale calibrated as described, cross checks were done by measuring the appearance potentials of $C_2F_4^+$ (from C_2F_4) and N_2^+ (from N_2). Our measured values agreed with the literature to within 0.1 V, indicating that our voltage scale is linear at least within the approximately 6-V range tested. In later experiments $C_2F_4^+$ and N_2^+ were used as secondary calibration standards.

We could reproduce exactly the shapes of ionization efficiency curves for CH_4^+ from CH_4 and $C_2H_6^+$, $C_2H_4^+$, and $C_2H_5^+$ from C_2H_6, which were reported by Melton and Hamill;[4] all reported "break points" agreed within a 0.1-V range. (The CH_4^+ curve is shown in Figure 1.) Although we always had a moderate air background, N_2^+ (28) does not interfere with $C_2H_4^+$ (28) as the appearance potential of N_2^+ is 15.6 V and N_2^+ has zero intensity below about 15.1 V (well above the region of interest for $C_2H_4^+$). In the spectrum of c-$C_4H_4F_4$, the appearance potential of CH_2^+ could not be carried out because of the interference by the CH_2^+ in the background and that of CF_2^+ and $C_3H_3F_2^+$ could not be done because of very low intensities.

The 1,1,2,2-tetrafluorocyclobutane was obtained from Columbia Organic Chemicals Co. It was dried and deaerated on a vacuum line through several freeze–pump–thaw cycles at liquid nitrogen and Dry Ice temperatures, and vacuum distilled into a glass bulb for transfer to the mass spectrometer.

Results and Calculations

The retarding potential difference curves which we obtained for $C_3H_4F^+$, $C_2H_2F_2^+$, $C_2F_4^+$, and $C_2H_4^+$ from c-$C_4H_4F_4$ are shown in Figures 1 and 2 along with N_2^+ as a standard and CH_4^+ for comparison with the work of Hamill and Melton.[4] The mass spectral fragmentation pattern which we obtained for c-$C_4H_4F_4$ is shown in Table I. In Table II we present the appearance potential values which were found for the several major product ions from c-$C_4H_4F_4$, along with values for certain other pertinent species from the literature.

TABLE I: Mass Spectral Cracking Pattern of c-$C_4H_4F_4$ at 70 V

Mass	Intensity	Assignment	Mass	Intensity	Assignment
14	18	CH_2	57	7	C_3H_2F
16	7	CH_4	59	16	C_3H_4F
26	9	C_2H_2	64	100	$C_2H_2F_2$
27	11	C_2H_3	69	5	CF_3 or C_4H_2F
28	23	C_2H_4	75	4	C_3HF_2
31	13	CF	77	9	$C_3H_3F_2$
32	37	CHF	89	16	$C_4H_3F_2$
39	9	C_3H_3	100	23	C_2F_4
40	30	C_3H_4	109	9	$C_4H_4F_3$
44	12	C_2HF	113	3	C_3HF_4
45	18	C_2H_2F	127	2	$C_4H_3F_4$
50	6	CF_2	128	3	$C_4H_4F_4$
51	16	CHF_2			

TABLE II: Appearance Potential Data

Ion	Reactant	Product	AP,V
$C_2F_4^+$	c-$C_4H_4F_4$	$C_2F_4^+ + C_2H_4$	12.60[a]
$C_2H_4^+$	c-$C_4H_4F_4$	$C_2H_4^+ + C_2F_4$	13.15[a]
$C_2H_2F_2^+$	c-$C_4H_4F_4$	$C_2H_2F_2^+ + C_2H_2F_2$	12.15[a]
$C_3H_4F^+$	c-$C_4H_4F_4$	$C_3H_4F^+ + CF_3$	12.85[a]
$C_2H_4^+$	C_2H_6	$C_2H_4^+ + H + H$	16.3[b]
$C_2H_4^+$	C_2H_4		10.48[c]
$C_2H_2F_2^+$	H_3C-CF_3	$C_2H_2F_2^+ + HF$	10.30[c]

[a] This work. [b] Reference 4. [c] Reference 6.

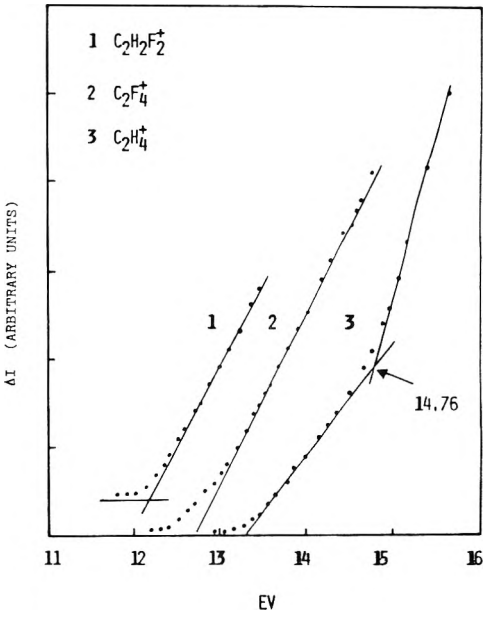

Figure 2. RPD curves for $C_2H_2F_2^+$, $C_2F_4^+$, and $C_2H_4^+$ from c-$C_4H_4F_4$, measured on a Bendix TOF mass spectrometer.

From the appearance potential values given in Table II, along with the standard enthalpy of formation for several species from the literature[5-7] (given in Table III), it is possible to calculate heats of formation of the ion $C_3H_4F^+$ and the neutral parent molecule c-$C_4H_4F_4$, as well as values for the energy of dissociation of C–C bonds in the C_4 ring. The heat of formation of the parent molecule can be formulated

TABLE III: Thermochemical Data

Ion or radical	$\Delta H_f°_{298}$, kcal/mol	Ref
$C_2F_4^+$	78	6
C_2H_4	12.49	6
$C_2H_4^+$	253	6
C_2F_4	−155.5	6
$C_2H_2F_2^+$	159	6
$C_2H_2F_2$	−78.6	6
CF_3	−112.6	7

in three different ways. First, using our measurements of the appearance potential of $C_2F_4^+$ we obtain:

$$c\text{-}C_4H_4F_4 \rightarrow C_2F_4^+ + C_2H_4 + e^- \quad (1a)$$

$$A(C_2F_4^+) \geq \Delta H_f°(C_2F_4^+) + \Delta H_f°(C_2H_4) - \Delta H_f°(c\text{-}C_4H_4F_4) \quad (1b)$$

Therefore

$$\Delta H_f°(c\text{-}C_4H_4F_4) \geq \Delta H_f°(C_2F_4^+) + \Delta H_f°(C_2H_4) - A(C_2F_4^+) \quad (1c)$$

$$\Delta H_f°(c\text{-}C_4H_4F_4) \geq 78 \text{ kcal/mol} + 12.49 \text{ kcal/mol} - 12.60 \text{ eV} \quad (1d)$$

$$\Delta H_f°(c\text{-}C_4H_4F_4) \geq -200 \text{ kcal/mol} \quad (1e)$$

Next, based on the appearance potential of $C_2H_4^+$, we can calculate:

$$c\text{-}C_4H_4F_4 \longrightarrow C_2H_4^+ + C_2F_4 + e^- \quad (2a)$$

$$A(C_2H_4^+) \geq \Delta H_f°(C_2H_4^+) + \Delta H_f°(C_2F_4) - \Delta H_f°(c\text{-}C_4H_4F_4) \quad (2b)$$

Therefore

$$\Delta H_f°(c\text{-}C_4H_4F_4) \geq \Delta H_f°(C_2H_4^+) + \Delta H_f°(C_2F_4) - A(C_2H_4^+) \quad (2c)$$

$$\Delta H_f°(c\text{-}C_4H_4F_4) \geq 253 \text{ kcal/mol} + (-155.5 \text{ kcal/mol}) - 13.1 \text{ eV} \quad (2d)$$

$$\Delta H_f°(c\text{-}C_4H_4F_4) \geq -206 \text{ kcal/mol} \quad (2e)$$

Finally, the measured appearance potential of $C_2H_2F_2^+$ gives

$$c\text{-}C_4H_4F_4 \longrightarrow C_2H_2F_2^+ + C_2H_2F_2 + e^- \quad (3a)$$

$$A(C_2H_2F_2^+) \geq \Delta H_f°(C_2H_2F_2^+) + \Delta H_f°(C_2H_2F_2) - \Delta H_f°(c\text{-}C_4H_4F_4) \quad (3b)$$

Therefore

$$\Delta H_f°(c\text{-}C_4H_4F_4) \geq \Delta H_f°(C_2H_2F_2^+) + \Delta H_f°(C_2H_2F_2) - A(C_2H_2F_2^+) \quad (3c)$$

$$\Delta H_f°(c\text{-}C_4H_4F_4) \geq 159 \text{ kcal/mol} + (-79 \text{ kcal/mol}) - 12.15 \text{ eV} \quad (3d)$$

$$\Delta H_f°(c\text{-}C_4H_4F_4) \geq -200 \text{ kcal/mol} \quad (3e)$$

Accordingly, the average value for $\Delta H_f°$ (c-$C_4H_4F_4$) is ≥ -202 kcal/mol. The satisfactory agreement between the three calculations is gratifying because the calculations constitute a rather severe test of the consistency of the published thermochemical data as well as our appearance potential measurements.

Using our value of −202 kcal/mol for the heat of formation of c-$C_4H_4F_4$ and the appearance potential of $C_3H_4F^+$, we can calculate a value for the heat of formation of this ion as follows:

$$c\text{-}C_4H_4F_4 \longrightarrow C_3H_4F^+ + CF_3^\cdot + e^- \quad (4a)$$

$$A(C_3H_4F^+) \geq \Delta H_f°(C_3H_4F^+) + \Delta H_f°(CF_3^\cdot) - \Delta H_f°(c\text{-}C_4H_4F_4) \quad (4b)$$

Therefore

$$\Delta H_f°(C_3H_4F^+) \leq A(C_3H_4F^+) - \Delta H_f°(CF_3^\cdot) + \Delta H_f°(c\text{-}C_4H_4F_4) \quad (4c)$$

$$\Delta H_f°(C_3H_4F^+) \leq 12.85 \text{ eV} - (-112.6 \text{ kcal/mol}) + (-202 \text{ kcal/mol}) \quad (4d)$$

$$\Delta H_f°(C_3H_4F^+) \leq +207 \text{ kcal/mol} \quad (4e)$$

In order to consider the energy of breaking C–C bonds in the c-$C_4H_4F_4$ ring, it is necessary to define our notation. First, we let $D_{F/F}$, $D_{H/H}$, and $D_{H/F}$ be the bond dissociation energy of the bonds shown below (Note that $D_{A/B}$ represents a C–C dissociation energy of a bond where A and B are substituents on the carbon atoms.):

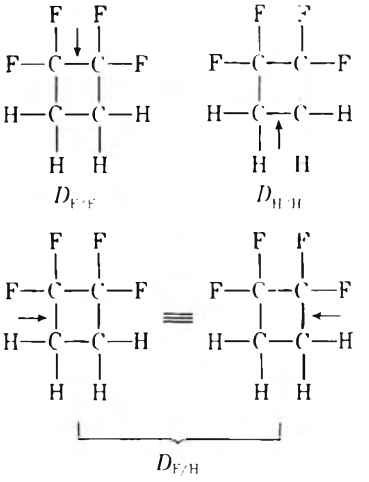

We also let $\Delta H_{(=H/H)}$ and $\Delta H_{(=H/F)}$ represent the energies for the *reverse* of the following processes:

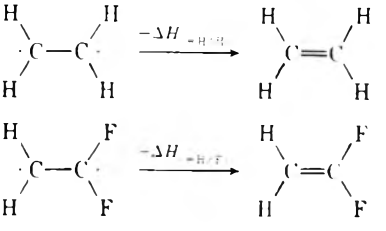

(5)

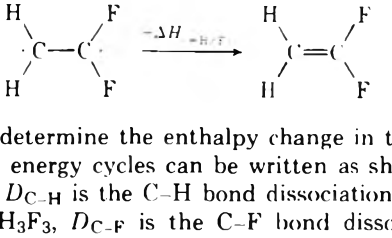

(6)

In order to determine the enthalpy change in these reactions, useful energy cycles can be written as shown in eq 7–12, where D_{C-H} is the C–H bond dissociation energy in C_2H_6 or $C_2H_3F_3$, D_{C-F} is the C–F bond dissociation in CH_3CF_3, and D_{H-F} is the H–F bond dissociation energy (equal to the bond energy in this case). We will use $I(C_2H_4^+/C_2H_4)$ to indicate the ionization potential (or appearance potential) of $C_2H_4^+$ from C_2H_4, and similarly for other

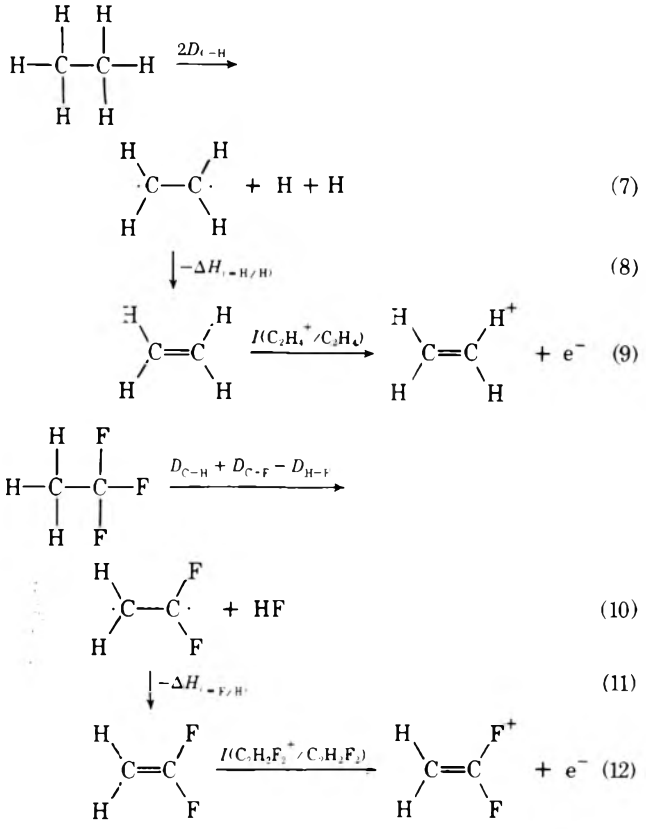

daughter ion–parent molecule pairs which are mentioned subsequently. Then we have:

$$A(C_2H_4^+/C_2H_6) = 2D_{C-H} - \Delta H_{(=H/H)} + I(C_2H_4^+/C_2H_4) \quad (13)$$

$$A(C_2H_2F_2^+/C_2H_3F_3) = D_{C-H} + D_{C-F} - D_{H-F} - \Delta H_{(=F/H)} + I(C_2H_2F_2^+/C_2H_2F_2) \quad (14)$$

Therefore, application of the energy cycle 7–9 to reaction 5 gives

$$\Delta H_{(=H/H)} = 2D_{C-H} + I(C_2H_4^+/C_2H_4) - A(C_2H_4^+/C_2H_6) \quad (15)$$

$$\Delta H_{(=H/H)} = 2(4.16) + 10.48 - 16.3 = 2.5 \text{ eV} \quad (16)$$

A similar calculation for reaction 6 using the energy cycle 10–12 gives:

$$\Delta H_{(=H/H)} = D_{C-H} + D_{C-F} - D_{H-F} + I(C_2H_2F_2^+/C_2H_2F_2) - A(C_2H_2F_2^+/C_2H_3F_3) \quad (17)$$

$$= (4.16 + 4.6 - 5.82 + 10.12 - 11.2) = 1.8 \text{ eV} \quad (18)$$

It would be of interest to calculate the quantity $\Delta H_{(=F/F)}$ for formation of tetrafluoroethylene from the corresponding diradical, but the necessary data are not accessable; $C_2F_4^+$ has zero abundance from C_2F_6 and C_2F_5H.[8]

We next consider the energetics of the unsymmetrical splitting of c-$C_4H_4F_4$ into $C_2H_4^+$ and C_2F_4:

$$c\text{-}C_4H_4F_4 \longrightarrow C_2H_4^+ + C_2F_4 + e^- \quad (19)$$

It is possible to make two reasonable, limiting assumptions about the energetics of this process (and the similar symmetrical split into $C_2H_2F_2^+$ and $C_2H_2F_2$): either the reorganization of the neutral fragment into a double-bonded species occurs before the split from the ion, or else it occurs afterwards. If the latter is the case, then the corresponding reorganization energy is not available to decrease the energy of formation of the observed ionic fragment:

$$A(C_2H_4^+/c\text{-}C_4H_4F_4) = 2D_{F/H} - \Delta H_{(=H-H)} + I(C_2H_4^+/C_2H_4) \quad (20)$$

This assumption leads to the following evaluation of $D_{F/H}$, the energy per bond to break the $CF_2\cdots CH_2$ carbon–carbon bonds in the c-$C_4H_4F_4$ ring:

$$2D_{F/H} = \Delta H_{(=H-H)} - I(C_2H_4^+/C_2H_4) + A(C_2H_4^+/c\text{-}C_4H_4F_4) \quad (21)$$

$$2D_{F/H} = 2.5 \text{ eV} - 10.48 \text{ eV} + 13.25 \text{ eV} \quad (22)$$

and

$$D_{F/H} = 2.64 \text{ eV} = 61 \text{ kcal/mol} \quad (23)$$

The magnitude of the resulting bond dissociation energy appears reasonable; the significance of this result will be considered further in the Discussion section.

In the case of the symmetrical dissociation process, the alternative limiting assumption appears to give reasonable results:

$$c\text{-}C_4H_4F_4 \longrightarrow C_2H_2F_2^+ + C_2H_2F_2 \quad (24)$$

Assuming that all of the reorganization energy is available to drive the process, we obtain:

$$A(C_2H_2F_2^+/c\text{-}C_4H_4F_4) = D_{F/F} + D_{H/H} - 2\Delta H_{(=F/H)} + I(C_2H_2F_2^+/C_2H_2F_2) \quad (25)$$

which rearranges to give

$$D_{F/F} + D_{H/H} = A(C_2H_2F_2^+/c\text{-}C_4H_4F_4) + 2\Delta H_{(=F/H)} - I(C_2H_2F_2^+/C_2H_2F_2) \quad (26)$$

$$D_{F/F} + D_{H-H} = 12.05 \text{ eV} + 2(1.86 \text{ eV}) - 10.30 \text{ eV} \quad (27)$$

$$D_{F/F} + D_{H-H} = 5.47 \text{ eV} = 126 \text{ kcal/mol} \quad (28)$$

Accordingly the average of these two bond dissociation energies is the reasonable value of 63 kcal/mol. This result will also be considered in the Discussion.

In order to carry out a calculation for the third dissociation process, into $C_2F_4^+$ and C_2H_4, we would need the energy of a tetrafluoroethylene diradical rearranging to tetrafluoroethylene. As noted above, we were not able to calculate this quantity.

Discussion

The overall mass spectral fragmentation pattern of c-$C_4H_4F_4$ is consistent with what might be expected for a saturated, cyclic C_4 compound.[9] Most compounds of this type give a small parent peak along with considerable fragmentation into lower molecular weight ions. Furthermore, Jennings[1] has postulated that the cyclic $C_4H_4F_4^+$ ion, formed as an intermediate complex in several ion–molecule reactions, has a very short lifetime. It appears reasonable to suggest that the structure of the c-$C_4H_4F_4^+$ system reached upon electron bombardment of the stable molecule is the same one formed in the ion–molecule reactions, although there could be differences in internal energies (especially vibrational energy). We note that c-$C_4H_4F_4$ shows a small

abundance of the parent ion, c-$C_4H_4F_4^+$; this is consistent with the fact that Jennings also saw a small amount of c-$C_4H_4F_4^+$ at high pressures (presumably, involving some collisional stabilization in the ion–molecule experiments).

As can be seen from the cracking pattern of c-$C_4H_4F_4$, there is no peak corresponding to $C_2H_3F^+$ or $C_2HF_3^+$. This fact lends some credibility to the assumption made by Jennings that the transition complex formed in the systems $[1,1\text{-}CF_2CH_2]^+$ on 1,1-$C_2H_2F_2$, $C_2H_4^+$ on C_2F_4, and $C_2F_4^+$ on C_2H_4 maintains a stable structure and does not scramble F and H atoms during its brief existence. We note a number of species which must involve some rearrangement, however, such as CHF^+. It is our suggestion that most (and perhaps all) such rearrangment occurs in connection with ring opening, which produces unsaturated carbon centers.

We calculate the heat of formation of c-$C_4H_4F_3^+$ to be about 190 kcal/mol by Franklin's group contribution method.[10] This value, when combined with our value for ΔH_f° of c-$C_4H_4F_4$, gives 14.4 V for the appearance potential of $C_4H_4F_3^+$ if we assume concurrent elimination of F^-, and a value of 18.0 V if we assume F atom elimination. We find an approximate appearance potential of c-$C_4H_4F_3^+$ of 13.5 ± 1 V. Although our data were not of high quality, due to the low abundance of the ion, its appearance potential is certainly not higher than 15.0 V. Accordingly we conclude that c-$C_4H_4F_3^+$ is formed by F^- elimination.

The two modes of splitting the cyclobutane ring into an ethylenic ion and an ethylenic molecule (reactions 19 and 24) clearly must proceed by two different mechanisms. For the unsymmetrical break (reaction 19) we utilized in the calculation only the reorganization energy of $\cdot CH_2CH_2\cdot$ into C_2H_4, and obtained 61 kcal/mol each for breaking two $CF_2\cdot\cdot\cdot CH_2$ bonds. If we had also utilized the reorganization energy of $\cdot CF_2CF_2\cdot$ into $CF_2{=}CF_2$ the resulting bond dissociation energies would increase by at least 15–20 kcal each, which would surely be too high for the badly strained c-$C_4H_4F_4$ molecule.

On the other hand, we utilized the reorganization energy for two $\cdot CF_2CH_2\cdot$ fragments into $CF_2{=}CH_2$, in order to interpret the data for the symmetric split. We obtained 126 kcal for $D_{F/F}$ plus $D_{H/H}$, or an average of 63 kcal/mol for dissociation of $CF_2\cdot\cdot\cdot CF_2$ and $CH_2\cdot\cdot\cdot CH_2$, which is of a reasonable magnitude. (If we apportion the two energies similar to the known dissociation energies of $CF_3\cdot\cdot\cdot CF_3$ and $CH_3\cdot\cdot\cdot CH_3$, the resulting values are 57 and 69 kcal/mol, respectively.) Use of only one reorganization energy term would give an impossibly low value of 46.5 kcal/mol for the average of $D_{F/F}$ and $D_{H/H}$. In fact, the postulate that anything much less than 100% of the two reorganization energy terms is available to drive reaction 24 would lead to an unrealistically low result.

Our specific suggestion for the mechanistic difference in reactions 19 and 24 (which forms the foundation of the different energetics) is that the former is a one-step dissociation giving $C_2H_4^+$ and an energy-rich $\cdot CF_2CF_2\cdot$ species (which later forms $CF_2{=}CF_2$ without aiding in the progress of the original dissociation) while reaction 24 is sequential, proceeding through an open-chain intermediate. Consistent with the conclusions reached by Jennings et al., as well as our own observations, the open-chain species formed in reaction 24a would have to be short lived (10^{-6} sec or less). Atom migration in the open-chain intermediate could explain occurrence of several additional species in the cracking pattern of c-$C_4H_4F_4$, in particular CF_3^+ and $C_3H_4F^+$. A similar ring opening of $C_4H_4F_3^+$ followed by a split into

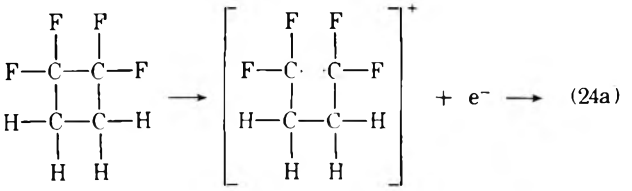

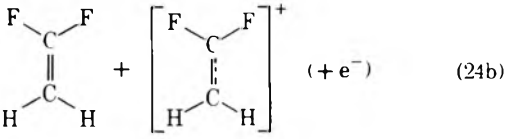

one-carbon and three-carbon fragments would explain the occurrence of CFH^+ (37%) and $C_3H_3F_2^+$ (9%). Several other similar decomposition sequences can be suggested.

The more favorable reaction path and energetics leading to $C_2H_2F_2^+$ compared to $C_2H_4^+$ (and probably also $C_2F_4^+$) are very likely related to the relative abundances of 100, 23, and 23% for these three species. Although the intensity of $C_2H_2F_2^+$ should equal the sum of the intensities of $C_2F_4^+$ and $C_2H_4^+$ due to statistical considerations, it is in fact even higher by a factor of 2.

Our appearance potential value (12.85 V) for the $C_3H_4F^+$ ion gives a value of 207 kcal/mol for ΔH_f° of this species, which is closer to a previously reported experimental value of 210 kcal/mol than to a theoretically estimated value of 175 kcal/mol.[11] The calculated ΔH_f° is apparently for a linear species; we suggest that the $C_3H_4F^+$ species formed in this work may have a cyclopropane structure. (Other C_3 species formed might also be cyclic.)

The utility of the electron impact method for determining thermodynamic quantities rests on the implicit assumption that the relevant but unmeasured corrections for excess energy in ionic and molecular fragments are small.[4-6,12] This situation is recognized by inequality signs in eq 1–4. In several instances (see eq 15, 17, 21, and 26) two ionization or appearance potential terms enter with opposite sign, so that partial cancellation of excess energy effects can be expected. (In these cases no inequality is indicated since its sign is not unambiguous.) An assumption of little or no excess energy is supported by Stevenson's law[13] in the case of $C_2F_4^+$ and $C_2H_4^+$, since the appearance potential of $C_2F_4^+$ is 0.55 V less than that of $C_2H_4^+$. This argument is not applicable in the case of $C_2H_2F_2^+$, but the good agreement of ΔH_f° (c-$C_4H_4F_4$) from eq 1–3 suggests that any excess energy correction needed for $A(C_2H_2F_2^+)$ must be small in the latter case as well; our results suggest that ΔH_f° (c-$C_4H_4F_4$) = −202 kcal/mol with little or no correction required for excess energy.

Although the RPD curves for $C_3H_4F^-$ and $C_2H_4^+$ both show well-defined breaks at higher energies (respectively 2.70 and 1.61 V above the appearance potentials) we have not attempted to interpret the electronic states or processes involved. However, Hamill and coworkers have had considerable success in understanding data of this type.[14]

Acknowledgment. This work was supported by the University of Florida Nuclear Science Program and by the Atomic Energy Commission under Contract No. AT-(40-1)-3106. These results were presented in Paper No. 308, Division of Physical Chemistry, 26th Southeastern Regional Meeting of the American Chemical Society, Norfolk, Va., Oct 23–25, 1974. This is Document No. ORO-3106-49.

References and Notes

(1) R. M. O'Malley, K. R. Jennings, M. T. Bowers, and V. G. Anicich, *Int. J. Mass Spectrom. Ion Phys.*, **11**, 89 (1973).
(2) A. J. Ferrer-Correia and K. R. Jennings, *Int. J. Mass Spectrom. Ion Phys.*, **11**, 111 (1973).
(3) R. E. Fox, W. M. Hickam, D. J. Grove, and T. Kjeldass, Jr., *Rev. Sci. Instrum.*, **26**, 1101 (1955).
(4) (a) C. E. Melton, Ph.D. Thesis, University of Notre Dame, 1964; (b) C. E. Melton and W. H. Hamill, *J. Chem. Phys.*, **41**, 546 (1964).
(5) T. L. Cottrell, "The Strength of Chemical Bonds", 2nd ed, Academic Press, New York, N.Y., 1958.
(6) J. L. Franklin, J. G. Dillard, H. M. Rosenstock, J. T. Herron, K. Draxl, and F. H. Field, *Nat. Stand. Ref. Data Ser., Nat. Bur. Stand.*, **No. 26** (1969).
(7) J. Heicklen, *Adv. Photochem.*, **7**, 57 (1969).
(8) The fragmentation pattern of C_2HF_5 is not listed in the API tables. We have examined the mass spectrum of this compound and found that there is no fragment at *m/e* 100.
(9) J. R. Majer, *Adv. Fluorine Chem.*, **2**, 55 (1961).
(10) J. L. Franklin, *Ind. Eng. Chem.*, **41**, 1070 (1949); *J. Chem. Phys.*, **21**, 2029 (1953).
(11) Both the experimental value of 210 kcal/mol and the theoretical value of 175 kcal/mol are given by Jennings and coworkers, ref 1. V. G. Anicich and M. T. Bowers have transmitted to us a preprint of an article currently in press, in which they argue that ΔH_f° ($C_3H_4F^+$) $\leq$ 185 kcal/mol based upon the assumption that the observed ion–molecule reaction $C_2H_4^+ + C_2H_3F \rightarrow C_3H_4F^+ + CH_3\cdot$ must be exothermic. Using ΔH_f° (C_2H_3F) = −32.5 kcal/mol and ΔH_f° ($CH_3\cdot$) = +33.0 kcal/mol as given by Jennings (ref 1) and ΔH_f° ($C_2H_4^+$) = 253 kcal/mol given in the NSRDS tables (ref 6), we obtain 187.5 kcal/mol in essential agreement with Bowers. This result clearly depends on the accuracy of the thermodynamic input data, as well as the validity of Bowers' assumption.
(12) F. W. McLafferty, "Mass Spectrometry of Organic Ions", Academic Press, New York, N.Y., 1963, p 145–156.
(13) R. W. Kiser, "Introduction to Mass Spectrometry and its Applications", Prentice-Hall, New York, N.Y., 1965.
(14) S. Tsuda and W. H. Hamill, *J. Chem. Phys.*, **41**, 2713 (1964).

Some Dielectric and Spectroscopic Studies of Molecular Interaction of Some 2,6-Dihalo-Substituted Phenols with Tertiary Amines

J. Kraft, S. Walker,*

Lakehead University, Ontario, Canada

and M. D. Magee

South Devon Technical College, England

(Received October 17, 1974)

Publication costs assisted by Lakehead University

Dielectric constants and losses of 2,4,6-trichlorophenol and 2,4,6-tribromophenol have been determined at four microwave frequencies and in a variety of solvents and solvent mixtures at 25°. In addition, dielectric measurements have been made on a 0.35 *M* solution of 2,4,6-trichlorophenol in *p*-xylene containing different concentrations of the strong electron-donor molecule, 1,4-diazabicyclo[2.2.2]octane (DBO). Infrared spectra of the symmetrical trihalophenols of the various systems in the hydroxyl stretching region are also reported. Both 1:1 and 2:1 complexes of symmetrical trichlorophenol with DBO appear to be formed, and the mean relaxation time and distribution parameter of the solutions increase enormously relative to their values in cyclohexane. If DBO is added to a 0.35 *M* solution of 2,4,6-trichlorophenol in *p*-xylene, then when the concentration of DBO equals that of the 2,4,6-trichlorophenol the measured moment has increased by 2.4 D. Conductance and electronic spectra have been obtained for some 2,6-dihalophenols–*tert*-amine systems with a view to studying any ionic forms produced. When the solvent has a low dielectric constant the equilibrium would seem to be largely over to the nonionic form. In alcoholic solution, where the dielectric constant is high, if the phenolic O–H is sufficiently protonic, then the presence of the ionic form may be readily inferred from both the conductance and electronic spectra data.

Introduction

While it has been known for some time[1] that weak intramolecular hydrogen bonds in 2-substituted phenols can rupture even in moderately strong electron-donor solvents, rupture of the hydrogen bond in 2-substituted nitrophenols has been demonstrated[2] only in the most powerful electron donors. Microwave measurements of dielectric constants and loss factors, for example, show that 1,4-diazabicyclo[2.2.2]octane (DBO) is a base sufficiently strong to complex with 2-nitrophenols, and easily ruptured the intramolecular hydrogen bond in 2-chlorophenol molecules, causing the hydroxyl group to swing into the trans position.[3] In 2,6-disubstituted halophenols the hydroxyl group is hydrogen bonded in both resonance stabilized positions. What in this case is the result of adding a powerful base to the solution? In both planar configurations, an intramolecular hydrogen bond exists but this is weaker than a bond with the DBO. To examine the nature of the hydrogen bond in such systems we have made a number of dielectric studies and have extended the investigation and obtained infrared and electronic spectra and conductivity data for a number of 2,6-dihalophenol–*tert*-amine mixtures in a variety of solvents.

Experimental Section

The apparatus and procedure for determining the dielectric constant and loss factor have been described previous-

TABLE I: Relaxation Times (in psec), Distribution Parameter, and Dipole Moments (in Debye Units) for Some Solutions of Symmetrical Trihalophenols in Various Solvents at 298°K[a]

Solute	Solvents	Concn	α	τ_0	μ
2,4,6-Trichlorophenol	C_6H_{12}	0.0414	0.02	17	1.0_0
2,4,6-Trichlorophenol	*p*-Xylene	0.0364	0.06	23	1.4_1
2,4,6-Trichlorophenol	1,4-Dioxan–*p*-xylene (1:4)	0.0285	0.12	39	1.7_8
2,4,6-Trichlorophenol	1,4-Dioxan	0.0296	0.26	40	2.0_0
2,4,6-Tribromophenol	*p*-Xylene	0.0074	0.13	34	1.7_8
2,4,6-Tribromophenol	1,4-Dioxan	0.0209	0.29	29	2.1_5

[a] Concentrations are in mole fractions.

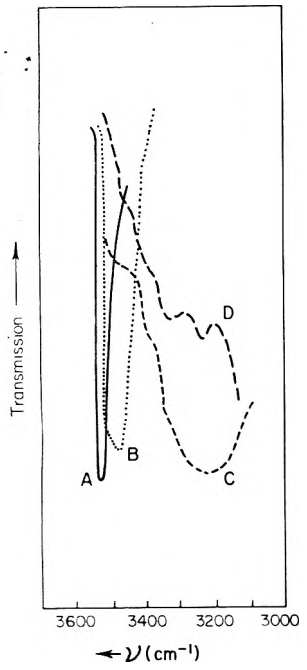

Figure 1. Infrared spectra of 2,4,6-trichlorophenol in (A) carbon tetrachloride, (B) *p*-xylene, (C) 1,4-dioxan, and (D) *p*-xylene + DBO.

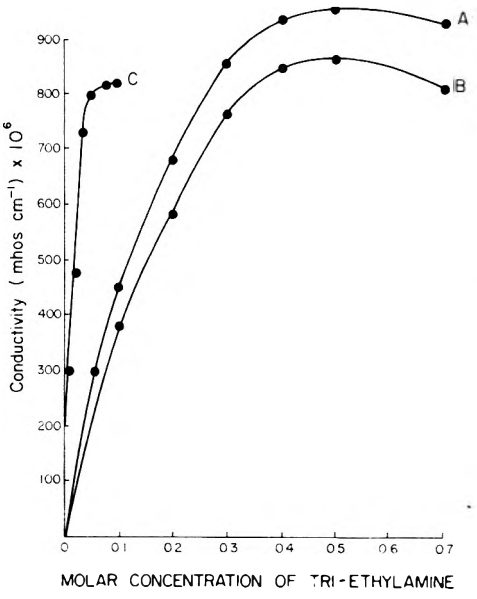

Figure 2. Plot of conductivity against concentration of triethylamine added to the following systems: (A) trichlorophenol (0.35 *M*) + ethyl alcohol, (B) tribromophenol (0.35 *M*) + ethyl alcohol, (C) 2,6-dichloro-4-nitrophenol (0.05 *M*) + ethyl alcohol.

ly.[4] Sources of error[5] and the validity of the method of analysis[6] have been considered elsewhere.

Conductivity values greater than 10^{-8} mhos cm^{-1} were measured using a conductivity measuring apparatus of the magic eye type. The cell had 1-cm^2 platinized electrodes on glass supports and a 10-mil Teflon body. The cell constant was determined using a standard potassium chloride solution.

For measurements in the range 10^{-8} to 10^{-} 15 mhos cm^{-1} a Balsbaugh three-terminal cell was used to eliminate errors due to erratic cell insulator conductivity and stray capacitance. Calibration of the cell constant was derived from the measured cell capacitance. The three-terminal cell was used in conjunction with a General Radio Type 1615-A bridge.

Purification and drying of the solvents have been described previously.[7] The solutes were recrystallized from the solvent in which measurements were to be made and stored in stoppered bottles in dry cupboards.

Results

The relaxation data are presented in Table I and some of the conductivity data are given in Figure 2 and the infrared and electronic spectra are presented in Figures 1 and 3.

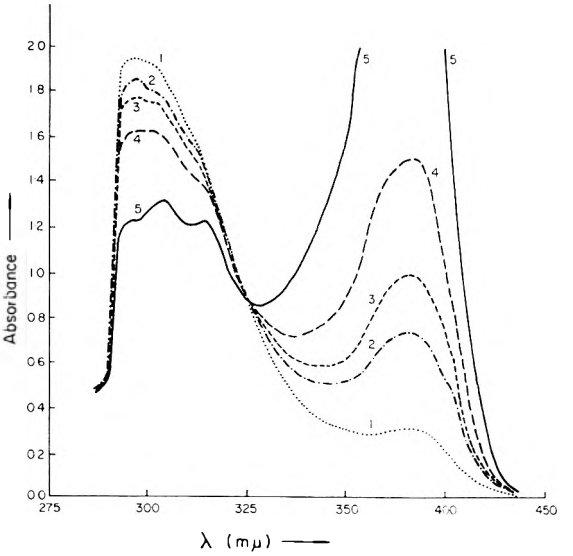

Figure 3. The uv spectra of the mixture of 2,6-dichloro-4-nitrophenol–*p*-xylene–triethylamine where the concentration of triethylamine increases from 1 to 2 to 3 etc.

Discussion

In 1,4-dioxan both 2,4,6-trichlorophenol and 2,4,6-tribromophenol show a large increase in distribution parameter

TABLE II: Relaxation Time (psec), Distribution Parameter, and Apparent Dipole Moments for a 0.3544 *M* Solution of 2,4,6-Trichlorophenol in *p*-Xylene with Varying Amounts of Added DBO at 298°K

DBO concn, *M*	τ_0	α	ϵ_∞	μ, D
0.000	23	0.06	2.28_5	1.4_1
0.018	38	0.28	2.28_9	1.7_0
0.047	86	0.34	2.30_4	2.1_0
0.065	91	0.38	2.31_4	2.2_8
0.090	141	0.37	2.31_9	2.5_0
0.357	152	0.36	2.38_8	3.8_4
0.714	146	0.39	2.40_5	4.1_3

compared with *p*-xylene and cyclohexane solutions, and for 2,4,6-trichlorophenol the mean relaxation time is much lengthened; both these observations are indications of interactions with the solvent.[14] The dipole moments also increased. Eric, Goode, and Ibbitsen[8] found that the dipole moment of 2,4,6-trichlorophenol was greater in 1,4-dioxan than in cyclohexane by 0.45 D and the moment of 2,4,6-tribromophenol was greater by 0.43 D. This is an increase of about 30% and such large values of $\Delta\mu$ are strong evidence of a hydrogen bonding interaction.

It is known that big increases in τ_0, α, and μ in 1,4-dioxan as opposed to the values in the inert solvent cyclohexane are indicative of a donor–acceptor interaction, and thus if the interaction of the 2,4,6-halophenols with the solvent leads to strong complex formation, then pronounced increases may be expected in these parameters.[3] A preliminary measurement on a fairly concentrated equimolar solution of 2,4,6-trichlorophenol gave a dipole moment of about 3.8 D, which is almost a fourfold increase relative to that in cyclohexane, a mean relaxation time of $>150 \times 10^{-12}$ sec (a tenfold increase relative to cyclohexane), and a distribution parameter of 0.40 (a twentyfold increase relative to cyclohexane). Strong complex formation seemed to be indicated. Further investigations were carried out in which the initial 2,4,6-trichlorophenol concentration was kept constant while the DBO concentration was varied. The resultant relaxation parameters are summarized in Table II. Both the mean relaxation time and distribution coefficient increase sharply even when very small quantities of DBO are added to the 2,4,6-trichlorophenol solution. At high concentrations of DBO, i.e., greater than that of the phenol, the relaxation times and distribution coefficients appear to level off, and this was the behavior to be expected if a strong complex was formed, since once all the 2,4,6-trichlorophenol was bonded to the DBO, further DBO additions should lead to little variation of such parameters. An interesting feature of the data is the shape of the curves at low DBO concentrations, the rate of increase of the parameter being lower than at intermediate concentrations. This could be attributed to the formation of a complex of relatively low dipole moment but long relaxation time at low DBO concentrations. DBO has two proton acceptor sites and can bond to two 2,4,6-trichlorophenol molecules. Such a complex might he expected to have a small dipole moment yet a very long relaxation time. Thus, the predominant formation of 2:1 2,4,6-trichlorophenol–DBO complex when 2,4,6-trichlorophenol is in a large excess could explain the form of the data. At intermediate and high concentrations, of course, the 1:1 complex would be present in greater concentration. Assuming that most, if not all, of the 2,4,6-trichlorophenol is complexed when DBO is in excess, the measured moment is a lower limit for the 1:1 complex since (i) the 2:1 complex would reduce its value and (ii) some of the phenol may be left uncomplexed. Such a high increment of the moment of ~2.7 D is much greater than that normally experienced for phenols hydrogen bonding with e.g., 1,4-dioxan (which lead to values of ~0.2 to 0.7 D) and suggests that the interaction may involve an equilibrium of the type

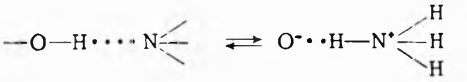

where an appreciable concentration of the ionic species on the right-hand side of the equation would lead to a high moment. Such an equilibrium was invoked by Jadzyn and Malecki[11] to explain the increased polarity of 2.7 D of the hydrogen bond of 2,4,6-trichlorophenol in a mixture of triethylamine and cyclohexane. When the cyclohexane was replaced by toluene, the polarity of the hydrogen bond increased to 5.1 D.[11] Thus, from dipole moment evidence alone it seemed likely for the system 2,4,6-trichlorophenol + triethylamine + *p*-xylene that an ionic form could best account for the increased polarity of the hydrogen bond and the large increments in moment we observed for the 2,4,6-trichlorophenol + DBO + *p*-xylene system with increasing DBO concentrations since the basicity of triethylamine and DBO should be similar.

In order to study the matter further we extended the investigation to include some measurements of conductivity and electronic spectra since both seemed capable of detecting ionic species; this would be feasible for the former method only provided some of the hydrogen bonded ion pairs dissociated and were in equilibrium with their ions. In addition, infrared spectra were also examined since this offered a means of detecting the species –O–H · · · N and of following the presence of nonintermolecularly hydrogen bonded O–H groups. Preliminary work indicated this was less readily feasible from the uv spectrum because of possible overlap of the parent phenol bands with that of the intermolecular hydrogen bonded phenol of the type O–H · · · N.

Infrared Spectra

Both 2,4,6-trichloro- and 2,4,6-tribromophenol show shifts of the hydroxyl stretching frequency relative to unassociated phenol[12] which has a value of 3611 cm^{-1}. In carbon tetrachloride 2,4,6-trichlorophenol has a single sharp absorption at 3542 cm^{-1}, while 2,4,6-tribromophenol has a single sharp band at 3526 cm^{-1}. Baker and Kaeding[13] found 3535 cm^{-1} for the hydroxyl group hydrogen bonded to the ortho chlorine substituent in 2,4-dichloro-6-bromophenol in carbon tetrachloride. In 2,4,6-tribromophenol a value of the hydroxyl stretching frequency in the fundamental region of 3515 cm^{-1} has been reported.[14] In *p*-xylene both phenols exhibit a doublet in the hydroxyl stretching region, bands occurring at 3534 and 3498 cm^{-1} for symmetrical trichlorophenol, and 3514 and 3498 cm^{-1} (shoulder) for tribromophenol. Doubling of the hydroxyl frequency has been noted for phenols in aromatic solvents by Mecke[15] and attributed to association isomerism, i.e., orientation of the solvent with its π electrons near the hydroxyl group or with its C–H groups near the hydroxyl group (in other words this amounts to "face" or "edge on" association between hydroxyl and the solvent). Since the solvent

has a different polarizibility in the two directions,[16] the interaction energy is different. These measurements, however, show that one frequency is common to both solutes, that at 3498 cm^{-1}, while the other is similar to the values for the single peak obtained for each substance in carbon tetrachloride. This suggests that for weakly bonded phenols the band at 3534 or 3514 cm^{-1} is due to intramolecularly hydrogen bonded hydroxyl.

In 1,4-dioxan a much greater change is observed (see Figure 1). The unsolvated hydroxyl peak occurs only as a weak band at 3500 cm^{-1} on the side of a broad band centred at about 3230 cm^{-1} for 2,4,6-trichlorophenol solutions. This compares with the hydroxyl stretching frequency of phenol in 1,4-dioxan of 3315 cm^{-1} and of *p*-nitrophenol in 1,4-dioxan of 3205 cm^{-1}.[17] For 2,4,6-tribromophenol the broad band is at 3250 cm^{-1}. The slightly lesser shift compared with 2,4,6-trichlorophenol may reflect the difference in mesomeric and inductive effects in the two cases or slight steric hindrance due to the greater volume of the bromine atoms compared with chlorine. The influence of added DBO on the infrared spectrum of 2,4,6-trichlorophenol is striking. To a solution of 0.35 *M* 2,4,6-trichlorophenol was added 0.18 *M* DBO, i.e., just over half the molarity of the phenol. If a 1:1 complex were formed then two hydroxyl stretching frequencies would be expected, one due to the complex and the other due to the excess uncomplexed phenol. In fact, there was only a trace of an uncomplexed band at about 3490 cm^{-1}, and a band appeared which was so broad as to overlap with solvent C–H bands and seemed to show some detailed structure.[18] At these low DBO concentrations it would seem that a strong 2:1 complex is formed with the trihalophenol and the DBO.

Conductivity Studies

Some of the conductivity data are given in Figure 2. When 2,4,6-trichloro- and 2,4,6-tribromophenol are dissolved in the nonpolar solvents carbon tetrachloride or *p*-xylene of static dielectric constant ~2.2 the conductivity is very small (of the order of the solvent (i.e., $\sim 10^{-12}$ mhos cm^{-1})). On addition of triethylamine to these solutions the conductivity increases but is still small and of the order of 10^{-7} mhos cm^{-1}. However, if the solvent for the 2,4,6-trichlorophenol–triethylamine mixture is changed to that of ethyl alcohol, the conductivity increases to $\sim 10^{-3}$ mhos cm^{-1} (the conductivity of the ethyl alcohol + triethylamine has been subtracted). The rise of conductivity with increasing concentration of phenols (with halogen substituents in the 2 and 6 position) + triethylamine + ethyl alcohol may be seen in Figure 2. In all three cases the curves are of a similar form, and the conductivity almost begins to level off when the phenol and the triethylamine are in a 1:1 ratio. For solubility reasons the concentration of the 2,6-dichloro-4-nitrophenol had an upper limit of ~0.05, and it follows from Figure 2 that the conductivity of the solutions of the 2,6-dichloro-4-nitrophenol may well be about 7 times greater than that of the two halophenols.

Estimates of the conductivity of 2,4,6-trichloro- and 2,4,6-tribromophenol in alcoholic solutions at 0.06 *M* concentration of triethylamine give a value of $\sim 2 \times 10^{-4}$ mhos cm^{-1}. It is striking how similar in value this is to that of salt sodium salicyclate in ethyl alcohol which has a conductivity of 4×10^{-4} mhos cm^{-1}. This, of course, is a salt, and although it would be totally ionized, may well have a large number of ion pairs which do not contribute to the conductivity. Potassium nitrophenolate (0.06 *M*) + *p*-nitrophenol + ethyl alcohol has a similar conductivity being 7×10^{-4} mhos cm^{-1}. Altogether from the conductivity data there would seem to be little doubt that both the trihalophenols and the 2,6-dichloro-4-nitrophenol form triethylamine salts in alcoholic solution where the ions contribute appreciably to the conductivity; this does not, of course, exclude the possibility of ion pairs which make no such contribution. In the solvents of low dielectric constant, though, the ionic contributions in the 2,4,6-trihalophenol–triethylamine + solvent systems would seem relatively low.

Uv and Visible Spectra

Previous work[19] has shown that in aprotic solvents with relatively high static dielectric constants (e.g., 1,2-dichloroethane $\epsilon_0 \sim 10$), *p*-nitrophenol can give rise to the following types of equilibria with triethylamine:

(A) simple hydrogen bonded complex

$$ArOH + NR_3 \rightleftharpoons ArOH \cdots NR_3 \quad (1)$$

(B) an ion-pair formation

$$ArOH \cdots NR_3 \rightleftharpoons ArO^- \cdots HN^+R_3 \quad (2)$$

in which there is an equilibrium involving an intermolecular proton shift.[19]

Type B equilibrium is characterized by the appearance of a new band in the visible region. Since the H in the OH of 2,4,6-trichlorophenol would appear to be more acidic than *p*-nitrophenol (their pK_a's being 6.0 and 7.15, respectively) it seemed possible that even in solvents of lower dielectric constant than 1,2-dichloroethane ion-pair formation might be feasible. Such ion-pair formation could account for the rapidly increasing apparent dipole moment of the 2,4,6-trichlorophenol with increasing DBO concentration.

A number of electronic spectra was determined in the uv and visible regions. The main features which emerged were as follows. (1) 2,4,6-Trichlorophenol in various solvents plus triethylamine gave three bands near 290, 296, and 320 mμ. The solvents were toluene, chloroform, *trans*-dichloroethylene, chlorobenzene, and trichloroethylene. In addition, 2,4,6-trichlorophenol + $CHCl_3$ + DBO and 2,4,6-triiodophenol + CCl_4 + $CHCl_3$ + DBO gave bands near 290, 300, and 325 mμ. (2) Mixtures of (a) 2,4,6-trichlorophenol + *p*-xylene + triethylamine, (b) 2,4,6-trichlorophenol + *p*-xylene + DBO, and (c) 2,4,6-trichlorophenol + 1,1,1-trichloroethane + triethylamine gave bands near 295 and 320 mμ. For the 2,4,6-trihalophenols the band at ~320 mμ which appears only in the presence of the tertiary amine may be ascribed to the presence of the normal hydrogen bond (i.e., type A). The band at 320 mμ increases in intensity with increasing triethylamine concentration while that of 2,4,6-trichlorophenol correspondingly decreases. When triethylamine is replaced by DBO the spectrum remains essentially the same. For the 2,4,6-trichlorophenol + triethylamine + solvent case when the solvent dielectric constant is varied from 2.2 to 7.2 no new band is observed. In addition this also proved to be the case when the solvent was ethyl alcohol.

For comparison the behavior of a more protonic O–H in a mixture of triethylamine + *p*-xylene was sought and 2,6-dichloro-4-nitrophenol was employed; its spectrum is given in Figure 3. An intense new band is observed at ~385 mμ which increases in intensity with increasing triethylamine concentration while the intensity of the parent phenol bands decrease. When the *p*-xylene is replaced by ethyl al-

cohol the band shifts to 410 mμ. To determine whether this band could be ascribed to the anion (case B) of the salt, potassium, 2,6-dichloro-4-nitrophenolate was examined and this also gave an intense band at 410 mμ.

It would seem within the limits of detection of this method that for the 2,4,6-trihalophenols no evidence is forthcoming for type B, that is, of ion-pair formation due to a tautomeric equilibrium.

Conclusions

The mean relaxation time and the distribution coefficient values establish the presence of more than one polar species in solutions of the trihalophenol, and hydrogen bonded complexes of the trihalophenol and DBO in a 1:1 and 2:1 ratio. When the dissolved amounts of 2,4,6-trichlorophenol and DBO are in a 1:1 ratio then the apparent dipole moment has increased by ~2.4 D. This appreciable increment suggests contributions from an ionic form which results from such an equilibrium as in eq 2. The conductivity data indicate a significant increase in ionic conductivity on addition of DBO or triethylamine to a solution of the trihalophenol in *p*-xylene. However, when the solvent *p*-xylene is replaced by ethyl alcohol, there is a dramatic rise in conductivity with increasing amine concentration. This could be explained by increased dissociation of the ion pairs which may be wholely or partly related to the high static dielectric constant (ϵ_0 24.30 at 25°) of the ethyl alcohol.

The electronic (and also the infrared) spectra of the 2,4,6-trihalophenols establishes the O–H ··· N< hydrogen bonded form for these phenols + triethylamine in a wide variety of solvents. In 2,6-dichloro-4-nitrophenol + triethylamine + either *p*-xylene or ethyl alcohol a new band is observed at ~400 mμ which may be attributed to the anion resulting from tautomeric equilibrium.

Finally it must be stressed that in these three component mixtures there may be a variety of species. Phenols certainly readily self associate; this would, of course, be radically altered by the presence of an adequate concentration of a strong donor, and some new associated species would ensue. A worthwhile extension of this work would be to make a spectroscopic examination over a wide range of concentration using band resolution techniques. This could well lead to more definite conclusions concerning the identity of the species present.

References and Notes

(1) J. J. Lindberg, *Acta Chem. Scand.*, **14**, 379 (1960).
(2) J. L. Roark and W. B. Smith, *J. Phys. Chem.*, **73**, 1043 (1969).
(3) M. D. Magee and S. Walker, *J. Chem. Phys.*, **55**, 3068 (1971).
(4) W. F. Hassell, M. D. Magee, S. W. Tucker, and S. Walker, *Tetrahedron*, **20**, 2137 (1964).
(5) M. D. Magee and S. Walker, *Trans. Faraday Soc.*, **62**, 3993 (1966).
(6) M. D. Magee and S. Walker, *J. Chem. Phys.*, **50**, 2580 (1969).
(7) M. D. Magee, Thesis, University of Aston, Birmingham, England, 1967.
(8) B. Eric, E. W. Goode, and D. A. Ibbitsen, *J. Chem. Soc.*, 55 (1960).
(9) M. D. Magee and S. Walker, *Can. J. Chem.*, **49**, 1106 (1971).
(10) J. W. Smith, "Electric Dipole Moments", Butterworths, London, 1955.
(11) J. Jadzyn and J. Malecki, *Acta Phys. Pol. A*, **41**, 599 (1972).
(12) M. St. C. Flett, *Spectrochim. Acta*, **10**, 21 (1957).
(13) A. W. Baker and W. W. Kaeding, *J. Am. Chem. Soc.*, **81**, 5904 (1959).
(14) I. Brown, G. Eglinton, and M. Martin-Smith, *Spectrochim. Acta*, **18**, 1593 (1962).
(15) R. Mecke, *Discuss. Faraday Soc.*, **9**, 161 (1950).
(16) R. J. W. Le Fèvre and C. G. Le Fèvre, *Rev. Pure Appl. Chem. (Aust.)*, **5**, 261 (1955).
(17) L. J. Bellamy and H. E. Hallam, *Trans. Faraday Soc.*, **55**, 220 (1959).
(18) Y. Manechal, *Commis. Energ. At. [Fr.], Rapp.* CEA-R-3683 (1969).
(19) C. I. Bell and G. M. Barrow, *J. Chem. Phys.*, 31, 1158 (1959).

Measurement of Adsorption and Surface Diffusion on Homogeneous Solid Surfaces

C. S. Lee and J. P. O'Connell*

Department of Chemical Engineering, University of Florida, Gainesville, Florida 32611

(Received September 16, 1974)

Adsorption and quasi-steady-state flux data for $CHCl_3$ in a porous bed of Graphon particles have been measured over the temperature range 5–85° with varying superficial bed densities. Knudsen flux of helium over the same conditions and some transient flux measurements were also made. While the gas-phase diffusivity is affected by bed densities, surface flux is independent of bed density. The time lags from the transient flux measurements are consistent with the quasi-steady-state measurements. Accurate correlation of the adsorption and surface flux data was made with our statistical mechanical model using parameters previously obtained. In particular, the geometric factor for surface flux is independent of bed density, temperature, and adsorbed species.

We have previously analyzed surface diffusion and adsorption of gases on homogeneous solid surfaces using a statistical mechanical model.[1,2] In the model, the interaction between adsorbed molecules is characterized by a hard-disk repulsion at diameter σ_H plus a long-range attractive potential with minimum ϵ_{gg}, while the structured surface potential field is replaced by a distribution of circular sites having interactions with the adsorbed molecules represented by an energy well depth ϵ and diameter σ_s. For transport, an empirical geometric factor f_e is also included to convert the superficial area and bed length to the cross section and diffusion path of the adsorbed molecules. Different parameters are sensitive to different properties and all can be determined quite well from adsorption isotherms

and surface diffusion data at two different temperatures. However, only the systems SO_2–Graphon and SF_6–Graphon had been studied previously. In this work experimental adsorption and diffusion data were taken on the $CHCl_3$–Graphon system to complement previous adsorption isotherm data of $CHCl_3$ on P33 (2700). Complete analysis of the graphitized carbon black systems within the model is yet to be made. However, indications are that the model can adequately describe all available data.

Theory

The use of the above molecular model with standard equilibrium statistical mechanical methods leads to an equilibrium isotherm of

$$P = K \frac{\theta}{[1 - \theta f_1/\theta_s]^{f_1}(1 - \theta)^R} \exp\left\{R\frac{3\theta - 2\theta^2}{(1 - \theta)^2} - 2\frac{\epsilon_{gg}}{kT}[f_{mo}(2 - f_{mo}) + (1 - f_{mo})^2 (\sigma_H/n\sigma_m)^4]\right\} \quad (1)$$

where K is Henry's constant, $\theta = \pi\sigma_H^2\rho/4$, ρ is the number of adsorbed molecules per unit surface area, $\theta_s = \pi\sigma_H^2\rho_s/4$, ρ_s is the surface site number density, f_1 is the fraction of molecules localized on sites (kinetic energy less than ϵ) while f_{mo} is the fraction of molecules not on sites (both fractions are calculated from partition functions described in ref 1), n is the smallest integer which makes $\sigma_H/n\sigma_m$ less than unity, σ_m is an average distance between centers, and R is a function of σ_m and f_m and can take on values from near zero to unity.

The form of the isotherm can vary from a Hill–deBoer form ($\epsilon = 0$) to a Langmuir form ($\epsilon = U_{00}$).

For the nonequilibrium properties, the statistical mechanical methods of the van der Waals theory of transport are used for admolecule–admolecule interactions while an analysis similar to the square-well transport theory is used for admolecule–surface interactions. A Boltzmann equation is solved for the single-particle surface distribution function to yield the surface "diffusion coefficient" for local one-dimensional surface flow of a pure component under a pressure gradient

$$D_s = \left[\frac{kT}{4\pi m}\right]^{1/2}\left[\frac{\partial \ln P}{\partial \ln \rho}\right]_T \times \left[\frac{1}{g_H(\sigma_H, \rho)\rho\sigma_H E_p(\epsilon/kT) + \rho_s\sigma_s E_s(\epsilon/kT)}\right] \quad (2)$$

where g_H is the rigid disk radial distribution function at contact and E_p and E_s are functions of reduced temperature tabulated in ref 1. Expressions are also given in ref 1 for the diffusion coefficient of a tracer under a concentration gradient at uniform total pressure.

Experimental Method

Unlike the adsorption isotherm measurement where the amount adsorbed is directly measured, the measurement of surface flow is usually an indirect one obtained from permeability through a porous bed of an adsorbable gas and of a nonadsorbable one. The assumption is that the surface flux, $F_{surface}$, and the bulk gas phase flux, F_{bulk}, are additive.[3]

$$F = F_{bulk} + F_{surface} \quad (3)$$

A model for strong interaction between the two fluxes has been developed,[4] but it is intended for very high gas-phase densities, and it is expected that if F_{bulk} is very small compared with $F_{surface}$, the effect of interaction is very small (if, indeed, it exists). For nonabsorbable gases, F_{bulk} is easily determined experimentally. Since the experimental bulk flow is usually in the Knudsen regime, the standard molecular weight and temperature corrections to the Knudsen diffusivities, D_{gK}, of nonadsorbable gases would give that for the adsorbable gases.[3]

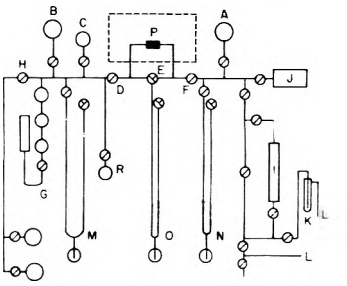

Figure 1. Schematic diagram of apparatus.

From this determination of F_{bulk} for adsorbable gases, $F_{surface}$ can be determined from eq 1. It is not clear whether the molecular weight correction alone is adequate,[4-9] so in order to minimize uncertainties, the conditions have been controlled so that calculated bulk flux, which is the maximum expected, is less than 15% of the total flux.

In a steady-state experiment, F_{total} is constant, but there is no reason that F_{bulk} or $F_{surface}$ should be so throughout the bed. However, eq 3 is valid locally, so the total flux can be written

$$F = \frac{A\rho_b}{f_e}\int D_s d\rho + D_{gk}\frac{\Delta P}{L}A_g \quad (4)$$

where D_s is given in eq 2, A is the surface area per unit mass of adsorbent, ρ_b is the mass of adsorbent per unit volume of the bed, f_e is an effectiveness factor for surface flow, P is the pressure, L is the bed length, and A_g is the gas-phase area determined from the bed diameter, d, and the void fraction, ϵ_v.

$$A_g = \pi d^2\epsilon_v/4 \quad (5)$$

D_{gk} varies with the square root of temperature and molecular weight.

Experimental Apparatus

The apparatus was similar to that of Pope[11] and is shown in Figure 1. Graphon (Cabot Corp.) was compacted in the stainless steel cylinder, P, of inside diameter 0.6 cm and inside length of 2.9 cm by adding and compressing four to seven portions of the adsorbent Graphon. The plugs labeled 1, 4, and 6 had void fractions of 0.36 ± 0.01, those labeled 2 and 5 had void fractions 0.43 ± 0.01, and plug 3 had void fraction of 0.32. Here we have assumed the specific gravity of solid Graphon to be 1.80. The cylinder was immersed in a constant temperature bath controlled to ±0.01°. The manometers, M and N, were mercury manometers and 12 mm i.d. tubing was used to minimize the error due to the mercury meniscus. The oil in manometer O, which was used for measurement of very small pressure changes, was separated from the system by mercury to avoid contacting the organic sample vapor. Pressure measurements were made with a cathetometer, accurate to ±0.01 mm, yielding accuracies of 0.5% for pressures over 0.2 mmHg. The buffer volumes, A, B and C, and the gas

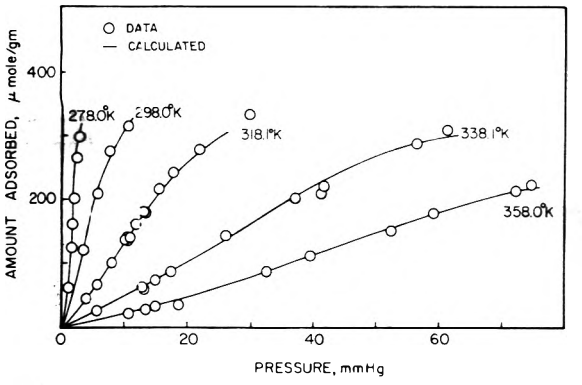

Figure 2. Adsorption isotherms for $CHCl_3$ on Graphon.

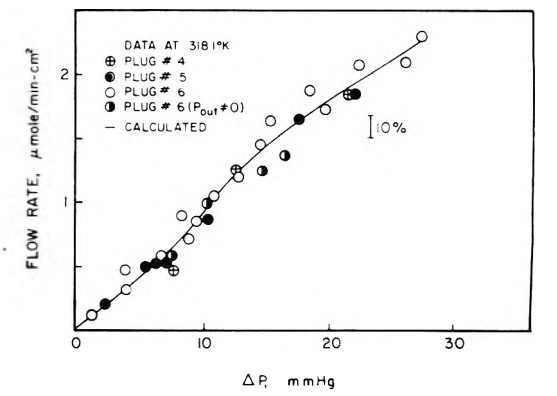

Figure 4. Flow rates for chloroform through different Graphon plugs.

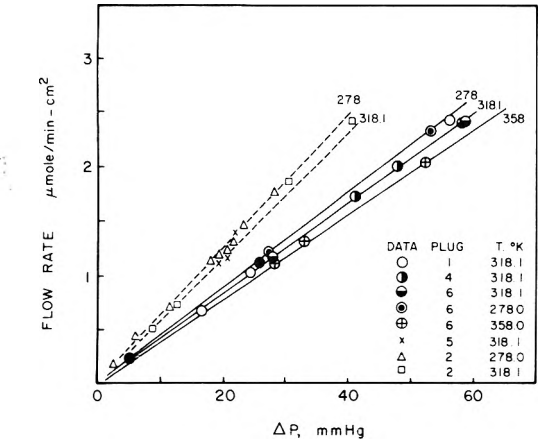

Figure 3. Flow rates for helium through Graphon plugs.

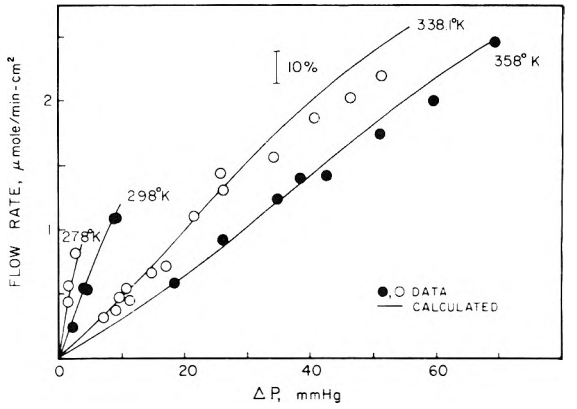

Figure 5. Flow rates for chloroform through a Graphon plug at different temperatures.

buret, G, were calibrated before connection to the system. All the stopcocks were high vacuum quality with vacuum bulbs. A cartesian manostat was installed before the pumping station to maintain constant downstream pressure.

Experimental Procedures

Spectral grade liquid chloroform (Matheson Coleman and Bell) was placed in the sample reservoir, R, which was isolated from the system by a mercury cut-off. The gases, CP grade SF_6 (Matheson) and high-purity grade helium (Air Reduction Co.), were connected to the stopcock H.

Initially the whole system was baked and pumped for 1 week. The plug temperature while baking was about 130°. Adsorption experiments were carried out using the system on the left side of stopcock F after it was closed. The method was the usual volumetric method[12] in which at a set temperature, the pressure of a vapor sample in a calibrated volume was measured before and after the sample was put in contact with the adsorbent. Whenever a new plug was made, the plug was baked at 130° for about 3 days. Between experiments with the same plug, the system was degassed at about 90° overnight. The good repeatability (within estimate error) of adsorption and flow measurements indicated little change in bed characteristics with time. Figure 2 shows the results for some of the data on each isotherm taken from plugs 3, 4, 5, and 6.

The flow measurement for both nonadsorbable helium and the adsorbable $CHCl_3$ was a quasi-steady-state measurement. The oil manometer, O, was opened to the outgoing-side volume of the plug. With the sample vapor introduced to the ingoing-side volume, the outgoing side was pumped for about 2 hr when a steady concentration profile should have been attained in the plug. By closing stopcock Q, the flow rate was determined from the pressure change in the outgoing-side volume using manometer O. Figure 3 shows representative helium flux measurements. Figure 4 shows the temperature dependence of the $CHCl_3$ surface flux in a single plug and Figure 5 shows the surface flux results for several conditions at 45°. Complete data are available.[13] The uncertainty of the flux measurements for adsorbable gases is larger than that of the adsorption isotherm. At high temperatures, F_{bulk} was calculated to be as large as 15% of the total flux. Since F_{bulk} for adsorbable gases is uncertain to some extent, the $F_{surface}$ values are also uncertain. Although the bulk gas contribution is negligible at low temperatures, the quasi-steady-state assumption is not as good under these conditions. Together with the uncertainty in measuring the low pressure and pressure difference, it is believed that the final fluxes are accurate to within ±10%. For the few transient measurements made (see below), the accuracy is about 15%.

Discussion

Detailed comparison of the present data with theory, plus those of other gases on graphetized carbon black, is presently being done. However, preliminary analysis of the present data yields some conclusions.

Values of the model parameters for the calculated values in Figures 2, 4, and 5 are given in Table I.

First, the equilibrium isotherm data show that the amount adsorbed per unit weight did not depend on the density of the plugs used. This would be expected if com-

TABLE I: Model Parameters[1] for $CHCl_3$–Graphon System over 5–85°

$2\epsilon_{ss}$ kcal/g mol	ϵ_s kcal/g mol	σ_H, Å	σ_s, Å	δ_s	f_e	ρ_s, Å^{-2}	σ_m, Å	n	A, m^2/g	ln B,[a] cmHg	U,[a] kcal/g mol
4.4	3.2	4.65	0.23	0.5	1.7	0.192	2.5	2	89	15.366	8.386

[a] Henry's constant, K, can be correlated by $K = B\exp(-U/RT)$ with units of cmHg.

pression does not affect the area exposed. This indicates that the differences in density are due to the size of the macropores, rather than micropores, between particles. The agreement of the data and the calculated values from eq 1 is satisfactory over a wide range of temperature. Dividing the present adsorbent surface area by a factor of 6.85 is all that is necessary to use the same parameters to accurately predict the $CHCl_3$–P33(2700) equilibrium data of Machin and Ross.[14] There are insufficient data to obtain isosteric heats of adsorption except at zero coverage where the values (values of U in Table I) are the same as those of Machin and Ross.

Second, several characteristics of the Knudsen flow can be observed from the helium flux data are shown in Figure 3. The square root temperature dependence of the Knudsen diffusion coefficient is clearly shown.[5-9] There is also a definite dependence of D_{gK} on the superficial density of the carbon plug. On the other hand, different plugs of the same density show essentially the same D_{gK}, a tentative indication that the plugs are reproducible to a large extent.

Third, studies of transient flow were made to see if transient measurements were consistent with the steady-state measurements. We used Frisch and Prager's definition of time lag.[15]

$$t_{lag} = \int (F_{steady} - F_{transient})\, dt / F_{steady} \qquad (6)$$

Measured time lags can be compared with Frisch's theoretical correlation

$$t_{lag} = \frac{L}{F_{steady}} \left| \langle C_s \rangle - \frac{\langle C_s^2 \rangle}{C_{s0}} \right| \qquad (7)$$

where

$$\langle C_s \rangle = \frac{1}{L}\int_0^L C_s(x)\, dx$$

and C_{s0} is the concentration at $x = 0$. Over the range of C_{s0} corresponding to 9–24 mmHg at 45° in plug 6, the calculated values of t_{lag} from eq 6 were 70 ± 1 min. For six data points using eq 5 the mean was 69 ± 5 min. Pope obtained similar agreement for his Spheron-6(2700) plug,[11] although Ash et al.[16] did not for heterogeneous substances. Disagreement has usually been attributed to the presence of "blind pores". While agreement apparently does not assure that "blind pores" are absent,[17] if any were present in these experiments, they did not affect the use of the same model parameters and surface areas for equilibrium and transport properties under varying bed densities.

Fourth, the surface flux is independent of bed density and temperature. This is expected if the surface-flux paths, determined by the amount of surface area and the form of its two-dimensional envelope, are unaffected by superficial density. Figure 4 shows that the data of plugs 4 and 6 which have essentially the same density agree within experimental error. This confirms the reproducibility of the plugs used and probably indicates that any nonhomogeneity effects of the plug were negligible. After accounting for the differences in gas-phase flux, the data from plug 5 agrees with the others. In the application of the model to these data, this would require that f_e be the same for all plugs. A value of 1.7 for f_e was found to describe all the data. In our previous analysis,[1] we found a value of 1.3 for the data of Ash et al. for SF_6 on Graphon. This indicates that the present surface flux was somewhat lower. To determine if this was caused by a difference in the bed or of the gas, three permeability data for SF_6 at −20° were also taken on plug 6. Using the molecular parameters obtained[1] from the data of Ash et al.,[3] and the value of 1.7 for f_e obtained from $CHCl_3$ in plug 6, the present SF_6 data could be reproduced quantitatively. The difference between the values of f_e obtained by Ash et al. and ourselves may be due to differences in the size and size distribution of the carbon black particles. The only obvious difference is in the bed density, our 1.04 compared to their 1.47 at the same porosity.

Finally, direct comparison of experimental surface fluxes with calculation (eq 4) is done here for the first time. All previous work[3,11] had determined "diffusion coefficients" by taking a graphical derivatives of flux data with the outlet pressure being essentially zero. Besides limiting the possible experimental conditions, this procedure can lead to highly uncertain values as is apparent from examination of the data in Figures 4 and 5. The flux equation allows for finite downstream pressures, so four of the data points were taken with nonzero downstream pressure. They are shown in Figure 4 after correction to the scale with zero outlet pressure by use of the model. They show good agreement with the others.

References and Notes

(1) C. S. Lee and J. P. O'Connell, *J. Colloid Interface Sci.*, **41**, 415 (1972).
(2) C. S. Lee and J. P. O'Connell, *Ind. Eng. Chem., Fundam.*, **13**, 165 (1974).
(3) R. Ash, R. W. Baker, and R. M. Barrer, *Proc. Roy. Soc., Ser. A*, **279**, 434 (1967).
(4) W. K. Bell, Ph.D. Dissertation, University of Colorado, 1971.
(5) E. R. Gilliland, R. F. Baddour, and J. L. Russell, *AIChE J.*, **4**, 90 (1958).
(6) F. M. Devienne in "The Solid-Gas Interface", Vol. II, E. A. Flood, Ed., Marcel Dekker, New York, N.Y., 1967, p 815.
(7) E. M. Reed, Jr., and J. B. Butt, *J. Phys. Chem.*, **75**, 133 (1971).
(8) S. T. Hiang and K. Kammermayer, *Can. J. Chem. Eng.*, **44**, 82 (1966); *Ind. Eng. Chem., Fundam.*, **7**, 671 (1968).
(9) C. N. Satterfield and P. J. Caddle, *Ind. Eng. Chem., Fundam.*, **7**, 202 (1968).
(10) R. M. Barrer and R. T. Lawson, *Surface Sci.*, **21**, 265 (1970).
(11) C. G. Pope, *Trans. Faraday Soc.*, **63**, 734 (1967).
(12) S. Ross and J. P. Olivier, "On Physical Adsorption", Interscience, New York, N.Y., 1964.
(13) C. S. Lee, Ph.D. Dissertation, University of Florida, 1972.
(14) W. D. Machin and S. Ross, *Proc. Roy. Soc., Ser. A*, **265**, 455 (1962).
(15) H. L. Frisch and S. Prager, *J. Chem. Phys.*, **54**, 1451 (1971).
(16) R. Ash, R. M. Barrer, and C. G. Pope, *Proc. Roy. Soc., Ser. A*, **271**, 1 (1963).
(17) J. H. Petropoulos and P. P. Roussis, *J. Chem. Phys.*, **47**, 1491 (1967).

Aggregation of Antihistamines in Aqueous Solution. Self-Association of Some Pyridine Derivatives

D. Attwood* and O. K. Udeala

Pharmacy Department, University of Manchester, Manchester M13 9PL, England *(Received August 20, 1974)*

The self-association of the antihistaminic drugs, tripelennamine hydrochloride, thenyldiamine hydrochloride, mepyramine maleate, pheniramine maleate, chloropheniramine maleate, and brompheniramine maleate, in aqueous solution has been investigated by light scattering methods. The scattering intensity was in excess of that calculated for the unassociated monomers for each compound. No significant discontinuity in the concentration dependence of the light scattering, attributable to a critical micelle concentration, could be detected. Attempts were made to simulate the experimental data using micellar and nonmicellar models of aggregation. The light scattering behavior of mepyramine maleate, chlorpheniramine maleate, and brompheniramine maleate was not consistent with the mass action model of micellar association but could be adequately reproduced by a nonmicellar model involving aggregate growth by the step-wise addition of monomers. The concentration dependence of the light scattering of tripelennamine hydrochloride, thenyldiamine hydrochloride, and pheniramine maleate could be simulated both by the micellar model, assuming aggregation numbers of 3 and 4 and micellar equilibrium constants of 10^{10} and 10^{14}, respectively, and by the nonmicellar model. It was not possible to detect a critical micelle concentration for any of these compounds from conductivity measurements.

It has been previously established[1] that some antihistaminic drugs based on the diphenylmethane nucleus formed micelles in aqueous solution. The physicochemical properties of the micelles of these compounds have been investigated.[2] This paper reports a study of the association of antihistaminic drugs with the general structures:

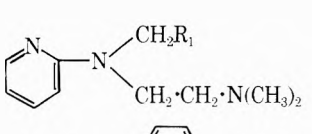

Ia, R_1 = 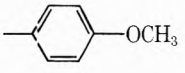

Ib, R_1 = 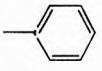

Ic, R_1 = 

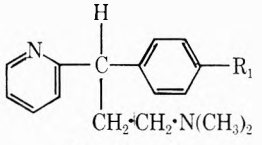

IIa, $R_1 = H$

IIb, $R_1 = Cl$

IIc, $R_1 = Br$

The compounds studied included mepyramine (pyrilamine) maleate (Ia), tripelennamine hydrochloride (Ib), thenyldiamine hydrochloride (Ic), pheniramine maleate (IIa), chlorpheniramine maleate (IIb), and brompheniramine maleate (IIc).

Farhadieh et al.[3] determined the concentration dependence of the conductivity and osmotic coefficients of aqueous solutions of mepyramine maleate and tripelennamine hydrochloride and suggested that small aggregates may be present in solution. They were unable to detect a critical micelle concentration (cmc) for either of these compounds.

Experimental Section

Materials. Mepyramine maleate and tripelennamine hydrochloride were obtained from May and Baker Ltd., and Ciba Laboratories, respectively. Thenyldiamine hydrochloride, pheniramine maleate, chlorpheniramine maleate, and brompheniramine maleate were gifts from Winthrop Laboratories, Hoechst Pharmaceuticals Ltd., and A. H. Robins and Co., Ltd., respectively. All drugs were used as received.

pK_a values have been reported[4] for a series of proprietary antihistamines, including the compounds investigated here. Values ranged between 8 and 10 and consequently almost complete ionization may be assumed over the concentration range at which measurements have been made.

Light scattering measurements were made at 303 K with a Fica 42000 photogoniodiffusometer (A.R.L. Ltd.) using a wavelength of 546 nm. Aqueous solutions were clarified by ultrafiltration through 0.1-μm Millipore filters until the ratio of the light scattering at angles of 30 and 150° did not exceed 1.10. The refractive index increments of the micellar species (dn/dm_{mic}) were measured at 546 nm using a differential refractometer (P.C.L. Ltd.). The following values (kg mol^{-1}) were obtained: tripelennamine hydrochloride, 0.0619; thenyldiamine hydrochloride, 0.0649; mepyramine maleate, 0.0795; pheniramine maleate, 0.0680; chlorpheniramine maleate, 0.0739; and brompheniramine maleate, 0.0797.

Conductivity measurements were made at 303 ± 0.01 K using a Wayne Kerr autobalance universal bridge (Model B641).

Treatment of Data

Light-scattering results are presented in Figure 1 as plots of the scattering at 90°, S_{90}, as a function of molal concentration, m. No discontinuity in the concentration dependence of S_{90} attributable to a cmc could be detected, although the scattering intensity was in excess of that calculated for unassociated monomers. This was in contrast to the diphenylmethane derivatives,[1] which exhibited significant discontinuities in their physicochemical properties at well-defined critical micelle concentrations. An attempt has been made to simulate the experimental data using two models of association.

Micellar Association. The mass action model of micellar association assumes that the cationic micelle, M^{p+}, is

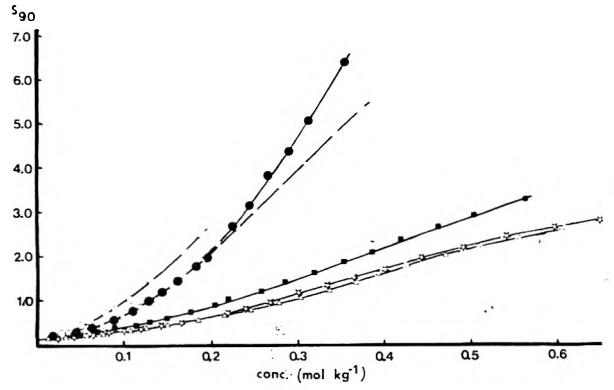

Figure 1. Concentration dependence of the scattering ratio, S_{90}, for aqueous solutions of tripelennamine hydrochloride (☆), thenyldiamine hydrochloride (△), mepyramine maleate (●), pheniramine maleate (■), chlorpheniramine maleate (□), and brompheniramine maleate (○).

formed by an all-or-none process from N monomers, D^+, and $N - p$ firmly bound anions, X^-.

$$ND^+ + (N - p)X^- \rightleftharpoons M^{p+} \quad (1)$$

In the absence of added electrolyte

$$[X^-] = [D^+] + p[M^{p+}] \quad (2)$$

and the micellar equilibrium constant, K_m, is given by

$$K_m = \frac{[M^{p+}]}{([X^-] - p[M^{p+}])^N [X^-]^{N-p}} \quad (3)$$

It is well known that the abruptness of the change in physicochemical properties at the cmc decreases with decreasing N (at constant K_m) and decreasing K_m (at constant N). The apparent absence of a cmc in Figure 1 may be a consequence of a combination of low N and K_m values. Theoretical curves were generated using eq 3 for a range of combinations of N, K_m, and p in an attempt to reproduce the experimental light-scattering curves. Concentrations in eq 3 were expressed as mole fractions. The scattering intensity, arising from the micellar species, S_{90mic}, was estimated using equations proposed by Anacker and Westwell.[5]

$$K^1 m_{mic}/R_{90mic} = A + Bm_{mic} \quad (4)$$

where $K^1 = 2\pi^2 n^2 (dn/dm_{mic})^2 V^0/L\lambda^4$; n is the refractive index of the solution; V^0 is the volume of solution containing 1 kg of water; L is Avogadro's number; λ is the wavelength of incident light, and m_{mic} is the molality of the micellar species (in terms of monomeric units) as determined from eq 3. The second virial coefficient, B, was calculated from

$$B = pA[(1 + p)N^{-1} - A](2m_{mon})^{-1} \quad (5)$$

where m_{mon} is the molality of monomer. The approximation $A = N^{-1}$ was made to simplify the calculations. S_{90mic} was calculated from R_{90mic} using the instrumental calibration constant. The scattering intensity due to monomeric species in solution, S_{90mon}, was estimated from eq 4, assuming a zero value of B. The total scattering intensity, S_{90}, was then a summation of S_{90mic}, S_{90mon}, and the intensity of the light scattered by the solvent.

Nonmicellar Association. Aggregate growth was assumed to occur by a process of monomeric addition.

$$M_{N-1} + M_1 \rightleftharpoons M_N \quad (6)$$

Several methods have been derived for the calculation of step-wise equilibrium constants, K_N, for such a system. A complicating factor in ionic systems is the nonideality arising from the interaction of charged species. Adams and Williams[6] have proposed a rigorous method for the treatment of the weight-average molecular weight data of associating nonideal systems. There is, however, no simple way of using these equations unless the equality of the values of the second virial coefficient for all species is assumed. A simpler approach is to assume the equality of all values of K_N. This is equivalent to assuming an identical free-energy change for the addition of each monomer. For systems of spherical ionic micelles, K_N is related to the free-energy change, ΔG_m, associated with the introduction of a monomer into a micelle with $N - 1$ monomers by

$$\Delta G_m = \Delta G_h + \Delta G_e = -RT \ln K_N \quad (7)$$

The magnitude of the hydrophobic free-energy component, ΔG_h, will be affected by the mode of packing within the micelle and for small micelles a significant dependence of ΔG_h on N might be expected.[7] Similarly ΔG_e varies with N, becoming more positive as N increases. Thus in the growth of small ionic aggregates, such as are present in the systems investigated here, it is clear that the assumption of equal K_N values is not reasonable.

An analytical treatment for ideal associating systems with nonequal K_N values has been derived by Steiner[8] and was applied here. The weight-average molecular weight, M_w, is related to weight concentration c (g dm^{-3}) by

$$M/M_w = 1 + d \ln x/d \ln c \quad (8)$$

where x is the weight fraction of compound of molecular weight, M, existing as the monomer. Consequently

$$\ln x = \int_0^c [(M/M_w) - 1] \, d \ln c \quad (9)$$

x was determined from the light-scattering data by graphical integration according to eq 9. Equilibrium constants were estimated from

$$[(M_w/xM) - 1]/(xc/M) = 4K_2 + 9K_2K_3(xc/M) \ldots + N^2\left(\prod_{N=2}^{N} K_N\right)(xc/M)^{N-2} \quad (10)$$

K_2 and K_3 were obtained from the intercept and limiting slope, respectively, of a plot of the quotient on the left of eq 10 vs. (xc/M). Curvature of such a plot is indicative of aggregates with $N > 3$ and higher equilibrium constants were thus evaluated in a similar manner until a linear plot of

$$\left\{[(M_w/xM) - 1] - \sum_{2}^{N=l-1} N^2 \prod_{2}^{N} K_N (xc/M)^{N-1}\right\}/(xc/M)$$

vs. (xc/M) was obtained, where l is the degree of association of the highest molecular species existing in solution in significant amounts. As a demonstration of the applicability of this model, the concentration dependence of the apparent M_w values, recalculated from the estimated values of k_N, has been compared with that indicated by experiment. It is emphasized that this method of treating the data ignores interactions between the charged species. This assumption becomes increasingly less valid as the solution concentration increases.

TABLE I: Equilibrium Constants and Limiting Aggregation Numbers for the Association of Antihistamines Calculated from Eq 10

	Equilibrium constants, $dm^3\ mol^{-1}$			Limiting aggregation number
	K_2	K_3	K_4	l
Tripelennamine HCl	0.62	1.75	3.1	7
Thenyldiamine HCl	0.38	1.93	0.8	6
Mepyramine maleate	2.00	7.19	6.3	10
Pheniramine maleate	1.61	5.17	0.4	7
Chlorpheniramine maleate	2.03	9.85	4.4	11
Brompheniramine maleate	3.50	20.95	7.9	15

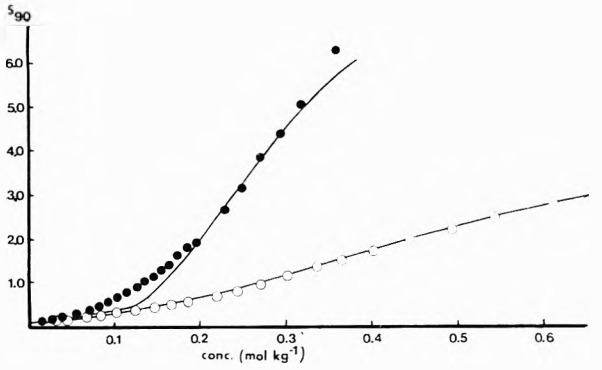

Figure 2. Simulation of the concentration dependence of scattering ratio, S_{90}, using mass action equations. Continuous lines represent values calculated using eq 1-5 with $N = 10$, $K_N = 10^{42}$, and $p/N = 0.2$ for mepyramine maleate (●) and $N = 3$, $K_N = 10^{10}$, and $p/N = 0.2$ for tripelennamine hydrochloride (O).

Results and Discussion

The light-scattering results for pheniramine maleate, thenyldiamine hydrochloride, and tripelennamine hydrochloride could be reproduced within the limits of error of the experimental data using eq 1-5 with $p/N = 0.2$ and values of $N = 3$ and 4 and $K_N = 10^{10}$ and 10^{14}, respectively (see Figure 2). The corresponding standard free energies of micellization ΔG (per mole of monomeric surfactant) were calculated from

$$\Delta G = -(RT/N) \ln K_N \qquad (11)$$

Both combinations of N and K_N gave a ΔG of approximately -20 kJ mol^{-1}. From the data of Kauzmann,[9] the formation of a micelle in which a phenyl ring is completely shielded from the aqueous environment would result in a free energy change of -17 kJ mol^{-1}. The ΔG value calculated assuming the applicability of the mass action law is thus not unreasonable.

Attempts to simulate the experimental scattering curves of mepyramine maleate, chlorpheniramine maleate, and brompheniramine maleate using eq 1-5 proved unsuccessful. In order to reproduce the appreciable scatter at the higher concentrations it was necessary to assume $N \geq 10$ and corresponding K_N values of the order of 10^{42}. Such combinations, however, produced significant inflections in the S_{90} vs. m curves at low concentrations (see Figure 2).

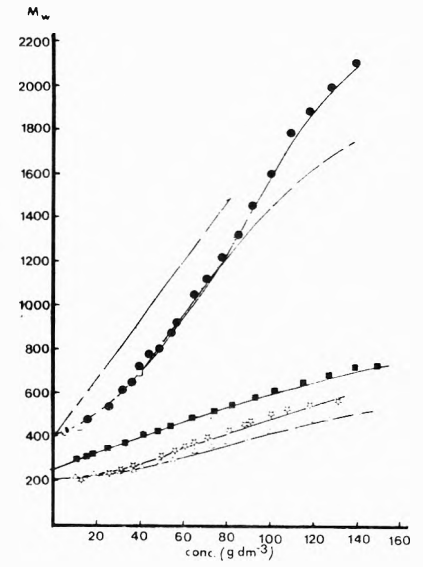

Figure 3. Simulation of the concentration dependence of apparent molecular weight, M_w, using a step-wise association model of aggregation. Continuous lines represent values calculated using eq 9 and 10. Experimental points represent apparent M_w values calculated from light-scattering results, assuming ideality, for tripelennamine hydrochloride (☆), thenyldiamine hydrochloride (△), mepyramine maleate (●), pheniramine maleate (■), chlorpheniramine maleate (□), and brompheniramine maleate (○).

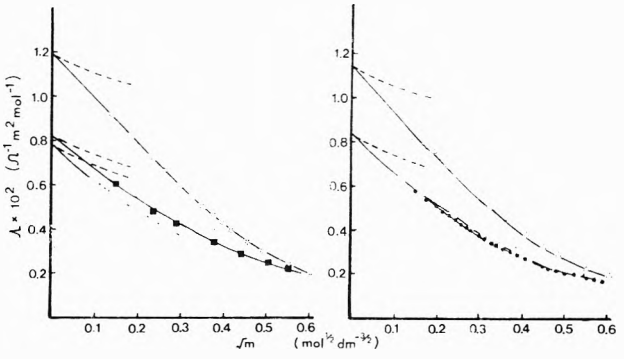

Figure 4. Equivalent conductivity of aqueous solutions of tripelennamine hydrochloride (☆), thenyldiamine hydrochloride (△), mepyramine maleate (●), pheniramine maleate (■), chlorpheniramine maleate (□), and brompheniramine maleate (○); eq 12 (- - - -).

The ΔG values for these combinations of N and K_N from eq 11 were approximately -24 kJ mol^{-1} giving poor agreement with the expected values.

Equations 9 and 10 gave an adequate description of the variation of apparent molecular weight with concentration for all compounds (Figure 3). Values of K_N are quoted in Table I. Small errors in the calculation of the lower K_N values accumulate and result in large errors in the higher constants. Consequently only the lower values have been quoted. The error in K_N arising from a neglect of the second virial coefficient is also least significant for these lower values. All compounds gave linear plots of

$$\left\{[(M_w/xM) - 1] - \sum_{2}^{N=l-1} N^2 \prod_{2}^{N} K_N (xc/M)^{N-1}\right\} / (xc/M)$$

vs. (xc/M) at characteristic values of l. This was assumed to be an indication of the attainment of a limiting aggre-

gate size, although similar effects may result from a neglect of nonideality in continually aggregating systems. The apparent increase in l in the series, pheniramine maleate, chlorpheniramine maleate, brompheniramine maleate (see Table I), might be expected from the increased hydrophobicity conferred by the -Cl and -Br substituents on the phenyl ring. Similarly the substituted $-OCH_3$ group of mepyramine maleate results in a greater hydrophobicity of this compound as compared to tripelennamine hydrochloride and this is again reflected in the values of l for these two compounds. Replacement of the phenyl ring of tripelennamine hydrochloride by a thiophene ring, as in thenyldiamine hydrochloride, had no apparent effect on the limiting aggregation number.

The conductivity data are presented as graphs of equivalent conductivity, Λ, against $m^{1/2}$ (see Figure 4). All compounds exhibited slopes greater than those predicted for 1:1 electrolytes by eq 12[10] which is reportedly valid for $m \leq$

$$\Lambda = \Lambda^0 - [(B_1\Lambda^0 + B_2)/(1 + \kappa a)]m^{1/2} \quad (12)$$

0.05 mol dm^{-3}. B_1 and B_2 are constants with values of 0.2321 $mol^{-1/2}$ $dm^{3/2}$ and 6.791 $\times$ 10^{-3} Ω^{-1} m^2 mol^{-1} (mol $dm^{-3})^{-1/2}$, respectively, at 303 K and $\kappa a = 1.04 \times 10^8 m^{1/2} a$ at this temperature. An assumed value of 0.4 nm (from molecular models) was assigned to the ionic radius, a. It was not possible to detect inflection points in the conductivity plots. This is in agreement with Farhadieh et al.[3] who also failed to detect a cmc from conductivity measurements on solutions of tripelennamine hydrochloride and mepyramine maleate over similar concentration ranges at 298 K.

In conclusion, the light-scattering data suggest that the self-association of mepyramine maleate, chlorpheniramine maleate, and brompheniramine maleate does not occur by the normal micellization process. It may occur by a form of step-wise association giving a polydisperse system with no clearly defined cmc. From the experimental evidence available it is not clear whether the self-association of tripelennamine hydrochloride, thenyldiamine hydrochloride, and pheniramine maleate is micellar or nonmicellar. Both forms of association will adequately describe the light-scattering data. The inability to detect a cmc for these three compounds may merely reflect the limitations of the physical methods used.

Acknowledgments. O. K. Udeala wishes to acknowledge financial support from a British Technical Aid award to the University of Nigeria.

References and Notes

(1) D. Attwood, *J. Pharm. Pharmacol.*, **24**, 751 (1972).
(2) D. Attwood and O. K. Udeala, *J. Pharm. Pharmacol.*, **26**, 854 (1974).
(3) B. Farhadieh, N. A. Hall, and E. R. Hammarlund, *J. Pharm. Sci.*, **56**, 18 (1967).
(4) P. B. Marshall, *Brit. J. Pharmacol.*, **10**, 270 (1955).
(5) E. W. Anacker and A. E. Westwell, *J. Phys. Chem.*, **68**, 3490 (1964).
(6) E. T. Adams and J. W. Williams, *J. Am. Chem. Soc.*, **86**, 3454 (1964).
(7) P. Mukerjee, *J. Phys. Chem.*, **76**, 565 (1972).
(8) R. F. Steiner, *Arch. Biochem. Biophys.*, **39**, 333 (1952).
(9) W. Kauzmann, *Adv. Protein Chem.*, **14**, 1 (1959).
(10) R. A. Robinson and R. H. Stokes, *J. Am. Chem. Soc.*, **76**, 1991 (1954).

Photooxidation of Sulfur Dioxide on the Surface of Magnesium Oxide

M. J. Lin and J. H. Lunsford*

Department of Chemistry, Texas A&M University, College Station, Texas 77843 *(Received November 13, 1974)*

Publication costs assisted by the Environmental Protection Agency

SO_2 is photochemically oxidized to SO_3^- on the surface of magnesium oxide in the presence of adsorbed water vapor and oxygen or nitrous oxide. Water reacts with adsorbed SO_2 to increase the concentration of sulfite ions and monodentate sulfito complexes. Subsequent photolysis leads to the formation of SO_3^-, which is confirmed by the EPR hyperfine structure of the ion enriched with sulfur-33. Molecular oxygen or N_2O serve as electron scavengers, thus increasing the surface concentration of SO_3^-. The greater stability of SO_3^- on the surface relative to aqueous solutions is attributed to the lack of mobility in the adsorbed water. The half-life of the surface SO_3^- is >10 hr at 25°, but drops to 0.5 min at 100°.

Introduction

It is generally agreed that aerosols adsorb or react with SO_2 from the atmosphere, and that the resulting compounds constitute a health hazard.[1-3] There is very little known, however, about the chemistry of adsorbed SO_2, particularly the photochemistry on aerosol materials. One of the most important problems in the chemistry of atmospheric aerosols is the mechanism by which SO_2 is photooxidized, either prior to or after adsorption. In the present work we have concentrated on the photochemistry of SO_2 on magnesium oxide, which is a typical basic oxide.

Previous studies have shown that magnesium oxide is active in adsorbing sulfur dioxide.[4-6] Infrared evidence suggests the adsorption of SO_2 on a clean MgO surface results in the formation of surface sulfite species, which may be oxidized at elevated temperatures to sulfates and sulfato complexes.[5,6] Ultraviolet irradiation of the sulfite ions at room temperature results in the production of SO_2^-,[4] and

this radical anion may be subsequently oxidized to SO_3^- with molecular oxygen.[7] Furthermore, photolysis studies in the atmosphere[8-10] have shown that SO_2 is more rapidly oxidized when adsorbed into water droplets.

This work has now been extended to determine the effect of adsorbed water vapor on the reactions of the surface sulfite ions. Conditions were used which would more closely simulate those found in the atmosphere. As will be shown here the photolysis of the sulfite ion on hydrated magnesium oxide has features which are in common with the photochemistry of aqueous solutions containing sulfite ions, in that the SO_3^- ion is formed; however, the reactivity of this ion on the surface is orders of magnitude less than that observed in solution.

Experimental Section

The magnesium oxide used in these experiments was reagent grade powder obtained from Mallinckrodt Chemical Works. For one set of samples, the powder was boiled in distilled water for about 20 hr, and the resulting paste was extruded into pellets with a hypodermic syringe. The pellets were dried at 120° and degassed at 300° for 2 hr and at 500° for 1 hr. The final pressure in the vacuum system was below 1.0×10^{-4} Torr. This material is referred to simply as magnesium oxide. A second sample was prepared by boiling the MgO powder in distilled water for 20 hr, and drying the slurry at 120° until a solid was formed. The resulting magnesium hydroxide was then heated in flowing nitrogen gas at 100° for 2 hr and at 400° for 10 hr. The MgO sample was subsequently exposed to the atmosphere where it was partially converted back to the hydroxide; hence, it is referred to as MgO–$Mg(OH)_2$. Before use the MgO–$Mg(OH)_2$ was evacuated for 2 min at room temperature.

In a typical experiment both the MgO and MgO–$Mg(OH)_2$ samples were exposed to 25 Torr of sulfur dioxide for 3 min. After having pumped off the gas phase SO_2 for 1 min, the sample was exposed to 23 Torr of water for 15 min. Finally, 100 Torr of oxygen or nitrous oxide was introduced. The samples were then irradiated individually under four different sources of light; a 2537-Å uv lamp, a 3660-Å uv lamp, sunlight, and four daylight fluorescent lamps. At 2537 Å the shorter wavelength uv lamp has an intensity of 140 $\mu W/cm^2$ at the distance of 6 in.; whereas at 3660 Å the longer wavelength lamp has an intensity of 6250 $\mu W/cm^2$ at 15 in. The intensity of the four daylight fluorescent lamps are approximately equivalent to the average sunlight intensity at sea level. The sample was placed in the middle of the four lamps which were surrounded by a reflecting cylinder. Irradiation was carried out for various periods of time up to 72 hr.

The sulfur dioxide gas used in these experiments was obtained from J. T. Baker Chemical Co. Sulfur-33 enriched SO_2 was prepared by treating 3 mg of sulfur containing 25.5% ^{33}S with an excess of pure oxygen at 450° for 2 hr. Prior to the adsorption the excess O_2 in SO_2 and in $^{33}SO_2$ was removed by the freeze–pump technique.

The EPR spectra were recorded at room temperature and liquid nitrogen temperature, using a Model E-6S Varian spectrometer. The g values were determined relative to the Cr^{3+} impurity line which has $g = 1.9797$. The error in estimating the g values is believed to be ±0.0005. Spin concentrations were determined using a single crystal of copper sulfate as a standard. The estimated error in the absolute spin concentration is ±25%.

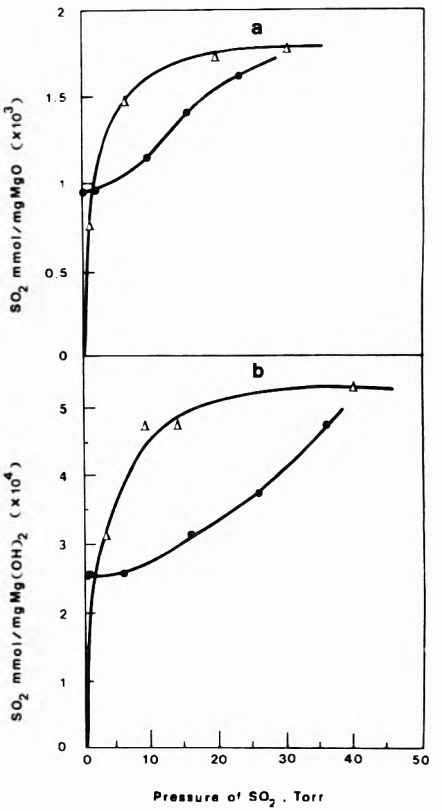

Figure 1. Adsorption isotherms of SO_2 at 25°: (a) on MgO; (b) on MgO–$Mg(OH)_2$; (Δ) adsorption; (●) desorption.

In the ir experiments a self-supporting MgO wafer was attached to a fused quartz holder. About 40 mg of the pretreated powder was used to make a wafer in a steel die at a pressure of 15 tons/in.^{2}. This wafer, which had an average thickness of 4 mg/cm^2, was then cut to a size of 0.9 cm × 2.0 cm. The sample was placed in an infrared cell and degassed under the conditions previously described. The spectra were recorded using a Beckman IR-9 spectrophotometer which was operated in transmittance mode. Silver bromide windows allowed us to cover the frequency range from 400 to 2000 cm^{-1}. The errors in assigning the wave numbers are estimated to be ±5 cm^{-1} for sharp bands and ±10 cm^{-1} for broad bands.

The adsorption experiments were carried out using a quartz spring with a sensitivity of 0.89 mm/mg. A cathetometer was used to detect the extension of the spring to a precision of ±0.1 mm. The BET surface areas of 158 and 64 m^2/g for MgO and MgO–$Mg(OH)_2$, respectively, were determined from nitrogen adsorption data.

Results

From the adsorption–desorption isotherms of Figure 1 one may conclude that 1.77×10^{-3} and 5.30×10^{-4} mmol of SO_2 was adsorbed per mg of MgO and MgO–$Mg(OH)_2$, respectively, at an equilibrium gas pressure of 25 Torr. Water was found to be adsorbed to a much greater extent than SO_2 (Figure 2). The monolayer coverages of SO_2 and H_2O are summarized in Table I where the area of an SO_2 molecule is taken as 19.2 Å^2 and the area of an H_2O molecule is 10.6 Å^2. Water was found to cover the surface to the extent of two to three monolayers, whereas less than a monolayer of sulfur dioxide was adsorbed following evacuation of excess SO_2.

TABLE I: Monolayer Coverage of SO_2 and H_2O

Sample	Reagent: SO_2 (25 Torr) followed by evacuation	Reagent: H_2O (23 Torr)
MgO	0.72	2.6
MgO–$Mg(OH)_2$	0.48	2.1

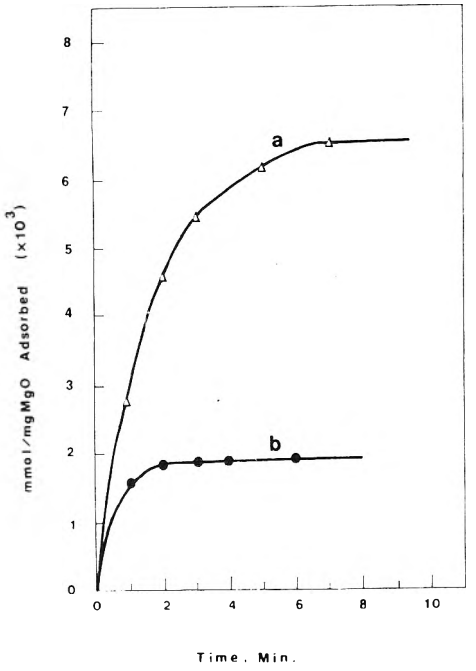

Figure 2. Adsorption of (a) H_2O (23 Torr) and (b) SO_2 (25 Torr) as a function of time for MgO at 25°.

After the adsorption of 25 Torr of SO_2 on the surface of MgO and MgO–$Mg(OH)_2$, a weak EPR signal of SO_2^- which is characterized by g_{xx} = 2.0014, g_{yy} = 2.0078, and g_{zz} = 2.003[4] was observed. The adsorbed species remained on the surface after pumping off the excess SO_2. After the addition of 23 Torr of water, the g_{yy} component of the SO_2^- spectrum was greatly reduced and the g_{xx} component vanished, while a new component at g = 2.0034 became apparent. After irradiation at 2537 Å a symmetric line with g value of 2.0034 was observed which is characteristic of SO_3^-.[7] A small peak of the remaining g_{yy} component of SO_2^- was frequently detected.

Upon the addition of 100 Torr of oxygen or nitrous oxide prior to irradiation, the intensity of the SO_3^- spectrum was increased by a factor of 3. It was also possible to form a small amount of SO_3^- by irradiating SO_2 on the surface of MgO in the ambient atmosphere; whereas, only SO_2^- was formed if the samples were irradiated under vacuum. The rate and extent of reaction to form SO_3^- increased with an increase in initial SO_2 concentration. A basic surface is preferred since the reaction was not observed on the surface of silica gel. The spectrum obtained using sulfur-33 enriched SO_2 is shown in Figure 3, and the presence of the four hyperfine lines with $a_\perp$ = 101 G and $a_\parallel$ = 142 G confirms the formation of $^{33}SO_3^-$. In contrast to the spectra of SO_3^- on dehydrated MgO[7] the spectra recorded with the sample at 77°K and 25° were the same.

TABLE II: Maximum Intensity of SO_3^- Obtained by Irradiating under the Four Sources (in Arbitrary Units)

Sample	Source: 2537 Å	Source: 3660 Å	Sunlight	4 daylight fluorescent lamps
MgO	115.4	20.2	6.3	10.0
MgO–$Mg(OH)_2$	16.8	2.0	1.0	4.3

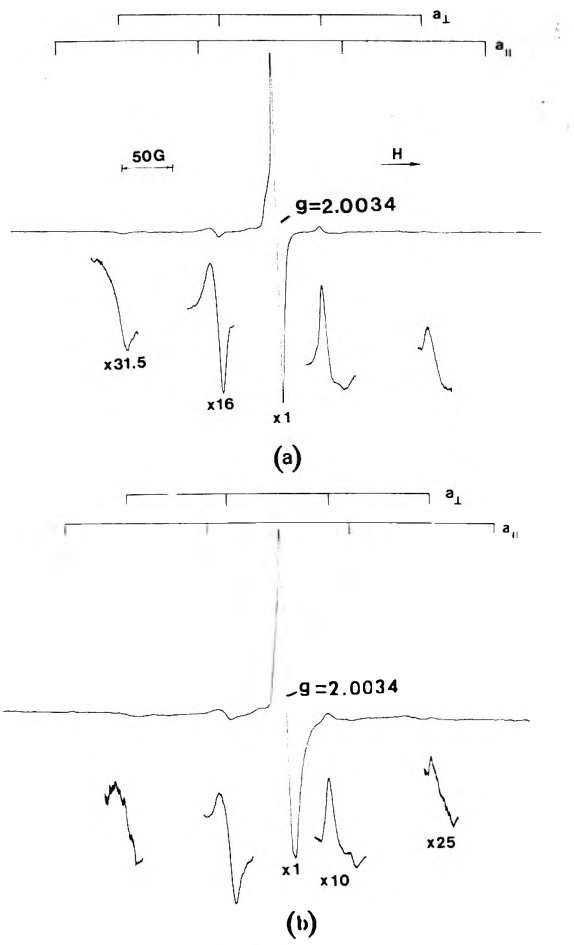

Figure 3. EPR spectra of $^{33}SO_3^-$ obtained by adding H_2O and O_2 to adsorbed $^{33}SO_2$ on the surface of MgO: (a) recorded at 25°; (b) recorded at 77°K.

The maximum intensity of the SO_3^- EPR signal was found to be greater upon irradiating with the shorter wavelength lamp (Table II). The final SO_3^- signal which was formed upon irradiation at 2537 Å was 5.7 times more intense than that which was formed upon irradiation at 3660 Å. The maximum signal of the resulting SO_3^- was 6.4 times stronger on MgO than on MgO–$Mg(OH)_2$. Exposure of the sample to direct sunlight also resulted in the formation of additional SO_3^-; however, the maximum signal was much less intense. Irradiation with four daylight fluorescent lamps gave a somewhat greater intensity.

If irradiation was begun immediately after the introduction of SO_2, H_2O, and O_2, an induction period of 24–36 hr was observed in the formation of SO_3^- (Figure 4); however, after allowing the sample to stand for 24 hr after the addition of the gases, no induction period was noted. A maxi-

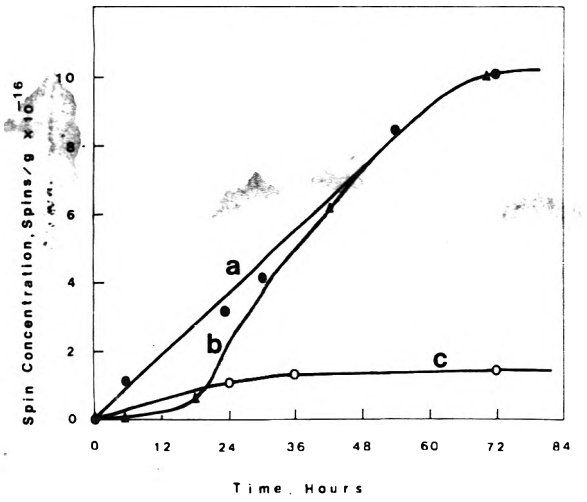

Figure 4. Spin concentrations of SO_3^- obtained by irradiating with a 2537-Å uv lamp vs. irradiation time: (a) with induction period on MgO, ●; (b) without induction period on MgO, ▲; (c) without induction period on MgO–$Mg(OH)_2$, O.

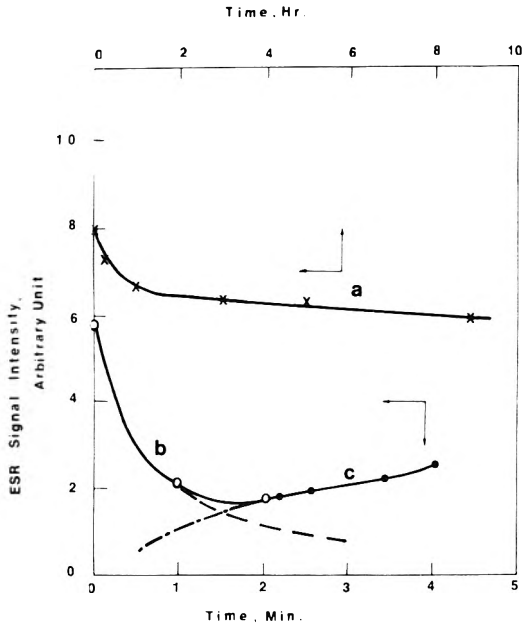

Figure 5. The stability of SO_3^- at 25 and 100°: (a) evacuating at 25°; (b) —— and - - - - -, heating at 100°; (c) - - - - and ——, SO_2^- re-forming.

mum spin concentration of 1.1×10^{17} spins/g of MgO was obtained by irradiating the reactants with the 2537-Å uv lamp for a period of 72 hr.

The resulting SO_3^- was found to be fairly stable, and the shape of the EPR spectrum remained unchanged after degassing the sample for 8 hr at room temperature. The addition of 500 Torr of oxygen to the sample with SO_3^- did not broaden the spectrum. The ion decomposed upon irradiation at 100° or upon heating for 2 min at 100° as shown in Figure 5. At that temperature water vapor was desorbed from the surface and the EPR spectrum showed that SO_2^- was formed.

In an attempt to identify the form of the surface species which were precursors of the SO_3^- ion infrared studies were carried out. Previous investigators[5,6] have failed to explore the 400–700-cm^{-1} region because of the opaqueness

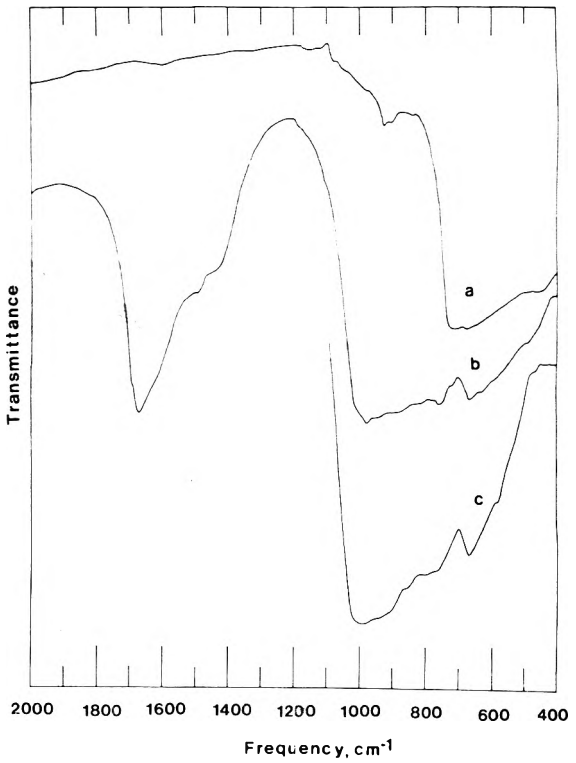

Figure 6. Infrared spectra of SO_2 and H_2O adsorbed on MgO: (a) background, (b) after 24 hr standing, (c) expanded scale.

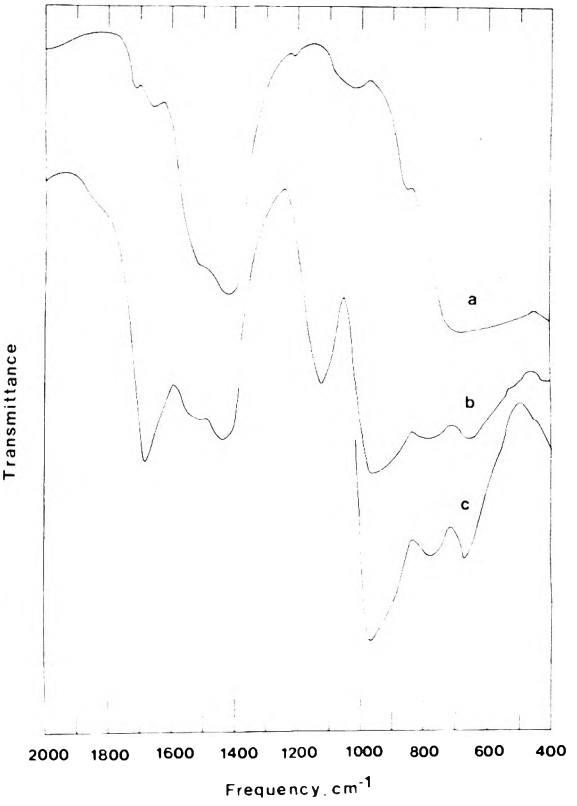

Figure 7. Infrared spectra of SO_2 and H_2O on MgO–$Mg(OH)_2$: (a) background, (b) after 24 hr standing, (c) expanded scale.

of the MgO films. In this work, both samples were slightly transparent in that region if the thickness of the wafer was approximately 4 mg/cm^2. Background spectra in the region

from 400 to 2000 cm^{-1} are shown as curves a of Figures 6 and 7 for MgO and MgO–$Mg(OH)_2$, respectively. After the addition of water to the sample, the physisorbed SO_2 species with bands at 1154 and 1340 cm^{-1}, as well as the remaining gas-phase SO_2 with bands at 1355, 1363, and 1379 cm^{-1}, disappeared. The band due to the symmetric stretch at 970 cm^{-1} became much more intense after the addition of water. The ir spectra of the species which were formed upon adsorption of SO_2 and H_2O after allowing the sample to remain for 24 hr at room temperature are shown as curves b and c of Figures 6 and 7. On MgO, new bands were found at 670, 990, and also 1680 cm^{-1}. Shoulders were also noted at 780, 930, and 1450 cm^{-1}. The shoulder at 1450 cm^{-1} is obviously due to the Mg–OH bending mode. The band at 1680 cm^{-1} is attributed to H–OH bending from molecular water. On MgO–$Mg(OH)_2$, new bands were detected at 670, 780, 970, 1130, and 1680 cm^{-1}. The Mg–OH bending band from 1420 to 1510 cm^{-1} was quite pronounced on the MgO–$Mg(OH)_2$ sample. The band at 1130 cm^{-1} did not form immediately after the adsorption of water, but grew with time. The addition of oxygen after the reaction of water and sulfur dioxide caused no change in band positions or intensities.

Discussion

The formation of SO_3^- in aqueous solutions is believed to occur via the photooxidation of sulfite ions and, as will be subsequently shown, the results from this study suggest that a similar mechanism is operative on the surface of a basic oxide. The EPR spectrum of SO_3^- at 77°K is found to be in good agreement with the earlier work on magnesium oxide.[7] In the present study the shape of the hyperfine lines was the same at both 25° and 77°K, indicating that the surface motion which was previously observed on the dehydrated samples at 25° was quenched by the presence of adsorbed water. Failure to observe any broadening by 500 Torr of molecular oxygen suggests that the SO_3^- is buried under several layers of water which are immobile at room temperature.

The infrared data provide reasonable evidence for the formation of sulfite ions on both samples. The simple sulfite ion is known to possess C_{3v} symmetry and four fundamental modes of vibrations: the symmetric stretching ν_1, symmetric bending ν_2, asymmetric stretching ν_3, and asymmetric bending ν_4. The fundamental frequencies of the SO_3^{2-} ion, for example, in the solid Na_2SO_3, appear at 1010 (ν_3), 961 (ν_1), 633 (ν_4), and 496 (ν_2) cm^{-1}.[11,12] The symmetric and asymmetric stretching vibrations, however, are sometimes very close to one another and are not resolved.[13] For the monodentate sulfito compounds, two structures are possible; coordination through sulfur and coordination through oxygen. Cotton and Francis[14] predicted that a shift to higher frequencies of the S–O stretching would be expected when coordinating through the sulfur. In addition, the band near 960 cm^{-1} is generally much sharper. Coordination through oxygen would lower the symmetry to C_s, and only three stretching vibrations would be expected due to the removal of the degeneracy in ν_3.[13] Occasionally an additional weak peak is also present near 1000 cm^{-1} due to an overtone.

The infrared spectra obtained in this work correlate reasonably well with the frequencies of sulfite ions and monodentate sulfito complexes. On MgO the band at 670 cm^{-1} corresponds to the symmetric bending, ν_4; whereas bands at 930–1000 cm^{-1} correspond to the symmetric stretch, ν_1, and may have some unresolved asymmetric stretch, ν_3. A band corresponding to the symmetric bending mode, ν_2, was not detected. Bands of MgO–$Mg(OH)_2$ appear at nearly the same position as those of MgO, except the band at 1130 cm^{-1} which grows with time. The band is attributed to a new sulfur-bonded sulfito ligand. The band near 780 cm^{-1} which was also observed by Schoonheydt and Lunsford[5] on the desorption of SO_2 at room temperature may be due to the existence of a strongly complexed sulfinato species, but this is difficult to verify by this experiment.

The participation of water in this reaction is important since only the EPR spectrum of SO_2^- was observed when SO_2 on MgO or MgO–$Mg(OH)_2$ was irradiated in the absence of adsorbed water. The much more intense band at 970 cm^{-1} after the addition of water indicates a greater concentration of the SO_3^{2-} ion.

In aqueous solution it has been proposed that water displaces the OH^- on bisulfite acid according to the following mechanism:[15]

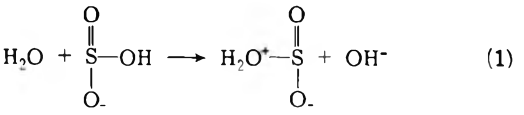

(1)

and

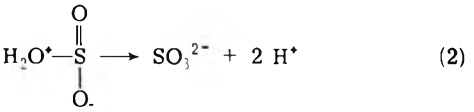

(2)

It is reasonable to assume that the reaction is carried out on the surface in the same fashion. Previous work[5] has shown that the surface hydroxyl ion strongly interacts with adsorbed SO_2; therefore, it is reasonable to expect that $HOSO_2^-$ is present on the surface. Water may attack $HOSO_2^-$ molecules subsequently and forms sulfite ions. The monodentate sulfito complex may be produced in a similar manner:

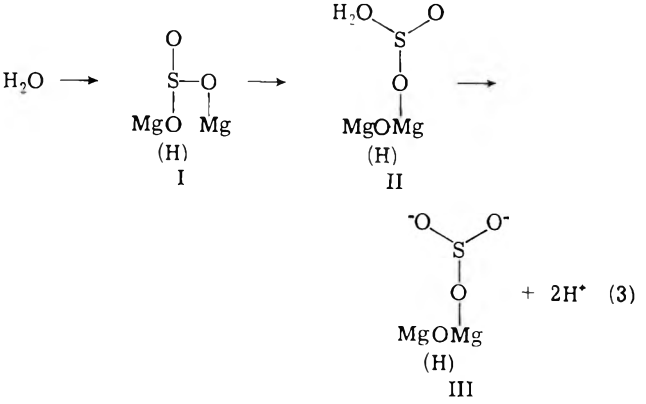

(3)

Both in the sulfite ion and the sulfito complex the third oxygen atom is thought to be derived from the water. Presumably on MgO–$Mg(OH)_2$ the surface species II also reacts with the hydroxide ion and rearranges to form the sulfur-bonded species over a period of 24 hr.

In aqueous sulfite solutions wavelengths less than 2500 Å were required to produce the SO_3^- ion.[16] On MgO and MgO–$Mg(OH)_2$, the process to produce SO_3^- from sulfites or sulfito complexes may involve the surface as an excited initiator similar to the photosensitization of aqueous sulfite solutions with ketones.[16] The excited MgO or MgO–$Mg(OH)_2$ which is formed by absorbing photochemical en-

ergy may react with the sulfites to produce an excited state in the ion. The excited sulfite ions may then release one electron to form SO_3^- according to the reaction

$$SO_3^{2-} \xrightarrow[MgO]{h\nu} SO_3^- + e_{aq}^- \quad (4)$$

Dogliotti and Hayon[17] studied this reaction by the photolysis of sulfite ions in solution. Later the absorption spectra of SO_3^- and e_{aq}^- were used to confirm the products.[18] More recently, Chawla et al. studied the same reaction and confirmed the formation of SO_3^- by its EPR spectrum.[16]

It was also observed in the solution studies that O_2 and N_2O increased the steady state concentration of SO_3^-. In the case of N_2O it has been proposed that the following reactions occur:[16-19]

$$e_{aq}^- + N_2O \xrightarrow{H_2O} OH + OH^- + N_2 \quad (5)$$

$$OH + SO_3^{2-} \longrightarrow SO_3^- + OH^- \quad (6)$$

thus N_2O serves both as a scavenger for the solvated electron and as a source of OH radicals. Presumably O_2 also traps an electron forming O_2^-, but this anion radical must react rapidly with water since there was no evidence for it in the EPR spectra.

The striking difference between the behavior of SO_3^- on the surface and in aqueous solution is found in the greatly increased stability of the ion on MgO or MgO–$Mg(OH)_2$. In solution, for example, the reaction

$$2SO_3^- \longrightarrow S_2O_6^{2-} \quad (7)$$

occurs with a rate constant of $2k = 1 \times 10^9\ M^{-1}\ sec^{-1}$;[18] whereas, the SO_3^- ion was stable on the surface for many hours. This increase in stability is attributed to the lack of mobility which the SO_3^- ion has on the surface. Another difference between the surface and the solution reactions is found in the reactivity of SO_3^- with O_2. In aqueous solution Hayon et al.[18] have proposed that the reaction

$$SO_3^- + O_2 \longrightarrow SO_5^- \quad (8)$$

is very rapid and is an important step in the oxidation of sulfite ions to sulfate ions.[18] In the present study there was no indication that O_2 reacted with SO_3^-. The absence of broadening of the EPR spectrum by molecular oxygen suggests that the SO_3^- is located in some inaccessible site on the surface.

As the temperature of the surface approaches 100° the mobility of the water and the SO_3^- must become more similar to that of aqueous solutions. At the elevated temperature the disappearance of the SO_3^- ion may be attributed to reactions 8 and 9. It is possible that the reaction

$$SO_3^- + SO_3^{2-} \longrightarrow SO_2^- + SO_3^{2-} \quad (9)$$

may lead to the formation of SO_2^- which was detected.

Conclusions

These results show that the heterogeneous photooxidation of SO_2 occurs on magnesium oxide particles. Apparently sulfite ions and monodentate sulfito complexes are formed on the surface of MgO and MgO–$Mg(OH)_2$ in the presence of sulfur dioxide and water, though the bonding in the presence of water may be different on the two surfaces. It is believed that water reacts with the adsorbed SO_2 to increase the concentration of sulfite ions and monodentate sulfito complexes on the surface. Upon irradiation the excited sulfite ions form SO_3^- by losing one electron. This ion may be a precursor to the formation of adsorbed sulfates in urban particulates.

Acknowledgment. This investigation was supported by research Grant No. R801136, Air Pollution Control Office, Environmental Protection Agency.

References and Notes

(1) C. M. Shy and J. F. Finklea, *Environ. Sci. Technol.*, **7**, 204 (1973).
(2) W. L. Faith and A. A. Atkisson, Jr., "Air Pollution", 2nd ed, Wiley-Interscience, New York, N.Y., 1972, p 19.
(3) A. C. Stern, Ed., "Air Pollution", Vol. I, Academic Press, New York, N.Y., 1962, Chapter 10.
(4) R. A. Schoonheydt and J. H. Lunsford, *J. Phys. Chem.*, **76**, 323 (1972).
(5) R. A. Schoonheydt and J. H. Lunsford, *J. Catal.*, **26**, 261 (1972).
(6) A. J. Goodsel, M. J. D. Low, and N. Takezawa, *Environ. Sci. Technol.*, **6**, 268 (1972).
(7) Y. Ben Taarit and J. H. Lunsford, *J. Phys. Chem.*, **77**, 1365 (1973).
(8) R. T. Cheng, M. Corn, and J. O. Frohliger, *Atomos. Environ.*, **5**, 987 (1971).
(9) P. Urone and W. H. Schroeder, *Environ. Sci. Technol.*, **3**, 436 (1969).
(10) H. F. Johnstone and D. R. Coughanowr, *Ind. Eng. Chem.*, **50**, 1169 (1958).
(11) J. C. Evans and H. J. Berstein, *Can. J. Chem.*, **33**, 1270 (1955).
(12) K. Nakamoto, "Infrared Spectra of Inorganic and Coordination Compounds", Wiley, New York, N.Y., 1963, p 87.
(13) G. Newman and D. B. Powell, *Spectrochim. Acta*, **10**, 213 (1963).
(14) F. A. Cotton and F. Francis, *J. Am. Chem. Soc.*, **82**, 2986 (1960).
(15) W. A. Pryor, "Mechanisms of Sulfur Reactions", McGraw-Hill, New York, N.Y., 1962, p 65.
(16) O. P. Chawla, N. L. Arthur, and R. W. Fessenden, *J. Phys. Chem.*, **77**, 772 (1973).
(17) L. Dogliotti and E. Hayon, *J. Phys. Chem.*, **72**, 1800 (1968).
(18) E. Hayon, A. Treinin, and J. Wilf, *J. Am. Chem. Soc.*, **94**, 47 (1972).
(19) D. Behar and R. W. Fessenden, *J. Phys. Chem.*, **76**, 1710 (1972).

Proton Beam Radiolysis of Matrix Samples. A New Technique for Infrared Spectroscopic Study of Charged Molecular Intermediates

Ralph O. Allen, Joseph M. Grzybowski, and Lester Andrews*

Department of Chemistry, University of Virginia, Charlottesville, Virginia 22901
(Received August 5, 1974; Revised Manuscript Received February 12, 1975)

A radio-frequency ion source capable of delivering 2.0-keV protons has been mated with a matrix-isolation apparatus and techniques for irradiating matrix samples with protons have been developed. Proton beam radiolysis of Ar/CCl_4 = 400/1 samples during 15°K deposition has produced a number of new infrared absorptions. Nernst glower photolysis of the matrix sample through a glass filter passing 500–3000-nm radiation, which is capable of releasing chemically trapped electrons, markedly reduced infrared absorptions at 1020, 927, 502, 374, and 290 cm^{-1}. These bands were assigned to isolated cations owing to their disappearance following the addition of thermal electrons to the sample. The chemical fate of the bombarding proton was also observed by this technique.

Introduction

Radiolysis of molecular solids produces free radicals, cations, and trapped electrons. Fundamental processes in the radiation chemistry of organic compounds in the solid state have been reviewed by Willard[1a] and radiolysis studies of carbon–halogen compounds have been recently discussed by Bühler.[1b] Of foremost interest is the fate of the electrons and cations produced by the incident ionizing radiation. γ radiolysis of solid CCl_4 at 77°K produced a near uv band attributed to a cationic species which was bleached by tungsten light or sample warming to 143°K.[2] Carbon tetrachloride is known to be an effective scavenger of electrons produced by ionizing radiation[3,4] which makes CCl_4 an interesting subject for studies in radiation chemistry.

Most of the early spectroscopic studies of radiation damage to solids have been limited to ESR and optical spectra. The extensive ESR work of Fessenden and coworkers[5] has, of course, been limited to free-radical radiolysis products. We report here a new experimental technique for producing and studying infrared spectra of charged *and* free-radical radiolysis products. This method involves proton beam irradiation of matrix samples during 15°K deposition which traps a large number of the intermediate radiolysis products. The matrix isolated cations can be reduced with thermal electrons which provides a means of discrimination between neutral and positively charged molecular species. Furthermore, chemically trapped electrons can be photodetached to neutralize the matrix isolated cations.

Another aspect of this technique is the possibility of studying the chemical fate of a high-energy charged particle such as a proton. Zeller et al.[6a] have shown that in solids, proton bombardment causes such solid state effects as the formation of color centers and the formation of radicals containing the bombarding hydrogen in a chemically bound form. Thus, the procedure described below provides a means of adding reactive hydrogen atoms as a reagent to study these binding effects.

Experimental Section

The proton beam with kinetic energies of up to 2.0 keV and currents up to 23 μA is provided by a High Voltage Engineering Model CSO-163 radio-frequency ion source of the type used for van de Graaff accelerators. Hydrogen is leaked into the Pyrex source, illustrated in Figure 1, through a small needle valve, then ionized and dissociated by a high-frequency oscillator operated at 60 MHz. In the rapidly reversing field the electrons move back and forth many times before being captured by the container walls so that efficient ionization occurs in the source at hydrogen pressures on the order of 50 μ. A magnetic field provided by a solenoid around the Pyrex source reduces the rf power requirements by restricting electron paths thus improving ionization efficiency and aiding in the extraction of the positive ions. Nevertheless, both the ion source and the rf source must be cooled by blowers during operation.

These sources are designed so that a large fraction (90%) of the extracted beam is the atomic ion (H^+). Parameters such as pressure, rf power, and magnet current are adjusted to give an intense red plasma indicative of a high percentage of monoatomic H^+ rather than the blue color of the molecular H_2^+ ions. The beam is extracted and accelerated to the desired energy by the positive potential applied to a small tungsten anode or probe at one end of the vessel. The extraction canal (1 mm i.d.) at the opposite end consists of a cylindrical aluminum tip which protrudes into the vessel and is hidden from the discharge by an insulating quartz sleeve mounted over the canal tip.[6b] Since the plasma is essentially at anode potential, almost all of the applied potential is across the cathode dark space. Thus, with proper design of the aluminum canal which is held at ground potential and the insulating sleeve which covers it, a large number of the positive ions which are extracted travel along paths which do not intercept the cathode walls. The extracted beam is electrostatically focused by applying a positive potential (about 80% of the anode potential) to a cylindrical electrode in order to maximize the fraction of the beam reaching the target area 67 cm down the beam tube. At the target, the beam is limited to a 5.6-cm diameter circle by an insulated stainless steel collimator. This collimator is continually discharged through a microammeter providing a means of monitoring the current from the source. Prior to actual operation, the settings for maximum beam on the target are found by isolating a Faraday cup on the beam line at the same distance from the source as used for the actual target. The matrix sample receives approximately 20% of the beam irradiating the target area.

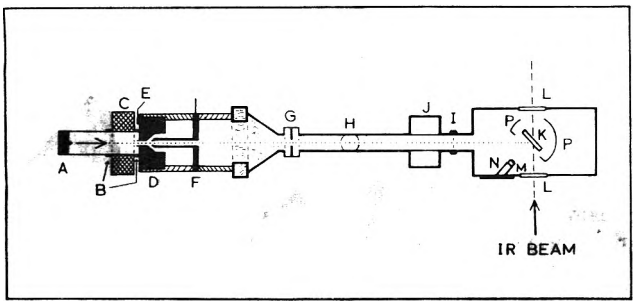

Figure 1. Experimental apparatus used to produce and observe ions and radicals. A is the probe of the rf ion source to which a positive potential of up tc 2000 V is applied. A plasma is created in the Pyrex cylinder by the oscillating potential between two brass rings (B) on the outside of the cylinder. The ring magnet (C) increases ionization efficiency and aids in the extraction of ions through the aluminum canal in the base (D) which is at ground potential. The gas to be ionized is emitted into the ion source (E) through another canal in the base. The extracted ion beam is focused by the adjustable positive potential on electrode F. The body of this portion of the apparatus is made of plexiglass in order to insulate the electrodes. The beam is collimated by stainless steel ring G which is insulated from the rest of the system and the current measured on the ring is used to monitor the performance of the ion source during an experiment. A diffusion pump below and an ion gauge above the plane at H allows this portion of the system to be evacuated independently by closing gate valve J and disconnecting APC connector at I. K is the CsI sample window attached to the 15°K refrigeration stage of a 3-W closed-cycle helium refrigerator. Two other CsI windows on the vacuum vessel (L) allow the infrared beam to pass through the sample which was deposited through a Cu nozzle (M) directed normal to K. The bare light bulb filament used to titrate cations is in position N. A radiation shield (P) improves the cooling efficiency of the refrigerator.

Four beam kinetic energies were used in these experiments, 0.5, 1.0, 1.5, and 2.0 keV. Owing to less efficient proton extraction at lower beam energy, the proton currents for these energies were 2, 7, 13, and 23 μA, respectively. A separate pumping system, cold cathode ionization gauge, and gate valve allowed the ion beam line to be separated from the target between experiments and maintained under vacuum.

The target for the argon matrix deposition was a $\frac{7}{8}$ in. × 1.25 in. CsI window cooled to 15°K by a Model 340 LS (Cryogenic Technology, Inc.) closed-cycle helium refrigerator. The argon was mixed with the reagent gas and the mixture entered the vessel through a copper tube directed toward the CsI window.[7] Since the target is an electrical insulator, charge builds up on the window during proton irradiation. Electrical charge on the CsI window during an actual experiment was verified by a Keithley 610 C electrometer and recorder connected to an insulated metal plate placed on the back face of the CsI sample window. The bare filament of a 12-V, 2.4-W light bulb placed 5 cm from the target can neutralize this excess charge when current flows through the filament since thermal electrons are attracted to the positively charged target. Photolysis and heating effects of the bulb were examined by operating a bulb with the glass globe intact. An aluminum shield partially surrounding the target reduced radiation heating of the sample.

The vacuum chamber was mounted in the sample compartment of a Beckman IR-12 filter-grating spectrophotometer so that the proton beam was in the same horizontal plane and perpendicular to the light beam, as is shown in Figure 1. The target window was positioned at a 45° angle to both beams, although by rotating the refrigerator, the window can be placed perpendicular to the spectrometer beam. Nernst glower photolysis of the sample was prevented during deposition in a number of experiments by blocking the source beam; visible and near-infrared light were kept from the sample while recording spectra by using a Kodak No. 220 far infrared transmitting filter (400–4000 cm^{-1}) or a MgO scatter plate. Photolysis studies were performed using the full Nernst source filtered by several colored glass filters.

Results and Discussion

Proton Bombardment. In order to observe any possible effects due to proton irradiation of the matrix, about 4 × 10^{-3} mol of argon (only) was deposited onto the CsI window and then the beam of 2-keV protons was turned on for 16 hr during which time another 0.03 mol of argon was sprayed onto the window. The physical properties of the matrix were not affected, and no bands were observed in the infrared spectrum. In another experiment a mixture of Ar and CCl_4 (Ar/CCl_4 = 400/1) was deposited for 10 hr and then irradiated with 0.5-keV protons for 11 hr and with 2-keV protons for 7 hr. The infrared spectrum showed only bands due to the reagent CCl_4. This is not unexpected since the penetration of 2.0-keV protons into solid argon is 1.3 × 10^{-5} cm (a maximum range calculated using extrapolations of data given by Northcliffe and Schilling[8]) while the thickness of argon on the sample window after 10 hr of deposition is on the order of 2 × 10^{-2} cm. Since such a small portion of the sample ($\frac{1}{1000}$) was affected by the proton bombardment, any radiation produced species would be at concentrations below our sensitivity of detection.

If, however, after an initial deposition of about 10^{-2} mol of the Ar–CCl_4 mixture, the proton beam was used to irradiate additional sample *during* its deposition on the window, several new intense bands were observed at 1037, 1020, 927, 898, 746, 502, 374, and 290 cm^{-1}. Trace a of Figure 2 illustrates a typical spectrum after 1.0-keV proton irradiation and sample deposition for 11 hr. The difference between infrared spectra observed for proton irradiation after and during the deposition of the sample indicates that the radiolysis products are produced on the sample surface during the condensation process and are then trapped in the argon matrix. Although it is difficult to estimate a gas pressure between the deposition nozzle and the 15°K window 5 cm away, a pressure of 1 μ appears reasonable. The mean free path for argon at 25° and 10^{-3} mm pressure is 8 cm. Accordingly, it is unlikely that any of the radiolysis observed here takes place in the gas phase; the radiolysis must occur on the surface of the matrix during sample condensation.

The new infrared absorptions were unstable. Comparison of the spectrum recorded after 11 hr of proton irradiation and sample deposition (Figure 2a) with that recorded after an additional 9 hr without blocking the Nernst glower source (Figure 2b) shows that the bands at 1020, 927, 502, 374, and 290 cm^{-1} decreased in intensity while the 1037- (0.33 OD) and 898-cm^{-1} (0.37 OD) absorptions increased to the given optical densities. In the 2.0-keV experiments reported in Table I, spectra recorded using the Kodak filter to block the Nernst glower showed that all of these bands increased through the complete deposition period. Also, further proton irradiation of a deposited sample decreased the bands at 1020-, 927-, 502-, 374-, and probably the weaker 290-cm^{-1} absorption, without much effect on the 1037- and 898-cm^{-1} bands. The former new absorptions appear to be due to extremely reactive species whose physical characterization is described below.

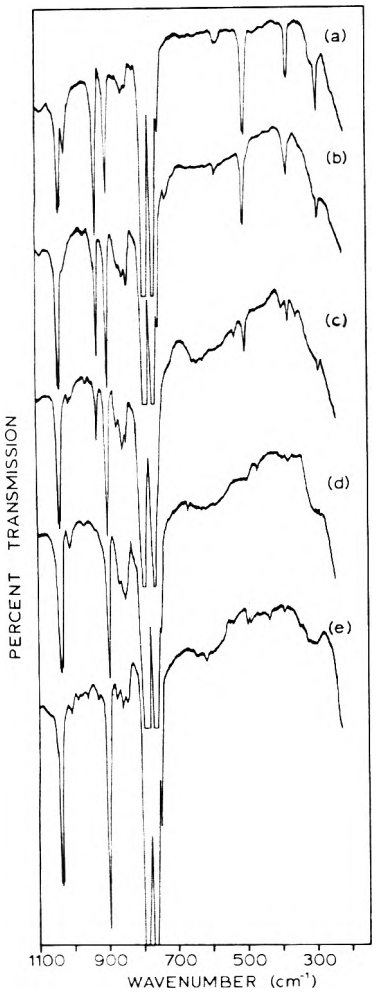

Figure 2. Infrared spectra in the 200–1100-cm^{-1} region for an Ar/CCl_4 = 400/1 sample deposited at 15°K for 11 hr while being bombarded with 1.0-keV protons (a) and after an additional 9 hr of deposition and bombardment (b). Subsequent exposure of the same sample to thermal electrons for 3 hr from filament with 5 V results in c. After 2 hr more exposure to the bulb filament at 10 V, the complete neutralization shown in d was observed. Trace e illustrates the spectrum for another sample deposited during bombardment with 1.0-keV protons and thermal electrons.

Detection of Positive Charge. In order to learn more about the physics of proton beam deposition into a matrix sample, a 1 in. × 0.25 in. copper plate was placed on the back surface of the CsI target and electrically insulated from the copper block. During sample deposition, this plate was monitored by an electrometer set on the 10^{-12} C range. No quantitative measure of charge buildup on the CsI window was possible; however, the meter oscillated ±20% of full scale with periods of less than 1 sec. This oscillation, observed only with the proton beam striking the sample, was recorded as a 150 unit (arbitrary) noise level; shutting off the beam by reducing the accelerating voltage to zero instantly stabilized the meter to a recorder noise level of 2 units. This coulometer oscillation is indicative of rapid charging and discharging of the sample during proton bombardment. Since this charging and discharging process took place in a fraction of a second, a ball-park measure of the charge accumulated by the sample before discharge is on the order of microcoulombs, which is the beam current for this brief period.

The charge–discharge process as determined by the meter oscillation was instantly quenched by turning on the bare filament of the light bulb which had no effect on the electrometer when the filament was operated alone. The recorder output gave a 2 unit noise level with both proton beam and bulb filament operating which produced an electrically neutral sample. Shutting off the filament immediately restored the 150 unit noise level caused by the proton beam charging the sample and its rapid discharge. This demonstrates that thermal electrons attracted to the positively charged sample from the bulb filament neutralized positive charge in the target sample.

Infrared spectra of the radiolysis products were also altered by the bulb filament. Figure 2c shows the effect of operating the bulb filament at 5 V for 3 hr. Changes from trace b are obvious, the 1020-cm^{-1} shoulder and the 927-, 502-, 374-, and 290-cm^{-1} bands decreased in intensity. After allowing current to flow through the bulb filament for another 2 hr with the voltage increased to 10 V, the bands at 927, 502, 374, and 290 cm^{-1} completely disappeared and 1020-cm^{-1} band was replaced by a 1010-cm^{-1} band as shown in Figure 2d. Note that the bands at 1037 and 898 cm^{-1} were unchanged. The latter band is due to the CCl_3 free radical.[7] Although the former band has been assigned[9] to CCl_3^+, its stability upon neutralization of the matrix indicates that it is not an isolated cation.

Figure 2e shows the vibrational spectrum of an 18-hr run where the Ar–CCl_4 mixture *and* proton beam were codeposited *and* the light bulb filament was operated during the entire process. In this neutralized sample, the species absorbing at 1020, 927, 502, 374, and 290 cm^{-1} were not trapped and the yield of the 1037-cm^{-1} (0.47 OD) absorber increased slightly and the CCl_3 radical band at 898 cm^{-1} (0.80 OD) doubled. A 2.0-keV proton experiment was conducted with the light bulb operating during deposition in an orientation normal to the proton beam such that radiation from the filament could not reach the sample but some thermal electrons could be attracted into the matrix. The yields of the 1020-, 927-, 502-, 374-, and 290-cm^{-1} bands were reduced 60% relative to the identical experiment without thermal electrons whereas the 898-cm^{-1} CCl_3 band increased by 40% and the 1037-cm^{-1} band decreased by 10%.

The increase in CCl_3 radical yield with the addition of extra electrons to the sample arises from the dissociative electron capture of CCl_4.

$$CCl_4 + e^- \rightarrow CCl_3 + Cl^- \quad (1)$$

In the deutron bombardment experiment illustrated in Figure 3, the spectroscopic effect of adding thermal electrons to the sample is clearly demonstrated. A 25-min period of electron deposition almost completely destroyed the 1020-, 927-, 502-, and 374-cm^{-1} bands and reduced the 290-cm^{-1} band to less than half of its original intensity. The intensity data are recorded in Table I (experiment 1).

The heating and photolytic effects of the bulb filament were considered. Operation of the filament at 10 V produced an increase in the sample block temperature from 15°K to between 16 and 17°K in all of the experiments which is clearly insignificant as far as the matrix sample is concerned. In another experiment (Table I, experiment 2) a sample was prepared with proton irradiation and the bulb filament was operated in a position perpendicular to the proton beam such that the filament was hidden from the sample by a quartz tube wrapped with aluminum foil. The original optical densities and those following this partial

TABLE I: Optical densities (OD) of New Absorption Bands (cm^{-1}) Produced by 2.0-keV Proton Beam Irradiation of Ar/CCl_4 = 400/1 Samples during Deposition at 15°K in the Absence of Nernst Glower Light

Experiment	1037	1020	927	898	746	502	374	290	242
1, 22 hr	0.45	0.09	0.38	>2.0	0.6	0.17	0.11	0.11	*a*
b	0.40	0.02	~0.02	>2.0	0.6	0.01	0.01	0.05	
2, 10 hr	0.30	0.17	0.71	2.0	0.37	0.33	0.17	0.15	*a*
c	0.27	0.09	0.51	2.0	0.37	0.21	0.11	0.09	
d	0.26	0.07	0.46	2.0	0.37	0.19	0.11	0.08	
3, 11 hr	0.28	0.16	0.66	1.4	0.3	0.28	0.15	0.12	*a*
e	0.28	0.04	0.22	1.4	0.3	0.10	0.07	0.04	
f	0.29	0.01	0.17	1.4	0.3	0.07	0.04	0.02	
g	0.26	0.0	0.01	1.4	0.3	0.0	0.0	0.0	
4, 11 hr	0.28	0.15	0.64	2.0	0.4	0.30	0.15	0.13	0.03
h	0.26	0.08	0.39	2.0	0.4	0.16	0.09	0.07	0.03
i	0.27	0.04	0.23	2.0	0.4	0.11	0.05	0.03	
j	0.27	0.02	0.15	2.0	0.4	0.06	0.03	0.00	0.0
5, 12 hr	0.21	0.28	1.8	>2	0.7	0.83	0.35	0.39	0.15
k	0.21	0.23	1.6	>2	0.7	0.65	0.25	0.30	0.10
l	0.19	0.09	0.46	>2	0.7	0.22	0.10	0.09	0.03
m	0.18	0.05	0.35	>2	0.7	0.17	0.09	0.09	0.03

[a] Observed as unresolved shoulder. [b] Bare filament operated at 10.5 V for 25 min. [c] Bare filament oriented normal to proton beam out of direct line with sample and operated at 10.5 V for 8 hr. [d] Sample exposed to Nernst glower radiation filtered through Corning 4303 glass. [e] Covered bulb directed at sample operated at 10.5 V for 1.0 hr. [f] Same as *e* for 0.5 hr more (1.5 hr total). [g] Same as *f* for 6.0 hr more (7.5 hr total). [h] Exposed filament directed at sample operated at 10.5 V for 20 min. [i] Same as *h* for 23 min more (43 min total). [j] Same as *i* for 17 min more (60 min total). [k] Sample exposed to full Nernst glower light for 1.5 hr. [l] Same as *k* for 10.5 hr more (12 hr total). [m] Sample exposed to covered filament at 10.5 V for 0.5 hr.

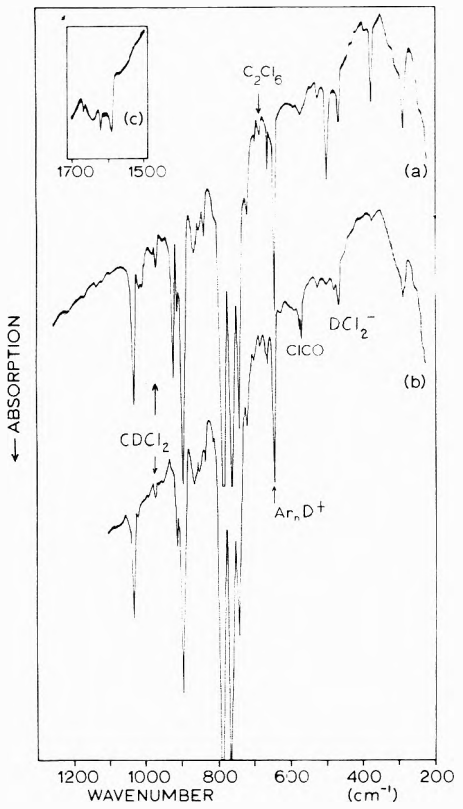

Figure 3. Infrared spectrum in the 200–1300-cm^{-1} region for an Ar/CCl_4 = 400/1 sample deposited at 15°K with 2.0-keV deuteron bombardment for 22 hr is illustrated in a. Trace b is for the same sample obtained after subsequent exposure to thermal electrons for 25 min from bulb filament operated at 10.5 V. The inset (trace c) displays the ν_2 bend region of H_2O for this sample, and illustrates the minor amount of water present (0.06 OD) as an impurity.

neutralization are listed in Table I. A 40% reduction in intensity of the five bands was affected by this relatively inefficient means of adding thermal electrons to the sample without electromagnetic radiation.

Photolysis by the bulb filament without thermal electrons was determined by using a complete bulb with the glass globe intact directed normal to the sample. Intensity data for the absorptions in an initial sample and following covered bulb operation for 1.0, 1.5, and 7.5 hr are listed in Table I as experiment 3. Note the essentially complete disappearance of the five bands. An identical experiment was done the following day with the bare filament from the same bulb in the same position; the intensity data for bare filament operation for 20, 43, and 60 min are listed as experiment 4 in Table I.

It is clear that the five bands of interest decrease faster when exposed to a bare heated filament as compared to the same filament covered by the bulb globe. Table II compares the percent decreases for the five bands exposed to the same covered and uncovered filament. Note that the ratios of percents decreased with the globe removed/covered for the first 20 min show a substantially greater (average factor of 1.8) decrease for the exposed filament. The last column lists the half-lives for the five bands which average a factor of 1.8 longer for the covered filament. The greater rate of decrease of the five absorptions with the bare filament is attributed to the addition of thermal electrons from the filament since the soft glass bulb globe (0.025-in. thick) is almost completely transparent to radiation from 3000 Å to below 25,000 Å but it cannot transmit thermal electrons.

Photobleaching. In several experiments, the effect of Nernst glower photolysis on the infrared spectrum was examined. First an Ar/CCl_4 = 400/1 sample was deposited with 2.0-keV protons for 12 hr with the light source blocked. The 1020-, 927-, 502-, 374-, and 290-cm^{-1} absorp-

TABLE II: Comparison of Percentage Decreases and Half-Lives of the Optical Densities for Five Absorptions Exposed to the Same 2.4-W Bulb Filament Operated at 10.5 V Covered (C) by the Lamp Globe and with the Globe Removed (R)

Absorptions, cm^{-1}	% decrease						Ratio, % decrease R/C for first 20 min	Absorption half-life, min	
	20 min		43 min		60 min				
	C	R	C	R	C	R		C	R
1020	27	47	56	73	75	87	1.7	40	23
927	29	39	55	64	66	77	1.4	38	29
502	23	47	50	63	63	80	2.0	45	25
374	18	37	46	66	54	77	2.1	60	28
290	25	46	46	77	71	100	1.8	40	25

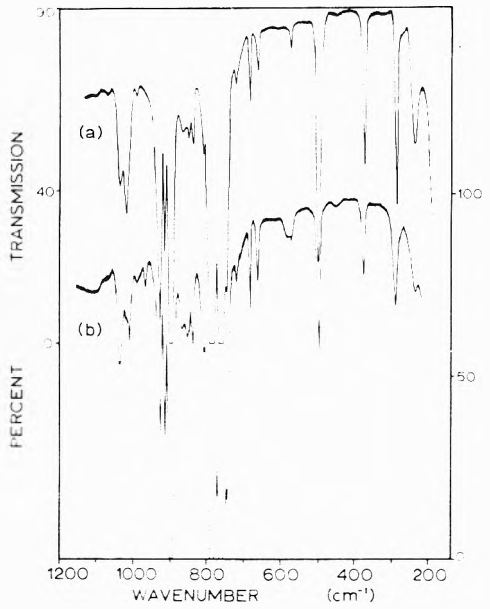

Figure 4. Infrared spectrum from 200 to 1100 cm^{-1} shown in trace a for an Ar/CCl_4 = 400/1 sample deposited at 15°K for 12 hr during 2.0-keV proton irradiation with Nernst glower source blocked. Spectrum b recorded after 12 hr of sample exposure to full light of Nernst glower with chopper operating. Transmission scale for spectrum a at left; scale for b on right.

tions were significantly more intense than in previous runs where the sample was exposed to the glower radiation, even with the glower current reduced. Figure 4a illustrates the spectrum in this extraordinarily productive experiment, which is in marked contrast to Figure 2a; the absorption intensities are listed in Table I as experiment 5. Trace b of Figure 4 shows the spectrum recorded after sample exposure to the full light of the Nernst glower (chopper operating) for 12 hr. Notice the major reduction in the 1020-, 927-, 502-, 374-, and 290-cm^{-1} band intensities. Expressed as a percent decrease, the bands of interest decreased as follows during 1.5 hr of full exposure to Nernst radiation: 1037(0%), 1020(16%), 927(8%), 502(21%), 374(28%), and 290(23%). Nernst photolysis for a total of 12 hr reduced the latter five bands by 65 ± 7%. In this experiment a moderately intense (0.15 OD) band was observed at 242 ± 2 cm^{-1}, which had been observed previously as a resolved shoulder. The 242-cm^{-1} band was also decreased by Nernst photolysis. Comparison between the product optical densities for 2.0-keV experiments using unblocked and blocked Nernst sources shows an increase in yields of the five bands when the sample was deposited in the absence of visible and near-infrared radiation.

In order to isolate the wavelength of photolysis light responsible for bleaching the five bands, the Nernst radiation was passed through colored glass filters. First, another sample was deposited in the absence of light and the spectra were recorded using the Kodak 220 filter or the MgO scatter plate. The sample was exposed to far-infrared radiation (400–4000 cm^{-1}) passing through the 220 filter for 13 hr and no decrease was observed in any of the five bands. The sample was then exposed to the 5000–30,000-Å Nernst output for 2 hr (OG-515 filter, Fish-Schurman Corp.) and the band intensities decreased substantially; the percent decrease from their original intensities are given in parentheses: 1037(0%), 1020(31%), 927(7%), 502(28%), 374(37%), and 290 cm^{-1} (21%). Exposure to radiation passing through a Corning 4303 (passes 3800–5400-Å radiation) filter produced no measurable changes in the bands of interest. Experiment 2 in Table I also shows a minimal effect for the Corning 4303 filtered Nernst photolysis of the sample.

From the above studies, it is apparent that the major amount of photobleaching of infrared absorptions occurs with radiation from the near-infrared through the green visible (5000 Å). The photochemistry of trapped electrons in the radiolysis of methyltetrahydrofuran[10] and 3-methylpentane[11a] glasses have been studied. Upon exposure to visible and near-infrared light, electrons were released from traps and diffused to positive ions and were captured, thus neutralizing the positive ion. It is not possible to specifically identify the electron traps in the irradiated argon–CCl_4 samples. The argon matrix itself is unlikely to trap electrons, but all types of chlorine species are excellent electron traps. The significant Nernst glower photobleaching of absorptions which may be assigned to cations suggests that electrons trapped by anionic species in the matrix can be released by near-infrared and visible radiation and subsequently neutralize trapped cations.

The five infrared bands at 1020, 927, 502, 374, and 290 cm^{-1} are related by their decrease during three physical operations which provide electrons for neutralizing positively charged species. First, additional proton irradiation of the deposited sample releases electrons by ionization at the surface of the argon matrix which are attracted to the positively charged species after the electrons lose the bulk of their excess kinetic energy.[11b] Second, owing to a residual positive charge in the sample following proton bombardment, thermal electrons attracted from a nearby heated filament selectively neutralize the positive species and pro-

vide a definitive identification of isolated cations in the matrix. Third, photobleaching of electrons trapped in the sample frees electrons for the neutralization of trapped cations. The 1020-, 927-, 502-, 374-, and 290-cm^{-1} infrared bands are therefore assigned to matrix-isolated cations. The absorbers will be identified in the following paper.[12]

Particle Chemistry. Most of the effects described above are due to the ionization of the high gas density surface by the proton as it loses energy. Thus the same effects should result from accelerating other small cations such as deuterons or α particles. Helium gas was put into the rf ion source producing He^{2+} and He^+ ions in the light green plasma, which were accelerated toward the target. Since the current was about twice that obtained for protons under the same conditions, most of the helium ions were doubly charged. With deuterium as the gas being ionized, the current is about the same as for hydrogen. In all three cases, using protons, deuterons, or α particles, the optical densities of the absorption bands are about the same when the same integrated current or total charge is used and the probe voltage in the ion source is the same. Interestingly, the spectrum observed by Current[13] following 200-eV electron bombardment of Ar–CCl_4 matrix samples during deposition was similar to the one in Figure 2a.

There are some differences in the bands observed, and it is these minor bands which reflect the fate of the bombarding particle. In the proton irradiations, a weak $CHCl_3$ band[14] was observed at 1224 cm^{-1} and HCl_2^- bands were recorded at 956 and 697 cm^{-1}.[15] In the deuteron experiments, these bands were replaced by the deuterium analogs; bands and species observed in Figure 3 were 911 cm^{-1}, $CDCl_3$; 974 cm^{-1}, $CDCl_2$;[14] 465 cm^{-1}, DCl_2^-;[15] 644 cm^{-1}, Ar_nD^+.[16] With α bombardment, bands due to hydrogen species disappear unless some water is present in the experiment to provide an H-atom source. This series of bands is strong evidence that a part of the 3 μmol of H^+ or D^+ ions (20% of 23 μA for 17 hr) lose enough kinetic energy to react chemically upon collision with a molecule in the sample. The yield of "hot hydrogen atom" reaction products is much smaller than the other radiolysis product yields.

The mechanism for the matrix radiolysis must center around primary ionizations of argon since it is the major component present. In conventional γ radiolysis studies, the addition of a noble gas increased the yield of products by charge and energy transfer from the noble gas.[17] A 2.0-keV proton produces approximately 76 energetic argon ion and electron pairs which undergo collisions with more argon and CCl_4 and cause fragmentation of CCl_4 leading to the observed radiolysis products. In this manner, the chemical effect of the proton beam is amplified.

The radiation dose in the present 2.0-keV proton experiments was calculated from beam parameters to be approximately 2×10^{21} eV/g. This is higher than the 1×10^{18} eV/g dose used in γ-irradiation studies[2] on solid CCl_4 where an electronic absorption was observed and attributed to a radiolysis product and the 2×10^{19} eV/g dose used in the 3-MP photobleaching study.[11a] Owing to the significantly lower sensitivity of infrared absorption as compared to optical absorption or ESR, the higher dose rates used in the present work were necessary to produce infrared observable quantities of intermediate radiolysis products.

Conclusions

The proton beam matrix technique provides unique insight into the radiolysis process. The rapid isolation of both ions and free-radical intermediates by the argon matrix during deposition allows observation of both charged and neutral radiolysis products in the same experiment, provided that the species is a strong infrared absorber.

Although collisions of ions and electrons produced by the proton give the majority of the observed species, after loss of its kinetic energy, the proton itself can react chemically. The products of the reaction with this "hot" hydrogen atom or ion can also be identified by this method. Relatively little study has been conducted on radiation damage related to the ultimate fate of a high-energy charged particle.

The proton radiolysis technique is nonselective and it can be applied to a wide variety of chemical systems whose intermediate radicals, cations, and anions have proven difficult to obtain for spectroscopic study using conventional methods.

As a method for producing positive molecular ions for matrix infrared study, proton beam irradiation is unique in that the sample contains a residual positive charge which can be neutralized with thermal electrons from a bulb filament. Therefore, infrared absorptions due to isolated cations can be titrated out and identified as isolated cations; this is not presently possible with other techniques for producing positive ions which form an electrically neutral sample. In addition, photobleaching of the irradiated sample can be used to release trapped electrons for the neutralization of isolated cations.

Acknowledgments. The authors gratefully acknowledge support for this research by a National Science Foundation Institutional Subgrant from the University of Virginia Research Policy Council and a fellowship from the Alfred P. Sloan Foundation for L.A. The help of Dr. G. Neal and Mr. D. Hills in construction of the experimental apparatus, part of which was furnished by the University of Virginia Physics Accelerator Laboratory, and the assistance of Dr. R. H. McKnight with the electrometer experiment, are gratefully acknowledged.

References and Notes

(1) (a) J. E. Willard, "Organic Compounds in the Solid State" in "Fundamental Processes in Radiation Chemistry", P. Ausloos, Ed., Interscience, New York, N. Y., 1968, Chapter 9; (b) R. E. Bühler, "Radiation Chemistry of the Carbon-Halogen Bond" in "The Chemistry of the Carbon-Halogen Bond", S. Patai, Ed., Wiley, New York, N. Y., 1973, Chapter 12.
(2) T. Shida and W. H. Hamill, *J. Chem. Phys.*, **44**, 2369 (1966).
(3) R. F. C. Claridge, R. M. Iyer, and J. E. Willard, *J. Phys. Chem.*, **71**, 3527 (1967).
(4) D. W. Skelly and W. H. Hamill, *J. Phys. Chem.*, **70**, 1630 (1966).
(5) R. W. Fessenden and R. H. Schuler, *J. Chem. Phys.*, **39**, 2147 (1963); **43**, 2704 (1965).
(6) (a) E. J. Zeller, G. Dreschhoff, and L. Kevan, *Mod. Geol.*, **1**, 141 (1970); E. J. Zeller, G. Dreschhoff, Y. Virmani, and J. Zimbrick, *Clgh. Fed. Sci. Tech. Inf.*, No. 718433 (1970). (b) Although some electromagnetic radiation from the plasma reaches the matrix sample, the solid angle of exposure is very small and the effect of this minute quantity of radiation is probably negligible.
(7) L. Andrews, *J. Chem. Phys.*, **48**, 972 (1968).
(8) L. C. Northcliffe and R. F. Schilling, *Nucl. Data Tables, USAEC*, **A7**, 233 (1970).
(9) M. E. Jacox and D. E. Milligan, *J. Chem. Phys.*, **54**, 3935 (1971).
(10) P. J. Dyne and O. A. Miller, *Can. J. Chem.*, **43**, 2696 (1965).
(11) (a) J. R. Miller and J. E. Willard, *J. Phys. Chem.*, **76**, 2341 (1972). (b) This could also be due to photobleaching by radiation from recombination of argon ions and electrons on the sample surface or from the hydrogen plasma.
(12) L. Andrews, J. M. Grzybowski, and R. O. Allen, *J. Phys. Chem.*, following paper.
(13) J. H. Current, unpublished results.
(14) T. G. Carver and L. Andrews, *J. Chem. Phys.*, **50**, 4235 (1969).
(15) P. N. Noble and G. C. Pimentel, *J. Chem. Phys.*, **49**, 3165 (1968); D. E.

Milligan and M. E. Jacox, *ibid.*, **53**, 2034 (1970). Work in progress in this laboratory, B. S. Ault and L. Andrews, has confirmed the anion identification.
(16) V. E. Bondybey and G. C. Pimentel, *J. Chem. Phys.*, **56**, 3832 (1972); D. E. Milligan and M. E. Jacox, *J. Mol. Spectrosc.*, **46**, 460 (1973); L. Andrews, B. S. Ault, J. M. Grzybowski, and R. O. Allen, *J. Chem. Phys.*, **62**, 2461 (1975).
(17) J. A. Stone, *Can. J. Chem.*, **46**, 1267 (1968), and references therein.

Infrared Spectra of the Molecular Ions and Radicals Produced by Proton Radiolysis of Carbon Tetrachloride in Argon during Condensation at 15°K

Lester Andrews,* Joseph M. Grzybowski, and Ralph O. Allen

Chemistry Department, University of Virginia, Charlottesville, Virginia 22901
(Received August 5, 1974; Revised Manuscript Received February 12, 1975)

Samples of CCl_4 and its carbon-13- or bromine-substituted counterparts at high dilution in argon were deposited at 15°K during simultaneous 2.0-keV proton beam irradiation. New infrared absorptions at 1037, 1020, 927, 898, 746, 502, 374, 290, and 242 cm^{-1} are attributed to CCl_4 radiolysis products and ion–molecule reaction products. The 898- and 746-cm^{-1} bands are due, respectively, to the CCl_3 and CCl_2 chemical intermediates. The 1020-, 927-, 502-, 374-, and 290-cm^{-1} bands, which disappear upon photobleaching and neutralization with thermal electrons, are assigned to the matrix-isolated positive molecular ions CCl_3^+, CCl_2^+, Cl_3^+, $Cl_2CCl_2^+$, and Cl_4^+, respectively. The 242-cm^{-1} absorption is likely due to Cl_3^- perturbed by a large cation. The 1037-cm^{-1} band is due to a CCl_3^+ vibration in an electrically neutral species, presumably $CCl_3^+Cl^-$. The fate of the bombarding proton is demonstrated by the observation of $CHCl_3$ and HCl_2^-, and in deuteron experiments, by the appearance of $CDCl_3$ and DCl_2^-.

Introduction

Ionic molecular species are of considerable spectroscopic and chemical interest for examination of mechanistic and bonding principles. Negatively charged species such as the superoxide anion have been synthesized using matrix reactions of alkali atoms which produced an ion pair. The first example of this type of species, $Li^+O_2^-$, was reported by Andrews[1] in 1968. Using electron bombardment and vacuum-uv photolysis, Milligan and Jacox subsequently produced matrix-isolated NO_2^-. A large number of negatively charged species have been produced as alkali cation–anion pairs using the matrix reaction technique.[3]

However, positively charged molecular ions are more difficult to produce and trap owing to the fact that ionization potentials are relatively high on a chemical energy scale. Lewis acid adducts provide one means of producing cations; Gillespie and Morton[4] have prepared $Cl_3^+AsF_6^-$ and obtained its vibrational spectrum from mixtures of ClF, Cl_2, and AsF_5. Jacox and Milligan[5] produced CCl_3^+ and $CHCl_2^+$ using vacuum-ultraviolet photolysis of chloroform. Electrical discharge techniques also provide positive species for matrix isolation; a discharged flow stream of argon and CCl_4 condensed at 15°K revealed the infrared spectrum of CCl_3^+ and the CCl_3 radical.[6] In unpublished studies, Current[7] irradiated a CCl_4–argon gas sample with 200-eV electrons *immediately prior* to condensation yielding several intense new bands. These bands included the trichloromethyl radical[8] and several positively charged molecular ions which were produced and identified in this study, using the proton bombardment technique described in the previous paper,[9] and in a preliminary communication.[10]

A detailed infrared spectroscopic study was conducted on the matrix-isolated products formed by proton irradiation of argon–CX_4 (X = Cl, Br) matrix samples during 15°K deposition. Since the neutral chlorocarbon[8] and bromocarbon[11] intermediate species are well known, the present study will be concerned only with identification of the several new molecular ions produced by radiolysis and any new ionic species synthesized by ion–molecule reactions during sample condensation.

Experimental Section

The proton beam apparatus, parameters, and experimental technique have been described in the previous paper.[9] While being bombarded with protons, samples of carbon tetrahalide vapor at high dilution in argon Ar/CX_4 = 400/1 (X = Cl, Br) were deposited on a CsI window[8] held at 15°K. The reagents CCl_4 (Mallinckrodt, reagent), CCl_3Br (Aldrich, spectroscopic), CCl_2Br_2 (Eastern Chemical), $CClBr_3$ (synthesized),[11] CBr_4 (Eastman Organic Chemicals, reagent), carbon-13 enriched CCl_4 (51 and 90%, Merck Sharpe and Dohme), nitrogen (Air Products, ultra high purity), and argon (Air Products, 99.995%) were used without purification except for CBr_4 which was recrystallized.[11] The gases used for ion production in the rf source, H_2, He (Matheson, high purity), and D_2 (Matheson, CP), were also used directly.

Infrared spectra were recorded in the 200–3000-cm^{-1} spectral range on a Beckman IR-12 filter-grating spectro-

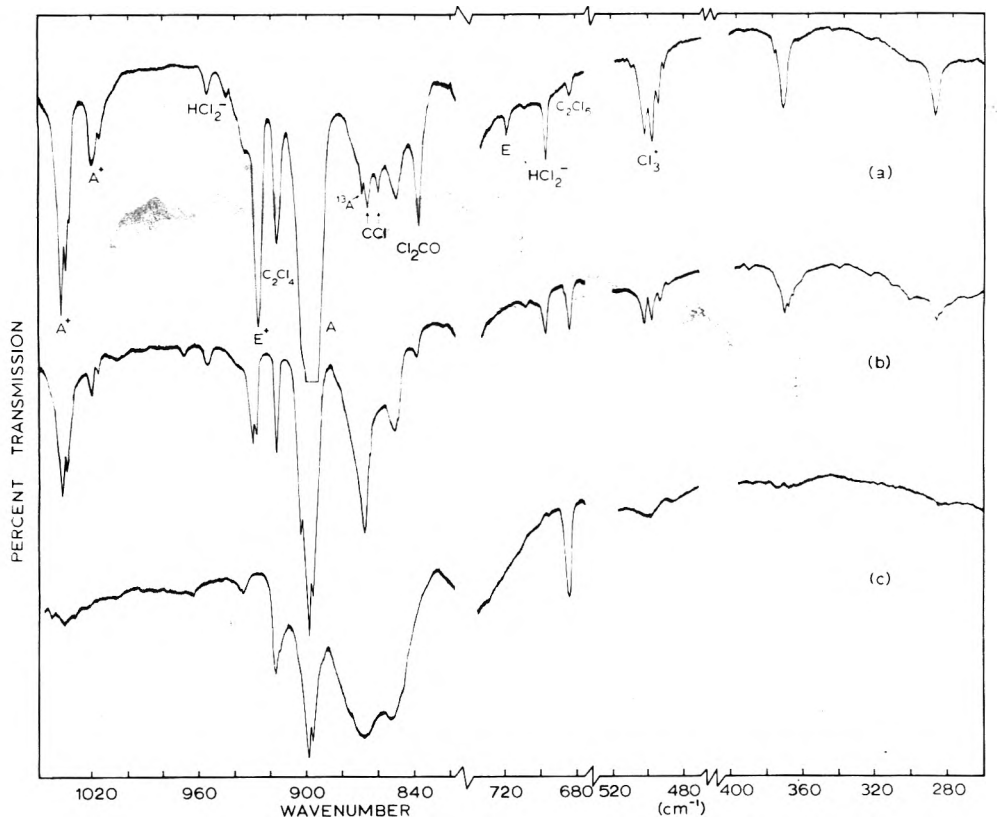

Figure 1. Infrared spectra of the major radiolysis products trapped during 2.0-keV proton irradiation and 15°K condensation of an Ar/CCl_4 = 400/1 sample for 17 hr, trace a. Spectrum b illustrates the effect of temperature cycling to 41°K and trace c is for a cycle to 50°K.

photometer. Survey scans at 20 or 40 cm^{-1}/min were recorded before, during, and after sample deposition. Expanded scale scans were taken at 8 and/or 1.6 cm^{-1}/min after sample deposition. The approximately 3-cm^{-1} resolution was limited by the observed band widths. Wave number accuracy was ±1 cm^{-1} except where otherwise indicated. In several experiments the infrared source beam was blocked to prevent radiation from reaching the sample during deposition and spectra were recorded using a Kodak No. 220 filter (transmits 400–4000 cm^{-1}) in front of the Nernst glower to eliminate visible light from the sample.

Results

A large number of matrix experiments have been performed in order to identify the intermediate radiolysis products of carbon tetrachloride. The results obtained by proton beam irradiation of CCl_4 will be presented first followed by carbon-13 and bromine substitution experiments.

Carbon Tetrachloride. Protons, deuterons, and α particles ranging in energy from 0.5 to 2.0 keV were used in this extensive matrix-isolation study of the radiolysis of CCl_4. The relative yields of two of the principal radiolysis products were a function of particle energy. However, the type of charged particle used in the bombardment did not affect the relative amounts of most of the observed species. The only exceptions were the products formed by chemically binding the bombarding particle, as will be discussed later.

Figure 1, trace a, illustrates the major radiolysis products trapped during simultaneous 2.0-keV proton irradiation and condensation of an Ar/CCl_4 = 400/1 sample for 17 hr. The most intense product band, 898 cm^{-1}, labeled A in Figure 1a to conform to the symbols used earlier, has been assigned to ν_3 of the CCl_3 radical.[8] The naturally occurring carbon-13 counterpart was observed at 869 cm^{-1} (0.1 OD). The intense A^+ band at 1037 cm^{-1} has been attributed[5] to CCl_3^+. Other known reactive species present include CCl_2 (720 cm^{-1}, labeled E, and 746 cm^{-1}, not shown),[12] CCl (866, 860 cm^{-1}),[13] and HCl_2^- (956, 697 cm^{-1}).[14] Stable molecules of interest include $CHCl_3$ (1224 cm^{-1}),[15] CH_2Cl_2 (1269 cm^{-1}),[16] C_2Cl_4 (915 cm^{-1}), and C_2Cl_6 (684 cm^{-1}).[8] The usual trace impurities, H_2O and CO_2, were also present and took part in the radiation chemistry forming ClCO (1879 cm^{-1} and a weak 572-cm^{-1} band, not shown),[17] Cl_2CO (1815 and 838 cm^{-1} and a 582-cm^{-1} band, not shown),[18] and CO (2141 cm^{-1}).[19] The hydrogen containing species resulted in part from the H_2O but, as shown by later deuteron experiments, also from reaction with the bombarding particles.

The bands of particular interest illustrated in Figure 1a are A^+ (1037 and 1020 cm^{-1}), E^+ (927 cm^{-1}), the Cl_3^+ (502 cm^{-1}) multiplet, a 374-cm^{-1} absorption, and the 290-cm^{-1} band. All of the new absorptions observed following CCl_4 radiolysis are listed in Table I.

Figure 1b shows the diffusion behavior of the trapped species following temperature cycling to 41°K and trace c is for a cycle to 50°K. Spectrum b shows the loss of CCl_2 (E, 720 cm^{-1}) and the partial decrease of CCl_3 (A, 898 cm^{-1}) and the growth of C_2Cl_6, which agrees with earlier findings.[8] The intensity of the sharp Cl_2CO band (838 cm^{-1}) was reduced due to aggregation, the new A^+ bands and the 374 and 290 cm^{-1} bands were halved and the new 927- and 502-cm^{-1} absorptions were reduced to one-third of their trace a intensities by the diffusion operation. An intense band appeared at 867 cm^{-1}. The final diffusion (c) shows only the most stable C_2Cl_4 and C_2Cl_6 species along with a

TABLE I: New Absorptions (cm^{-1}) Produced by the Radiolysis of Argon-CCl_4 Samples during 15°K Deposition[a]

Absorptions		Absorptions	
2140	CO	838	Cl_2CO
1879	ClCO	746	CCl_2
1815	Cl_2CO	720	CCl_2
1269	CH_2Cl_2	697	HCl_2^-
1224	$CHCl_3$	684	C_2Cl_6
1037	$CCl_3^+(Cl^-)$	582	Cl_2CO
1020	CCl_3^+	572	ClCO
956	HCl_2^-	502	Cl_3^+
927	CCl_2^+	498	Cl_3^+
915	C_2Cl_4	494	Cl_3^+
898	CCl_3	491	Cl_3^+
869	$^{13}CCl_3$	374	$CCl_2Cl_2^{+*}$
866	$C^{35}Cl$	290	Cl_4^{+*}
860	$C^{37}Cl$	242	$CCl_3^+Cl_3^{-*}$
850 broad	?		

[a] Traces of H_2O, CO_2, and air are unavoidably present. An asterisk denotes tentative identification.

small amount of CCl_3 remaining and the growth of a broad aggregate band at 850–870 cm^{-1}.

An analogous experiment was run for 22 hr irradiating with 2.0-keV deutrons. The spectrum, which is shown in Figure 3a of the previous paper,[9] was essentially identical with that of Figure 1a except for several new deuterium containing species. The deuteron irradiated sample was subsequently neutralized by applying 10 V to the exposed bulb filament for 25 min. Resulting changes in the spectrum were as follows (see Figure 3b of the previous paper[9]): the 1020-, 927-, 502-, and 374-cm^{-1} bands disappeared almost completely and the 645- and 290-cm^{-1} bands were reduced to 70 and 45%, respectively, of their original intensities. The A^+ band (1037 cm^{-1}) along with the C_2Cl_4 (915 cm^{-1}), CCl_3 (A, 898 cm^{-1}), CCl_2 (E, 746, 720 cm^{-1}), Cl_2CO (838 cm^{-1}), and DCl_2^- (465 cm^{-1}) bands were not affected by photobleaching and adding thermal electrons. The electron titration and photobleaching of numerous samples irradiated with protons or α particles followed the same pattern.[9] Removal of the 1020-cm^{-1} band by photobleaching revealed a weaker counterpart at 1010 cm^{-1} which was also ultimately photobleached.

In the most productive experiment, illustrated in Figure 4a of the previous paper,[9] a moderately intense band was observed at 242 ± 2 cm^{-1} which was noted as a shoulder in most of the other experiments. This new band decreased with photobleaching of the matrix sample, Figure 4b in the previous paper, as did the five bands of interest here.

A 2.0-keV proton experiment was conducted with a nitrogen matrix sample, N_2/CCl_4 = 400/1, for 18 hr. The chlorocarbon absorptions were broadened and shifted 5–10 cm^{-1} higher relative to their argon matrix counterparts, including the CCl_4 precursor. The CCl_3 radical band was observed at 904 cm^{-1} (0.38 OD); CCl_2 was not detected. In the higher frequency region, new bands were observed at 1042 (0.19 OD, 18-cm^{-1} half-width) and 942 cm^{-1} (0.27 OD, 16-cm^{-1} half-width). The lower frequency region yielded a sharp triplet at 505.3, 501.0, and 496.7 cm^{-1} (0.68, 0.63, 0.18 OD), a broad 385-cm^{-1} (0.12 OD) feature, a sharp 292-cm^{-1} band (0.35 OD), and a sharp 243-cm^{-1} absorption (~0.3 OD). The exposed bulb filament was operated at

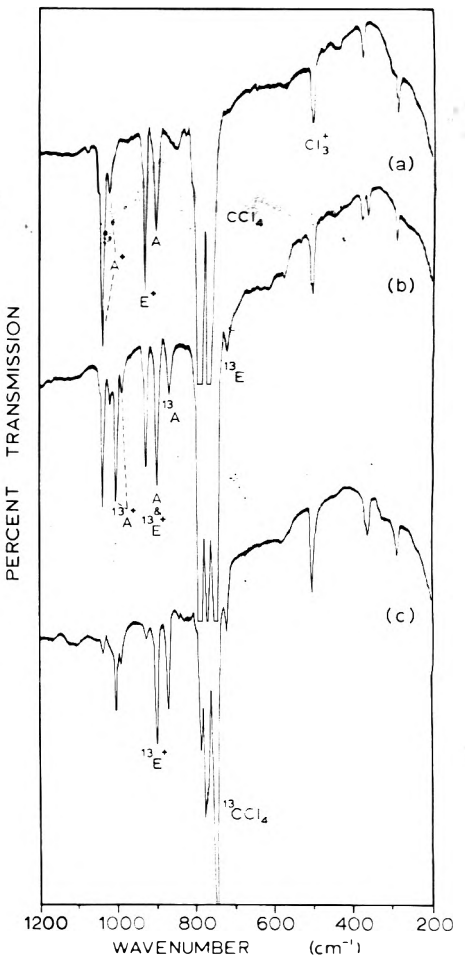

Figure 2. Infrared spectra of the proton beam radiolysis products of carbon tetrachloride and the carbon-13 enriched molecules: spectrum a, natural CCl_4, 0.5-keV proton beam; spectrum b, 51% carbon-13 enriched CCl_4, 0.5-keV proton beam; spectrum c, 90% carbon-13 enriched CCl_4, 1.0-keV proton beam.

10.5 V for 0.5 hr and the 942-, 500-cm^{-1} triplet, and 385-, 292-, and 243-cm^{-1} bands disappeared completely.

Carbon-13 Tetrachloride. Experiments were conducted with carbon-13 enriched CCl_4 using 0.5-, 1.0-, and 2.0-keV proton beam irradiations. Two of these experiments are contrasted with the natural isotopic material in Figure 2 using the lower beam energies which produced smaller yields of the trichloromethyl radical. Trace a illustrates a 0.5-keV experiment with natural isotopic CCl_4; note the reduced A band intensity. In a similar 51% $^{13}CCl_4$ experiment, shown in trace b, the A^+, E^+, A, and 374-cm^{-1} bands appeared as equal intensity doublets, which indicates that these species contain a single carbon atom. The 90% $^{13}CCl_4$ experiment, illustrated in trace c, shows the dominant carbon-13 counterparts of the observed bands; Table II lists the observed wave numbers. In a particularly productive 2.0-keV 90% $^{13}CCl_4$ experiment, the E^+ band was observed at 927.0 ± 0.2 cm^{-1} (0.080 OD) and the $^{13}E^+$ band was measured at 897.7 ± 0.2 cm^{-1} (0.84 OD) on several high-resolution scans. Photobleaching of the sample markedly reduced the 988-, 898-, 502-, 361-, and 290-cm^{-1} band intensities without affecting the 1003- and 869-cm^{-1} absorptions. A 980-cm^{-1} side band emerged upon reduction of the 988-cm^{-1} feature. The 810-cm^{-1} $^{13}COCl_2$ and 723-cm^{-1} $^{13}CCl_2$ bands were not affected by the bulb filament. The 502-cm^{-1} multiplet, the 290-cm^{-1} band, and the 242-cm^{-1}

TABLE II: Effect of Bromine Substitution on the New Absorptions (cm $^{-1}$) Produced by Radiolysis of Argon-CX_4 Samples[a]

Precursor	CX_3^+ (X^-)	$CX_3^\cdot$	$CX_2^\cdot$	CX_3	CX_2	$X_3^\cdot$	$CX_2X_2^\cdot$	$X_4^\cdot$	X_3^-
CCl_4	($A^\cdot$) 1037.0	1020 (1010)	($E^\cdot$) 927.0	(A) 898	(E) 746, 720	502, 498, 494, 491 sh	374	290	242
$^{13}CCl_4$	($^{13}A^\cdot$) 1003.0	988 (980)	($^{13}E^\cdot$) 897.7	(^{13}A) 869	(^{13}E) 723	502, 498, 494, 491 sh	361	290	242
CCl_3Br	($A^\cdot$) 1036.0, 1034.0		($E^\cdot$) 925	(A) 898	(E) 746	492, 488, 484 sh		251	225
	($B^\cdot$) 1019, 957		($F^\cdot$) 870	(B) 889, 836	(F) 612	437, 420	356		221
CCl_2Br_2	($B^\cdot$) 1019, 958		($E^\cdot$) 925	(B) 891 un, 836	(F) 612	432, 416	355	230	
	($C^\cdot$) 976, 891 un		($F^\cdot$) 868	(C) 856	(G) 640	362, 339			
$CClBr_3$	($C^\cdot$) 978, 975; 894, 891		($F^\cdot$) 870 sh	(C) 856, 783 sh	(F) 612		355		
	($D^\cdot$) 874, 880		($G^\cdot$) 778	(D) 773	(G) 641, 596	283	326		
CBr_4	($D^\cdot$) 874, 880		($G^\cdot$) 778	(D) 773	(G) 641, 596	283	326		

[a] sh denotes shoulder, un denotes unresolved C$^+$, B band.

feature showed *no* measurable carbon-13 shift in the 90% $^{13}CCl_4$ experiments.

Bromine Substitution. Bromine substitution in the CX_4 precursor molecule provided a pseudo-isotope for chlorine. Figure 3 contrasts the 750–1050-cm^{-1} regions of the infrared spectra for 0.5-keV proton irradiations of CCl_4, CCl_3Br (1.0 keV in this case), CCl_2Br_2, $CClBr_3$, and CBr_4 samples. Figure 4 illustrates the 200–700-cm^{-1} regions for these same precursors following 2.0-keV proton bombardment. The new absorptions found upon bromine substitution are tabulated in Table II. For all reagent molecules, the analogous 2.0-keV experiments produced more intense bands; however, the primary cation/radical ratio was greater for the 0.5-keV experiment, and for this reason these spectra were used for Figure 3. The CCl_4 spectrum revealed the very intense A^+ band at 1037 cm^{-1} with a high-wave number shoulder at 1041 cm^{-1} and a satellite band at 1020 cm^{-1} along with the intense E^+ band at 927 cm^{-1} and A band at 898 cm^{-1}. These same bands were observed in the CCl_3Br spectrum with lower intensities but identical wave numbers, except E^+ which appeared at 925 cm^{-1}. In addition CCl_3Br gave rise to bands at 1019 cm^{-1} and a 957.0-, 953.5-cm^{-1} doublet labeled B^+, B (CCl_2Br)[8] absorptions at 889 and 835 cm^{-1}, and a band at 870 cm^{-1} designated F^+. Both the F^+ and the E^+ bands were almost completely removed by a 30-min titration with thermal electrons while the A, A^+, B, and B^+ bands were not affected. In the CCl_2Br_2 spectrum the B^+ bands at 1019 cm^{-1} and at 958, 953 cm^{-1} (doublet), and the B bands at 891 (unresolved from C^+ at 893 cm^{-1}) and 836 cm^{-1} were more intense. New C^+ bands were observed at 976 and 891 cm^{-1} (unresolved from B at 889 cm^{-1}), and E^+ at 925 cm^{-1}, F^+ at 868 cm^{-1}, and a weak C band at 856 cm^{-1} also resulted. Continuing in the series, the $CClBr_3$ spectrum produced two C^+ doublets 978, 975 cm^{-1} and 894, 891 cm^{-1} along with weak C bands ($CClBr_2$) at 856 and 783 cm^{-1} (shoulder). An intense new doublet at 880, 874 cm^{-1} is labeled D^+ and the sharp D (CBr_3)[11] band is noted at 773 cm^{-1} along with another new band G^+, at 778 cm^{-1}. The label I denotes impurity bands from the precursor sample. The CBr_4 spectrum contains these last three bands which are labeled D^+ (880, 874 cm^{-1}, 0.65 OD), G^+ (778 cm^{-1} 0.12 OD), and D (773 cm^{-1}, 0.08 OD). In CBr_4 experiments using 2.0-keV proton and α particle beams, the D^+ doublet became a single sharp band at 874.0 (0.43 OD) cm^{-1} with a sharp 878-cm^{-1} shoulder, the D radical band at 773 cm^{-1} (1.5 OD) and the G^+ (0.75 OD) absorption increased markedly in intensity. Other species of interest observed in these CBr_4 experiments were $CHBr_3$ (1154 cm^{-1}), CH_2Br_2 (651 cm^{-1}),

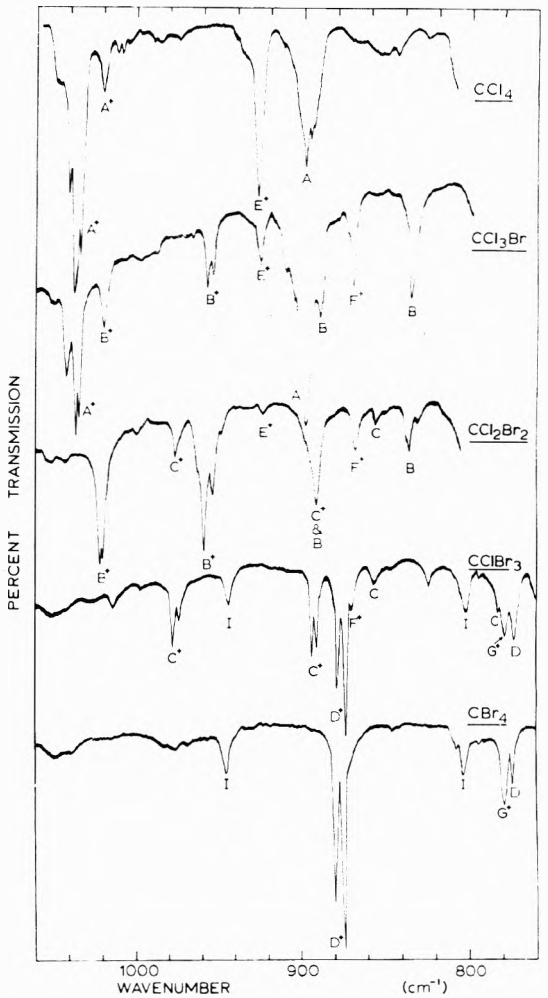

Figure 3. Infrared spectra in the 750–1050-cm^{-1} region for 0.5-keV proton radiolysis products of CX_4 molecules (X = Cl, Br). Ar/CX_4 = 400/1. CCl_3Br experiment used 1.0-keV proton beam.

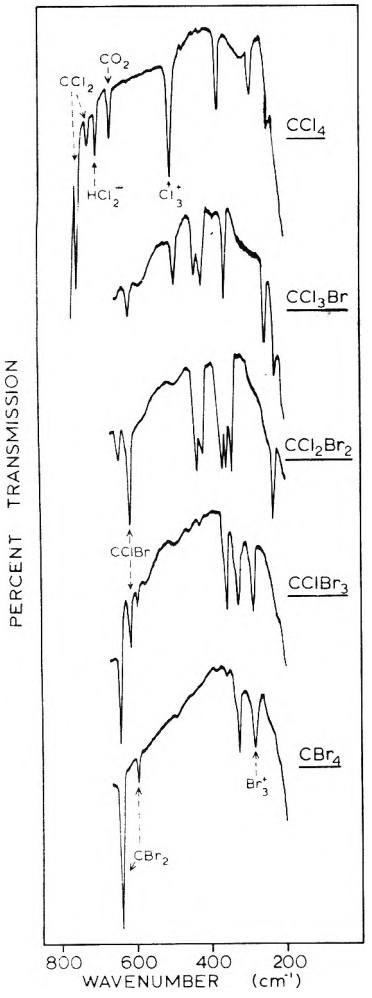

Figure 4. Infrared spectra from 200 to 700 cm^{-1} for a 2.0-keV proton beam irradiation of CX_4 matrix samples during 15°K deposition.

HBr_2^- (729, 894 cm^{-1}),[20] and CBr_2 (640.5 cm^{-1}, 0.54 OD and 595.7 cm^{-1}, 0.06 OD).[11]

In the low-frequency region, Figure 4 shows CCl_2 bands at 746 and 720 cm^{-1}, the HCl_2^- band at 697 cm^{-1}, and previously unidentified bands at 502, 374, 290, and 242 cm^{-1} in the CCl_4 spectrum. The CCl_3Br parent gave a new band at 490 cm^{-1}, two bands at 437, 420 cm^{-1}, a sharp 356-cm^{-1} band, an absorption at 251 cm^{-1}, and a doublet at 221, 225 cm^{-1}. These bands are listed in Table II. In the 1.0-keV experiment, all but the latter doublet were observed, and all of these bands almost completely disappeared upon addition of thermal electrons for 3 hr. The 502-cm^{-1} multiplet in CCl_4 experiments consisted of four bands: 502.0 (0.12 OD), 498.0 (0.14 OD), 494.5 (0.07 OD), and 491 cm^{-1} (shoulder, 0.02 OD). The 490-cm^{-1} band in CCl_3Br experiments was resolved into absorptions at 492.4 (0.09 OD), 488.4 (0.07 OD), and 484 cm^{-1} (shoulder, 0.02 OD). Expanded-scale spectra of these multiplets are contrasted in Figure 5. For these and the other halogen containing species in Table II, a gradual shift was observed to lower wave numbers with increasing bromine substitution.

In the 1.0-keV proton radiolysis study of CBr_4, the final sample was neutralized with thermal electrons for 5 hr with the filament at 6 V and for an additional 5 hr at 10 V. The 778-cm^{-1} G^+ band was reduced from 0.36 to 0.25 OD and the 283-cm^{-1} absorption decreased from 0.06 to 0.04 OD while the 326-cm^{-1} absorption decreased almost completely from 0.05 to 0.01 OD. The D (0.28 OD) and D^+ (0.27 OD) bands were unchanged.

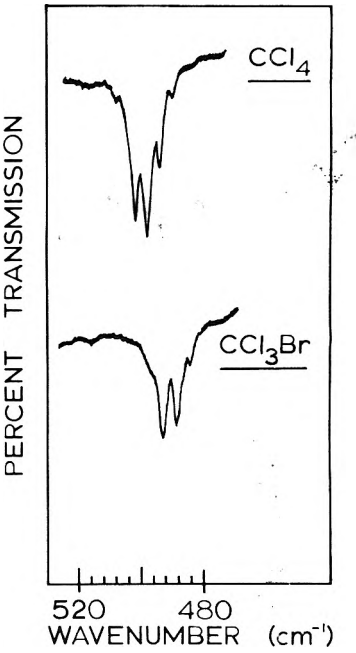

Figure 5. Expanded-scale infrared spectra of the multiplets near 500 cm^{-1} in CCl_4 and CCl_3Br experiments.

Discussion

Chemical identification of the new ionic species produced here will each be discussed along with some postulates of the mechanisms responsible for their formation. In the previous paper,[9] five infrared absorptions, 1020, 927, 502, 374 and 290 cm^{-1}, were attributed to matrix-isolated cations owing to their marked decrease when the sample was photolyzed with near-infrared and visible light which releases trapped electrons and when thermal electrons were added to the sample. Since the counterparts of the new argon matrix bands were also observed in solid nitrogen (assuming the broad 1042-cm^{-1} nitrogen matrix band incorporates both of the 1037- and 1020-cm^{-1} argon matrix features), the matrix host is not chemically combined in any of the new molecular species derived from CCl_4. The cations responsible for each of the five infrared absorptions will be identified from the available spectroscopic evidence in the following discussion.

CCl_3^+. The trichloromethyl carbonium ion was first identified by Jacox and Milligan (hereafter JM) following hydrogen resonance vacuum-uv photolysis of $CHCl_3$ samples without any mention of the possibility of a counterion.[5] The JM experiment was similar to the present technique; both irradiations were performed during sample deposition but the JM ionizing radiation was 10-eV photons while 2000-eV protons were utilized in this study. In both cases the major molecular species were the same. The 1036.6-cm^{-1} band observed by JM was seen as sharp band peaks at 1036.5 to 1037.0 cm^{-1} in this work. This band was not affected when the sample was neutralized with thermal electrons or photobleached while the new band observed nearby at 1020 cm^{-1} was completely neutralized, revealing a weak band at 1010 cm^{-1} which itself was ultimately destroyed. This indicates that the 1037-cm^{-1} absorber is part of an electrically neutral species and the 1020-cm^{-1} band is a matrix-isolated cation. The unusually high frequency for

these carbon–chlorine vibrational modes suggests cationic species. Since the most abundant anion produced by either type of radiation, other than electrons, must be Cl^- owing to the fact that atomic chlorine is an excellent electron trap, it is proposed that the 1037-cm^{-1} absorber is the $CCl_3^+Cl^-$ ion pair, which results from the combination of CCl_3^+ and Cl^- ions during sample condensation. Chloride ion is also produced by the dissociative electron capture of CCl_4. The 1020-cm^{-1} absorption is assigned to ν_3 of the isolated CCl_3^+ species; the 1010-cm^{-1} band is presumably due to CCl_3^+ isolated in a matrix site more resistant to photobleaching. The 1037-cm^{-1} band is assigned to the ν_3 mode of CCl_3^+ in the $CCl_3^+Cl^-$ species.

Support for this assignment comes from the bromine substitution data which indicate that the 1037-cm^{-1} band is doubly degenerate and that two bands result upon partial bromine substitution. That four, and only four, unique species can be produced from the five tetrahalide precursors in Figure 3 defines the new species as containing three equivalent halogen atoms. Similar data has been presented for the CX_3 radicals.[8] The mixed-carbon isotopic experiment indicates a single carbon atom species, and the carbon-13 shift is appropriate for the ν_3 mode. In agreement with JM, the 1037-cm^{-1} absorption must be caused by a CCl_3^+ vibration; however, the failure to neutralize the species with electrons indicates the immediate presence of a counterion.

The unique and perhaps unexpected stability of CCl_3^+ in the presence of a counterion is probably due to its planar geometry. CCl_3^+ must be a D_{3h} species since it is isoelectronic with BCl_3. For $CCl_3^+Cl^-$ to charge transfer to give CCl_4, the planar CCl_3^+ group must deform to the tetrahedral geometry and this process requires an activation energy. Interestingly, the $CCl_3^+Cl^-$ ion pair is not very unstable thermodynamically.[21]

$$CCl_4 \xrightarrow{D = 68 \pm 3 \text{ kcal/mol}} CCl_3 + Cl \qquad (1)$$

$$\downarrow I = 202 \qquad \downarrow E = -83$$

$$CCl_3^+ \quad Cl^-$$

The gaseous ion pair requires 187 kcal/mol for its production, but electrostatic attraction between the ions can provide some of this energy. If the interionic distance is 2.0 Å, the conversion $CCl_4 \rightarrow CCl_3^+Cl^-$ is endothermic by only 21 kcal/mol.

It appears that a coplanar ion-pair arrangement 1 might

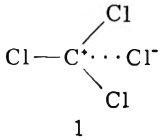

1

resist conversion to CCl_4 more than a C_{3v} structure with Cl^- above the positive carbon center. Thus, if CCl_3^+ and Cl^- produced by radiolysis approach each other during condensation of the matrix sample, the ion pair could be stabilized in the matrix *unless* the kinetic energy of the ions is greater than the activation energy necessary to deform the CCl_3^+ group and charge transfer to yield CCl_4.

Resistance of the sharp 874-cm^{-1} band in the CBr_4 experiments to photobleaching and neutralization with thermal electrons indicates the formation of the analogous $CBr_3^+Br^-$ ion pair which is presumably stabilized by the planar geometry of CBr_3^+. In fact all of the B^+ and C^+ species must also be $CX_3^+X^-$ ion pairs; the B^+ bands are assigned to CCl_2Br^+ modes and the C^+ absorptions are due to $CClBr_2^+$ vibrations. The 2- (two) cm^{-1} variation in splittings and band positions might be due to a change in counterion between Cl^- and Br^-.

In the π molecular orbital scheme for a planar CCl_3 radical, the free-radical electron is in an antibonding molecular orbital and its removal to form planar CCl_3^+ clearly leads to stronger C–Cl bonds as indicated by the increase in ν_3 frequencies from 898 to 1020 or 1037 cm^{-1}. This is, of course, expected since the binding in the cation will be greater due to increased nuclear attractions for the remaining electrons and decreased electron–electron repulsions as compared to the radical.

CCl_2^+. An electron-impact mass spectrum of CCl_4 showed CCl_3^+ to be the major ion produced; however, the CCl_2^+ ion signal was one-fourth as intense. The sharp E^+ band at 927.0 cm^{-1} exhibited a carbon-13 counterpart at 897.7 cm^{-1}. It was markedly decreased by sample diffusion, by bombardment with protons after sample deposition, and it could be completely eliminated with thermal electrons and by photobleaching (see Figures 2 and 3 of the previous paper[9]) all of which indicates that it is due to an isolated cation.

The bromine substitution data show three different species, E^+ (927 cm^{-1}), F^+ (869 cm^{-1}), and G^+ (778 cm^{-1}), all of which could be neutralized by thermal electrons. The observation of three different bands indicates two equivalent halogen atoms in the absorber. In fact, the observation of the E^+ band in CCl_4, CCl_3Br, and CCl_2Br_2 experiments is indicative of a two chlorine species. Confirmation of this stoichiometry was found in the high-resolution spectrum of the 927-cm^{-1} band recorded by Current[7] which showed resolved chlorine isotopic splittings with a 9/6/1 relative intensity. This observation requires two equivalent chlorine atoms for the absorbing species.

The 927.0 ± 0.2-cm^{-1} band and its 897.7 ± 0.2-cm^{-1} carbon-isotopic counterpart are therefore assigned to ν_3 of the $^{12}CCl_2^+$ and $^{13}CCl_2^+$ species, respectively. This isotopic data can be used to predict a lower limit of 115° for the $(Cl–C–Cl)^+$ valence angle which is larger than the 100° value found for CCl_2[12] and is consistent with the known relationship between 17 and 18 valence electron molecules (NO_2, 134° and O_3, 117°, for example). The true bond angle for CCl_2^+ is probably 125 ± 10 °.

The bromine substitution work supports these assignments. An absorption in the CBr_4 experiments at 778 cm^{-1} is assigned to ν_3 of CBr_2^+. The F^+ bands at 869 ± 1 cm^{-1} are assigned to $CClBr^+$.

Here the electrons removed from CCl_2 and CBr_2 to form CCl_2^+ and CBr_2^+ are probably nonbonding as far as the carbon–halogen bond is concerned. Nevertheless, the ν_3 frequencies increase substantially. This is in part due to expanding the valence angle which incorporates more s character into the bonding *and* the fact that n nuclear charges can bind $n - 1$ electrons in a halogen system more tightly and give rise to a stronger bonding.

The infrared spectrum was closely examined for double positively charged species, CCl_2^{2+} and CCl_3^{2+}, which were present in the mass spectrum with 2–3% of the CCl_2^+ and CCl_3^+ intensities. CCl_2^{2+}, isoelectronic with CO_2, would be expected to have an intense ν_3 absorption above 1050 cm^{-1}. No additional bands were observed which could be assigned to double positively charged species. Such species are produced by radiolysis in lower yields than single charged cations, and are presumably more reactive during

sample condensation. Thus, if present, the yields were too low to be observed. Furthermore, if the second ionization potentials of the CCl_2 and CCl_3 species exceed the ionization potential of argon, charge transfer would produce Ar^+ and the singly charged cation.

It can be noted from Figure 3 that bromine detachment occurs more readily upon radiolysis than chlorine separation. This is consistent with mass spectra for the CCl_3Br and CCl_2Br_2 compounds. In the former, the Br^+/Cl^+ ratio was 23/10 while the latter gave 16/4. Accordingly, the CCl^+/CBr^+ ratios were 27/10 and 11/8 for the two precursors, respectively. The $CCl_2^+/CClBr^+$ ratio from CCl_3Br was 52/12 and the $CCl_2^+/CClBr^+/CBr_2^+$ yield from CCl_2Br_2 was 18/16/1. The carbonium ion yields in Figure 3 and in the mass spectra also matched nicely. The CCl_3Br mass spectrum yielded a CCl_3^+/CCl_2Br^+ ratio of 75/33 and the CCl_2Br_2 mass spectrum gave $CCl_2Br^+/CClBr_2^+$ = 48/10. The CX_3 radical absorptions in Figure 3 followed the intensities of their CX_3^+ analogs with more intense radical bands for the departed bromine atom.

Since the prominent 1037-cm^{-1} band has been assigned to the $CCl_3^+Cl^-$ ion pair, the possibility of a $CCl_2^+Cl^-$ ion pair should be explored. However, there is no geometry barrier to resist the formation of planar CCl_3 from $CCl_2^+Cl^-$ when the latter ions approach each other during sample condensation. So the CCl_2^+ and Cl^- ion association increases the yield of CCl_3 radical. In the case of $CCl_3^+Cl^-$, the different planar CCl_3^+ geometry in the ion and in the tetrahedral CCl_4 neutral makes it possible to trap some $CCl_3^+Cl^-$ as a stable ion pair in the solid matrix.

Cl_3^+. The quartet near 500 cm^{-1} in Figure 1 exhibits chlorine isotopic splittings which requires three chlorine atoms, and since no carbon-13 shift could be detected, the absorber probably contains no carbon. Statistical weights of the six naturally occurring chlorine isotopic species with three chlorine atoms are as follows:

35–35–35	27/64	27
35–35–37	18/64	27
35–37–35	9/64	
37–37–35	6/64	9
37–35–37	3/64	
37–37–37	1/64	1

If the position of the different isotopes within the molecule cause splittings which can not be resolved, a 27/27/9/1 quartet should result. The observed bands are in excellent agreement with this possibility.

The complete and rapid neutralization of the 500-cm^{-1} band by thermal electrons indicates that this absorber is also an isolated cation, which must therefore be Cl_3^+. Strong support for assigning this infrared band to ν_3 of Cl_3^+ is found in the vibrational spectrum of $Cl_3^+AsF_6^-$, where the antisymmetric stretch of Cl_3^+ has been attributed to a 508-cm^{-1} Raman band.[4] The agreement between the argon matrix and Lewis acid adduct Cl_3^+ frequencies is excellent. The frequency analogy to the isoelectronic SCl_2 (ν_3 = 535 cm^{-1})[22a] molecule is also supportive.

The bromine substitution data add strength to this assignment. The first band at 492, 488, 484 cm^{-1} in the CCl_3Br experiment arises from a Cl_2Br^+ species. The isotopic triplet shown in Figure 5 is more consistent with a (Cl–Br–Cl)$^+$ species with two equivalent chlorine atoms. The 437-, 420-cm^{-1} bands are candidates for a (Cl–Cl–Br)$^+$ arrangement.[22b] The CCl_2Br_2 experiment produced four bands at 432, 416, 362, and 339 cm^{-1} which could be due to two isomeric Br_2Cl^+ species. Finally, the perbromo species, Br_3^+, was observed at 283 cm^{-1} in the $CClBr_3$ and CBr_4 experiments. The failure to observe Cl_3^+ in the CCl_3Br experiment is due to the fact that bromine detachment is favored over chlorine separation by an approximate factor of 3 (see Figure 3). Accordingly, ion–molecule reaction products containing halogen species will be preferentially bromine substituted using mixed chloro–bromo precursors. The chlorine–bromine shift in the fundamental ratio of 502/283 = 1.77 is appropriate for a pure halogen vibrational mode and is in excellent agreement with the Cl_2/Br_2 fundamental ratio[23] of 554/318 = 1.74.

These trihalo cations are presumably synthesized by the ion–molecule reaction 2 during sample condensation rather

$$Cl_2 + Cl^+ \longrightarrow Cl_3^+ \qquad (2)$$

than by a direct ionization process since no Cl_3^+ was detected in the mass spectrum of CCl_4. Gillespie and Morton[4] have proposed an analogous mechanism for the formation of $Cl_3^+AsF_6^-$ from an AsF_5 solution of ClF and Cl_2 where $Cl^+AsF_6^-$ is first formed followed by the addition of Cl_2 to give $Cl_3^+AsF_6^-$.

The bonding in trihalide ions has been discussed by Pimentel[24] in simple molecular orbital terms using only p_z atomic orbitals. Very recently, matrix isolated Cl_3^- has been observed at 374 cm^{-1} in proton bombardment experiments with Cl_2.[25] The two electrons removed in forming Cl_3^+ from Cl_3^- are nonbonding. However, chemical binding is strengthened owing to the greater attraction of 51 nuclear charges for 50 electrons in the trichloride cation as compared to 52 electrons in the trichloride anion. Accordingly, ν_3 increases from 374 cm^{-1} for Cl_3^- to 502 cm^{-1} for Cl_3^+ as the number of nonbonding electrons is decreased and the effective nuclear charge for the remaining electrons is increased.

Evidence for $CCl_2(Cl_2)^+$. The 374-cm^{-1} band observed here exhibits a large carbon-13 shift consistent with the vibration of carbon against two chlorine atoms. The bromine substitution data provide two counterpart bands at 355 and 326 cm^{-1} which form a uniform progression and indicate that this vibrational mode involves two equivalent halogen atoms. The rapid and complete disappearance of these three bands following the addition of thermal electrons indicates that the absorber is an isolated cation. The chlorine–bromine shift from 374 to 326 cm^{-1} (a ratio of 1.15) is consistent with a carbon–halogen stretching mode (ratios for ν_3 of CCl_2/CBr_2 = 1.16 and for ν_1 of CCl_2/CBr_2 = 1.21)[8,11] and not an X–C–X bending mode (ratios for ν_4 of CCl_4/CBr_4 = 314/183 = 1.72 and for ν_2 of CCl_2/CBr_2 = 326/196 = 1.66).[26a] However, 374 cm^{-1} is about half of the wave number of a normal C–Cl stretching fundamental, so the 374-cm^{-1} absorber involves particularly weak carbon–halogen bonds. This suggests another ion–molecule reaction product.

The data limit the possible sources for this C--Cl_2 stretching mode to the ions CCl_3^+ or CCl_2^+ bonded to molecular Cl_2 or the molecules CCl_3 or CCl_2 bonded to the ion Cl_2^+, the latter of which could be formed by reaction 3. Ste-

$$Cl + Cl^+ \longrightarrow Cl_2^+ \qquad (3)$$

ric arguments suggest a preference for the $(CCl_2\text{--}Cl_2)^+$ species, which satisfies tetravalent carbon, over the more hindered $(CCl_3\text{--}Cl_2)^+$ possibility. Thus, a reasonable explanation for the 374-cm^{-1} absorption is the product of

reactions 4 which occur during sample condensation. This

$$\left.\begin{matrix} CCl_2 + Cl_2^+ \\ CCl_2^+ + Cl_2 \end{matrix}\right\rangle \longrightarrow Cl_2C{:}Cl_2^+ \qquad (4)$$

$Cl_2C{:}Cl_2^+$ species might be a nonclassical carbonium ion which has the C_{2v} structure suggested in 2. Two carbon–

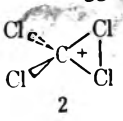

2

chlorine bonds involve normal electron pair bonding while the other two involve electron-deficient bonding with presumably delocalized electrons around the cation center. This structure nicely accounts for the low 374-cm^{-1} C–Cl_2 vibrational frequency and the large carbon-13 isotopic shift. The structure suggested is a more stable form of CCl_4^+ than the tetrahedral structure formed upon electron impact since the latter decomposes before detection in the mass spectrometer. The formation of a Cl–Cl bond about the cation center provides a mechanism for stabilization of CCl_4^+.

Support for this nonclassical ion structure is found in very recent studies[26b] on CH_5^+ which indicate a C_s structure containing three normal C–H bonds and two weaker C–H bonds involved in three-center electron deficient bonding around the cation.

It should be pointed out that the 4800-Å optical band observed by Hamill and coworkers[27] following radiolysis of CCl_4 in hydrocarbon glasses and attributed to the positive ion CCl_4^+ could, in fact, be due to the species 2 suggested here.

Evidence for Cl_4^+. The 290-cm^{-1} absorber is probably a halogen species since no carbon-13 shift was detected in the 90% carbon-13 experiment. Bromine substitution products were observed at 251 cm^{-1} in CCl_3Br and at 230 cm^{-1} in CCl_2Br_2 experiments. The more completely bromine substituted species were not observed due to the 200-cm^{-1} spectrophotometer limit; however, if the Br_2/Cl_2 wave number ratio is multiplied by 290 cm^{-1}, a 167-cm^{-1} absorption is predicted for the perbromo species. Although we cannot be certain, the space between the observed 230-cm^{-1} band and the predicted perbromo band at 167 cm^{-1} *suggests* another unobserved band around 200 cm^{-1}. This possible interpretation provides five bands which suggests a four-halogen atom species for the cation absorbing at 290 cm^{-1}. Interestingly, the 290-cm^{-1} band appeared to photobleach faster and neutralize with thermal electrons slower than the other cation bands.

On the basis of the present data, the 290-cm^{-1} band is tentatively assigned to the weak intermolecular bond stretching mode of the $Cl_2 \cdots Cl_2^+$ species. It is proposed that a three-electron bond is formed between Cl_2 and Cl_2^+ using the $(\pi^*-\pi^*)\sigma$ scheme of Spratley and Pimentel[28] following ion–molecule reaction 5. In support of this assign-

$$Cl_2 + Cl_2^+ \longrightarrow Cl_2 \cdots Cl_2^+ \qquad (5)$$

ment is the half-order bond stretching frequency of Cl_2^- observed near 250 cm^{-1} for the $M^+Cl_2^-$ species.[29] While the Cl_4^+ stoichiometry and assignment cannot be regarded as definitive, it is the best present explanation for the 290-cm^{-1} absorber.

Evidence for Cl_3^-. The 242-cm^{-1} band appeared as a shoulder in samples exposed to the Nernst glower during deposition; however, in the most productive experiment where the sample was protected from the glower, the 242-cm^{-1} band was observed to be moderately intense (0.15 OD) on the first infrared scan. It was reduced to 0.03 OD following prolonged exposure to the full light of the glower. In fact, this absorption was the most sensitive to photobleaching of all the observed bands. No carbon-13 shift was observed for the 242-cm^{-1} band so it is presumed to arise from a halogen species. The only bromine-substituted counterpart that could be observed was the 221-, 225-cm^{-1} doublet in CCl_3Br experiments.

Although it is not possible to eliminate positively charged species from consideration, the agreement between the 242-cm^{-1} argon matrix band and the broad 242-cm^{-1} absorption assigned to ν_3 of Cl_3^- in the $R_4N^+Cl_3^-$ species dissolved in acetonitrile[30] suggests the tentative assignment of the former to Cl_3^-. Likewise, the 221-, 225-cm^{-1} doublet is in very good agreement with the 227-cm^{-1} band of Cl_2Br^- in $R_4N^+Cl_2Br^-$. However, matrix-isolated Cl_3^- has been observed at 374 cm^{-1} in recent proton bombardment experiments with Cl_2.[25] If the 242-cm^{-1} band is due to Cl_3^- as its agreement with the earlier assignment suggests, it must likewise be perturbed by a large cation. It is conceivable that CCl_3^+ could be a possible counterion, and its own absorption is obscured by the bands already discussed between 1000 and 1040 cm^{-1}. Reaction 6 suggests

$$CCl_3^+Cl^- + Cl_2 \longrightarrow CCl_3^+Cl_3^- \qquad (6)$$

a mechanism for the formation of this species which could readily photolyze to give the initial reactants or CCl_4 and Cl_2. This reaction is consistent with the formation of Br_2Cl^- by the reaction of $R_4N^+Cl^-$ with Br_2.[30]

Finally, observation of the isolated ions HCl_2^- and DCl_2^- in these experiments[14,25] indicates the participation of chloride ion in the matrix reactions and supports the presence of the related trichloride ion. Bichloride ion is formed by reaction 7, and it contributes to the charge balance in the matrix sample.

$$HCl + Cl^- \longrightarrow HCl_2^- \qquad (7)$$

Matrix-Isolated Cations. This work has shown that isolated cations can exist in an argon matrix which also must contain isolated anions including Cl^-, Cl_2^-, and HCl_2^-. The subject of isolated ions in rare gas matrices has been discussed by Kasai, who presented ESR evidence for cations and anions isolated in argon matrices at distances on the order of 10-Å apart.[31] The existence of matrix-isolated ions indicates an argon–cation "solvation" energy arising from ion–induced dipole forces (probably somewhat larger than van der Waals energies) which is instrumental in holding unlike charged ions apart. In order to determine the average separation of reactive species in these experiments, it is necessary to determine the concentration of products. Not all of the 1 part of CCl_4 in 400 argon atoms are decomposed; however, more than one product may be formed from a given CCl_4 molecule. If the concentration of charged species were as high as 1 in 500 argon atoms, the average separation between these species would be approximately eight argon atoms or approximately 30 Å. The electrostatic attractive energy between a cation and anion separated by this distance in solid argon of dielectric constant 1.53 is approximately 7 kcal/mol. The rigidity of the matrix which provides a barrier to diffusion and the "solvation" of cations by the matrix are sufficient to overcome this attractive energy and hold cations and anions apart at these low temperatures and dilute concentrations.

It is therefore reasonable for several of the charged

species observed here to be "effectively isolated" within the matrix without adjacent counterions.

Conclusions

The simultaneous radiolysis of an argon–CCl_4 sample with 2.0-keV protons during condensation at 15°K provides a fruitful method for studying the chemical intermediates (radicals and cations) of CCl_4 radiolysis, and the ion–molecule reactions of these products. Photobleaching of the sample releases trapped electrons to neutralize isolated cations. The residual positive charge on the matrix sample allows the isolated cations to be neutralized by thermal electrons and, therefore, identified as cations.

The CCl_3 and CCl_2 intermediate species were observed in good yields. A significant amount of the principal charged radiolysis product CCl_3^+ undergoes reaction with an anion, presumably Cl^-, to give an electrically neutral ion pair $CCl_3^+Cl^-$ which was not photobleached or neutralized by thermal electrons; some isolated CCl_3^+ was also trapped. The CCl_2^+ species was observed to be isolated in the matrix, based upon its complete and rapid neutralization with the addition of thermal electrons to the sample and upon photolysis. Three absorptions were identified as the cation–molecule reaction products Cl_3^+, $Cl_2C{:}Cl_2^+$, and Cl_4^+, which were photobleached and neutralized by thermal electrons. Spectroscopic evidence was also presented for the anion–molecule reaction product HCl_2^- and the species $CCl_3^+Cl_3^-$.

This work demonstrates that cations can be trapped in an argon matrix at 15°K. Solvation of the cation by argon arising from ion-induced dipole interactions and the activation energy for diffusion through the dielectric solid argon prevent neutralization and allow their preservation as isolated ions.

Acknowledgments. The authors gratefully acknowledge financial support for this research by a National Science Foundation Institutional Subgrant from the University of Virginia Research Policy Council and an Alfred P. Sloan Fellowship for L.A. We thank Dr. J.W. Nibler for the tesla coil discharge spectrum and Dr. D.F. Hunt for the mass spectra. Special acknowledgment is due Dr. J.H. Current for providing an unpublished report on his significant electron impact work and for permission to quote his experimental results here.

References and Notes

(1) L. Andrews, *J. Chem. Phys.*, **50**, 4288 (1969).
(2) D. E. Milligan and M. E. Jacox, *J. Chem. Phys.*, **52**, 3864 (1970).
(3) L. Andrews, "Infrared and Raman Spectroscopic Studies of Alkali-Metal Atom–Matrix-Reaction Products", in "Cryogenic Chemistry", Wiley-Interscience, New York, N.Y., 1975.
(4) R. J. Gillespie and M. J. Morton, *Inorg. Chem.*, **9**, 811 (1970).
(5) M. E. Jacox and D. E. Milligan, *J. Chem. Phys.*, **54**, 3935 (1971).
(6) J. W. Nibler, unpublished results.
(7) J. H. Current, unpublished results.
(8) L. Andrews, *J. Chem. Phys.*, **48**, 972 (1968).
(9) R. O. Allen, J. M. Grzybowski, and L. Andrews, *J. Phys. Chem.*, previous paper.
(10) L. Andrews, R. O. Allen, and J. M. Grzybowski, *J. Chem. Phys.*, **61**, 2156 (1974).
(11) L. Andrews and T. G. Carver, *J. Chem. Phys.*, **49**, 896 (1968).
(12) L. Andrews, *J. Chem. Phys.*, **48**, 979 (1968).
(13) M. E. Jacox and D. E. Milligan, *J. Chem. Phys.*, **53**, 2688 (1970).
(14) P. N. Noble and G. C. Pimentel, *J. Chem. Phys.*, **49**, 3165 (1968); D. E. Milligan and M. E. Jacox, *ibid.*, **53**, 2034 (1970). Work in progress in this laboratory, B. S. Ault and L. Andrews, has confirmed the anion identification.
(15) T. G. Carver and L. Andrews, *J. Chem. Phys.*, **50**, 4235 (1969).
(16) L. Andrews and D. W. Smith, *J. Chem. Phys.*, **53**, 2956 (1970).
(17) M. E. Jacox and D. E. Milligan, *J. Chem. Phys.*, **43**, 866 (1965).
(18) A phosgene (Matheson) sample, Ar/Cl_2CO = 400/1 was examined after 20 min of sample deposition to accurately measure the 582.0-, 838.0-, and 1816-cm^{-1} Cl_2CO bands. 2.0-keV proton irradiation and sample deposition for 15 hr produced an excellent spectrum of ClCO in solid argon; the bands were observed at 1878 (0.50 OD), 572 (0.14 OD), and 285 cm^{-1} (0.04 OD).
(19) G. E. Leroi, G. E. Ewing, and G. C. Pimentel, *J. Chem. Phys.*, **40**, 2298 (1964).
(20) V. E. Bondybey, G. C. Pimentel, and P. N. Noble, *J. Chem. Phys.*, **55**, 540 (1971); D. E. Milligan and M. E. Jacox, *ibid.*, **55**, 2550 (1971). Work in progress in this laboratory has confirmed the anion identification.
(21) V. I. Vedeneyev et al., "Bond Energies, Ionization Potentials and Electron Affinities", Edward Arnold, London, 1966.
(22) (a) H. Stammeriech, R. Forneris, and K. Sone, *J. Chem. Phys.*, **23**, 972 (1955). (b) BrCl in solid argon absorbs at 436 and 428 cm^{-1}. The 437-cm^{-1} band may include absorption due to BrCl.
(23) W. Holzer, W. F. Murphy, and H. J. Bernstein, *J. Chem. Phys.*, **52**, 399 (1970).
(24) G. C. Pimentel, *J. Chem. Phys.*, **19**, 446 (1951).
(25) L. Andrews, B. S. Ault, J. M. Grzybowski, and R. O. Allen, *J. Chem. Phys.*, **62**, 2461 (1975).
(26) (a) D. E. Tevault and L. Andrews, *J. Mol. Spectrosc.*, **54**, 110 (1975); *J. Am. Chem. Soc.*, in press; (b) M. D. Sefcik, J. M. S. Henis, and P. P. Gaspar, *J. Chem. Phys.*, **61**, 4321 (1974), and references therein.
(27) J. P. Guarino and W. H. Hamill, *J. Am. Chem. Soc.*, **86**, 777 (1964); D. W. Skelly and W. H. Hamill, *J. Phys. Chem.*, **70**, 1630 (1966); T. Shida and W. H. Hamill, *J. Chem. Phys.*, **44**, 2369 (1966).
(28) R. J. Spratley and G. C. Pimentel, *J. Am. Chem. Soc.*, **88**, 2394 (1966).
(29) W. F. Howard, Jr., and L. Andrews, *J. Am. Chem. Soc.*, **95**, 2056 (1973).
(30) J. C. Evans and G. Y-S. Lo, *J. Chem. Phys.*, **44**, 3638 (1966); **45**, 1069 (1966).
(31) P. H. Kasai, *Acc. Chem. Res.*, **4**, 329 (1971).

A Raman Study of the Influence of Cesium Bromide, Tetramethylammonium Bromide, Ammonium Bromide, and Tetrabutylammonium Bromide on Water Structure at 40 and 80°

M. Lucas,* A. De Trobriand,

Commissariat à l'Energie Atomique, D.G.R., 92260 Fontenay-aux-Roses, France

and M. Ceccaldi

Commissariat à l'Energie Atomique, D.R.A., 91190 Gif-Sur-Yvette, France

(Received March 1, 1974; Revised Manuscript Received January 7, 1975)

Publication costs assisted by the Commissariat à l'Energie Atomique

The influence of CsBr, NH_4Br, Me_4NBr, and Bu_4NBr on the band ν_{OD} (HOD in H_2O) near 2500 cm^{-1} and ν_{OH} (HOD in D_2O) near 3400 cm^{-1} has been considered at 40 and 80°. At unit molality all bromides decrease the relative magnitude of the high-frequency component ascribed to nonbonded water, and the effect increases with cation size. This may possibly be ascribed to anion hydration which may not be cation independent at the salt concentration considered. At 40° all salts shift the position of the band ascribed to bonded water toward higher wave numbers. This is at least consistent with the structure breaking capability of Br^-, at 80° the shift is more important for Bu_4NBr than for CsBr. The addition of these various salts to water is not equivalent to a modification of pure water temperature. Differential spectra have been considered, in order to subtract any contribution from Br^-. They are not similar to that caused by a change of temperature for pure water, in the spectral region considered in the present investigation.

I. Introduction

Comparatively few spectroscopic studies of the influence of quaternary ammonium salts on water structure have appeared in the literature. Among studies in the region 2000–4000 cm^{-1}, Hartman's study of the influence of added salt on the position of the band ν_{OH} (HDO in D_2O) near 3400 cm^{-1} yields the result that R_4NCl salts displace the band in the same direction as a temperature increase for pure water, and the bigger the cation, the larger is the effect.[1] A study of the displacement of the combination band of pure water near 2135 cm^{-1} yields the same result,[2] but the less well understood behavior of the combination band precludes a simple interpretation.

From a Raman study of the influence of Bu_4NCl on ν_{OD} (HDO in H_2O) near 2500 cm^{-1} Walrafen has concluded that this salt is a strong structure former from the appearance of an OD stretching component near 2480 cm^{-1} on the low-frequency side of the band.[3]

Near-ir studies are all based on the concept of structural temperature, that is, that addition of a salt induces changes on a particular water band, which are equivalent to that produced by a temperature modification. Then the salt is classified as either a structure former or a structure breaker depending upon the direction of the temperature variation. Although this interpretation may seem naive, it is the only one which is possible, since near-ir bands are usually combination bands of fundamentals and overtones, and it is not known how they combine and with which percentage of each. However, there is general agreement that bands due to (OH) free groups are, relative to the more hydrogen bonded H_2O polymers bands, far more intense in the overtone regions.[4]

Among these studies, Bunzl[5] has considered the influence of R_4NBr salts on the near-ir band of water near 0.94 μm, ascribed to $2\nu_1 + \nu_3$,[6,20] with the result that all halides including CsCl, which is considered a strong structure breaker from other type of measurements,[7] produced a structural temperature t_{str} smaller than the actual solution temperature t_{soln}, so that Δt defined as $t_{str} - t_{soln}$ is negative. Bunzl concluded on the salts structural influence on water, by assuming that salts for which $\partial\Delta t/\partial t_{soln}$ is negative, e.g., Bu_4NBr, are structure formers. This type of probe is somewhat unfortunate since, if applied to $NaClO_4$, it yields that this salt does not influence water structure since $\partial\Delta t/\partial t_{soln}$ is shown to be zero. In addition by the same probe NaF should be considered a structure breaker since $\partial\Delta t/\partial t_{soln}$ is positive for this salt.[9] (Bunzl also took into account a Δt caused by "charge induced shift", but is is not clear how this Δt changes with the temperature.)

The hydration of Br^- in aqueous solution is now well documented, either by Raman spectroscopy[10,11] or X-ray spectrometry in aqueous solutions.[12] This hydration has the effect (although Br^- acts mainly as a net structure breaker[12]) to lower the concentration of "free" water molecules in solution,[13] so that Bunzl's results may be explained on the basis that the apparent negative Δt observed is caused mainly by Br^- hydration.

However NH_4Br causes a much smaller negative Δt than Me_4NBr. There is then a problem since NH_4^+ is assumed to have no influence on water structure.[14] If one subtracts the Δt caused by Me_4NBr from that caused by NH_4Br a negative value is still found although Me_4N^+ is considered a structure breaker. If this is ascribed to "charge induced shift" it is not clear why this should exist for Me_4N^+ and not for NH_4^+.

Worley and Klotz have considered the near-ir band of HOD in D_2O, 1.3–1.8 μm, and interpreted again the influence of salts in terms of structural temperature.[15] This band contains four[15] to six components,[16] which are ascribed to overtones and combinations of overtones and fun-

TABLE I: List of Position, Relative Percentage, and Half-Width of the Gaussian Components of HOD in H_2O and Aqueous Solutions, and HOD in D_2O and Salt Solutions

40°	H_2O			1 *m* CsBr			1 *m* Me_4NBr			1 *m* Bu_4NBr		
cm^{-1}	2660	2535	2350	2660	2543	2335	2660	2540	2345	2657	2540	2350
HW, cm^{-1}	80	167	90	75	167	90	80	167	90	70	167	80
%	12	85	3	8	89	3	7	90.5	2.5	5	93.5	1.5
80°	H_2O			1 *m* CsBr			1 *m* Me_4NBr			1 *m* Bu_4NBr		
cm^{-1}	2660	2552	2370	2655	2552	2370	2660	2557	2365	2660	2562	2365
HW, cm^{-1}	90	167	90	85	167	95	85	167	90	85	167	95
%	16	80	4	11	85	4	8.5	88	3.5	7	90.5	2.5
40°	1 *m* CsCl			1 *m* Bu_4NCl			1 *m* NH_4Br			80° 1 *m* NH_4Br		
cm^{-1}	2660	2537	2350	2670	2537	2350	2660	2543	2335	2655	2554	2370
HW, cm^{-1}	80	167	90	70	167	80	75	167	90	85	167	95
%	9	88	3	6	92.5	1.5	7.5	86.5	6	10.9	83	6.5
40°	D_2O			1 *m* CsBr			Bu_4NBr					
cm^{-1}	3615	3450	3230	3625	3460	3245	3625	3455	3245			
HW, cm^{-1}	100	250	120	90	240	125	80	235	120			
%	11	86	3	8.5	90	3	5	92	3			
80°	D_2O			1 *m* CsBr			Bu_4NBr					
cm^{-1}	3620	3477	3255	3620	3477	3250	3625	3483	3265			
HW, cm^{-1}	95	235	120	80	235	120	76	235	110			
%	14	83	3	9	88	3	6.5	90.5	3			

damentals. It has been found that Me_4NBr does not change the structural temperature of the solution ($\Delta t = 0$) and that Bu_4NBr causes Δt to be $-10°$ for a 1 *m* solution at an actual solution temperature of 5°, whereas Bunzl finds Δt's which are respectively -6 and $-30°$ for Me_4NBr and Bu_4NBr.[5] It is not surprising that these studies have led to different results since Worley and Klotz have based their conclusions on the variation of the ratios of ir intensities at 1.416 and 1.556 μm. In both regions several bands overlap,[16] so that it is difficult to decide what is really measured. In addition the relative decrease of the intensity at 1.416 μm which is caused by addition of Bu_4NBr may be partly caused by Br^- hydration since this band is ascribed to "free" HOD molecules.

Jolicoeur and Philip[6] have examined the band at 0.96 μm and have greatly improved Bunzl's study, since they have considered the influence of salts on the band shape parameters instead of the position only. They also compare the influence of R_4NBr on the band to the influence of a temperature modification of pure water, subtracting the influence of NaBr, and conclude that all R_4N^+ enhance water structure relative to Na^+. To explain this, it is hypothesized that the overlap of the cosphere around the structure breaking Br^- and Me_4N^+ leads to structure promotion. Whereas this is in agreement with a qualitative explanation of thermodynamic excess functions,[19] it may be argued that spectroscopy does not give a measure of an excess function, since the overall state of water in both ionic cospheres and not only in the overlapped region is examined.

The study of the influence of salts on the 8300-cm^{-1} band ($\nu_1 + \nu_2 + \nu_3$) in H_2O by Yamatera et al.[20] leads also to the same general conclusions.

In all these studies it may be noted that the concept of structural temperature is used, the "free" OH band is predominant, and that this band is modified in an apparent structure promotion direction by Br^- or Cl^- hydration. It is useful to note at this point that from proton NMR Br^- appears as effective a structure breaker as ClO_4^-,[9] whereas by near-ir spectroscopy it is found much less efficient. The reason for this discrepancy may well be that Br^- hydration is sometimes neglected in the interpretation of the ir spectra.

In view of all the discrepancies listed above, it has been found necessary to reexamine the influence of some R_4NX salts in the water structure. This paper describes the influence of the salts in the OD stretching band (20% HOD in H_2O) near 2500 cm^{-1} and the OH stretching band (HOD in D_2O) near 3400 cm^{-1} at 40 and 80°.

II. Experimental Section

A 1 aquamolal solution of CsCl, Bu_4NCl, CsBr, Me_4NBr, NH_4Br, and Bu_4NBr in H_2O–D_2O, 10% by weight H_2O in D_2O or D_2O in H_2O, has been filtered on 0.1-μ millipore filter and spectra have been recorded on samples in a thermo-

stated cell at 40 ± 0.5° and 80 ± 0.5°. The spectra were run on a PHO 60 Coderg spectrometer with a spectral resolution of 6 cm^{-1}. A Spectrophysics 165 argon ion laser operating at 4880 Å at power levels ranging from 600 to 800 mW was used for excitation. The polarization of the emerging laser beam could be rotated 90° by a quartz half-wave plate. The laser beam was then focused and passed into the sample cell. Scattered light from the sample was collected by a lens at right angle to the laser beam, and entered the double monochromator. After detection with a photomultiplier EMI 9598, amplification, and discrimination, the signal was displayed on a strip chart recorder.

The base line was recorded (either salt in pure D_2O or H_2O) since it has been shown that it is not a straight line for pure water,[21] and since the absorption from the CH_3 must be substracted. Corrected relative intensities have been determined as given in ref 21. The spectra have been corrected for spectral sensitivity. This has been calibrated as a function of frequency using a tungsten ribbon filament lamp which was temperature calibrated. As outlined previously,[22] this correction is rather important.

Results. The relative intensities are corrected for H_2O, D_2O, or CH_3 intensity, and spectral sensitivity. They are proportional to $45\alpha^2 + 7\beta^2$, where α is the mean polarizability derivative and β is the anisotropy derivative.

Before decomposition into gaussian components the spectra are transformed by multiplication of the tabulated values by

$$\frac{\nu(1 - e^{-h\nu}/kT)}{(\nu_L - \nu)^4}$$

where ν is the vibrational frequency and ν_L is the exciting frequency, as recommended by Szymanski[23] and Scherer et al.[24] It has the advantage, if no others, that the number of gaussian components needed to fit the spectra is smaller after multiplication by the factor given above, than before. Table I gives the various gaussian components for the solutions considered.

III. Discussion

First let us consider the positions of the gaussian components found for HOD in H_2O at 40°. A main component at 2535 cm^{-1} and two others at 2660 and 2350 cm^{-1} are found. The most recent gaussian decomposition[21] yields a main component at 2539 cm^{-1}, a very small one at 2664 cm^{-1}, and two others at 2420 and 2498 cm^{-1} at 25°. Another investigation[22] yields a main component at 2488 cm^{-1} and two at 2610 and 2664 cm^{-1}. At 40° Lindner[31] found a main component near 2525 cm^{-1} and two small ones at 2640 and 2360 cm^{-1}. At 40° Walrafen[26] found a main component at 2530 cm^{-1} and another near 2660 cm^{-1}, and Weston[32] a main component near 2450 cm^{-1}. In these investigations the correction by the factor $\nu(1 - e^{-h\nu/kT})/(\nu_L - \nu)^4$ does not seem to have been performed.

In any case no general agreement on the position and number of gaussian components seems to exist.

There is however general agreement that the high frequency component near 2660 cm^{-1} must be ascribed to "free" (or less H-bonded) water molecules. This is substantiated by Lindner's[31] and Walrafen's work.[26] The main component around 2530 cm^{-1} is ascribed to hydrogen-bonded water molecules.

Figure 1 shows plots of the spectra obtained for HOD in H_2O without salt or in 1 *m* CsBr, Me_4NBr, and Bu_4BNr solutions at 40°. For comparison all intensities have been plotted in such a manner that they are unity at the frequency of maximum intensity. When Figure 1 is considered, it is obvious that all bromides decrease the intensity of the high-frequency OD nonbonded component near 2660 cm^{-1} and that the bigger the cation, the more important is the effect. Another interesting feature is that, at 40°, the frequency of the main OD bonded component is shifted by all bromides toward higher frequency by about 7 cm^{-1}.

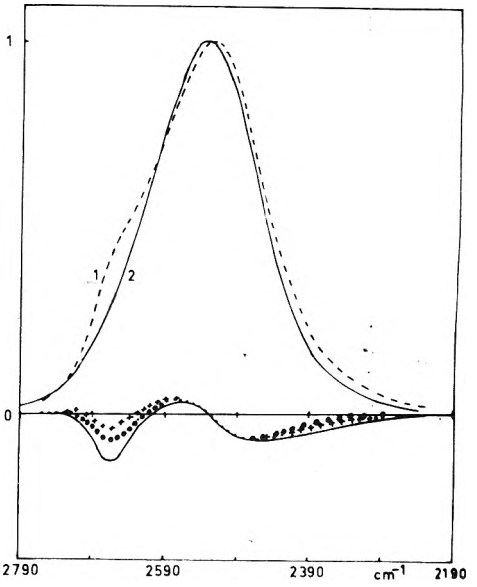

Figure 1. Plots of the band intensity *i* against wave numbers: (1) HOD in pure water; (2) HOD in 1 *m* Bu_4NBr aqueous solution. Differential intensity defined as *i*(salt solution) minus *i*(water): solid line, 1 *m* Bu_4NBr; dotted line, 1 *m* Me_4NBr; crosses, 1 *m* CsBr.

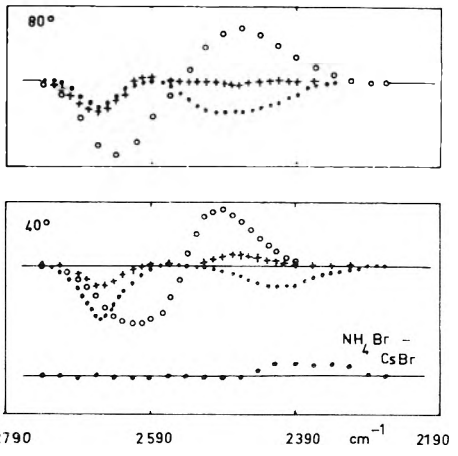

Figure 2. Plots of the differential spectra of 1 *m* Me_4NBr and Bu_4NBr aqueous solutions after subtracting the 1 *m* CsBr spectra (temperature 40 and 80°): crosses, Me_4NBr; filled circles, Bu_4NBr; open circles, plots of the differential spectra of HOD in H_2O; upper plot, water at 60° minus water at 80°; lower plot, water at 20° minus water at 40°.

The consideration of the gaussian components percentages and positions listed in Table I leads obviously to the same conclusions. At 80° the salts influence on the high-frequency component is the same as at 40°, but Bu_4NBr still shifts the main band position toward higher wave numbers than Me_4NBr, whereas when CsBr is added no shift is found. The frequency shifts induced by salts at various temperatures are qualitatively consistent with ir[2] findings.

When Bu_4NBr (and Bu_4NCl) is added to water, no low-frequency component is found near 2480 cm^{-1}.

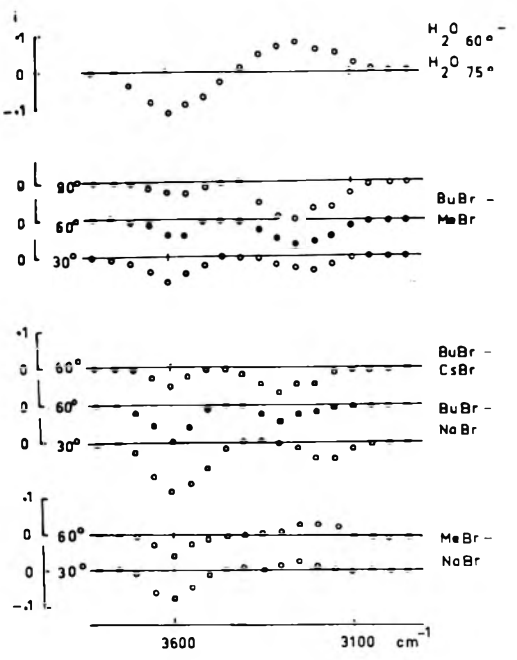

Figure 3. Plots of the differential ir spectra of 0.8 *m* Me_4NBr and Bu_4NBr aqueous solutions after subtracting the 0.8 *m* CsBr on NaBr spectra. MeBr and BuBr are short-hand notation for Me_4NBr and Bu_4NBr.

If we want to rationalize the influence of the salts in terms of "structural temperature", it is found that if the high-frequency component only is considered, all salts shift the solution structural temperature under its actual value ($\Delta t = t_{str} - t_{soln} < 0$), whereas if the main component is considered, an increase in the structural temperature ($\Delta t > 0$) is observed, since the effect of a temperature increase is to shift the main component position toward higher wave numbers for HDO in pure water.

As the ammonium ion is considered unique in its similarity with water,[14] we expect a 1 *m* solution of NH_4Br to reflect mainly the behavior of the Br^- ions. However, comparison of our spectra shows that the spectra of a 1 *m* solution of NH_4Br and CsBr are very similar, the only difference is that at wave numbers lower than 2440 cm^{-1}, a small band appears in the NH_4Br spectra, which is caused by N–H stretching.[33] As suggested by one referee, we have shown in Figure 2 the differential spectra obtained by subtracting the spectrum of HOD in a 1 *m* solution of CsBr from that of HOD in a 1 *m* solution of Me_4NBr and Bu_4NBr at 40 and 80°. We have also plotted on the same figure the spectra obtained by subtracting the spectra of HOD in H_2O at 40° (80°) from that of HOD in H_2O at 20° (60°).

The consideration of these spectra shows that the differential spectra which is expected to show the influence of the cation R_4N^+ relative to Cs^+ is not equivalent to that caused by a change of temperature for water only. (Me_4N^+ relative to Cs^+ is perhaps an exception with $\Delta t = -3°$ at 40°.)

Clearly the addition of a halide to water is not equivalent to a change of temperature, a conclusion already arrived at by other workers.[25,27,29] It is not therefore surprising that each combination band considered in the near-ir yields different results, difficult to interpret since it averages in some unknown way the two apparently contradictory informations obtained in the present work.

On the other hand, the structural informations obtained here are equally difficult to interpret. The decrease of the "free" OD (or OH) band near 2660 cm^{-1} (or 3620 cm^{-1}) cannot, in the case of CsBr or Me_4NBr relative to pure water, be ascribed safely to water structure promotion by these salts in view of all other evidence against this interpretation.[17,18] A tentative hypothesis is that this decrease may be caused by a decrease in the molal absorbance of the "free OH" band in the solution, caused by the influence of large cations.

In order to substantiate the conclusions drawn from results obtained with the Raman technique, we have recorded the infrared spectra of H_2O in various 0.8 *m* halides solutions (NaBr, CsBr, Me_4NBr, and Bu_4NBr) at 30, 60, and 90° between 2900 and 3800 cm^{-1}.[34] The vibrations in the spectra are symmetric and asymmetric stretching, an overtone of H–O–H bending,[35] and possibly Fermi resonance between these.[35] We have not attempted to dissect the spectra into their components. We have plotted the spectra in such a manner that intensity are unity at the wave number of maximum intensity and obtained by subtraction differential spectra which are shown in Figure 3. Comparison between Figure 2 and 3 shows that the spectra are very similar and that in both cases the conclusions are the same.

References and Notes

(1) K. A. Hartman, *J. Phys. Chem.*, **70**, 270 (1966).
(2) A. de Trobriand, M. Henry, M. Ceccaldi, M. M. Marciacq Rousselot, and M. Lucas, *C. R. Acad. Sci., Ser. C*, **274**, 919 (1972).
(3) G. E. Walrafen, *J. Chem. Phys.*, **55**, 768 (1971).
(4) L. M. Kleiss, H. A. Strobel, and M. C. R. Symons, *Spectrochim. Acta, Part A*, **29**, 829 (1973).
(5) K. W. Bunzl, *J. Phys. Chem.*, **71**, 1358 (1967).
(6) C. Jolicoeur and P. R. Philip, *J. Phys. Chem.*, **77**, 3071 (1973).
(7) H. S. Franck and M. W. Evans, *J. Chem. Phys.*, **13**, 507 (1945).
(8) W. A. P. Luck, *Ber. Bunsenges. Phys. Chem.*, **69**, 69 (1965).
(9) J. Davies, S. Ormondroyd, and M. C. R. Symons, *Trans. Faraday Soc.*, **67**, 3465 (1971).
(10) G. E. Walrafen, *J. Chem. Phys.*, **52**, 4176 (1970).
(11) Z. Kecki, P. Dryjanski, and E. Kozlowska, *Rocz. Chem.*, **42**, 1749 (1968).
(12) A. H. Narten, *J. Phys. Chem.*, **74**, 765 (1970).
(13) R. E. Verrall in "Water a Comprehensive Treatise", Vol. 3, F. Franks, Ed., Plenum Press, New York, N.Y., 1973, p 243 (this refers to Cl^- hydration, but the effect for Br^- is supposed by us to be the same).
(14) P. M. Vollmar, *J. Chem. Phys.*, **39**, 2236 (1963).
(15) J. D. Worley and I. M. Klotz, *J. Chem. Phys.*, **45**, 2868 (1966).
(16) W. A. P. Luck and W. Ditter, *Z. Naturforsch. B*, **24**, 482 (1969).
(17) R. L. Kay, *Adv. Chem. Ser.*, **No. 73**, 1 (1968).
(18) "Chemical Physics of Ionic Solutions", B. E. Conway and R. G. Barradas, Ed., Wiley, New York, N.Y., 1967, p 92.
(19) J. E. Desnoyers, M. Arel, G. Perron, and C. Jolicoeur, *J. Phys. Chem.*, **73**, 3346 (1969).
(20) H. Yamatera, B. Fitzpatrick, and G. Gordon, *J. Mol. Spectrosc.*, **14**, 268 (1964).
(21) W. C. Mundy, L. Gutierrez, and F. H. Spedding, *J. Chem. Phys.*, **59**, 2173 (1973).
(22) W. F. Murphy and H. H. Bernstein, *J. Phys. Chem.*, **76**, 1147 (1972).
(23) "Raman Spectroscopy", H. A. Szymanski, Ed., Plenum Press, New York, N.Y., 1967.
(24) J. R. Scherer, M. L. Go, and S. Kint, *J. Phys. Chem.*, **77**, 2108 (1973).
(25) P. Rhine, O. Williams, G. M. Hale, and M. R. Querris, *J. Phys. Chem.*, **78**, 238 (1974).
(26) G. E. Walrafen, *J. Chem. Phys.*, **48**, 244 (1968).
(27) P. Dryjanski and Z. Kecki, *J. Mol. Structure*, **12**, 219 (1972).
(28) Z. Kecki, J. Witanowski, K. Akst-Lipszyc, and S. Minc, *Rocz. Chem.*, **40**, 919 (1966).
(29) H. R. Wyss and M. Falk, *Can. J. Chem.*, **48**, 607 (1970).
(30) Reference 13, p 245.
(31) H. A. Lindner, Doctoral Dissertation, Karlsruhe, 1970.
(32) R. E. Weston, *Spectrochim. Acta*, **18**, 1257 (1962).
(33) M. Freymann, R. Freymann, and Yeou Ta, *C. R. Acad. Sci.*, **207**, 728 (1938); ref 23; I. R. Rao and C. S. Rao, *Z. Phys.*, **88**, 127 (1934).
(34) Spectra were recorded on a Perkin-Elmer 521 with a cell with CaF_2 windows and a home-made temperature control, cell thickness: ca. 1 μ. Each spectrum is the average of four independent measurements.
(35) This is what is deduced from the position of these components in the water vapor. In another investigation, five components are found in the ir spectra of liquid water, in agreement with Raman spectra: G. E. Walrafen in "Water a Comprehensive Treatise", Vol. 1, F. Franks, Ed., Plenum Press, New York, N.Y., 1972, p 202.

Proton Magnetic Resonance Investigations of Alkylammonium Carboxylate Micelles in Nonaqueous Solvents. VI.[1] Aggregation of Hexylammonium Propionate in Dimethyl Sulfoxide–Benzene and Dimethyl Sulfoxide–Water Mixed Solvent Systems

E. J. Fendler, V. G. Constien,[2] and J. H. Fendler*

Department of Chemistry, Texas A & M University, College Station, Texas 77843
(Received July 5, 1974; Revised Manuscript Received January 13, 1975)

Changes in the chemical shifts of the magnetically discrete protons of hexylammonium propionate (HAP) have been utilized in DMSO–benzene and DMSO–water solvent systems to establish aggregation behavior. Over the ranges of 100 to 0 wt % water to DMSO and 100 to 0 wt % DMSO to benzene, the aggregation behavior ranged from that of normal micelles in pure water to that of reversed aggregates in benzene.

Introduction

Typical of reversed aggregate-forming surfactants exhibiting considerable catalytic activity are alkylammonium carboxylates which have been observed to catalyze reactions by factors of up to 5×10^6-fold.[3-9] In order to obtain a better understanding of the substrate–aggregate interactions involved and the mechanism of catalysis by alkylammonium carboxylate reversed "micellar" aggregates, systematic investigations of the physiochemical properties of several of these surfactant systems have been carried out in various nonaqueous solvents using ^{1}H NMR spectroscopy and vapor-phase osmometry.[10-14] These investigations indicated that alkylammonium carboxylate surfactants in nonaqueous solvents generally tend to form rather small aggregates consisting of less than eight monomers in which the polar headgroups are located in the interior while the hydrophobic hydrocarbon chains are oriented toward and partially in contact with the bulk solvent. These data are, however, also compatible with a multiple-equilibrium model which does not exclude the possibility of higher aggregates, i.e., relatively large micelles in the more concentrated solutions.[14,15] In addition, there appears to be a good relationship between the critical micelle concentrations and both macroscopic (e.g., dielectric constants) and microscopic (e.g., $E_T(30)$ values) solvent polarity parameters; however, the predominant solvent–surfactant headgroup interactions are explicable in terms of bulk solvent polarity.[12] (The greater the interaction of the ionic surfactant monomers with the solvent, the less is the tendency to aggregate as manifested by higher critical micelle concentrations.) Also, based on the single monomer–n-mer equilibrium model, the aggregation number of alkylammonium propionates appears to increase with an increasing number of carbon atoms in the alkyl chain and slightly with increasing solvent polarity.[12] Since the structure and catalytic properties of alkylammonium carboxylate aggregates are altered by changes in solvent properties such as polarity, bulk, and geometry,[12] aggregation behavior in overlapping mixed solvent systems would shed light on micellar properties as a function of changing solvent composition. To accomplish this end, we have investigated the aggregation of hexylammonium propionate (HAP) in the overlapping solvent systems benzene–dimethyl sulfoxide and dimethyl sulfoxide–water using ^{1}H NMR spectroscopy, surface tensiometry, and dye absorption spectrophotometry.

Experimental Section

Reagent grade benzene-d_6 (Thompson-Packard, 99.5% d) was distilled from calcium hydride onto and stored over freshly dried Linde Type 5A molecular sieve. Dimethyl-d_6 sulfoxide (DMSO-d_6) (Diaprep, Aldrich, and Merck Sharp and Dohme of Canada, 99.5% d) was stored over freshly activated Linde Type 5A molecular sieves. If ^{1}H NMR analysis of the DMSO-d_6 revealed trace amounts of water present, the DMSO-d_6 was further dried by storing over calcium hydride for 2 or 3 days followed by filtering in a drybox onto fresh molecular sieve. Deuterium oxide (Thompson-Packard, 99.8% d) was used as received. DMSO-d_6 and benzene-d_6–DMSO-d_6 solutions were prepared in a dry nitrogen atmosphere to avoid contamination with atmospheric moisture. In the surface tension and spectral change measurements doubly distilled water and Fisher certified spectroanalyzed dimethyl sulfoxide which had been stored over Linde Type 5A molecular sieves were used. All mixed solvent solutions were prepared on a weight percent basis.

Hexylammonium propionate (HAP) was prepared by the method of Kitahara.[16] Reagent grade propionic acid (53.4 g, 0.94 mol) was added to a refluxing solution containing 95.0 g (0.94 mol) of n-hexylamine (dried and purified by vacuum distillation from calcium hydride) in 80 ml of dry reagent grade hexane over a period of 1 hr. The solution was refluxed for 4 hr, the solvent removed by vacuum rotary evaporation, and the product doubly distilled in vacuo, yielding colorless product, bp 69–70° at 0.44 Torr. The purity of the HAP was established from its sharp boiling point and from its ^{1}H NMR spectrum.[10]

The 100-MHz nuclear magnetic resonance spectra were obtained on a modified Varian Associates HA-100 spectrometer equipped with a Hewlett-Packard Model 200 ABR audio oscillator and frequency counter. Each spectrum was recorded at least three times after equilibration to the ambient probe temperature of 33.5 ± 0.5°. All spectra were determined on freshly prepared solutions and were measured relative to neat tetramethylsilane contained in a Wilmad 520-2 internal coaxial tube. Individual chemical shift measurements are accurate to ±0.2 Hz. Coupling constants were measured from spectra obtained at 500-Hz sweep widths and are accurate to at least ±0.4 Hz. Bulk susceptibility corrections have not been applied; however, the differences have been predicted and/or found to be

TABLE I: ^{1}H NMR Chemical Shifts of Hexylammonium Propionate in Benzene-d_6–DMSO-d_6 Solvent Systems

Benzene-d_6–DMSO-d_6, w/w[b]	HAP, M	δ, ppm[a]				
		$CH_3(CH_2)_4$-$CH_2NH_3^+$	$CH_3CH_2CO_2^-$	$CH_3CH_2CO_2^-$	$CH_3(CH_2)_4$-$CH_2NH_3^+$	$CH_3(CH_2)_4$-$CH_2NH_3^+$
100/0	0.487	0.670	1.052	2.219	2.640	9.382
	0.442	0.660	1.045	2.212	2.623	9.351
	0.390	0.650	1.042	2.200	2.618	9.292
	0.293	0.647	1.037	2.203	2.609	9.270
	0.147	0.641	1.023	2.195	2.576	9.000
	0.073	0.642	1.016	2.182	2.544	8.480
	0.037	0.640	0.996	2.156	2.499	7.877
	0.027	0.681	0.973	2.132	2.467	7.839
	0.021	0.667	0.957	2.114	2.433	7.621
	0.018		0.939	2.102		6.157
75/25	0.26	0.777	1.122	2.267	2.730	8.249
	0.20	0.775	1.105	2.256	2.688	7.837
	0.17	0.773	1.100	2.249	2.693	7.176
	0.13	0.771	1.096	2.242	2.672	6.816
	0.10	0.769	1.084	2.247	2.650	6.630
	0.064	0.764	1.069	2.236	2.620	5.923
	0.042	0.766	1.057	2.221	2.599	4.907
	0.032	0.773	1.027	2.189	2.561	4.460
	0.025	0.781	1.016	2.180	2.542	4.241
	0.016	0.793	0.991	2.156	2.518	3.989
50/50	0.48	0.882	1.169	2.297	2.833	8.807
	0.40	0.880	1.167	2.297	2.827	8.671
	0.32	0.875	1.160	2.292	2.805	8.208
	0.24	0.874	1.158	2.293	2.800	7.849
	0.22	0.873	1.162	2.292	2.798	7.695
	0.16	0.870	1.146	2.291	2.770	7.251
	0.12	0.884	1.155	2.290	2.767	7.050
	0.11	0.875	1.140	2.288	2.761	6.569
	0.08	0.879	1.135	2.285	2.694	6.003
	0.05	0.882	1.129	2.283	2.734	5.691
	0.04	0.886	1.122	2.282	2.708	5.340
25/75	1.96	1.061	1.253	2.363	3.006	9.583
	1.19	1.050	1.251	2.354	2.981	9.234
	0.98	1.052	1.247	2.348	2.965	9.229
	0.60	1.040	1.243	2.341	2.951	8.518
	0.49	1.035	1.242	2.345	2.950	8.366
	0.25	1.030	1.232	2.343	2.919	7.699
	0.12		1.213	2.341	2.875	6.550
	0.06	1.025	1.218	2.359	2.788	5.663
	0.03	1.020	1.208	2.363	2.398	4.730
	0.02	1.022	1.207	2.373		4.169
16/84	2.02	1.113	1.276	2.371	3.039	9.633
	1.01	1.110	1.275	2.371	3.017	8.940
	0.51	1.094	1.261	2.362	2.986	8.359
	0.18	1.083	1.246	2.357	2.932	7.007
	0.09	1.087	1.246	2.366	2.906	5.668
	0.04	1.097	1.257	2.393	2.893	4.684
	0.02	1.087	1.246	2.405	2.854	4.368

[a] Obtained at 100 MHz and 33.5° relative to external TMS; see Experimental Section for details. [b] For data in pure DMSO, see Table II.

small for a variety of aqueous and nonaqueous micellar systems[10-13, 18-20] and would not affect the interpretation of the data significantly.

Surface tension–HAP concentration profiles were obtained at 25.0 ± 0.1° for water, DMSO, and DMSO–H_2O solutions by use of a Cenco du Noüy tensiometer with a 6-cm platinum–iridium ring. The surface tension was calculated from an expression[21] involving the measured force, ring dimensions, and the correction factor. The absence of minima[22] in these plots of surface tension vs. concentration indicates the absence of impurities in the surfactant.

Critical micelle concentration determinations using dye absorption spectrophotometry were carried out using Cary 14 and Beckman DU spectrophotometers on HAP solutions

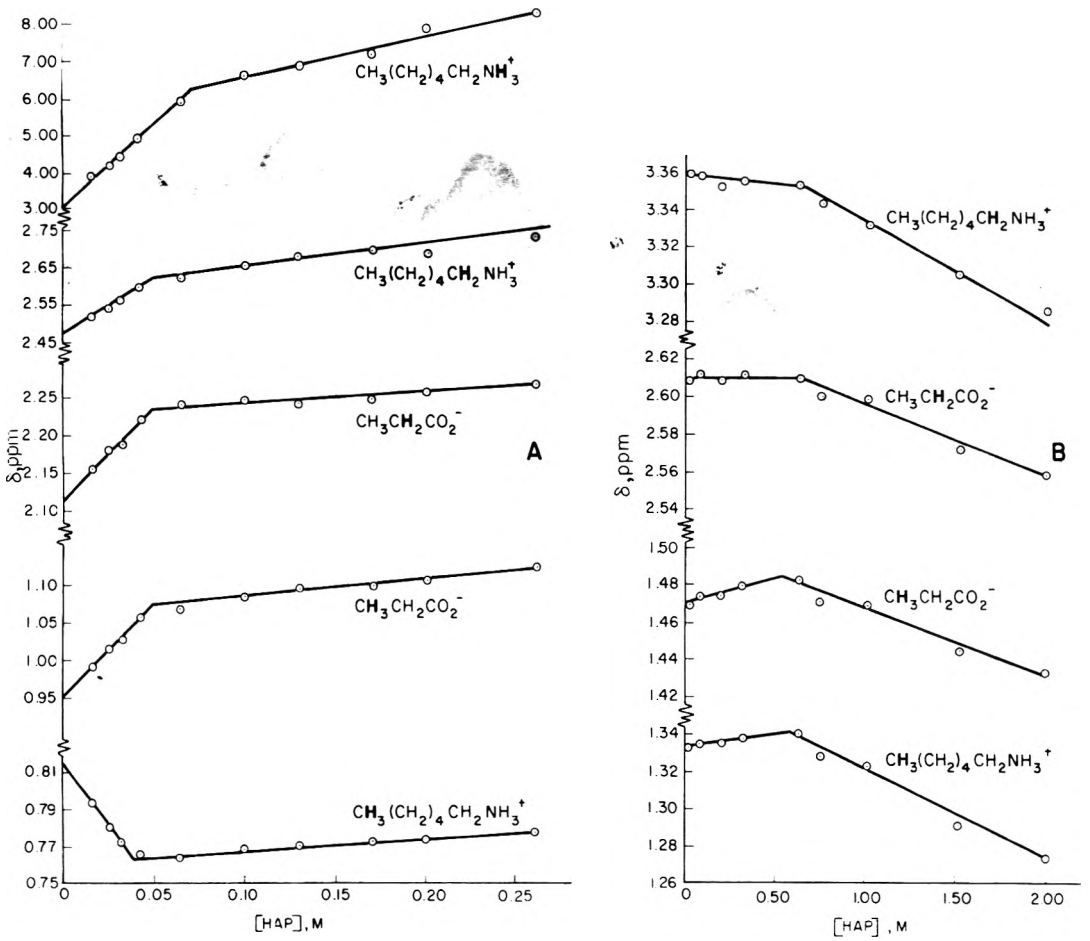

Figure 1. Chemical shifts (δ, ppm) of hexylammonium propionate (HAP) as a function of stoichiometric concentration (M): (A) 75/25% benzene-d_6–DMSO-d_6 (w/w); (B) 50/50 DMSO-d_6–D_2O (w/w).

containing a low concentration of the appropriate dye. The dyes, rhodamine-B (Allied Chemical and Dye Corp.) and pinacyanol chloride (Eastman), were used without further purification.

Results and Discussion

^1H NMR Spectra of HAP. The proton NMR spectra of hexylammonium propionate (HAP) in the overlapping mixed solvent systems of benzene-d_6–DMSO-d_6 and DMSO-d_6–D_2O exhibit the same general appearance in terms of resonances and multiplicities as those reported for HAP in other solvent systems[10,12] and consist of a sharp triplet for the terminal methyl protons of the hexylammonium ion and for those of the propionate ion, a poorly resolved broad resonance for the intermediate methylene protons of the hexylammonium ion, a quartet for the propionate methylene protons, an apparent triplet for the methylene protons adjacent to the ammonium ion, and a relatively sharp singlet for the ammonium protons in the benzene-d_6–DMSO-d_6 solvent systems. Chemical shifts, δ, of the magnetically discrete protons of HAP in the pure solvents and in the overlapping mixed solvent systems comprised of benzene-d_6–DMSO-d_6 and DMSO-d_6–D_2O are given in Tables I and II and are illustrated for all of the protons in the 75% benzene-d_6–25% DMSO-d_6 and the 50% DMSO-d_6–50% D_2O systems in Figure 1. As in the cases of other micelle-forming surfactant systems, only single weight-averaged resonances are observed for the protons of the monomeric and aggregated surfactant due to rapid exchange on the NMR time scale (10^{-4} sec). It is apparent (see Figure 1 for example) that relatively well-defined discontinuities occur at approximately the same surfactant concentration for a given solvent system. The point of this break in the plots may be considered an operational NMR critical micelle concentration (cmc) since the values are in reasonable agreement with those obtained using other techniques (vide infra). The discontinuities exist for all of the benzene-d_6–DMSO-d_6 concentrations examined; in the DMSO-d_6–D_2O system, however, there are significant discontinuities with the exception of the 75–95% DMSO-d_6–D_2O region (see Figure 2). This region coincides with one in which DMSO undergoes hydration changes[23-25] and it is conceivable that this solvent reorganization, e.g., strong bonding of water to DMSO, alters the aggregation behavior.

Observable coupling constants for HAP in the overlapping benzene-d_6–DMSO-d_6—DMSO-d_6–D_2O solvent systems are given in Table III. Not unexpectedly, these values show little dependence on solvent composition within experimental error.

From plots of δ vs. C_D and $1/C_D$, the monomeric, δ_m, and micellar, δ_M, chemical shifts were obtained upon extrapolation to zero and infinite HAP concentration, respectively, according to

$$\delta = \delta_M + \frac{\mathrm{cmc}}{C_D}(\delta_M - \delta_M) \qquad (1)$$

TABLE II: ^{1}H NMR Chemical Shifts of Hexylammonium Propionate in DMSO-d_6–D_2O Solvent Systems

DMSO-d_6–D_2O, w/w	HAP, M	δ, ppm[a]				
		$CH_3(CH_2)_4$-$CH_2NH_3^+$	$CH_3CH_2CO_2^-$	$CH_3CH_2CO_2^-$	$CH_3(CH_2)_4$-$CH_2NH_3^+$	$CH_3(CH_2)_4$-$CH_2NH_3^+$
100/0	0.38		1.311	2.393	3.053	8.536
	0.32		1.305	2.386	3.386	8.319
	0.19		1.300	2.392	3.025	7.585
	0.10		1.304	2.410		6.195
	0.06		1.307	2.423	2.992	5.800
	0.05		1.307	2.433	2.970	5.575
	0.03		1.322	2.459	2.969	5.073
	0.02		1.324	2.474		4.887
95/5	1.98	1.222	1.331	2.413	3.123	
	1.00	1.235	1.331	2.406	3.112	
	0.50		1.334	2.409	3.116	
	0.27		1.332	2.409	3.107	
	0.16		1.337	2.416	3.098	
	0.12		1.344	2.441		
	0.08		1.332	2.413		
	0.06		1.349	2.423		
85/15	2.05	1.245	1.360	2.456	3.169	
	1.03	1.272	1.376	2.463	3.183	
	0.51	1.288	1.383	2.466	3.189	
	0.26	1.294	1.385	2.461	3.198	
	0.13	1.297	1.387	2.464	3.193	
	0.06		1.387	2.470	3.202	
75/25	2.02	1.258	1.391	2.491	3.218	
	1.51	1.279	1.404	2.503	3.232	
	1.01	1.292	1.412	2.510	3.249	
	0.75	1.303	1.415	2.513	3.247	
	0.50	1.313	1.423	2.520	3.257	
	0.38	1.315	1.422	2.514	3.259	
	0.25	1.324	1.429	2.519	3.268	
	0.19	1.327	1.433	2.525	3.272	
	0.10	1.331	1.429	2.519	3.272	
	0.04	1.332	1.431	2.510	3.278	
	0.02	1.334	1.433	2.523		
65/35	2.02	1.275	1.417	2.527	3.258	
	1.01	1.316	1.446	2.554	3.289	
	0.51	1.338	1.461	2.567	3.312	
	0.25	1.345	1.464	2.572	3.318	
	0.13	1.347	1.464	2.571	3.319	
	0.06	1.348	1.466	2.569	3.318	
50/50	1.99	1.274	1.433	2.559	3.286	
	1.51	1.291	1.445	2.572	3.305	
	1.01	1.323	1.469	2.599	3.332	
	0.75	1.328	1.471	2.600	3.343	
	0.63	1.340	1.482	2.610	3.353	
	0.32	1.337	1.479	2.611	3.355	
	0.20	1.335	1.476	2.609	3.353	
	0.08	1.334	1.473	2.612	3.358	
	0.02	1.332	1.469	2.609	3.359	
25/75	2.04	1.287	1.462	2.602	3.346	
	1.51	1.295	1.471	2.613	3.357	
	1.24	1.316	1.485	2.632	3.379	
	1.02	1.319	1.490	2.636	3.384	
	0.76	1.325	1.491	2.640	3.392	
	0.62	1.331	1.499	2.651	3.402	
	0.51	1.329	1.491	2.646	3.401	
	0.26	1.328	1.498	2.655	3.414	
	0.16	1.329	1.498	2.652	3.413	

Table II *(Continued)*

DMSO-d_6–D_2O, w/w	HAP, M	δ, ppm[a] $CH_3(CH_2)_1$-$CH_2NH_3^+$	$CH_3CH_2CO_2^-$	$CH_3CH_2CO_2^-$	$CH_2(CH_2)_1$-$CH_2NH_3^+$	$CH_3(CH_2)_1$-$CH_2NH_3^+$
5/95	2.03	1.296	1.488	2.630	3.374	
	1.54	1.318	1.499	2.651	3.400	
	0.77	1.333	1.515	2.685	3.432	
	0.38	1.332	1.517	2.691	3.443	
	0.19	1.320	1.506	2.690	3.436	
	0.10	1.317	1.503	2.688	3.432	
0/100	3.00	1.264	1.445	2.594	3.338	
	2.04	1.285	1.476	2.630	3.373	
	1.52	1.299	1.487	2.648	3.389	
	1.01	1.312	1.498	2.669	3.415	
	0.63	1.328	1.516	2.692	3.444	
	0.50	1.326	1.517	2.696	3.450	
	0.33	1.322	1.513	2.691	3.443	
	0.10	1.319	1.505	2.690	3.446	
	0.08	1.317	1.508	2.696	3.444	
	0.07	1.313	1.507	2.691	3.448	

[a] Obtained at 100 MHz and 33.5° relative to external TMS; see Experimental Section for details.

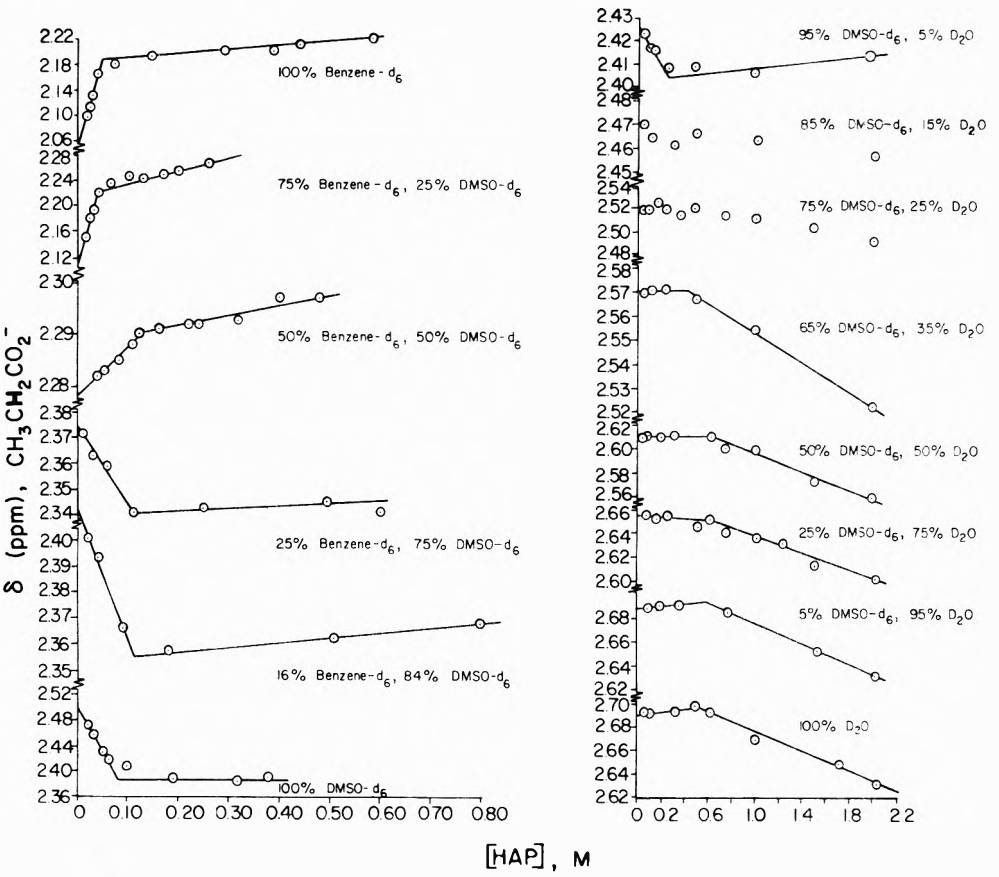

Figure 2. Chemical shifts (δ, ppm) of the propionate methylene protons ($CH_3CH_2CO_2^-$) of HAP as a function of stoichiometric concentration (C_D, M) in benzene-d_6–DMSO-d_6 and DMSO-d_6–D_2O solvent systems.

where δ, δ_M, and δ_m are the observed, micellar, and monomeric chemical shifts, cmc is the critical micelle concentration, and C_D is the stoichiometric surfactant concentration. This treatment is essentially based, however, on a single equilibrium model and involves the assumption that above the cmc the concentration of monomers remains constant and is equal to the cmc. Although these assumptions are most likely invalid in some cases, this treatment has been profitably employed previously to compare qualitatively the effects of changes in surfactant chain length and of solvent on the structure of alkylammonium carboxylate aggregates.[10-13] Values of δ_M and δ_m for the various protons in

TABLE III: Coupling Constants for Hexylammonium Propionate in Benzene-d_6–DMSO-d_6–D_2O Solvent Systems

% DMSO-d_6	0	25	50	75	84	100	95	85	75	65	50	25	5	0
% Benzene-d_6	100	75	50	25	16	0								
% D_2O							5	15	25	35	50	75	95	100
HAP, M	0.39	0.20	0.22	0.49	1.01	0.38	0.08	0.51	1.51	0.50	0.02	1.51	1.54	0.25
Proton measured	J, Hz													
$CH_3CH_2CO_2^-$	7.6 ± 0.4	7.5 ± 0.1	7.6 ± 0.1	7.4 ± 0.1	7.5 ± 0.1	7.6 ± 0.2	7.7 ± 0.1	7.6 ± 0.2	7.6 ± 0.1		7.0 ± 0.2	7.5 ± 0.4	7.7 ± 0.2	7.6 ± 0.2
$CH_3CH_2CO_2^-$	7.4 ± 0.5	7.5 ± 0.2	7.3 ± 0.2	7.7 ± 0.2	7.6 ± 0.3	7.5 ± 0.4	7.3 ± 0.2	7.4 ± 0.1	7.6 ± 0.1	7.7 ± 0.1	7.7 ± 0.2	7.5 ± 0.1	7.5 ± 0.1	7.5 ± 0.1
$CH_3(CH_2)_4CH_2NH_3^+$	6.3 ± 0.3	6.1 ± 0.4	6.0 ± 0.4	5.9 ± 0.4	6.0 ± 0.7			7.1 ± 0.2	7.4 ± 0.4			6.5 ± 0.4	6.0 ± 0.5	6.3 ± 0.4
$CH_3(CH_2)_4CH_2NH_3^+$	7.8 ± 0.3	7.3 ± 0.2	7.3 ± 0.1	6.9 ± 0.1	7.4 ± 0.6	7.0 ± 0.4					7.5 ± 0.4	7.5 ± 0.5	7.4 ± 0.5	7.5 ± 0.4

TABLE IV: Monomeric (δ_m) and Micellar (δ_M) Chemical Shifts of Hexylammonium Propionate in Benzene-d_6–DMSO-d_6 and DMSO-d_6–D_2O[a]

Solvent system	Proton									
	$CH_3CH_2CO_2^-$		$CH_3CH_2CO_2^-$		$CH_3(CH_2)_4$-$CH_2NH_3^+$		$CH_3(CH_2)_4$-$CH_3CH_2NH_3^+$		$CH_3(CH_2)_4$-$CH_3NH_3^+$	
	δ_m	δ_M	δ_m	δ_M	δ_m	δ_M	δ_m	δ_M	δ_m	δ_M
Benzene-d_6	0.758	1.063	1.983	2.110	0.746	0.685	2.287	2.660	1.430	9.430
Benzene-d_6–DMSO-d_6, w/w										
75/25	0.952	1.183	2.118	2.230	0.817	0.784	2.475	2.772	3.200	9.485
50/50	1.106	1.181	2.276	2.305	0.902	0.884	2.694	2.865	4.500	9.640
25/75	1.197	1.257	2.384	2.373	1.020	1.070	2.970	2.694	3.825	10.050
16/84	1.251	1.285	2.419	2.377	1.067	1.113	2.800	3.050	3.800	9.800
DMSO-d_6	1.337	1.327	2.505	2.402			2.940	3.144	4.254	12.08
DMSO-d_6-D_2O, w/w										
95/5	1.357	1.331	2.464	2.415						
85/15	1.389	1.363	2.474	2.453	1.301	1.251	3.302	3.168		
75/25	1.433	1.374	2.524	2.477	1.334	1.227	3.281	3.190		
65/35	1.467	1.426	2.570	2.505	1.349	1.292	3.319	3.246		
50/50	1.470	1.414	2 606	2.540	1.333	1.247	3.359	3.263		
25/75	1.499	1.432	2.655	2.560	1.331	1.249	3.422	3.241		
5/95	1.497	1.471	2.685	2.609	1.311	1.289	3.429	3.357		
D_2O	1.505	1.450	2.689	2.569	1.315	1.253	3.444	3.334		

[a] Mean chemical shifts in ppm relative to external TMS at 33.5° according to eq 1 using plots of δ vs. C_D for δ_m and plots of δ vs. $1/C_D$ for δ_M.

TABLE V: Chemical Shift Dependence of HAP Protons on Solvent Composition[a]

Proton	Solvent composition ranges								
	100% benzene-d_6 to 100% DMSO-d_6			100% DMSO-d_6 to 60% DMSO-d_6–40% D_2O			60% DMSO-d_6–40% D_2O to 100% D_2O		
	δ^b	δ_M	δ_m	δ^c	δ_M	δ_m	δ^c	δ_M	δ_m
$CH_3CH_2CO_2^-$	0.25	0.28	0.58	0.41	0.23	0.28	0.10	0.07	0.05
$CH_3CH_2CO_2^-$	0.18	0.20	0.53	0.44	0.25	0.19	0.18	0.23	0.19
$CH_3(CH_2)_4CH_2NH_3^+$	0.52	0.22	0.22	0.25	0.30	0.60	0.	0	0
$CH_3(CH_2)_4CH_2NH_3^+$	0.42	0.45	0.77 0.90	0.65	0.14	1.35	0.20	0.14	0.20
$CH_3(CH_2)_4CH_2NH_3^+$	4.1	0.75	6.5 0						

[a] Slope (× 100) of plots of δ_M, δ_m, and δ vs. solvent composition. [b] [HAP] = 0.50 M. [c] [HAP] = 1.00 M.

TABLE VI: Equilibrium Constants (K) and Aggregation Numbers (n) for Hexylammonium Propionate in Benzene-d_6 and DMSO-d_6–D_2O[a]

Solvent system	Surfactant protons utilized	n[b]	K, M^{1-n}[b]
Benzene-d_6	$\mathbf{CH_3}CH_2CO_2^-$ $CH_3(CH_2)_4CH_2NH_3^+$	2.4	6×10^2
Benzene-d_6–DMSO-d_6, w/w			
75/25	$CH_3CH_2CO_2^-$ $CH_3(CH_2)_4CH_2NH_3^+$ $CH_3(CH_2)_4CH_2NH_3^+$	3.0	8×10^3
50/50	$CH_3CH_2CO_2^-$ $CH_3CH_2CO_2^-$ $CH_3(CH_2)_4CH_2NH_3^+$ $CH_3(CH_2)_4CH_2NH_3^+$	3.0	1×10^2
25/75	$CH_3CH_2CO_2^-$ $CH_3(CH_2)_4CH_2NH_3^+$	2.6	5×10^1
16/84	$CH_3(CH_2)_4CH_2NH_3^+$ $CH_3(CH_2)_4CH_2NH_3^+$ $CH_3(CH_2)_4CH_2NH_3^+$	1.9	1×10^1
DMSO-d_6	$CH_3(CH_2)_4CH_2NH_3^+$ $CH_3(CH_2)_4CH_2NH_3^+$	2.2	4
DMSO-d_6–D_2O, w/w			
85/15	$CH_3CH_2CO_2^-$ $CH_3CH_2CO_2^-$ $CH_3(CH_2)_4CH_2NH_3^+$ $CH_3(CH_2)_4CH_2NH_3^+$	2.3	3
75/25	$CH_3CH_2CO_2^-$ $CH_3(CH_2)_4CH_2NH_3^+$ $CH_3(CH_2)_4CH_2NH_3^+$	2.4	0.8
65/35	$CH_3CH_2CO_2^-$ $CH_3(CH)_4CH_2NH_3^+$	2.2	0.5
25/75	$CH_3CH_2CO_2^-$ $CH_3CH_2CO_2^-$ $CH_3(CH_2)_4CH_2NH_3^+$ $CH_3(CH_2)_4CH_2NH_3^+$	2.5	0.2

[a] Values of n and K are considered to be accurate within ±0.5 and ±20%, respectively. [b] Calculated assuming a simple equilibrium model, eq 3-5.

TABLE VII: Critical Micelle Concentrations of HAP in Benzene-d_6–DMSO-d_6–D_2O Solvent Systems from ^1H Chemical Shift Data[a]

% DMSO-d_6	0	25	50	75	84	100	95	85	75	65	50	25	5	0
% benzene-d_6	100	75	50	25	16	0								
% D_2O							5	15	25	35	50	75	95	100
Proton	Critical micelle concentration, M													
$CH_3CH_2CO_2^-$	0.026 to 0.035	0.048	0.12	0.09 to 0.14	0.11	0.10	0.12 to 0.18			0.51	0.62	0.64 to 0.72	0.48	0.56
$CH_3CH_2CO_2^-$	0.028 to 0.042	0.048 to 0.042	0.12	0.08	0.10	0.08	0.16 to 0.28	≈0.18		0.30 to 0.44	0.51 to 0.63	0.60	0.48 to 0.58	0.50 to 0.58
$CH_3(CH_2)_4CH_2NH_3^+$	0.030 to 0.040	0.040	0.14	0.09 to 0.15	0.08 to 0.13				~0.38	0.41	0.62	0.61 to 0.72	0.52	0.52
$CH_3(CH_2)_4CH_2NH_3^+$	0.037 to 0.044	0.056 to 0.048	0.11 to 0.15	0.08 to 0.13	0.09	0.10			≈0.37	0.37 to 0.40	0.62		0.45	0.50 to 0.62
$CH_3(CH_2)_4CH_2NH_3^+$	0.024 to 0.034	0.076	0.11 to 0.16	0.14	0.18 to 0.20									
Av values	0.034	0.052	0.13	0.11	0.12	0.10	0.19	≈0.18	≈0.38	0.42	0.61	0.65	0.50	0.55

[a] At 33.5°; see Experimental Section for additional details.

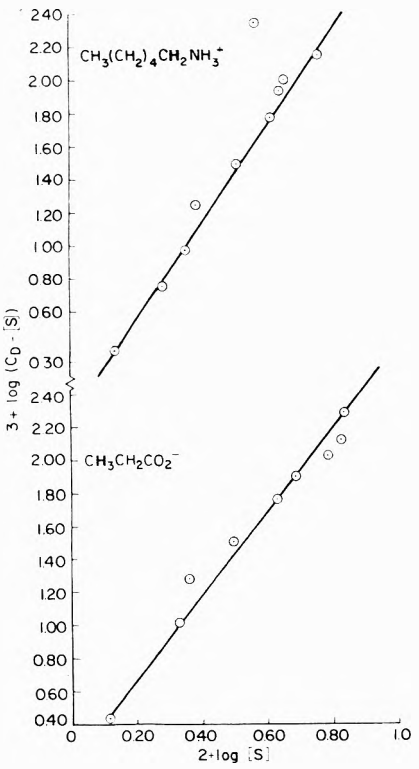

Figure 3. Aggregation number plots for HAP in 75/25% benzene-d_6–DMSO-d_6 (w/w) according to eq 3.

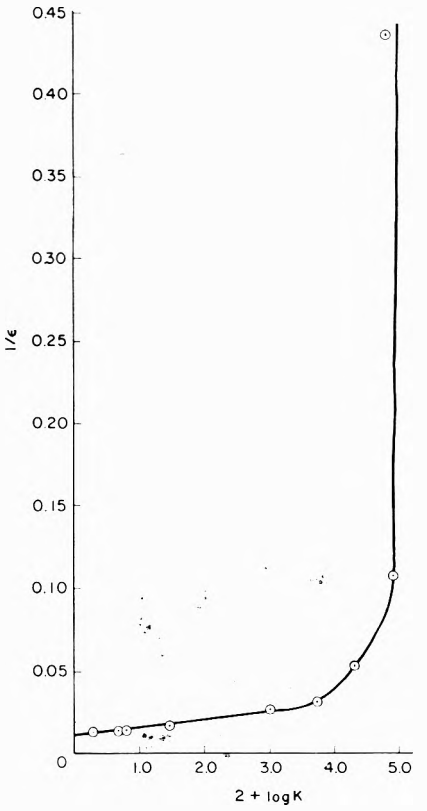

Figure 4. Dependence of the equilibrium association constant, K, of HAP on the reciprocal dielectric constant, ϵ, of the benzene-d_6–DMSO-d_6 and DMSO-d_6–D_2O solvent systems at 33.5°.

the benzene-d_6–DMSO-d_6 and DMSO-d_6–D_2O solvent systems are given in Table IV. For purposes of comparison, the observed chemical shifts, and those of the monomeric, δ_m, and micellar, δ_M, species for 0.50 M HAP in the benzene-d_6–DMSO-d_6 systems and 1.0 M HAP in the DMSO-d_6–D_2O systems have been fitted to

$$\delta_X = \delta_0 + aX \tag{2}$$

where δ_x is δ, δ_M, or δ_m; δ_0 is the chemical shift in pure benzene-d_6 or DMSO-d_6, and a is the dependence on solvent composition (i.e., the slope of plots of δ_x vs. solvent composition (w/w)). The values of a are given in Table V for the ranges in which the dependence is linear within experimental error.

From the values of the micellar, δ_M, and monomeric, δ_m, chemical shifts approximate values for the concentration of the monomer, [S], aggregation number, n, and equilibrium constant for micelle formation, K, have been calculated from eq 1, 3, and 4 as described previously.[10-12] This treatment involves an idealized single equilibrium between surfactant monomers, S, and micelles, S_n, i.e.

$$\log (C_D - [S]) = \log nK + n \log [S] \tag{3}$$

$$[S] = C_D(\delta_M - \delta)/(\delta_M - \delta_m) \tag{4}$$

$$nS \overset{K}{\rightleftharpoons} S_n \qquad K = [S_n]/[S]^n \tag{5}$$

which indeed may not be the case (vide supra). However, good linear plots of the data are obtained in the majority of cases (e.g., Figure 3) and the data are internally consistent and hence useful for purposes of comparison. The values of n and K calculated from data for the various protons of HAP are given in Table VI. Using this single equilibrium treatment, HAP appears to aggregate as approximately tri-

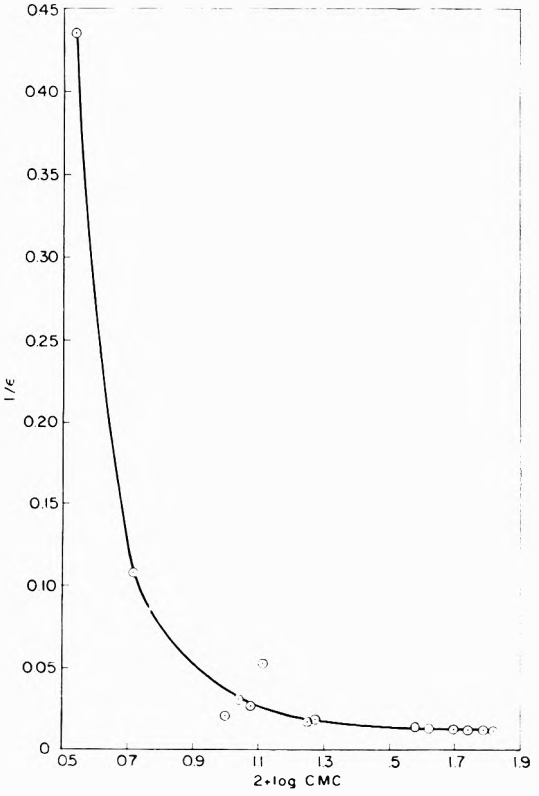

Figure 5. Dependence of the molar critical micelle concentration, cmc, of HAP on the reciprocal dielectric constant, ϵ, of the benzene-d_6–DMSO-d_6–D_2O solvent systems at 33.5°.

TABLE VIII: Surface Tension of Hexylammonium Propionate in DMSO-H_2O Solutions at 25°

100% H_2O	M^a	0.10	0.15	0.23	0.30	0.38	0.51	0.60	0.75	1.00	1.50	2.00
	γ^b	51.1	47.3	43.6	39.1	36.9	34.5	33.3	32.3	30.6	30.3	29.4
75% H_2O	M	0.05	0.09	0.19	0.28	0.35	0.44	0.63	1.05	1.51	2.01	
25% DMSO	γ	59.4	55.1	49.2	41.8	39.7	37.7	36.1	33.5	32.7	31.9	
50% H_2O	M	0.03	0.10	0.20	0.28	0.35	0.44	0.63	1.05	1.51	2.01	
50% DMSO	γ	55.1	51.4	45.7	42.4	40.2	38.4	35.9	33.4	32.6	32.0	
25% H_2O	M	0.03	0.05	0.11	0.22	0.31	0.44	0.63	1.05	1.28	1.50	1.70
75% DMSO	γ	49.7	48.2	46.5	43.0	40.8	38.5	36.5	34.2	33.6	33.1	32.7
18.7% H_2O	M	0.04	0.08	0.16	0.26	0.37	0.53	0.76	1.09	1.36	1.64	2.00
81.3% DMSO	γ	47.2	45.7	44.2	41.8	39.9	38.0	36.4	34.6	33.8	33.4	32.9
7.1% H_2O	M	0.07	0.14	0.25	0.35	0.50	0.71	1.02	1.46	1.71	2.01	
92.9% DMSO	γ	44.8	43.7	42.1	40.3	38.9	37.0	35.5	34.2	34.1	33.3	
100% DMSO	M	0.05	0.10	0.20	0.48	0.69	0.99	1.23	1.45	1.71	2.01	
	γ	43.4	42.8	41.6	37.6	35.8	33.9	33.2	32.6	34.4	34.1	

[a] HAP concentration, molar. [b] Surface tension, dyne/cm.

TABLE IX: Comparison of Critical Micelle Concentrations Obtained by Different Methods

Solvent system		cmc, HAP, M		
% H_2O	% DMSO	^{1}H NMR	Surface tension	Uv dye absorption
100.0	00.0	0.55	0.42	0.72
75.0	25.0	0.65	0.37	
50.0	50.0	0.61	0.35	
25.0	75.0	0.38	0.40	
18.7	81.3		0.59	
15.0	85.0	~0.18		
7.1	92.9		0.74	
5.0	95.0	0.19		
0.0	100.0	0.10	~0.70	0.13

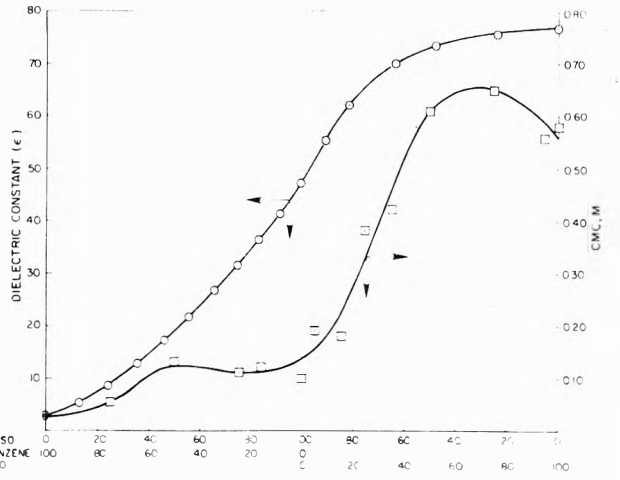

Figure 6. Plots of the dielectric constant, ϵ (O), of the benzene-d_6–DMSO-d_6 and DMSO-d_6–D_2O solvent systems and the molar critical micelle concentration, cmc (□), of HAP at 33.5° as a function of solvent composition in weight/weight per cent.

mers in both the benzene–DMSO and DMSO–water solvent systems (Table VI). The association of alkylammonium carboxylates is equally compatible with a multiple equilibrium treatment[15] which does not exclude the possibility of aggregates composed of 20 or more monomers in the solutions of relatively high surfactant concentration. Indeed, dodecylammonium propionate has been found to exhibit an indefinite (rather than a monomer–n-mer) self-association in benzene and cyclohexane.[14] It is probable that HAP in benzene and in at least the higher weight per cent benzene–DMSO solutions also behaves in the same fashion, i.e., above the cmc a multiple equilibrium exists between the monomers and the aggregates or micelles.

In any case, the structure of the aggregates changes with solvent composition. In pure benzene and other nonpolar solvents, hexylammonium propionate forms "reversed micelles" with the ammonium and carboxylate groups in the interior and the hydrocarbon chains oriented toward and penetrated by the bulk solvent.[10] As the polarity of the solvent is changed by addition of DMSO, the "reversed" or nonpolar aggregate structure of HAP is retained until about 50 wt % of the solvent is composed of DMSO. In this solvent range, the aggregate structure begins to dramatically change as evidenced by a rapid decrease in the equilibrium constant (Table VI and Figure 4), rapid increase in the cmc (Figure 5), and reversal of the relative magnitude of the micellar, δ_M, and monomeric, δ_m, chemically shifts (Table IV). These data suggest that the aggregate structure is changing to one more compatible with the more polar bulk solvent. Such a structure would allow the polar head groups to have greater contact with the bulk solvent while at least partially shielding the hydrocarbon chains from it. This type of aggregate structure apparently exists as the polarity of the solvent system is further increased until a solvent composition of approximately 50% DMSO–50% water is reached. In this solvent range, the structure of the solvent itself may begin to undergo changes. Several investigations have indicated that DMSO–water solutions form an association complex of the form $(DMSO \cdot 2H_2O)_n$ in solutions containing 65–75% DMSO and that the solution structure between approximately 80% DMSO–20% water and 100% water varies little with composition.[25]

Critical micelle concentrations, cmc's, of HAP have been determined for these solvent systems using ^{1}H NMR spectroscopy, surface tensiometry, and absorption spectrophotometry of dyes. Critical micelle concentrations determined from ^{1}H NMR data are given in Table VII. The critical micelle concentrations of HAP in the benzene-d_6–DMSO-d_6 and DMSO-d_6–D_2O solvent systems sharply increase at about 50% benzene-d_6–50% DMSO-d_6 and again at about 75% DMSO-d_6–25% D_2O (Table VII). The critical micelle concentration of HAP in the overlapping solvent systems generally increases with increasing solvent polarity (Figures 5 and 6), although the aggregate structure changes completely from a "reversed" to a normal micelle type. The

cmc in the region of "reversed" aggregates is, however, far less dependent on solvent composition than in the region composed of normal micelles. Also, in both of the solvent ranges comprising reversed and normal micellar aggregates the cmc is quite dependent upon the dielectric constant while in the intermediate or transition region the cmc is almost independent of dielectric constant (Figure 6).

For purposes of comparison the cmc's of HAP were also determined from surface tension measurements in the DMSO–water system and the data are given in Table VIII. Plots of surface tension, γ in dynes/cm vs. stoichiometric HAP concentration, were typical of those for aqueous surfactant solutions being linear in the low and high concentration ranges and curvilinear in a small range between the two. The point of intersection of straight lines drawn through the points of the former ranges was taken as the cmc. As a means of checking the accuracy of this method, the surface tension plots were extrapolated to zero HAP concentration to obtain the surface tension of the solvent. Plots of these numbers against solvent composition were in good agreement with published values for DMSO–H_2O solutions.[26,27]

Dye absorption spectrophotometry was also used to determine cmc's of HAP in pure water and DMSO. Individual measurements of DMSO–HAP solutions containing rhodamine-B were made at 550 nm and individual measurements of H_2O–HAP solutions were made at 610 nm using pinacyanol chloride as the dye. The discontinuities in plots of absorbance of the dye vs. stoichiometric HAP concentration were taken as the cmc's. Good plots were obtained in both DMSO and in water. It should be noted, however, that relatively large organic additives such as dyes typically lower the cmc of surfactants in aqueous solution[28,29] but insufficient data prohibit generalizations in nonpolar solvents.

The cmc data for HAP in DMSO–water obtained using ^1H NMR spectroscopy, surface tensiometry, and dye absorption spectrophotometry are compiled in Table IX. The agreement between the independently determined values is remarkably good considering the differences in these methods.[29]

Conclusion

It is apparent that the association behavior of HAP, and most probably longer chain alkylammonium carboxylates, is highly dependent upon solvent composition. The aggregate structure, critical micelle concentration, aggregation number, and aggregate (micelle) association constant are all affected by solvent properties such as polarity and structure. These interdependencies and the interactions involved are essential for an understanding of the mechanisms of catalysis of organic and inorganic reactions which occur in the presence of surfactants in mixed solvent systems. Consequently these factors for anionic and nonionic surfactants are currently being investigated in our laboratories.

Acknowledgments. Support of this work by the National Science Foundation is gratefully acknowledged. E.J. Fendler is a Research Career Development Awardee of the National Institution of Health.

References and Notes

(1) O. A. El Seoud, E. J. Fendler, and J. H. Fendler, *J. Chem. Soc., Faraday Trans. 1*, **70**, 459 (1974).
(2) Submitted for partial fulfillment of the requirements for the M.S. degree, Texas A & M University, May 1974.
(3) J. H. Fendler, E. J. Fendler, R. T. Medary, and V. A. Woods, *J. Am. Chem. Soc.*, **94**, 7288 (1972).
(4) J. H. Fendler, E. J. Fendler, and S. A. Chang, *J. Am. Chem. Soc.*, **95**, 3272 (1973).
(5) C. J. O'Connor, E. J. Fendler, and J. H Fendler, *J. Org. Chem.*, **38**, 3371 (1973).
(6) C. J. O'Connor, E. J. Fendler, and J. H. Fendler, *J. Chem. Soc., Dalton Trans.*, 625 (1974)
(7) C. J. O'Connor, E. J. Fendler, and J. H. Fendler, *J. Am. Chem. Soc.*, **96**, 370 (1974).
(8) J. H. Fendler, F. Nome, and H. C. Van Woert, *J. Am. Chem. Soc.*, **96**, 6745 (1974).
(9) W. Hinze and J. H. Fendler, *J. Chem. Soc., Dalton Trans.*, in press.
(10) J. H. Fendler, E. J. Fendler, R. T. Medary, and O. A. El Seoud, *J. Chem. Soc., Faraday Trans. 1*, **69**, 280 (1973).
(11) E. J. Fendler, J. H. Fendler, R. T. Medary, and O. A. El Seoud, *J. Phys. Chem.*, **77**, 1432 (1973)
(12) O. A. El Seoud, E. J. Fendler, J. H. Fendler, and R. T. Medary, *J. Phys. Chem.*, **77**, 1876 (1973).
(13) O. A. El Seoud, E. J. Fendler, and J. H. Fendler, *J. Chem. Soc., Faraday Trans. 1*, **70**, 450 (1974).
(14) Y.-F. Low, E. J. Fendler, and E. T. Adams, Jr., Presented at the 29th Southwest Regional Meeting of the American Chemical Society, El Paso, Texas, Dec 5–7, 1973, Abstract No. 284.
(15) N. Muller, *J. Phys. Chem.*, **79**, 287 (1975).
(16) A. Kitahara, *Bull. Chem. Soc. Jpn.*, **28**, 234 (1955); **30**, 586 (1957).
(17) J. C. Eriksson and G. Gillberg, *Acta Chem. Scand.*, **20**, 2019 (1966).
(18) R. Hague, *J. Phys. Chem.*, **72**, 3056 (1968).
(19) P. A. Arrington, A. Clouse, D. Doddrell, R. B. Dunlap, and E. H. Cordes, *J. Phys. Chem.*, **74**, 665 (1970).
(20) F. Podo, A. Ray, and G. Némethy, *J. Am. Chem. Soc.*, **95**, 6164 (1973).
(21) W. D. Harkins and H. F. Jordan, *J. Am. Chem. Soc.*, **52**, 1751 (1930).
(22) S. P. Harrold, *J. Colloid Sci.*, **15**, 280 (1960).
(23) S. A. Schichman and R. L. Amery, *J. Phys. Chem.*, **75**, 98 (1971).
(24) J. M. G. Cowie and P. M. Toporowski, *Can. J. Chem.*, **39**, 2240 (1961).
(25) D. D. MacDonald and J. B. Hyne, *Can. J. Chem.*, **49**, 611 (1971).
(26) E. Tommila and T. Autio, *Suom. Kemistil. B*, **42**, 107 (1969).
(27) E. Tommila and A. Pajunen, *Suom. Kemistil. B*, **41**, 172 (1968).
(28) E. J. Fendler and J. H. Fendler, *Adv. Phys. Org. Chem.*, **8**, 271 (1970).
(29) P. Mukerjee and K. J. Mysels, *Natl. Stand. Ref. Data Ser., Natl. Bur. Stand.*, **No. 36** (1971).

Hydrogen Bonding Interaction of Some Naturally Occurring Isomeric Juglones with Dioxane

S. B. Padhye* and B. A. Kulkarni

Department of Chemistry, University of Poona, Poona 411007, India
(Received June 27, 1974; Revised Manuscript Received December 5, 1974)

The hydrogen bonding interaction of isojuglones, viz. lawsone (I) and phthiocol (II), with dioxane in *n*-hexane solution studied at 25° revealed the absence of chelated hydroxyl groups. Strong intramolecular hydrogen bonding was confirmed in juglone (III) and plumbagin (IV).

Absorption spectra of 1,4-naphthoquinone and its derivatives have been reported earlier mainly for the identification of a new pigment or for confirmation of the purity of the synthesized quinone.[1-5] Solvent effect studies to elucidate the pecularities of the molecular structures of the hydroxy derivatives of 1,4-naphthoquinone such as juglones, which involve the possibility of both types of hydrogen bonding, viz. intra- and intermolecular, are, however, lacking. The present communication describes such a study of the hydrogen bonding interaction of four naturally occurring isomeric juglones, viz. lawsone (I), phthiocol (II), juglone (III), and plumbagin (IV), with dioxane in an attempt to examine the nature of hydrogen bonding in these compounds. This is in continuation of our work with PMR and near-infrared spectra of these compounds described recently.[6,7]

Scheme I

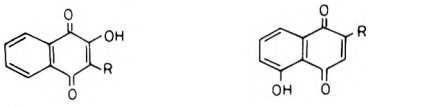

I, R = H (Lawsone)
II, R = CH_3 (Phthiocol)

III, R = H (Juglone)
IV, R = CH_3 (Plumbagin)

Lawsone (I) and juglone (III) were products of Fluka A.G., while phthiocol (II) was synthesized according to Fieser.[8] The isolation and characterization of plumbagin (IV) has been described elsewhere.[9] All the juglones were carefully crystallized and dried prior to their use. The absorption spectra were obtained with a Beckman DK-2 spectrophotometer using matched 10-mm quartz cells in a thermostated cell holder. All solvents were of spectroscopic grade (E. Merck, Darmstadt) and were tested to that effect.

It is well known that when a phenolic hydroxyl group is involved as a proton donor in the formation of a hydrogen bond, red shifts are observed for the $\pi \rightarrow \pi^*$ transition due to the inductive effect.[10] These red spectral shifts which can very advantageously be used for distinguishing the intra- vs. intermolecular hydrogen bonding[11-13] form the basis of present communication. Thus, on comparing the uv spectra of I or II in an aprotic solvent (such as *n*-hexane) with its spectra in a proton acceptor solvent (such as dioxane), appreciable red shifts are observed for the $\pi \rightarrow \pi^*$ transition (i.e., 410 cm^{-1} for I and 210 cm^{-1} for II). It is clear from the pattern of the spectra shown in Figure 1, for the interaction between I and dioxane that a simple equilibrium is occurring as judged from the clear isosbestic points. The presence of intramolecular hydrogen bonding assumed in the parent compound for equilibrium A is ruled

Scheme II

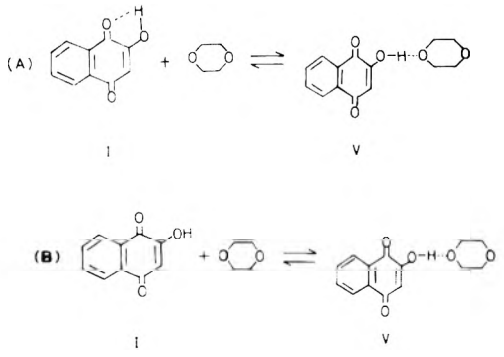

out on the grounds that it would show as a negligible red shift in the aprotic and proton acceptor solvent[14] and would certainly tend to destroy the fine spectral structure observed for these compounds especially in the uv region.[15] Further, the absence of intramolecular hydrogen bonding in I and II has already been reported by us based on the PMR and near ir spectral evidence.[6,7] Equilibrium B is, therefore, the only possible mode of interaction for these compounds with dioxane and explains the present experimental data adequately. Plots of the log of the ratio of the concentration of hydrogen bonded to nonhydrogen bonded I (estimated from the absorbance at 246 and 248 nm) vs. log dioxane concentration were made as suggested by Scott and Lin.[13] The slope of such plots also provided a clear indication of 1:1 complex formation (V).

The values obtained for the equilibrium constant of this hydrogen bonding interaction (3.4 M^{-1} at 25° for I and 1.9 M^{-1} at 25° for II) by the calculation of Rose and Drago[16] are comparable with those obtained in case of phenols,[17,18] halophenols,[13] thioamides,[19] and naphthols[20] undergoing similar equilibrium with dioxane.

The unavailability of the proton for intermolecular association with dioxane in III and IV as seen from the absence of the red spectral shifts clearly indicates the presence of a strong intramolecular hydrogen bonding in these compounds and confirms our earlier conclusion in ruling out the possibility of equilibrium A for I and II.

Contrary to the earlier assumptions the present study has revealed the absence of chelated hydroxyl groups in I and II which may well be due to the unfavorable interatomic distances and bond angles for the completion of a five-

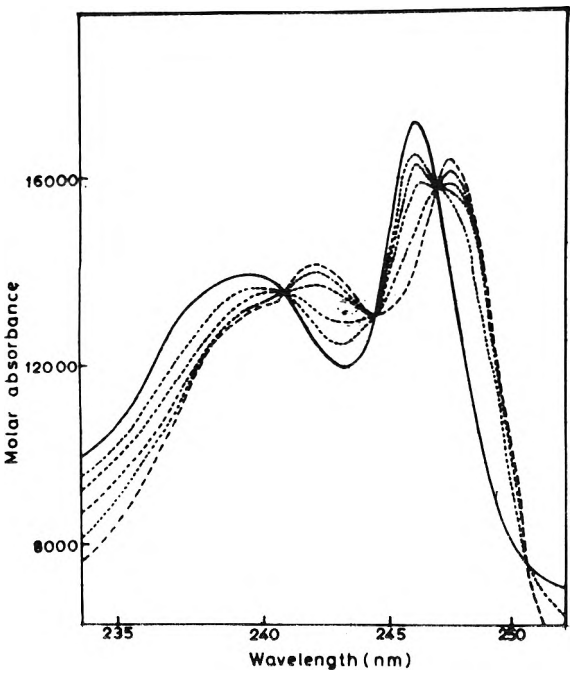

Figure 1. Uv absorption spectra of I at 25°: (a) solid curve, lawsone in *n*-hexane (5×10^{-5} *M*); (b) broken curve, lawsone in dioxane (4×10^{-5} *M*); (c) dotted curves, lawsone in dioxane at intermediate concentrations.

membered chelated ring system. X-Ray crystallographic data provided in case of some halo derivatives of 1,4-naphthoquinone by Schvoerer et al.[21,22] strongly supports such a conclusion.

Acknowledgment. The authors thank Professor H.J. Arnikar for providing the laboratory facilities.

References and Notes

(1) C. J. P. Spruit, *Recl. Trav. Chim. Pays-Bas*, **68**, 809 (1949).
(2) P. J. Scheuer, I. Singh, R. T. Ogata, R. E. Moore, and C. W. J. Chang, *Tetrahedron*, **24**, 6053 (1968).
(3) R. R. Hill and G. H. Mitchell, *J. Chem. Soc. B*, 61 (1969).
(4) R. A. Morton, Ed., "Biochemistry of Quinones", Academic Press, New York, N.Y., 1965.
(5) R. H. Thomson, "Naturally Occurring Quinones", 2nd ed, Academic Press, New York, N.Y., 1971.
(6) S. B. Padhyé and B. A. Kulkarni, *J. Magn. Resonance*, **16**, 150 (1974).
(7) S. B. Padhyé and B. A. Kulkarni, *J. Univ. Poona Sci. Technol.*, **46**, 93 (1974).
(8) L. F. Fieser, *J. Biol. Chem.*, **133**, 391 (1940).
(9) S. B. Padhyé and B. A. Kulkarni, *J. Univ. Poona*, **44**, 27 (1973).
(10) G. Némethy and A. Ray, *J. Phys. Chem.*, **77**, 64 (1973).
(11) N. S. Baylies and E. G. McRae, *J. Phys. Chem.*, **58**, 1002 (1954).
(12) A. E. Lutskii, *J. Phys. Chem. (USSR)*, **19**, 282 (1945).
(13) R. M. Scott and M.-L. Lin, *J. Phys. Chem.*, **76**, 587 (1972).
(14) S. N. Vinogradov and R. H. Linnell, "Hydrogen Bonding", Van Nostrand-Reinhold, New York, N.Y., 1971, p 108.
(15) A. I. Scott, "Interpretation of the UV Spectra of Natural Products", Pergamon Press, Oxford, 1964, pp 6 and 125.
(16) N. J. Rose and R. S. Drago, *J. Am. Chem. Soc.*, **81**, 6138 (1959).
(17) H. Baba and S. Suzuki, *J. Chem. Phys.*, **35**, 1118 (1961).
(18) W. A. Lees and A. Buraway, *Tetrahedron*, **19**, 419 (1963).
(19) B. Ellis and P. J. F. Griffiths, *Spectrochim. Acta*, **22**, 2005 (1966).
(20) W. B. Person, *J. Am. Chem. Soc.*, **87**, 167 (1965).
(21) M. Schvoerer, J. Gaultier, C. Hauw, and J. Housty, *C. R. Acad. Sci.*, **273**, 956 (1971).
(22) M. Schvoerer, C. Courseille, and S. Geoffre, *C. R. Acad. Sci.*, **273**, 1633 (1971).

An Electron Spin Resonance Study of the Effect of Electron Releasing Groups upon the Molecular Orbitals of Substituted Phenylcyclooctatetraene Anion Radicals

Gerald R. Stevenson* and Luis Echegoyen

Department of Chemistry, University of Puerto Rico, Rio Piedras, Puerto Rico 00931 *(Received September 20, 1974)*

Publication costs assisted by the University of Puerto Rico

Several substituted phenylcyclooctatetraenes have been reduced to their respective anion radicals in hexamethylphosphoramide. The ESR spectra of the anion radicals confirm that the phenyl moiety is weakly electron withdrawing relative to the cyclooctatetraene ring system, and that electron-releasing groups on the phenyl group reduce this effect. The presence of the substituted phenyl group removes the degeneracy of the two nonbonding molecular orbitals. The splitting of the nonbonding molecular orbitals is about −0.26 kcal/mol for the phenyl group but is +0.26 kcal/mol for the 2,4,6-trimethylphenyl substituent. From this and the fact that there is a large line width reduction upon substitution of the phenyl protons with deuteriums in the mono-substituted phenylcyclooctatetraene systems, it is concluded that the dihedral angle between the phenyl ring and the cyclooctatetraene ring system is large but smaller than 90°. The steric interaction between the methyl groups and the cyclooctatetraene ring forces this dihedral angle much closer to 90° in the case of 2,4,6-trimethylphenylcyclooctatetraene.

The electron spin resonance spectrum of the phenylcyclooctatetraene anion radical is of considerable interest since it should provide information as to the degree of conjugation between the two ring systems (one of which is aromatic and the other antiaromatic in the neutral state), the effect of the phenyl substituent upon the molecular orbitals of the cyclooctatetraene (COT) ring system, and the relative electron-withdrawing character of these two ring systems.

The anion radical of phenylcyclooctatetraene (I) was first generated in 1966 by Carrington and coworkers.[1] However, in tetrahydrofuran, even at −100°, they were able to observe only a poorly resolved ESR pattern, which they interpreted in terms of a quartet and a quintet due to three and four equivalent protons on the COT rings, respectively. From this it was concluded that the energies of the two nonbonding orbitals are not the same and that ψ_{n-} is slightly higher in energy than ψ_{n+}.[1] Thus the phenyl group is slightly electron withdrawing relative to the COT moiety. At that time there was still no experimental proof that the phenyl protons were not contributing to the observed hyperfine splitting.

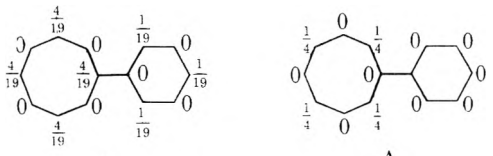

B A

The results of the reduction of phenyl-d_5-cyclooctatetraene confirms all of the conclusions drawn by Carrington.[2] Further, the reduction in line width in substituting phenylcyclooctatetraene for the deuterated compound indicates that the large line width observed by Carrington and coworkers was due to unresolved splitting from the phenyl protons. The presence of the electron-attracting phenyl group splits the degeneracy of the two nonbonding orbitals as shown in Figure 1.

The splitting is negative, since it has been previously defined that ϵ is positive when ψ_{n+} is of higher energy than ψ_{n-}.[2b] For the case of phenyl-d_5-cyclooctatetraene, ϵ was found to be about −0.26 kcal/mol.[2b]

To better understand the bonding and bond angle between these two ring systems and the effect of substituted phenyl groups upon the molecular orbitals of the COT ring system, we have synthesized and formed the anion radicals of several substituted phenylcyclooctatetraenes.

Results

The electrolytic reduction of *p-tert*-butylphenylcyclooctatetraene (II) in hexamethylphosphoramide (HMPA) leads to the formation of an anion radical solution yielding a poorly resolved ESR spectrum (Figure 2) consisting of 13 broad lines. The line width for the first hyperfine line is 1.0 G. Upon substitution of the phenyl protons by deuteriums, the resolution of the ESR spectrum increases considerably, and the line width reduces to 0.4 G, Figure 1. Both of these spectra can be accounted for as being due to a quartet of 2.58 ± 0.02 G from three equivalent protons and a pentet of 3.57 ± 0.02 G from four equivalent protons. The error of 0.02 G reported here is taken from the deuterated system and is much larger for the anion radical of II itself.

Describing the wave function for the odd electron in the COT moiety as a linear combination of the two nonbonding molecular orbitals of COT, we obtain

$$\Psi = C_{n-}\psi_{n-} + C_{n+}\psi_{n+} \quad (1)$$

From the ESR coupling constants $C_{n-}^2 = 3.57/(3.57 + 2.58) = 0.58$ and thus $\Psi = 0.76\psi_{n-} + 0.65\psi_{n+}$. The difference in energy between ψ_{n-} and ψ_{n+} can now be obtained by the use of eq 2.[3] Solving this expression for ϵ yields a value of −0.19 kcal/mol, Table I.

$$C_{n-}^2 = e^{-\epsilon/kT}/(1 + e^{-\epsilon/kT}) \quad (2)$$

The reduction of *p*-methylphenylcyclooctatetraene (III) in an identical manner yields an ESR spectrum consisting of eight broad lines (line width = 1.4 G). The resolution is greatly enhanced by perdeuterating the toluyl moiety. The

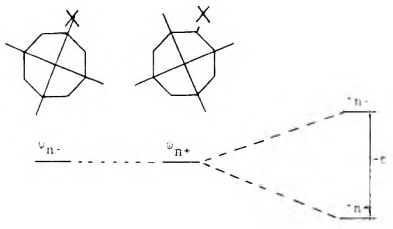

Figure 1. The two nonbonding degenerate orbitals of planar COT and the splitting due to the presence of an electron-attracting group. X represents the substituent.

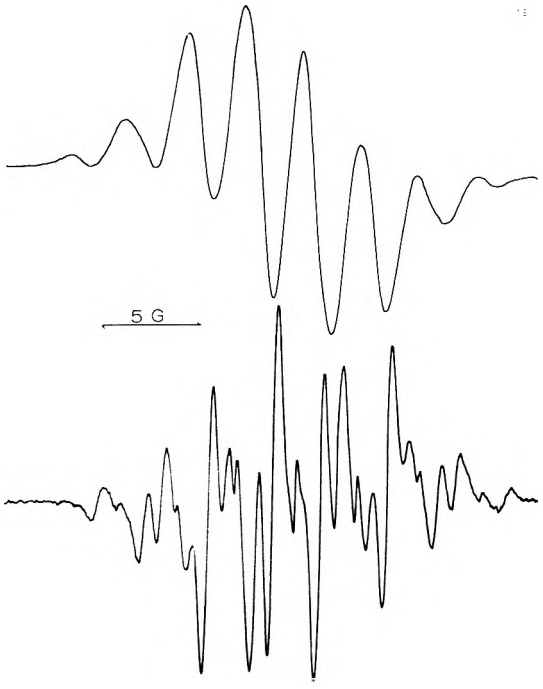

Figure 2. ESR spectra of the anion radicals of II (upper) and II-d_4 (lower) in HMPA.

ESR spectrum for tolyl-d_7-cyclooctatetraene (III-d_7) consists of a quartet due to three equivalent protons with a coupling constant of 3.04 ± 0.02 G and a pentet due to four equivalent protons with a coupling constant of 3.56 ± 0.03 G. The parameters calculated from these coupling constants are given in Table I.

When solutions of biphenylcyclooctatetraene (IV) are reduced in the same way a reasonably well-resolved ESR spectrum was obtained consisting of 12 esr lines (line width 0.9 G) and coupling constants of 2.00 ± 0.06 and 4.00 ± 0.06 G due to three and four equivalent protons, respectively. The line width for this system is still quite large, however, the difference between the two coupling constants is large enough so that the error due to the line width is minimized, Figure 3.

Reduced in this same manner, *p*-dimethylaminophenylcyclooctatetraene (V) gave an ESR signal consisting of eight broad lines due to seven roughly equivalent protons with a coupling constant of 2.97 ± 0.27 G. A resolved spectrum of this compound would probably yield a pentet of quartets, but the large error in the coupling constants due to the large line width of 1.1 G makes this impossible. A deuteration study of this compound was not carried out due to the fact that unresolved splitting from the nitrogen would still remain, and a more precise determination of the coupling constants is not necessary for a consistent interpretation of the results, Table I.

TABLE I: Values for C_{n-}^2, C_{n-}^2, ϵ, and σ for Substituted Phenylcyclooctatetraene Anion Radicals

Anion radical	C_{n-}^2	C_{n+}^2	ϵ	σ
I-d_5•⁻	0.61	0.39	−0.26	0
II-d_4•⁻	0.58	0.42	−0.19	−0.20
III-d_7•⁻	0.54	0.46	−0.09	−0.17
IV•⁻	0.67	0.33	−0.41	−0.01
V	0.5	0.5	0	−0.60
VI•⁻	0.39	0.61	+0.26	−0.51

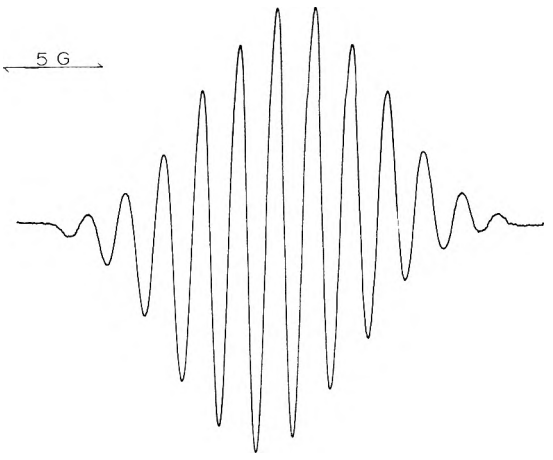

Figure 3. ESR spectrum of the anion radical of IV in HMPA.

All of the undeuterated substituted phenylcyclooctatetraenes mentioned above yield ESR spectra with very large line widths. However, the reduction of 2,4,6-trimethylphenylcyclooctatetraene (VI) in the same manner resulted in a solution exhibiting a well-resolved ESR pattern with a relatively narrow line width of 0.45 G. This pattern is due to a quartet from three equivalent protons with a coupling constant of 3.78 ± 0.02 G and a pentet due to four equivalent protons with a coupling constant of 2.42 ± 0.02 G. Note that for this anion radical the quartet splitting is larger than that for the pentet, in contrast to the other compounds.

The reversal in the ground state from ψ_{n+} to ψ_{n-} for 2,4,6-trimethylphenylcyclooctatetraene indicates that the trimethylphenyl substituent is slightly electron releasing relative to the COT ring system. Thus for this system there is a lower spin density in the phenyl ring and consequently the unresolved coupling due to the phenyl protons is small and does not result in extensive line broadening.

Discussion

All of the mono-substituted phenylcyclooctatetraene anion radicals exhibit a hyperfine pattern consisting of a quintet of quartets. This hyperfine pattern is the same for a particular anion radical whether or not the phenyl protons are replaced with deuteriums. Deuteration of the phenyl group leads only to line width reduction and thus better resolution. This, coupled with the fact that the pentet splitting is larger than the quartet splitting meaning that ψ_{n+} is of lower energy than ψ_{n-} and ϵ is less than zero, indicates that the mono-substituted phenyl group is acting as a

weak electron-withdrawing substituent relative to the COT ring system. However, it is expected that the electron-withdrawing ability of the phenyl moiety will decrease as the electron-releasing character of the substituent increases. This is clearly borne out by experiment as evidenced by a Hammett type plot of ρ of the substituent vs. the difference in energy between ψ_{n-} and ψ_{n+}, Figure 4. The negative slope of this plot indicates that ψ_{n-} is stabilized with respect to ψ_{n+} as the electron-withdrawing ability of the substituted phenyl system is decreased, Figure 5. A plot of ϵ vs. the σ value for the substituent on substituted cyclooctatetraene also yields a negative slope.[2b] The magnitude of the slope of the Hammett plot for the substituted phenyl cycloctatetraenes (−0.9) is less than that for the substituted cyclooctatetraenes (−2.5) because in the present work the effect of the substituent upon the molecular orbitals of the COT moiety is diluted through the phenyl ring system.

It has been previously mentioned that the dihedral angle between the two rings in $I^{\cdot-}$ is quite large.[2b] However, no quantitative estimate of this dihedral angle exists. It is safe to assume that the dihedral angle for the mono-substituted phenylcyclooctatetraene anion radicals is about the same as for $I^{\cdot-}$. Regardless of this bond angle, electron-releasing groups in the para position of the phenylcyclooctatetraene anion radical decrease the spin density in the phenyl system and increase that in the COT moiety. Thus, off hand, it would be expected that the line width would decrease upon substitution of a methyl group in the para position of I. However, the line width does not decrease, because the decreased spin density in the phenyl group is offset by the fact that the number of protons that can result in unresolved splitting is increased by two.

Similarly little change in the line width would be expected for substitution of a methyl group in the ortho position of I, since the spin densities in the ortho and para positions are about the same. Thus without a change in the dihedral angle, the anion radical of 2,4,6-trimethylphenylcyclooctatetraene (VI) would be expected to give an ESR spectrum consisting of broad lines. However, if the presence of the *o*-methyl groups results in an increase of the dihedral angle due to a steric interaction with the COT ring system, the spin density in the phenyl group would undergo a further decrease, and narrower line widths should be observed. Experimentally the anion radical of VI yields a well-resolved ESR pattern with relatively narrow lines. This indicates that the dihedral angle in the anion radical of I is large but smaller than 90°, while the steric interaction between the *o*-methyl groups of VI and the COT ring forces the dihedral angle closer to 90°. This increased dihedral angle further decreases the resonance between the two rings causing the substituted phenyl group to act as an electron-releasing substituent. Thus for this system ψ_{n-} is less stable than ψ_{n+}.

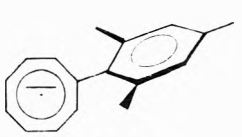

VI·⁻

Experimental Section

X-band ESR spectra were recorded using a Varian E-3 ESR spectrometer. All of the electrolytic reductions were carried out in hexamethylphosphoramide (HMPA) with tetra-*n*-butylammonium perchlorate added as an electrolyte. The HMPA was purified as previously described.[4]

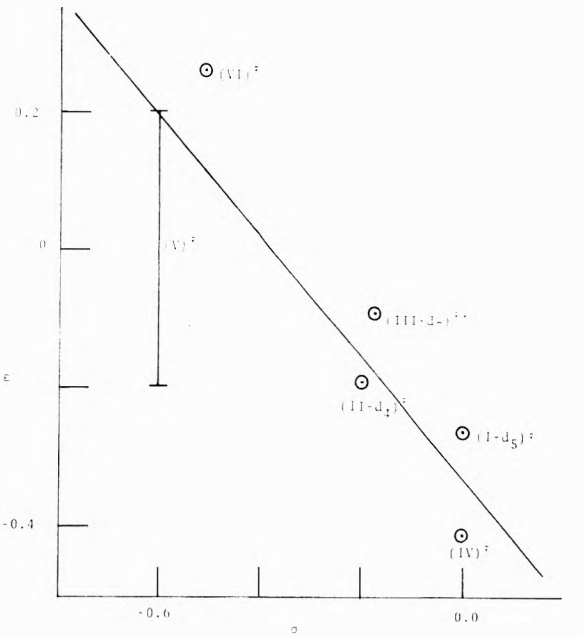

Figure 4. A plot of ϵ vs. σ of the sustituent on phenylcycloctatetraene. The vertical line represents the point of the *N,N*-dimethylamino substituent. This point is subject to large error due to the fact that there is an unresolved splitting from the amino nitrogen, and the phenyl group is not deuterated.

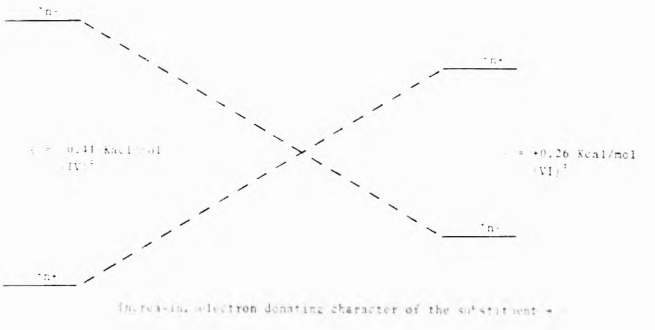

Figure 5. Graphical representation of the variation of ϵ with the electron-donating ability of the substituent on phenylcyclooctatetraene.

All of the phenylcyclooctatetraenes were prepared by the general method described below. This method of preparation is essentially identical with that described by Cope[5] for the preparation of the parent phenylcyclooctatetraene.

A dry 250-ml flask was equipped with a magnetic stirrer, a dropping funnel, and a reflux condenser. The entire system was then flushed with nitrogen and 1.4 g (0.2 mol) of lithium was placed in the flask. A solution of 0.1 mol of the appropriately substituted bromobenzene in 100 ml of dry ether was then added with stirring over a period of 1 hr. This mixture was then refluxed for a period of 10 hr to ensure complete formation of the lithium reagent. COT (0.11 mol) was then added and the reflux condenser was replaced with a Vigreux column. The temperature of the reaction mixture was then raised to 90° over a period of 1 hr. During this time the majority of the ether distilled out of the reaction flask. The reaction flask was maintained at this temperature for another 2 hr with rapid stirring of the slurry. After cooling in an ice bath, the ether was poured back into the reaction flask, and about 75 ml of water was slowly added. The ether layer was separated and combined with two ether extractions of the water layer. After drying with

magnesium sulfate, the ether was stripped off under reduced pressure, and the remaining oil was distilled under vacuum.

p-Methylphenylcyclooctatetraene (*III*) was distilled through a short path distillation head to yield 5.8 g (29%) of III as an orange liquid, bp 90–92° (0.6 mm): PMR ($CDCl_3$) δ 7.01 (m, 4), 5.84 (m, 7), 2.23 (s, 3). The mass spectrum shows a parent and base peak at 196 mass units.

p-Methylphenyl-d_7-cyclooctatetraene (III-d_7) was purified in the same manner giving the same yield and physical properties: PMR ($CDCl_3$) 5.84 (m). The mass spectrum shows a base and parent peak at 201 mass units.

p-tert-Butylphenylcyclooctatetraene (*II*) was distilled through a short path distillation head to yield 5.2 g (22%) of II as an orange liquid, bp 180–184 (0.3 mm): PMR ($CDCl_3$) δ 7.33 (m, 4), 5.86 (m, 7), 1.23 (s, 9). The mass spectrum shows a parent and base peak at 236 mass units.

p-tert-Butylphenyl-d_4-cyclooctatetraene (II-d_4) was made in the same manner and has the same physical properties: PMR ($CDCl_3$) 5.98 (m, 7), 1.30 (s, 9). The mass spectrum shows a parent and base peak at 240 mass units.

Biphenylcyclooctatetraene (*IV*) was prepared in the same manner and the crude product was distilled through a short path distillation head and collected from 192 to 196° at a pressure of 0.1 mm. The yellow solid was recrystallized from methanol to yield light yellow leaflets (yield 16%) mp 101–102°: PMR ($CDCl_3$) δ 7.63 (m, 9), 6.04 (m, 7). The mass spectrum shows a parent and base peak at 256 mass units. *Anal.* Calcd C 93.75; H, 6.25. Found C, 93.79; H, 6.27.

p-Dimethylaminophenylcyclooctatetraene (*V*) was distilled in the same manner. The distillation product solidified rapidly and was recrystallized from methanol to yield orange leaflets (21% yield) mp 90–91° (lit. 90–90.5°).[5] PMR ($CDCl_3$) δ 7.26 (d, 4, J = 8.8 Hz), 6.63 (d, 2, J = 8.8 Hz), 5.98 (m, 7), 2.93 (s, 6). The mass spectrum shows a parent and base peak at 223 mass units.

2,4,6-Trimethylphenylcyclooctatetraene (*VI*) upon distillation gave a yellow oil, which was collected from 90 to 95° at 0.05 mm (6% yield). The NMR spectrum indicated that this oil contained an impurity of about 10% of 2,4,6-trimethylphenylcyclooctatriene (probably a mixture of isomers). Attempts to separate the two components of the mixture by the formation of the silver complex of the triene (previously described by Cope)[5] were unsuccessful probably due to the steric interaction from the *o*-methyl groups. Attempts to purify VI were abandoned, and the mixture was submitted to electrolytic reduction and ESR analysis. This was not too disappointing, since the reduction potential of COT[6] is lower than that for cyclooctatriene,[7] and the anion radical of COT is much more stable than that for cyclooctatriene. Thus the electrolytic reduction of this mixture should lead to the formation of only one stable anion radical, that of VI: PMR of VI δ ($CDCl_3$) 6.89 (m, 2), 5.75 (m, 7), 2.24 (m, 9).

Acknowledgments. We are indebted to the Research Corporation for support of this work.

References and Notes

(1) A. Carrington, R. E. Moss, and P. E. Todd, *Mol. Phys.*, **12**, 95 (1966).
(2) (a) G. R. Stevenson, M. Colón, J. G. Concepción, and A. McB. Block, *J. Am. Chem. Soc.*, **96**, 2283 (1974); (b) G. R. Stevenson and L. Echegoyen, *ibid.*, **96**, 5452 (1974).
(3) G. R. Stevenson and J. G. Concepción, *J. Phys. Chem.*, **78**, 90 (1974).
(4) G. R. Stevenson, L. Echegoyen, and L. R. Lizardi, *J. Phys. Chem.*, **76**, 1439 (1972).
(5) A. C. Cope and M. R. Kinter, *J. Am. Chem. Soc.*, **73**, 3424 (1951).
(6) L. B. Anderson and L. A. Paquette, *J. Am. Chem. Soc.*, **94**, 4915 (1972).
(7) L. B. Anderson, M. J. Broadhurst, and L. A. Paquette, *J. Am. Chem. Soc.*, **95**, 2198 (1973).

Reactions Involving Electron Transfer at Semiconductor Surfaces.[1] VI. Electron Spin Resonance Studies on Dark and Illuminated Aqueous Suspensions of Zinc Oxides

Joseph Cunningham* and Sean Corkery

Chemistry Department, University College, Cork, Ireland *(Received May 9, 1974; Revised Manuscript Received December 17, 1974)*

Techniques are described permitting ESR studies on continuously circulating suspensions of powdered zinc oxides in aqueous media with pH and ionic strength carefully controlled. Only suspensions prepared from indium-doped ZnO gave any ESR signal in the dark at room temperature and the observed singlet had $\Delta H_{1/2} \sim 5.2$ G and $g = 1.9545$. Incidence of uv light onto circulating suspensions of high-purity zinc oxide yielded a new ESR singlet with $g = 1.9558$ and $\Delta H_{1/2} \sim 4.1$ G. Intensity vs. duration of illumination plots were obtained for these photogenerated signals by varying the residence time of particles in the uv light. These plots distinguish a "fast" component reaching its limiting concentration in 0.05 sec and a "slow" component leveling off in 40 sec. Data are presented on dependence of the intensity of the "fast" component upon electrolyte pH, showing a 50% increase in I_{fp} (1.96) as the pH changed from 10 to 7. This pH dependence and observed effects of other additives are compared with requirements of a model attributing the ESR signal to unpaired conduction band electrons in the bulk of ZnO coexisting with unpaired electrons on partially ionized donors near the surface. Values of the paramagnetic centers detected were two orders of magnitude lower than reported electron densities in the conduction band of dry samples.

Introduction

Electron spin resonance signals in zinc oxide powders or single crystals under vacuum or various gases have been recently reviewed.[2a] There is general agreement that samples prepared by prior heating under vacuum exhibit a single-line ESR signal, usually referred to as the $g \sim 1.96$ singlet since the spectroscopic splitting factor has approximately that value. Some workers report partial resolution of two components with $g \sim 1.955 \pm 0.002$ and $g \sim 1.958 \pm 0.002$ in favorable conditions.[2b,3] The significant measure of agreement on the g factor contrasts with a divergence of views on the paramagnetic centers responsible; some workers[4-6] assign the singlet with $g \sim 1.96$ to "conduction band" electrons, (e_{cb}^-); others[3,7,8] identify one component of the signal with interstitial zinc centers, (Zn_i^+); and some[3,8,9] suggest that f^+ centers (an electron trapped in an oxygen ion vacancy) are responsible for one component of the complex signal at $g \sim 1.96$. The third interpretation is not convincing in the light of evidence presented[10] that the ESR singlet signal of F^+ centers in single crystals of ZnO has $g_\perp = 1.9963$, $g_\parallel = 1.9948$ and hence should show $g_{av} \sim 1.996$, which would readily be distinguished from the complex singlet at $g \sim 1.96$. The literature does not however distinguish definitely between (Zn_i^+) and (e_{cb}^-) as possible contributors to the singlet at $g \sim 1.96$ and does not exclude the possibility that unpaired electrons exchange between environments characteristic of each. Both such environments represent electron-excess regions and it was felt, in undertaking the present study on aqueous suspensions of zinc oxides, that detection and study of any ESR singlet with $g \sim 1.96$ might provide valuable experimental information on the number and behavior of electron-excess paramagnetic centers present either in the bulk of ZnO particles suspended in an electrolyte or at the surface of these ZnO particles. The latter possibility merits more serious consideration for ZnO than has yet been accorded it in the literature, since paramagnetic surface centers have been shown to make a major contribution to ESR signals observed in powdered samples of rutile (TiO_2) treated and studied in similar conditions.[2a,11]

Experimental Section

ESR Technique. Elementary considerations indicate high probability for dielectric loss from incident microwave energy via interaction with the strongly polar aqueous electrolyte and via interaction with conduction band electrons of the semiconductor. It was imperative therefore that the ZnO–electrolyte suspensions be located within the cavity of an ESR spectrometer as a thin layer parallel to the microwave electric field. An all-quartz "aqueous solution flat cell" was utilized for this purpose in the present study. Thick suspensions (8 g/100 ml) could be circulated at constant density through the flat region (0.3 mm thick × 5 mm wide × 20 mm long) of this cell, or could be held static therein. All the ESR studies here reported were made at room temperature with the flat cell located in the multipurpose rectangular cavity (TE_{102} mode) of a Decca XI ESR spectrometer operating in the simple homodyne detection mode. Facilities available on this instrument for monitoring the "Q value" of the loaded or unloaded cavity showed that aqueous suspensions containing particles of semiconducting zinc oxide did not reduce the Q value, and hence the spectrometer sensitivity, significantly below that recorded with aqueous solutions in the flat cell.

The ESR spectrometer, as normally operated, recorded the first derivative of the ESR signals. Dilute solutions of $MnCl_2$ were utilized to calibrate the instrument sensitivity for paramagnetic species in the aqueous phase within the flat cell. The limit for detection of the sextet of lines from Mn^{2+} transitions corresponded to spectrometer sensitivity adequate only for detecting ca. 7×10^{12} spins in the flat cell in conditions of present experiments. The g values of signals detected in the flat cell were carefully checked and calibrated against a powdered reference of DPPH or of manganese-doped MgO attached to the outside of the aqueous solution flat cell. In the "fixed frequency" mode of opera-

tion of the Decca spectrometer g factors could be measured and reproduced to ±0.0005. Operation in "cavity lock" mode was often more convenient, however, and in such cases Klystron frequencies were read on a Hewlett-Packard frequency counter, again allowing absolute determination of g factors to ±0.0005. Within a sequence of measurements on a suspension, changes of $\Delta g = \pm 0.0003$ could readily be observed as shifts in position of the center of the ESR singlet relative to the fourth and fifth member of a sextet of lines originating from Mn^{2+} in the reference.

Materials. Three types of powdered zinc oxide were utilized for this study very high purity oxide, termed ZnO-SP500, supplied by New Jersey Zinc Co., with reported[12] carrier density of 3×10^{16} g^{-1} at room temperature,[1] measured surface area of 4 m^2 g^{-1} and particle sizes 0.2–2 μm; type SP500 later doped with indium to increase carrier density to 1.8×10^{-8} g^{-1}, termed ZnO–In, with measured surface area <0.1 m^2 g^{-1} and particle sizes 5–10 μm; high purity ZnO later doped with lithium, termed ZnO–Li with carrier density 10^{14} g^{-1} and surface area of 1.0 m^2 g^{-1}.

Utilizing equipment shown diagrammatically in Figure 1, strenuous efforts were made to prepare suspensions from these materials in reproducible conditions which excluded oxygen, CO_2, or other impurities. In step 1, a sample of the powdered zinc oxide was first heated for 3 hr at 400 ± 5° in a stream of preheated highly purified nitrogen or argon, in order to remove adsorbed O_2, H_2O, or CO_2. Such thermally outgassed samples were cooled to 20° in the flow of purified gas prior to the next step. In step 2 the aqueous phase to be used for the suspension was refluxed in a stream of purified gas and cooled to 20° over 30 min during which it was continuously flushed by N_2. In step 3 the deoxygenated and decarboxylated solid and aqueous phases were mixed in the reaction vessel shown in Figure 1, where they were magnetically stirred for at east 30 min prior to ESR measurement. The pH of the suspension was continuously monitored and maintained at a preselected value through automatic addition of deoxygenated NaOH or $HClO_4$ into the mixing chamber. Except where otherwise noted, all chemicals were AR quality and only water purified by distillation from alkaline $KMnO_4$ and again distilled was used. In most experiments $NaClO_4$ present at 10^{-2} M was used to maintain constant ionic strength in the suspensions. For purposes of comparison a few measurements were made on suspensions prepared from untreated ZnO (i.e., not outgassed).

Circulation and Illumination. Use of a peristaltic pump to continuously recirculate the suspensions from the mixing chamber out through the ESR flat cell and back was found to offer several advantages over a previously reported technique for ESR measurement on static suspensions.[13] These advantages included: (a) the maintenance of a uniform suspension in the sensitive area of the ESR flat cell, as opposed to slow settling of suspension in static systems; (b) better probability that the "sample" present in the sensitive volume at a given instant is representative of the total suspension volume of known pH, because of the rapid mixing; (c) the ease with which "residence time" of sample in the ESR flat cell could be varied simply by varying the pumping rate of the peristaltic pump. This latter facility was particularly important for studies made under illumination by light from a 150-W medium-pressure Hg lamp or a 200-W xenon-arc lamp. In some experiments Zeiss narrow band-pass filters were used to pass to the suspension emission centered on only one line of the Hg-emission spectrum at 365, 405, 435 or 546 nm. In other illuminations a 2-cm cell filled with appropriate aqueous solution was used to filter out undesireable infrared radiation. Test runs with any of these illuminations incident on the flat cell with aqueous electrolyte, but no zinc oxide, flowing through it, showed no ESR signals were generated in the flat cell or in the aqueous media.

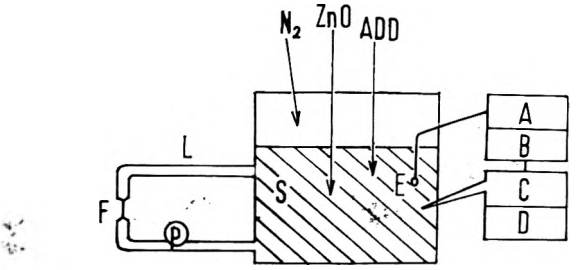

Figure 1. Schematic representation of equipment for observing ESR signals in circulating aqueous suspensions at fixed pH and ionic strength: S, suspension in glass mixing vessel; L, circulating loop; F, aqueous flat cell in ESR cavity; N_2, ZnO, and ADD, ports for introducing N_2, ZnO, and additives without exposure to air; A and E, pH electrode and meter; B, automatic titrator; C, autoburet; D, recorder.

Results

A. Nonilluminated Suspensions. The ESR signal illustrated in Figure 2a curve 1 was readily detected with a measured g factor of 1.9545 for any rigorously deoxygenated suspension of ZnO–In circulating continuously through the flat cell. A half-width $\Delta H_{1/2}$ of 5.2 ± 0.4 G was associated with this signal at the lowest microwave power (60 mW) and modulation depth (2.3 G) which yielded measurable signals in these experiments. Comparison of the integrated area under this signal with integrated area under the Mn^{2+} sextet, measured with similar instrumental settings on 10^{-5} M solutions of $MnCl_2$ in the same flat cell, indicated that the signal in curve 1 of Figure 2a originated from 5.5 ± 1.5 × 10^{15} paramagnetic centers per gram of ZnO–In particles. Additional comparisons run against external reference samples (DPPH dispersed in KCl) attached to the back of the flat cell and measured simultaneously with the singlet at $g \sim 1.96$ were in agreement with this concentration value. No signal similar to that in Figure 2a(1) was detected in nonilluminated suspensions identically prepared from either ZnO-SP500 or from ZnO–Li and studied under conditions identical with those used for ZnO–In. It may be estimated from the above calibration and from the observed signal-to-noise ratio that no paramagnetic centers capable of yielding ESR signal with $g \sim 1.96$ could therefore have been present at concentrations $>5 \times 10^{14}$ g^{-1} in suspensions of either ZnO-SP500 or ZnO–Li.

Influence of Electrolyte Composition on Signal Intensity from ZnO–In. Addition of $NaClO_4$ to an aqueous phase at 10^{-2} M to establish ionic strength control had no appreciable effect on $I_d(1.96)$, the intensity of the ESR signal observed from ZnO–In suspensions in the dark. After addition of 10^{-2} M $NaClO_4$ to maintain constant ionic strength, then the effect of electrolyte pH upon $I_d(1.96)$ was tested by varying pH between 7 and 10.5, through small additions of aqueous NaOH or $HClO_4$. Results indicating negligible influence of pH on $I_d(1.96)$ in ZnO–In are illustrated in Figure 3a. It was also observed that addition of ethanol to the suspension, even up to 50% composition by volume, had no detectable effect on the signal intensity, thus indicating

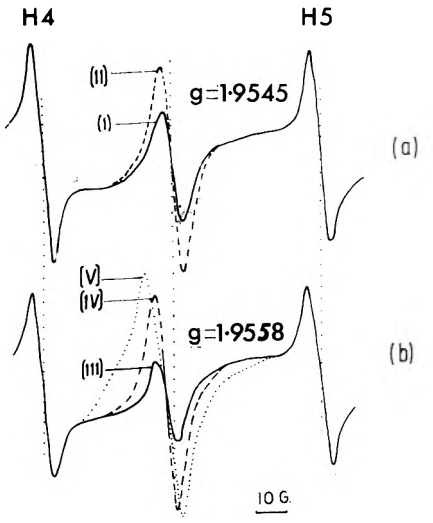

Figure 2. ESR singlet from zinc oxide suspensions shown together with two reference signals from Mn^{+} reference. (i) Signal from aqueous suspension of ZnO–in (ZnO–In outgassed in N_2 at 380°) in the dark; (ii) under illumination; (iii) and (iv) the fast and slow signal from uv illuminated suspension of ZnO-SP500 (outgassed in N_2 at 380°); (v) as in (iii) but with zinc dust or formate added.

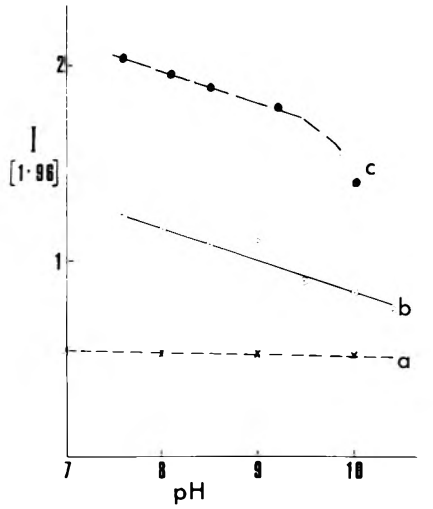

Figure 3. Intensity of ESR singlets with $g \sim 1.96$ from aqueous suspension of various zinc oxides, as a function of electrolyte pH: (a) data illustrating lack of pH dependence for I_d (1.96) from ZnO–In suspensions in the dark; (b) pH dependence of I_{fp} (1.96) for fast photogenerated component in ZnO-SP500. (c) pH dependence of I_{sp} (1.96) for slow photogenerated component in ZnO-SP500.

that $I_d(1.96)$ was not unduly sensitive to the dielectric constant of the liquid phase.

B. Uv Illuminated Suspensions of Zinc Oxides. Wavelength Dependence. Rigorously deoxygenated suspensions of ZnO-SP500, which had not shown any measurable ESR signal in the dark, immediately developed a readily measurable singlet with $g \sim 1.96$ under uv illumination. Tests with Zeiss narrow band-pass filters indicated that only light inside the bandedge of ZnO at 390 nm was effective, since the Hg emission 350–380 nm centered on the line at 365 nm caused the signal to appear, whereas use of narrow band filters passing mercury lamp emissions at 404, 444, and 546 nm showed that those wavelengths were ineffective in producing the signal. The measured g value of the photoproduced signal was 1.9558 in all suspensions prepared from thermally outgassed samples of ZnO-SP500.

ZnO–In. When uv light became incident on a circulating suspension the intensity of the signal with $g \sim 1.96$ increased from that noted in the same suspension prior to illumination. This increase in signal intensity was not, for ZnO–In suspensions, accompanied by any shift of the central point of the signal. Thus the g factor of both the dark and photoinduced components of the ESR singlet observed in illuminated suspensions had $g = 1.9545$, which differs by more than experimental error from the $g = 1.9558$ observed for illuminated suspensions of ZnO-SP500.

ZnO–Li. No signal was produced in aqueous suspensions of ZnO–Li prepared and illuminated under conditions identical with those used for ZnO-SP500.

Dependence of Signal Intensity and g Value on Residence Time. Residence time of individual zinc oxide particles in the flat cell coincided with the time interval for which the particle experienced uv illumination. Decreasing the pumping rate of the peristaltic pump from its maximum value therefore effectively increased the average number of photons absorbed by suspended ZnO particles during their passage through the cell. Figure 4 illustrates how the intensity of the singlet with $g \sim 1.96$ increased with increasing residence time, and hence with increasing number of photons absorbed per particle. The data indicate that two components contribute to growth of the ESR signal with $g \sim 1.96$ under uv illumination: a fast component which rapidly approaches a limiting value I_{fp} (1.96) at 0.05–0.1-sec residence times (cf. Figure 4a); and a slow component which only makes appreciable additional contribution to the total intensity at $g \sim 1.96$ when average residence time exceeded *ca.* 10 sec. A decrease in rate of growth of this slow component, I_{sp} (1.96), is apparent in Figure 4b at residence times 20–40 sec. In addition to providing good evidence for fast and slow components, the data in Figure 4 show that observations made with residence times 0.03–0.1 sec should mainly yield information (initially at least) on properties of the fast component, whereas observations made at residence times 40–50 sec should be further influenced by sizeable contribution made by the slow component. Such measurements showed no shift of the center point of the photoinduced ESR signal between fast and slow components, provided that the ZnO-SP500 suspensions were prepared from thermally outgassed ZnO-SP500. A g value greater by $\Delta g = +0.001$ than for the fast component measured on the same suspension was observed for the slow component photogenerated in suspensions prepared from untreated ZnO-SP500.

pH Dependence of I_{fp} (1.96). Results showing how the measured intensity of the fast component in ZnO-SP500 suspensions varied with the pH of the supporting electrolyte are shown in curve b of Figure 3. The series of points shown were taken on a single suspension of (ZnO-SP500) with fixed residence time of 0.033 sec and indicate ca. 50% increase in I_{fp} (1.96) from pH 10 to pH 7.5. Similar data were obtained with other suspensions and the mean value of ($I_{1.96}$ at pH 7)/($I_{1.96}$ at pH 10) was 1.5 for three suspensions prepared from ZnO-SP500.

pH Dependence of I_{sp} (1.96). From a set of residence time vs. $I_{1.96}$ plots similar to Figure 4 but recorded at various preset pH values it was possible to compare $I_{1.96}$ values at any chosen residence time but for different pH values. Curve c of Figure 3 illustrates the apparent pH dependent of $I_{1.96}$ for residence time of 40 sec, i.e., corresponding to the inflection of the slow component. This pH dependence of I_{sp} (1.96) is very similar to that for I_{fp} (1.96) (cf. curves b

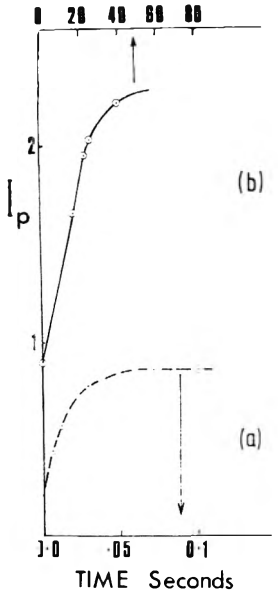

Figure 4. Variation of the intensity of the photogenerated ESR singlet in suspensions of ZnO-SP500 with "residence time" of particles in uv illumination: (a) fast component I_{fp} (1.96); (b) slow component I_{sp} (1.96).

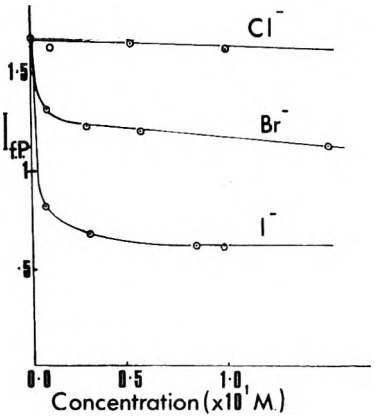

Figure 5. Effect of increasing concentrations of halide ion additives on I_{fp} (1.96) for uv illuminated suspensions of ZnO-SP500 at constant pH.

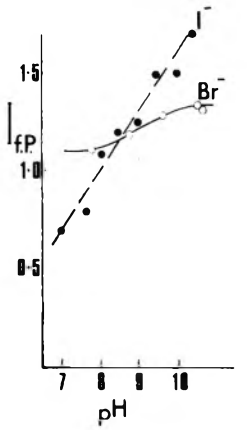

Figure 6. pH dependence of the magnitude of fast photogenerated signal intensity observed in the presence of inhibiting additives I^- and Br^-: ●, signal intensity (arbitrary units) observed at various pH in the presence of 6×10^{-3} *M* I^-; O, intensities at various pH in the presence of 0.15 *M* Br^-.

and c in Figure 3). Further evidence for similar pH dependences of the fast and slow components was provided by the constancy of the ratio I_{sp} (1.96)/I_{fp} (1.96) = 1.6 ± 0.1 for various pH values, irrespective of the residence time chosen for comparison.

Influence of Electrolyte Composition on Photoinduced $I_{1.96}$. Tests with suspensions of ZnO-SP500 in aqueous phases maintained at different ionic strength by concentrations of $NaClO_4$ in the range 10^{-4} to 10^{-1} *M* showed that this material did not affect the magnitude of I_{fp} (1.96) or I_{sp} (1.96). Use of 10^{-2} *M* $NaClO_4$ was therefore standard practice in maintaining constant ionic strength in the present study and data usually refer to this condition. The observation of I_{fp} (1.96) at similar magnitude in illuminated suspensions of ZnO-SP500 in 10^{-2} *M* $KClO_4$ or 10^{-2} *M* $NaClO_4$ indicated, however, that the identity of the alkali-metal cation did not significantly affect the ESR signal intensity.

Anionic Additives. The mixing chamber of the circulating system (see Figure 1) facilitated studies of the influence of various water-soluble additives upon I_{fp} (1.96) in conditions of constant pH, approximately constant ionic strength, and constant residence time. Figure 5 illustrates how progressive additions of halide ions affected I_{fp} (1.96), with I^- and Br^- reducing signal intensity appreciably but with Cl^- having no significant effect at any pH. The magnitude of the inhibitory effect of I^- and Br^- upon the magnitude of I_{fp} (1.96) varied with pH and Figure 6 illustrates the pH dependence of the inhibitory effect for 6×10^{-3} *M* I^- or for 0.15 *M* Br^-.

Oxidizable Additives. The recent literature on ZnO–electrolyte interfaces assigns an important role to holes photoproduced in ZnO via their interaction with oxidizable species such as formate ion or alcohols present in the electrolyte.[14] The effects of alcohols and formate ion were therefore examined and Figure 7a illustrates progressive increases in I_{fp} (1.96) at increasing concentrations of ethanol. Figure 7b illustrates that very much lower concentrations of formate (ca. 5×10^{-3} *M*) sufficed to achieve enhancements similar to that produced by 0.2 *M* ethanol. These increases confirm the sensitivity of I_{fp} (1.96) toward the availability of hole-trapping species at the ZnO–electrolyte interface. The introduction of NO_3^- into illuminated suspensions also produced increases in I_{fp} (1.96) but experiments with narrow band-pass filters suggested that direct light absorption by nitrate to produce electronically excited NO_3^{-*} was necessary and that ground state NO_3^- did not interact.

Reducible Additives. The effect of reoxygenation upon I_{fp} (1.96) in previously deoxygenated suspensions of ZnO-SP500 was examined, in view of literature reports that O_2 localizes electrons at the illuminated interface and thereby undergoes photoassisted reduction to H_2O_2.[15,16] The average value of the ratio of I_{fp} (1.96) in oxygenated suspension to I_{fp} (1.96) measured on the same suspension prior to reoxygenation was 0.8 ± 0.1. This relatively small reduction, effected by the saturation concentration of 10^{-3} *M* oxygen, contrasted with the reduction of I_{fp} (1.96) by 50% in the presence of 10^{-3} *M* of another reducible additive viz., *p*-nitrosodimethylaniline, PNDA (cf. Figure 8 and note that these experiments were made with an external filter of $PNDA_{aq}$ to reduce possible inner filter effects). This latter molecule has also been shown to undergo photoassisted reduction at the ZnO–electrolyte interface.[13] Figure 8 presents data on the progressive decreases in I_{fp}

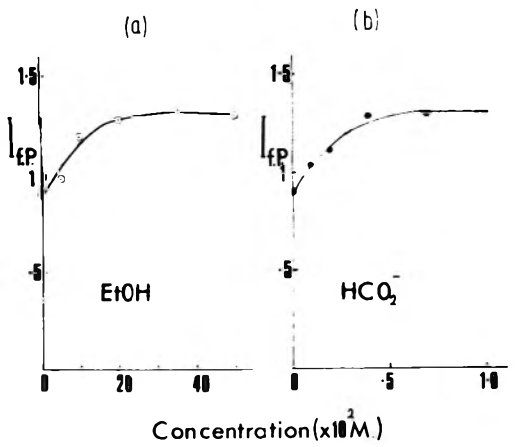

Figure 7. (a) Effect of increasing concentration of ethanol as an oxidizable additive upon I_{fp} (1.96) for uv illuminated aqueous suspensions of ZnO-SP500. (b) Increase in I_{fp} (1.96) achieved with additions of HCO_2^-.

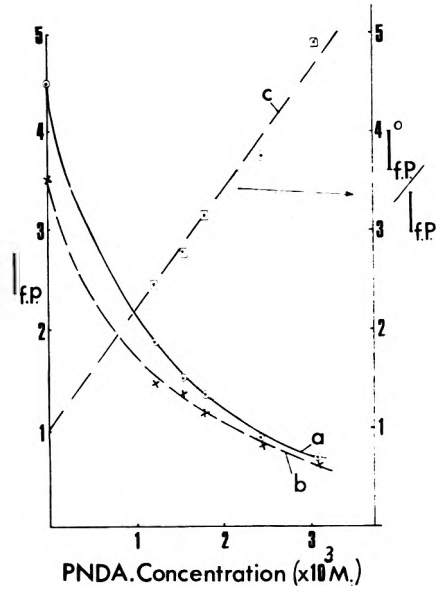

Figure 8. Effects of increasing concentration of PNDA as a reducible additive upon I_{fp} (1.96) for uv illuminated aqueous suspensions of ZnO-SP500: (a) data at pH 8; (b) data at pH 10; (c) Stern-Volmer plot of data as per eq 1.

(1.96) effected by increasing concentration of PNDA. Figure 8c shows that "quenching" of I_{fp} (1.96) by added PNDA obeys a Stern-Volmer type relationship of the form expected if $PNDA_{aq}$ enters into competition with the process producing paramagnetic species, viz.

$$(I_{1.96})_0/(I_{1.96})_c = 1 + k_q\{PNDA\}/k_p \qquad (1)$$

In this expression I_0 and I_c refer to signal intensities for {PNDA} = 0 or C respectively; k_q and k_p refer respectively to rate constants for quenching and for $I_{(1.96)}$ production.

Test of Possible Involvement of Surface States. The demonstrated sensitivity of ESR signal intensity on pH and on the presence of various additives pointed to location of the photogenerated paramagnetic centers (or their precursors) close to the ZnO-electrolyte interface. Earlier capacitance studies of this interface in the dark[17] were interpreted as indicating very low concentrations of surface states (10^9/cm^2). Consequently identification of the paramagnetic centers as surface states could be consistent with our failure to detect unpaired spins at levels $>10^{10}$/cm^2 in the dark from suspensions of ZnO-SP500. Our detection of a measurable ESR signal at levels $\sim 5 \times 10^{12}$/cm^2 from suspensions of ZnO–In in the dark were not necessarily inconsistent with assignment of the ESR signal to surface states, since recent studies[18] indicate that addition of altervalent ions to metal oxides, including zinc oxide, greatly modify the number and type of catalytically active surface sites. Fortunately it was possible experimentally to test the involvement of such surface states in the ESR signal observed from suspensions of ZnO–In in the absence of uv illumination. Reports by various workers that surface states on zinc oxide crystals correspond to energy levels situated at depths between 2.0 and 0.3 eV beneath the conduction band,[19,20] and that transitions of electrons into or out of these levels could be promoted by visible or ir radiation, provided the basis for an experimental test. It was expected on the basis of these reports that changes in the number of electrons trapped at such surface states would result from incidence of visible and ir radiation on a circulating suspension of ZnO–In. The output of a 450-W xenon-arc lamp focussed by a quartz lens was filtered by a glass filter which removed all photons of wavelength <600 nm. Lamp output thus filtered contained photons of energies 2.0–0.3 eV and was allowed to fall on the circulating suspension of ZnO–In–H_2O. No change in ESR signal intensity was noted and the negative result of this experiment is interpreted as strong evidence against the involvement of surface states at depths 2–0.3 eV below the conduction band in producing the signal with $g \sim 1.96$ in ZnO–In.

Influence of Surface Nonstoichiometry and Hydroxylation upon Dark and Photogenerated Signals. Increases in the degree of metal-excess nonstoichiometry of ZnO, and in the conductivity, have been reported to result from heating ZnO samples in zinc vapor, in vacuo or in reducing atmospheres.[2a,3,21] Attempts were therefore made in the present work to simulate this increase in nonstoichiometry for ZnO particles suspended in aqueous solution and to observe any influence of nonstoichiometry upon intensity of dark or photoinduced ESR signal with $g \sim 1.96$. Addition of zinc dust to aqueous suspensions of ZnO-SP500 did yield an ESR signal in the dark (cf. Figure 2b(V)), in contrast to lack of any observable signal from suspensions containing either the ZnO-SP500 or the zinc dust. The signal from the mixed (ZnO-SP500 plus zinc) suspension was much broader ($\Delta H_{1/2} = 16 \pm 4$ G) than any other ESR signal observed in the present study. It also had a different g factor of 1.958 ± 0.001, making it appear that zinc and ZnO particles present simultaneously in the suspension generated paramagnetic centers in which the unpaired electron experienced a significantly different environment from that of the unpaired electrons detected in indium-doped zinc oxide in the dark ($g = 1.9545 \pm 0.0005$; $\Delta H_{1/2} = 5.2 \pm 0.4$ G). Signal intensity from Zn-SP500 plus zinc suspensions in the dark were greatest immediately after addition of zinc dust and decayed with $t_{1/2}$ ca. 20 min for mixtures initially equimolar in ZnO and zinc. When illumination became incident on such suspension in which the signal at 1.958 had decayed to low values, a photoinduced ESR signal was observed having $g = 1.9558$, as normally observed for photoinduced signals in ZnO-SP500.

Varying the extent of nonstoichiometry of the ZnO surface was also expected to result when the gaseous atmosphere around ZnO was varied during thermal outgassing at 400° (prior to introduction into the aqueous phase).

However no significant variation from the g factor of 1.9558 for photogenerated signals was detected when samples of ZnO-SP500 were (i) preoxidized in O_2; (ii) preheated in N_2, which is reported not to reduce ZnO; or (iii) preheated in argon, which was expected to result in loss of oxygen from the surface. A slight shift of the g factor to 1.9565 was noted above for the slow photogenerated component (but not the fast component) in suspensions prepared using ZnO-SP500 taken directly from the tin and not outgassed prior to use. This is thought to be associated with surface carbonation of untreated oxide, rather than with variations in nonstoichiometry.

The influence of surface hydroxylation upon intensity of the photogenerated signal was examined by first establishing an ESR signal with $g = 1.9558$ in an illuminated circulating suspension of ZnO-SP500 and then adding NaOH and $Zn(ClO_4)_2$ to the mixing chamber. It seemed probable that resultant zinc hydroxide would adhere to the interface between electrolyte and the ZnO-SP500 particles. These experiments did not, however, produce any significant change in the intensity of the photogenerated ESR signal, thereby suggesting that the depth of hydroxylation of the ZnO–H_2O interface was not a rate-limiting factor in production of the photogenerated ESR signal.

Discussion

In view of the negative result of our experimental test for involvement of surface states in the ESR signal with $g \sim 1.9545$ in ZnO–In suspensions, this discussion does not further consider possible roles of paramagnetic surface states. Emphasis is concentrated instead on demonstrating that a reasonable and self-consistent explanation of the observed results can be given by assigning ESR signals with $g \sim 1.96$ to unpaired electrons in the conduction band of ZnO *coexisting* with partially ionized donors. The background for choice of this model was that extensive literature support existed for the involvement of unpaired electrons in the ZnO conduction band with ESR signals at $g \sim 1.96$,[4-6] and that many workers did not exclude some (usually unspecified) involvement of Zn^+ donor sites.[2a,3,8]

Figure 9 summarises published band-theory descriptions[22] of electronic energy levels available in pure or indium-doped ZnO. In nominally pure ZnO-SP500 excess zinc provides the donor centers, each of which contains an unpaired electron while in the partially ionized Zn_i^+ state. Partially ionized donors, In^{2+}, should be paramagnetic centers in ZnO–In. The literature indicates that donor levels associated with those partially ionized In^{2+} or Zn^+ donors lie only 0.01 and 0.03 eV, respectively, beneath the ZnO conduction band in the "flat band" condition.[22] Coexistence of the two types of paramagnetic center represented respectively by unpaired electrons in the conduction band or by partially ionized donors is thus guaranteed at room temperature in the "flat band" condition. Our observations of slight, but significant differences between the g values of the ESR signals observed from suspensions of pure and indium-doped ZnO could result in two ways from the situations depicted in Figure 9: *either* as a time-averaged single ESR signal caused by very rapid exchange of unpaired electrons between the environments of the conduction band and partially ionized donors, *or* as a composite of two separate but overlapping ESR singlets originating respectively from unpaired electrons in the conduction band or from unpaired electrons at partially ionized donors. A slow rate of exchange between the two possible environments of the

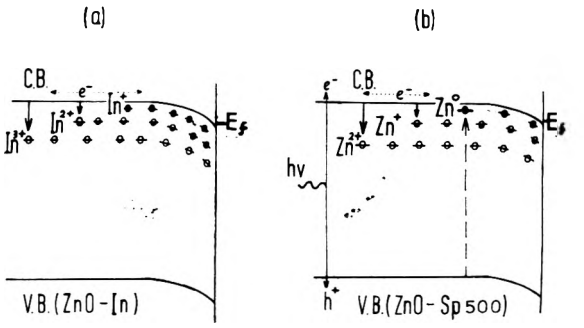

Figure 9. Schematic representation of energy levels in zinc oxides bearing excess positive surface charge arising either from proton adsorption or oriented water dipoles: (a) energy levels for indium-doped zinc oxide; (b) energy levels and photoassisted processes in pure ZnO-SP500.

unpaired electron is not excluded by the latter model, which requires only that such exchange be slow relative to the ESR transition in order to yield two separate signals. Either description could be consistent with the slight but significant differences here noted between g factors from suspensions of pure ZnO-SP500 ($g = 1.9558$) or from ZnO–In ($g = 1.9545$). The following paragraphs show that kinetics of photogenerated growth of the former signal (cf. Figure 4) are consistent with exchange of photogenerated electrons between conduction band and donors within the bulk of ZnO, prior to their ultimate removal by recombination with holes irreversibly trapped adjacent to the ZnO–H_2O interface. A kinetic analysis of this model can be based on the following equations

$$ZnO + h\nu \longrightarrow e^- + h^\bullet \qquad \text{rate} = I\beta \tag{2}$$

$$h^\bullet + ZnOH_s \longrightarrow H_2O - Zn_s^\bullet \qquad \text{rate} = k_3 p^* \tag{3}$$

$$H_2O\text{–}Zn^\bullet + e^- \longrightarrow ZnOH_s \qquad \text{rate} = k_4 n^* [\overline{Zn}^\bullet\text{–}OH_s] \tag{4}$$

Here $ZnOH_s$ represents hydroxyls adjacent to the ZnO–H_2O interface; e^- and h^+ are photogenerated electrons and holes with densities n^* and p^* respectively in the conduction band or valence band of ZnO; β, k_3, and k_4 are rate constants for the equations as written; I is the radiation intensity and Zn_s^+–OH_s denotes a paramagnetic Zn^+-type species formed at the interface by fast trapping of photogenerated holes. In this model no attempt is made to distinguish the fast electron exchange limiting case from the slow electron exchange limiting case and it is assumed that unpaired electrons prior to recombination contribute to n^* whether in the conduction band or temporarily trapped on bulk donors. It is considered however that both n^* and [Zn^+–OH] contribute to the net concentration, [R], of radical-type centers. Growth of [R] was followed experimentally as growth of the observed composite ESR signal intensity, I_{fp} (1.96) and relationship (5) should apply. Assuming processes (2) and (3) are fast but (4) is slow, then the

$$\frac{dI_{fp}^*(1.96)}{dt} \equiv \frac{d[R]}{dt} \equiv \frac{dn^*}{dt} + \frac{d[Zn_s^\bullet\text{–}OH_s]}{dt} \tag{5}$$

steady-state approximation may be applied to the hole concentration, leading to

$$p^* = \beta I / k_3 \tag{6}$$

The net rate of growth of photogenerated electrons may then be written as

$$dn^*/dt = \beta I - k_4 n^* [Zn_s^\bullet\text{–}OH_s] \tag{7}$$

Expression 7 is also true for net rate of growth of $[Zn_s^+–OH_s]$ and substitution of these equalities into (5) results in

$$\frac{dI_{fp}(1.96)}{dt} = \frac{d[R]}{dt} = 2\beta I - 2k_4 n^*[Zn_s^+–OH_s] \quad (8)$$

Requirements of charge balance between photogenerated electron-excess and electron-deficient species may be expressed as

$$[Zn_s^+–OH_s] = n^* - p^* \quad (9)$$

Substitution of (9) and (6) into (8) leads to the quadratic expression

$$\frac{dI_{fp}(1.96)}{dt} = 2\beta I + \frac{2k_4}{k_3}\beta I n^* - 2k_4 n^{*2} \quad (10)$$

Equation 10 upon appropriate integration yields an equation of form

$$[R] = (n^* + [Zn_s^+–OH_s]) = M \tanh (t^*C) \quad (11)$$

where

$$M = \frac{BI}{2C}\left(2 + \frac{Bik_4}{2k_3^2}\right)$$

$$C = BIk_4 + \frac{k_4}{4k_3}BI$$

and t^* is the duration of illumination. Equation 11 requires that, if the experimentally measured values of ESR signal intensity I_{fp} (1.96) is proportional to [R] and the residence time of particles in the ESR cavity is proportional to t^*, then a constant M should exist such that signal intensity increases linearly with tanh (t^*M). Figure 10 illustrates that data such as those in Figure 4 on growth of ESR signal intensity with residence time could be well represented in this manner, with arbitrarily chosen values of M.

A more detailed consideration is given elsewhere[23] of the relationship between the experimentally observed ESR signal intensity and growth in the number of paramagnetic centers in individual ZnO particles in their "transit time" across the flat cell in the ESR cavity. These considerations show that, for the conditions of our experiments, growth of paramagnetic centers in individual particles according to eq 11 should result in similar rate expression for growth of the composite ESR signal.

The "slow exchange" model for the photogenerated ESR signal thus appears to be both physically reasonable and fully consistent with the kinetic requirements of appropriate kinetic equations. No other model was found which satisfied both these criteria; thus models based on growth of paramagnetic centers in illuminated particles according to Elovich, zero-order or second-order rate expression did not reproduce the experimentally observed kinetics of signal growth; whereas models based on growth of signal intensity within illuminated particles according to first-order expression could reproduce the observed signal growth but did not appear physically reasonable. The chief difficulty for first-order models was in assigning physical significance to the limiting value $[R]_{max}$ to which a number of paramagnetic centers would approach as transit time though the illuminated cavity increased (e.g., surface states were excluded from consideration by the negative results of our experiments with suspensions exposed to visible and ir illumination).

Our identification of the ESR signal with conduction band electrons coexisting with partially ionized donors and our explanation of growth in signal intensity as arising from photogeneration of electrons and holes appear fully

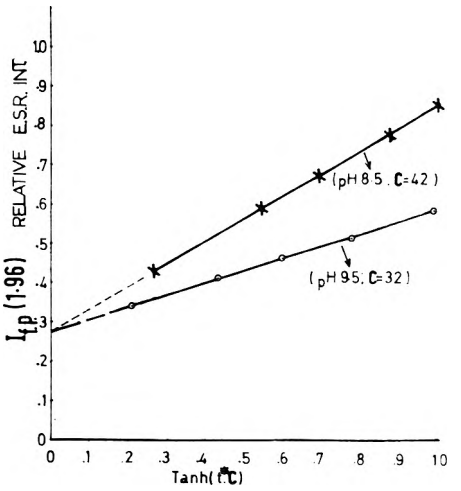

Figure 10. Plots illustrating good agreement between kinetic expression II (see text) and experimentally determined ESR signal intensity I_{fp} (1.96) measured for different transit times t^* for particles of ZnO-SP500 through the uv illuminated region of the flat cell: (a) Points, ⊗, on upper line were determined for different transit times in suspensions with pH fixed at 8.5. The line corresponds to expression II with C arbitrarily set to 42; (b) same as a except that the pH was 9.5 and choice of C = 32 gave best fit of line to experimental values, O.

consistent with literature reports on photoconductivity in zinc oxide.[22] This has been attributed to photogenerated increases in concentration of conduction band electrons and has been reported as exhibiting a fast component approaching saturation in ca. 0.1 sec and attributed to purely electronic processes. A slow component of photoconductivity has been reported for illuminated ZnO crystals just as a slow ESR component has here been detected from the illuminated suspensions. Difficulties associated with "settling" of the suspension in the flat cell at long illumination times prevent meaningful kinetic analysis of growth of this slow component of the ESR signal but most other ESR results presented in this paper can be satisfactorily accounted for in terms of the coexistence of conduction band electrons and donors, provided that due account is taken of characteristics of the ZnO–electrolyte interface. The necessity of taking these characteristics into account is demonstrated by the discrepancy of 10^2–10^3 between number of unpaired electrons here measured for well-outgassed particles in aqueous suspension (5×10^{15} and $<5 \times 10^{14}$ g^{-1} for ZnO–In and ZnO-SP 500, respectively) and reported electron densities measured by an a.c. Hall technique on the same oxides when dry and well outgassed in vacuo (1.8×10^{18} and 3×10^{16} g^{-1}, respectively). Two electrical double-layer processes could markedly affect the number of electrons mobile in the bulk conduction band of ZnO particles suspended in aqueous electrolyte: first, a build-up of an excess of positive or negative charge at the interface can result from surface excess of H^+ or OH^- ions caused by adsorption and hydrolysis equilibria;[24a] secondly, a large capacitive effect can occur across interfaces[24c] arising from dipolar interactions between electrons within ZnO and the dipolar water molecules which are available in abundance at the ZnO–H_2O interface. The former process tends to produce *downward* band bending at the interface at electrolyte pH values lower than the point of zero charge, pzc, which is reported to occur at pH ~9.5[24b] for ZnO–H_2O. A modified form of the Nernst equation

$$\Delta\psi_s(\text{volt}) = -0.059\Delta\text{pH} \quad (12)$$

predicts a positive surface potential, ψ_s, of 0.118 V at electrolyte pH of 7.5, due to surface excess of H^+ ions, and this situation is schematically depicted in Figure 9a. High probability for occupancy of donor levels close to the positively charged interface and reduced numbers of unpaired electrons in the conduction band should accompany such downward band bending. Surface capacitance changes of ca. 1 C cm^{-2} (pH unit)$^{-1}$ have been associated in the literature with pH dependence of such adsorption of H^+ and OH^- on zinc oxide.[24b] The equivalent separation of charge across the ZnO–H_2O interface for the net interfacial area of ZnO–In present in the ESR flat cell would correspond to a change of 3×10^{15} separated charges at the interface per unit change in pH. Since the ESR signal intensity observed from the ZnO–In particles present in the ESR flat cell corresponded to $\sim 10^{14}$ unpaired electrons, a marked effect of pH upon ESR signal intensity from ZnO–In in the dark could be expected from this capacitive effect of adsorbed potential determining (pd) ions. No such pH dependence was observed (cf. Figure 3) and it may be argued that another process, less dependent on pH, determined the number of unpaired electrons detectable by ESR within the ZnO–In particles. Existance of sufficient downward band bending to localize a large fraction of conduction band electrons adjacent to the interface and thereby couple their spins would be such a process, and could operate even at pH 9.5, since it is reported that the "fleet-band" condition is not achieved at the point of zero charge. Localization and pairing of a large fraction of electrons at the interface through such downward band bending of the type illustrated in Figure 9 could also account for our experimental observation that the numbers of unpaired electrons here observed by ESR were much lower than reported for the same zinc oxides in vacuo.[12]

The model described above for the photogenerated signal envisages rapid irreversible hole trapping, adjacent to surface hydroxyls, reversible electron trapping, and hole–electron recombination at the site of the previously trapped hole. Effects of pH and of additives upon intensity of the photogenerated signal can be accounted for as follows in terms of their effects upon hole–electron recombination.

pH Dependence of I_{fp} (1.96). Faster hole–electron recombination at pH 9.5 than at 7.5 is predicted by the model on the basis of greater surface concentration of hydroxyls at pH 9.5. An additional factor possibly contributing to the observed lower steady-state concentration of unpaired electrons at pH 9.5 is that capacitative effects associated with surface charge should then be lowest. Dewald has given evidence that surface states are negligible at the ZnO–H_2O interface in the dark[17] and, if this situation is assumed also to prevail at the illuminated interface, application of boundary layer theory[25] is permissible and indicates that the potential associated with adsorption of potential-determining ions should decrease to zero over a depth of approximately 100 nm within particles of ZnO-SP500. This depletion depth is comparable to particle size and to penetration depth of uv illumination. Consequently, most electron–hole pairs photogenerated at pH 7.5 are "born" in a potential gradient tending to separate them by moving electrons toward the interface and holes toward the interior of the particles. Capacitative effects of the positive surface potential existing at pH 7 tend to maintain separation between photogenerated electrons and holes and to reduce recombination by opposing their diffusion toward one another.

Hole-Attaching Additives. The presence of effective traps for photogenerated holes in the aqueous suspensions of ZnO-SP500 corresponds to introduction into energy-level diagram 9b of a new acceptor level capable of competing for available holes and so reducing hole–electron recombination at surface hydroxyls. Higher photostationary state concentration of electrons could then result. The enhancing effects of the good hole-attaching additives, ethanol and formate, as illustrated in Figure 7, are consistent with such competition for available holes between the normal surface and surface sites bearing formate ion or ethanol molecules. Morrison et al.[14] have noted previously that these additives produce a doubling in the number of charge carriers (conduction-band electrons) when ZnO electrodes immersed in electrolyte were exposed to uv illumination. The explanation advanced by Morrison et al. to explain their "current doubling" effect identified hole trapping by the additives as the essential first step. They envisaged (13b) or (14b) as additional steps in which resultant surface radicals then inject an electron into the conduction band, thereby producing two conduction band electrons per trapped hole. A qualitative explanation of the enhancing effect of formate and ethanol on I_{fp} (1.96) in the present study can be based on (13) and (14).

$$HCO_2^-{}_{(ads)} + h^+{}_{(ZnO)} \xrightarrow{a} \dot{H}CO_{2\,(ads)} \xrightarrow{b} H^+ + CO_2 + e_{cb}^- \quad (13)$$

or

$$C_2H_5OH_{(ads)} + h^+{}_{(ZnO)} \xrightarrow{a} C_2H_5\dot{O}H^+{}_{(ads)} \xrightarrow{b} C_2H_4O + 2H^+ + e_{cb}^- \quad (14)$$

Inhibiting Additives. The very small inhibiting effect here noted for 10^{-3} *M* oxygen upon I_{fp} (1.96) and the much larger effect of 10^{-3} *M* I^- do not appear consistent with simple electron attachment as the mechanism effecting reductions in photostationary concentration of unpaired electrons in suspended particles of ZnO-SP500. Published rate constants for reaction with solvated electrons[26] would require O_2 {$k(O_2 + e^-) \sim 10^{10}\ M^{-1}\ sec^{-1}$} to be much more effective than I^- {$(e^- + I^-) < 10^5\ M^{-1}\ sec^{-1}$}. Alternative possibilities of reducing the photostationary concentration of unpaired electrons include: (i) action of the additives as effective hole–electron recombination centers in the ZnO–electrolyte interface, as already suggested[14] for I^- and, (ii) excitation transfer to an appropriate excited state of the additive from the excited state of the ZnO lattice, ZnO*. The energy levels of ZnO* at 3.2 eV is situated above the lowest singlet excited state of PNDA at 2.8 eV. The process, ZnO* + PNDA → ZnO + PNDA*, is energetically feasible and this could account for the agreement noted in Figure 8 between the quenching effect of PNDA upon I_{fp} (1.96) and the Stern–Volmer quenching expression. Use of solution concentration, [$PNDA_{aq}$], rather than surface concentration in this expression is justified by absence of significant adsorption of PNDA onto ZnO. Agreement with (1) is consistent with excitation transfer out to PNDA molecules in the aqueous phase.

Acknowledgments. Financial support of this research in part by the U.S. Air Force Office of Scientific Research and in part by the National Science Council of Ireland is acknowledged. The authors are also grateful to the New Jersey Zinc Company for supplying zinc oxides used in the study.

References and Notes

(1) Work supported in part by the U.S. Air Force Office of Scientific Research through the European Office of Aerospace Research under Grant No. AF7[illegible]-2148.
(2) (a) R. D. Iyengar and M. Codell, *Adv. Colloid Interface Sci.*, **3**, 365 (1972); (b) D. Hahn, R. Nink, and D. Severin, *Phys. Kondens. Mater.*, **5**, 371 (1966).
(3) J. Schneider and A. Rauber, *Z. Naturforsch., Teil B*, **16**, 712 (1961).
(4) R. J. Kokes, *J. Phys. Chem.*, **66**, 99 (1962).
(5) M. Setaka, S. Fujieda, and T. Kwan, *Bull. Chem. Soc. Jpn.*, **43**, 2377 (1970).
(6) K. M. Sancier, *Surface Sci.*, **21**, 1 (1970).
(7) H. Uetta, *Can. J. Chem.*, **46**, 891 (1968).
(8) M. Codell, H. Gisser and R. D. Iyengar, *Can. J. Chem.*, **46**, 2239 (1968).
(9) P. H. Kasai, *Phys. Rev.*, **130**, 989 (1963).
(10) J. M. Smith and W. E. Vehse, *Phys. lett. A*, **31**, 147 (1970).
(11) J. Cunningham and A. L. Penny, *J. Phys. Chem.*, **78**, 870 (1974).
(12) H. Chon and D. Prater, *Discuss. Faraday Soc.*, **41**, 380 (1960).
(13) J. Cunningham and H. Zainal, *J. Phys. Chem.*, **76**, 2362 (1972).
(14) (a) S. R. Morrison, "Current Problems in Electrophotography," Walter de Gruyter, Berlin, 1972; (b) S. R. Morrison and T. Freund, *Electrochem. Acta*, **13**, 1343 (1968).
(15) W. Doerfler and K. Hauffe, *J. Catal.*, **3**, 171 (1964).
(16) T. Wolkenstein, *Adv. Catal.*, **23**, 157.
(17) J. F. Dewald, *Bell System Tech. J.*, **39**, 615 (1960).
(18) P. J. Crane, *Trans. Faraday Soc.*, **63**, 693 (1967).
(19) (a) G. Heiland and W. Bauer, *J. Phys. Chem. Solids*, **32**, 2605 (1971); (b) G. Heiland and H. Luth, *Phys. Status Solidi*, **14**, 573 (1972); (c) G. Heiland, W. Bauer, and M. Neuhaus, *Photochem. Photobiol.*, **16**, 315 (1972).
(20) (a) J. Lagowski, E. S. Sproules, and H. C. Gatos, *Surface Sci.*, **30**, 653 (1972); (b) J. Lagowski, C. L. Balestra, and H. C. Gatos, *ibid.*, **29**, 203, 213 (1972).
(21) M. J. Duck and R. L. Nelson, *J. Chem. Soc., Faraday Trans. 1*, **70**, 436 (1970).
(22) G. Heiland, E. Mollwo, and F. Stockman, *Solid State Phys.*, **8**, 278 (1959).
(23) S. Corkery, Ph.D. Thesis, University College, Cork, Ireland, 1974.
(24) (a) H. P. Boehm, *Discuss. Faraday Soc.*, **52**, 264 (1971); (b) V. G. Barube and P. L. de Bruyn, *J. Colloid. Interface Sci.*, **27**, 305 (1968); (c) K. Muller, "Electroadsorption," E. Gileadi, Ed., Plenum Press, New York, N.Y., 1967, Chapter 6, p 117.
(25) P. B. Weisz, *J. Chem. Phys.*, **21**, 1531 (1953).
(26) M. Anbar and P. Neta, *Int. J. Appl. Radiat. Isot.*, **18**, 493 (1967).

Magnetic Orientation of Poly(γ-methyl-D-glutamate) Liquid Crystals

Robert W. Filas* and Harry Stefanou

Frick Chemical Laboratories, Princeton University, Princeton, New Jersey 08540 *(Received June 6, 1973; Revised Manuscript Received August 16, 1974)*

NMR was used to detect the magnetic orientation of a biphasic solution of poly(γ-methyl-D-glutamate) in dichloromethane. The observed triplet is interpreted in terms of an outer doublet produced by the direct dipolar coupling between the protons on the solvent molecules in oriented liquid crystalline regions, and a central resonance corresponding to solvent in an isotropic environment. The time dependence of the magnetic reorientation is compared with an equation derived in an earlier paper utilizing a continuum mechanics approach.

Nuclear magnetic resonance[1-3] (NMR) and light scattering[4] have been employed to show that liquid crystalline solutions of poly(γ-benzyl-L-glutamate) (PBLG) and poly(γ-ethyl-L-glutamate) (PELG) can be oriented by magnetic fields. In each case the long axis of the polypeptide was found to align parallel to the field direction. The results reported herein concern the use of NMR to detect the magnetic orientation of biphasic solutions of poly(γ-methyl-D-glutamate) (PMDG) in dichloromethane.

A convenient method of investigating the magnetic orientation of a lyotropic mesophase is to observe the effect of the ordered structure on the dipolar splitting of the solvent molecules. The separation of the doublet in the NMR signal for a pair of protons is given by[5,6]

$$\Delta H = 3\mu\left\langle \frac{3\cos^2\theta - 1}{r^3} \right\rangle \qquad (1)$$

where μ is the proton magnetic moment, r is the interproton distance, and θ is the angle between the interproton vector and the magnetic field direction. The averaging over all values of θ indicated by the brackets can drastically reduce the magnitude of the observed splitting compared to the rigid lattice value.[1]

PMDG, isolated from Ajinomoto's Ajicoat polyamino acid solution, was purified by precipitation in ethanol from chloroform, dried, then redissolved in reagent grade dichloromethane. After filtration, the solutions were sealed in NMR tubes and the bulk weight per cent of each determined gravimetrically from aliquots of solution and their dried residues. The intrinsic viscosity of the polypeptide was 0.995 ± 0.003 in dichloroacetic acid at 25.0°. Magnetic field strengths of either 14.1 or 23.5 kG were produced by a Varian A60 or a Varian HA100 NMR spectrometer, respectively. An external oscillator and frequency counter were used to calibrate the sweep parameters of the HA100. Each sample was allowed to remain in the field without spinning until no further change in the signal was observed.

A concentration range in which isotropic and liquid crystal phases coexist in equilibrium is to be expected for solutions of rod-like molecules.[7] According to the phase rule, the concentration of the polymer-rich phase will remain constant as the bulk concentration increases until the entire solution is liquid crystalline. By observing the samples between crossed polarizers the lower limit of this biphasic region was found to be about 11% polymer. Below this concentration the NMR absorption signal was a singlet, as expected for an isotropic solution. However, a 13.2% sample, which was partially birefringent and appeared speckled between crossed polarizers, initially produced a singlet which broadened with time and eventually became a triplet as

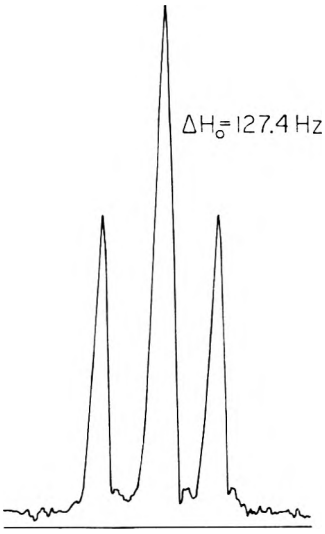

Figure 1. 100-MHz NMR signal of a 13.2% solution of PMDG in dichloromethane at 30.1°.

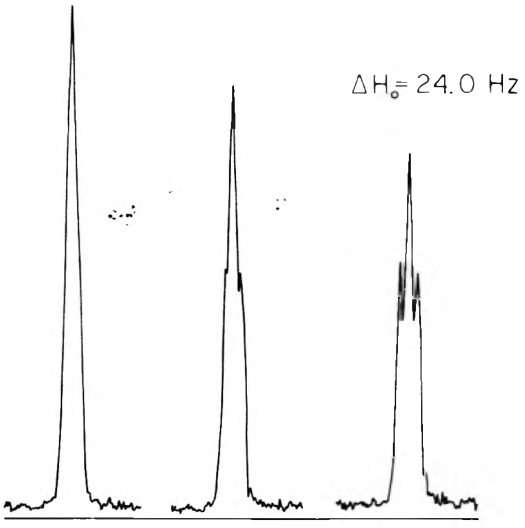

Figure 2. 100-MHz NMR signal of an 8.8% PBDG solution in dichloromethane at several stages of orientation from an initially random structure at 31.1°.

shown in Figure 1. The two outer peaks correspond to dichloromethane molecules in liquid crystalline regions while the central peak represents solvent in an isotropic environment. Integration of the signal revealed that 41% of the solvent is in an anisotropic environment. The same kind of signal is produced in a 60-MHz instrument, except that the resonances are not as sharp.

To further test the hypothesis that a biphasic material will give a triplet absorption signal, a biphasic solution[8] (8.8%) of poly-γ-benzyl-D-glutamate (PBDG) in dichloromethane was prepared. The molecular weight of the polymer as determined by viscosity[9] was 261,000. Its appearance between crossed polarizers was similar to that of the PMDG solution. The 100-MHz NMR signal of this solution was initially a singlet and gradually split into a triplet (Figure 2). This process took several hours in a freshly prepared sample, but proceeded much more rapidly in the same solution allowed to age for 1 week out of the magnetic field. Further aging effects were evident after several months when positive spherulites could be observed in the sample, similar to those found in chloroform solutions of PMLG.[10] Since the rate of magnetic orientation of the liquid crystalline regions of the biphasic solution is strongly time dependent, insufficient time in the magnetic field could explain the broadened singlet reported by earlier workers[8] for biphasic solutions of PBLG (M = 275,000) in dichloromethane.

If an aligned sample is rotated by an angle θ_0, the realignment of the polypeptide rods with the field can be related to the time dependence of ΔH by rewriting eq 1 in terms of the observed equilibrium separation, ΔH_0:

$$\Delta H(t) = \frac{\Delta H_0}{2}(3\cos^2\theta(t) - 1) \qquad (2)$$

By removing the averaging brackets, it is assumed that the influence of the polymer on the solvent and the local distribution of helices remains constant during reorientation. These assumptions have recently been justified[11] in a study of the time dependence of the reorientation of a racemic mixture of PBG in dichloromethane for $\theta_0 \leq 45°$. Using a continuum mechanics approach, it was shown[11] that

$$\theta(t) = \tan^{-1}(\tan\theta_0 e^{-At}) \qquad (3)$$

where $A \equiv \mu H^2/c$. Since the magnetic field strength is known, the only constant to be determined by experiment

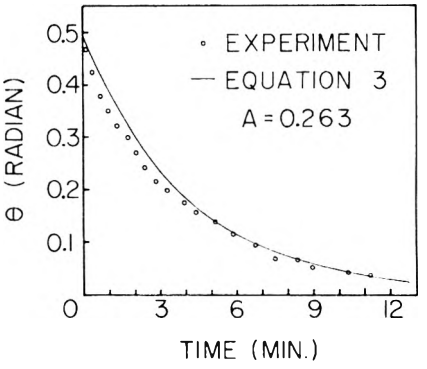

Figure 3. Reorientation of a 13.2% PMDG solution following a 28.1° rotation of the sample tube in a 23.5 kg field at −18.3°.

is μ/c: the ratio of the anisotropy of the diamagnetic susceptibility to the apparent rotational viscosity. A comparison of the calculated values of $\theta(t)$ with eq 3 is shown in Figure 3 for θ_0 = 28.1°. The value of A was chosen to fit the data at 5 min. During the first minute of the reorientation, the outer peaks rapidly broadened and decreased in height making measurement of the splitting less accurate. The central peak remained unchanged in shape as expected. In the subsequent time, the outer peaks sharpened and increased in height until their initial shape was achieved after about 10 min. A second 28.1° rotation 20 min after the first one produced similar behavior.

Reorientations of biphasic solutions of PBDG and racemic PBG were found to obey eq 3 quite well. In these cases, however, the shape of the outer peaks did not change as with the PMDG. This observation would seem to indicate that the broadening was not due to the biphasic nature of the solution. One possible explanation is that incomplete alignment of the PMDG helices results in counterrotation during reorientation, disrupting the structure and broadening the outer peaks. Further studies are certainly needed to resolve this question.

References and Notes

(1) S. Sobajima, *J. Phys. Soc. Jpn.*, **23**, 1070 (1967).
(2) M. Panar and W. D. Phillips, *J. Am. Chem. Soc.*, **90**, 3880 (1968).

(3) R. D. Orwoll and R. L. Vold, *J. Am. Chem. Soc.*, **93**, 5335 (1971).
(4) N. Miyata, K. Tohyama, and Y. Go, *J. Phys. Soc. Jpn.*, **33**, 1180 (1972).
(5) G. E. Pake, *J. Chem. Phys.*, **16**, 327 (1948).
(6) J. C. Rowell, W. D. Phillips, L. R. Melby, and M. Panar, *J. Chem. Phys.*, **43**, 3442 (1965).
(7) P. J. Flory, *Proc. R. Soc., London, Ser. A*, **234**, 73 (1956).
(8) E. T. Samulski and A. V. Tobolsky, *Mol. Cryst. Liq. Cryst.*, **7**, 433 (1969).
(9) P. Doty, J. H. Bradbury, and A. M. Holtzer, *J. Am. Chem. Soc.*, **78**, 947 (1956).
(10) S. Ishikawa, T. Kurita, and E. Suzuki, *Polym. Lett.*, **1**, 127 (1963).
(11) R. W. Filas, L. E. Hajdo, and A. C. Eringen, *J. Chem. Phys.*, **61**, 3037 (1974).

Transference Numbers and Ionic Conductances in 100% Sulfuric Acid at 25°[1]

David P. Sidebottom and Michael Spiro*

Department of Chemistry, Imperial College of Science and Technology, London SW7 2AY, England (*Received November 11, 1974*)

The cation transference numbers of lithium, sodium, potassium, ammonium, silver, and barium hydrogen sulfates, and of solutions of water and of acetic acid, have been measured in 100% sulfuric acid at 25° by the direct moving boundary method. Most determinations were carried out in the range 0.07–0.2 mol dm^{-3}. The transference numbers were of the order of 0.005, much smaller than had been believed previously. Individual ionic conductances were calculated from these results and literature conductances. Estimates were made of the limiting ionic conductances and their values compared with the predictions of the Zwanzig theory.

Introduction

The behavior of solutions in pure sulfuric acid is governed by three main properties of the solvent.[2-4] It is extremely acid and so converts many simple inorganic and organic solutes into hydrogen sulfate salts[2-4] and it possesses

$$\tfrac{1}{2}Na_2SO_4 + \tfrac{1}{2}H_2SO_4 \longrightarrow Na^+ + HSO_4^-$$

$$H_2O + H_2SO_4 \longrightarrow H_3O^+ + HSO_4^-$$

$$HOAc + H_2SO_4 \longrightarrow H_2OAc^+ + HSO_4^-$$

such a large dielectric constant (D = 100 at 25°)[2,3] that these salts are almost completely dissociated. Third, the high viscosity of sulfuric acid (η = 0.2454 P at 25°)[5] forces ions to migrate very slowly unless (such as HSO_4^-) they conduct by proton jumping. As a result, the conductivities of solutions of the various hydrogen sulfates are almost identical at low concentrations.[6,7] The only method, therefore, of obtaining values of individual ionic conductances is by measuring transference numbers.

A fourth property of sulfuric acid makes it difficult even to derive values of the limiting molar conductances of the hydrogen sulfate salts.[8] The acid is extensively self-dissociated by reactions such as[2-4]

$$2H_2SO_4 \rightleftharpoons H_3SO_4^+ + HSO_4^-$$

$$2H_2SO_4 \rightleftharpoons H_3O^+ + HS_2O_7^-$$

and the ionic strength of the pure solvent is high,[8] 0.082 mol dm^{-3} at 25°. Thus extrapolation of the molar conductances to infinitesimal ionic strength[9] involves large and somewhat uncertain solvent corrections.[8] However, combination of experimental conductivities (κ) and experimental transference numbers (T) yields molar ionic conductances (λ) free from any solvent correction error. For the cation

$$\lambda_+c_+ = \kappa(\text{corr})T_+(\text{corr}) = \kappa T_+ \quad (1)$$

since

$$\kappa(\text{corr}) = \lambda_+c_+ + \lambda_-c_-;\ \kappa = \Sigma\lambda_i c_i \quad (2)$$

$$T_+(\text{corr}) = \frac{\lambda_+c_+}{\lambda_+c_+ + \lambda_-c_-};\ T_+ = \frac{\lambda_+c_+}{\Sigma\lambda_i c_i} \quad (3)$$

where c_+ is the molarity of added cation and c_- the molarity of the accompanying hydrogen sulfate ion. The overall summations contain contributions from the various solvonium and solvate species.

Three earlier papers[10-12] reported cation transference measurements in sulfuric acid solutions, all by the Hittorf method. This method depends on the determination of small differences between large quantities, and thus becomes unreliable when the transference numbers are as small as they are in sulfuric acid. We therefore decided to carry out a series of transference measurements using the more accurate moving boundary method.

Experimental Section

Materials. The preparation of the solvent was based on that of Gillespie et al.[13,14] Sulfur trioxide was slowly distilled from warm 20% oleum (Fisons) and passed into British Drug Houses AnalaR 98% sulfuric acid until SO_3 was in excess. The weak oleum produced (ca. 1500 cm^3) was titrated with 200–300 cm^3 AnalaR acid at 25° until a minimum in the specific conductance of the solution (1.0432 ohm^{-1} m^{-1}) was obtained, and further AnalaR acid was then added until the specific conductance of the 100% acid (1.0439 ohm^{-1} m^{-1}) was reached. The Pyrex distillation and titration flasks were fitted with Quickfit ground joints which were lubricated with Hilflon P.T.F.E. aerosol if in the gas phase and with a few drops of AnalaR acid if in contact with the liquid. Sovirel Rotulex ball joints with

P.T.F.E. sealing rings were found useful for connecting the different vessels. The titration flask was stirred at 200 rpm with a pressure-tight Sovirel 4-588-07 stirrer with four P.T.F.E. sealing chevrons. Very dry nitrogen was employed as a carrier gas in the distillation, and to transfer acid samples to and from the S-shaped conductivity cell (cell constant 47745 m^{-1}). The conductance bridge was constructed from high-grade Sullivan and Pye resistors and condensers and incorporated a Wagner earth. The sensitivity at balance at 2000 Hz was 0.002% using a Telequipment D43 oscilloscope. The reaction vessel and conductivity cell were accurately thermostated at 25° in an oil bath. It was found that, if exposed to light, the sulfuric acid turned yellow after several days and increased slightly in conductance. The acid was therefore stored in an air-tight Pyrex flask painted black, where periodic checks showed that it remained colorless and of constant conductance.

All solid solutes were stored in vacuum desiccators. AnalaR sodium, potassium, ammonium, and silver sulfates were first dried in an oven at 150–180°, while AnalaR $Li_2SO_4 \cdot H_2O$ was fiercely heated to constant weight. To avoid coprecipitation, barium sulfate was prepared by slow precipitation at 100° by adding a dilute aqueous filtered solution of barium hydroxide to excess aqueous sulfuric acid. The precipitate was thoroughly washed and dried at 700°. Benzoic acid was Hopkin and Williams standard reagent, acetic acid British Drug Houses Aristar, and water doubly distilled conductivity water. All solutions were made up by weight in a dry atmosphere. In the case of water and acetic acid, a weighed amount of the liquid solute was frozen in a small stoppered bottle which was then slid into a flask of solvent inside a dry bag. The flask was stoppered and shaken to open the sample bottle and ensure thorough mixing. Concentrations were converted to molarities by means of literature density data.[15]

Apparatus. The basic moving boundary technique has been described elsewhere.[16] The current was controlled by a high-voltage galvanostat[17] and determined by measuring the potential drop with a Racal 9075 digital voltmeter across a 1000-ohm Sullivan standard resistor. The boundaries, followed optically (Figures 4.12 and 4.13 in ref 16), were timed with a Zenith battery-operated clock and a metronome. Because the cation transference numbers are so tiny the boundaries moved extremely slowly; a few centimeters in 2 days. Extended electrode sections of large volume were therefore sealed into the cells to avoid electrode products reaching the boundaries. The main problem was that of lubricating the large hollow stopcocks in the rising and falling boundary cells (Figures 4.17 and 4.18 in ref 16). Sulfuric acid solutions dissolved or attacked hydrocarbon and silicone greases and even, though more slowly, Voltalef 90 fluorocarbon grease. Use of P.T.F.E. aerosol or sleeves led to leakage around the glass key (barrel). However, specially designed four-way P.T.F.E. keys (Springham) proved satisfactory. These were of solid P.T.F.E. with two grooves, each covering 90° of arc, cut into the outside (Figure 1). Solution inside the grooves and subject to Joule heating could then be cooled on the glass side by the thermostat oil. A similar four-way tap was fitted to a redesigned falling cell. The etchmarks on the tubes were calibrated by carrying out runs with an aqueous 0.1 *M* KCl solution whose transference number is well known.[16]

Electrodes. Moving boundary experiments require a closed electrode compartment in which the electrode is chemically stable and undergoes a known reaction of known volume change. No gas must be evolved. The few relevant cathodic electrode studies in the literature[18] did not suggest a system meeting these criteria, except possibly the reduction of dilute oleums at low over-potentials. No anodic studies have been carried out. The behavior of a number of possible electrode systems in 100% sulfuric acid was therefore investigated. Unfortunately metals capable of dissolving according to

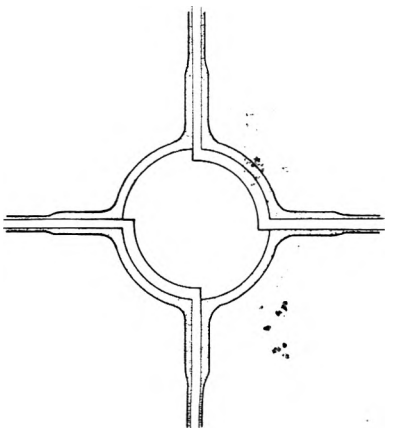

Figure 1. Schematic illustration of the grooved four-way moving boundary stopcocks.

$$M \longrightarrow M^{n+} + ne^-$$

(M = Pb, Cu, Ni, Cd, Tl, Hg, Ag) tended to dissolve to some extent even in the absence of current, silver being the most stable. Redox systems of the type

$$M^{x+} + (x - y)e^- \rightleftharpoons M^{y+}$$

(M = Pb, Fe, Ce, Hg) were unsuited as either anodes or cathodes by the low solubilities of their sulfates and the gassing that occurred when the solid salts, or a saturated solution of $Hg_2(HSO_4)_2$, were tried. The only electrode system satisfying the necessary conditions was

$$Ag^+ + e^- \longrightarrow Ag$$

Low yields (60–70%) were obtained if silver particles fell off during the electrolysis. A large platinum foil was therefore employed as cathode, part of the foil being allowed to lie flat at the bottom of the electrode compartment to catch any silver that became loose and to protect it cathodically. Analyses after runs then gave silver metal yields of 90–93% of the theoretical. Only ca. 1% of the yield could be accounted for by sulfuric acid reduction products (titration with dichromate), and the missing few percent were attributed to slow dissolution of metal in the ca. 20-min interval between switching off the current and removing the electrode. The closed cathode compartments in the cells held about 35 cm^3, and an initial Ag^+ concentration of 0.35 *M* was always employed. The open anode compartments held gassing platinum electrodes.

Preliminary Experiments. Many systems gave boundaries of good visibility. The earlier Hittorf work[11] suggested that Ba^{2+} ions were slower than those of the alkali metals, and indeed barium hydrogen sulfate as following electrolyte produced good rising boundaries with Na^+, NH_4^+, and H_3O^+ leading, a poor rising boundary with K^+ leading, and falling boundaries with Ag^+ leading. A second indicator species was required to test the independence of the boundary velocity on the nature of the following ion; H_2OAc^+ met this need for the relatively fast ions K^+,

NH_4^+, and Ag^+ although these falling boundaries were hard to see below 5 mA. For the slower leading ions Li^+, Na^+, Ba^{2+}, H_3O^+, and H_2OAc^+, excellent falling boundaries were formed with H_2OBz^+ as indicator. The Kohlrausch concentrations for Ba^{2+} and H_2OAc^+ could be estimated from experimental transference measurements; for H_2OBz^+ a variation of 24% in concentration had no significant effect on the boundary velocities.

A curious feature of the systems $Ag^+ \leftarrow Ba^{2+}$, $Ag^+ \leftarrow H_2OAc^+$, and $Ba^{2+} \leftarrow H_2OBz^+$ was the frequent appearance of double falling boundaries. In some runs the two boundaries had the same velocity, in others they gradually moved closer together or further apart (see Table II). No boundary at all was seen when the falling cell was entirely filled with 0.223 *M* $AgHSO_4$ solution, thus ruling out such extraneous reasons as solution leakage. The double boundaries can be understood only by discovering the compositions of the solutions they separate. Attempts were therefore made to take samples for analysis. This could not be done with the four-way stopcocks normally employed, and special cells were used with straight-through two-way taps through which a capillary could be inserted after a run and successive samples of solution removed. Unfortunately no boundaries were seen with these cells, whether the tap held a hollow glass key lubricated with Voltalef 90 or a P.T.F.E. key. Presumably chemical attack on the lubricant in the former case, and Joule heating inside the poorly conducting solid P.T.F.E. in the latter, disturbed boundary adjustment. Nevertheless, samples were taken in two experiments. In the run 0.223 *M* $AgHSO_4 \leftarrow$ 0.0207 *M* $Ba(HSO_4)_2$ with a glass key, the bottom samples contained silver (tested by adding aqueous KCl and then ammonia) but no barium (tested by adding water and then ammonia) while the upper samples contained barium but no silver. The existence of only one boundary is thereby indicated. In the run 0.114 *M* $AgHSO_4 \leftarrow$ 0.060 *M* $H_2OAcHSO_4$ with a glass key, samples (ca. 0.1 g) were diluted with water and analyzed for silver by atomic absorption spectroscopy at 328.1 nm. The silver concentrations of successively higher layers were found to be 0.11_7, 0.10_0, 0.05_2, 0.02_5, and 0.00 *M* (all ±20%). This points to the possible existence of two or more silver solutions, the leading one having the highest concentration.

Parsons has suggested[19] that the extra boundary might have been formed between a solution of Ag^+ ions and one of silver in a higher oxidation state such as Ag^{3+}. A similar idea could well explain unpublished observations of double boundaries in certain other systems: $AgI \leftarrow HgI_2|Hg$ (autogenic) and $Cu(NO_3)_2 \leftarrow Hg(NO_3)_2|Hg$ (autogenic) at −40° in liquid ammonia[20] and in some uranium systems at 25° in water.[21] A common feature of all these systems (except $Ba^{2+} \leftarrow H_2OBz^+$ in sulfuric acid) is the participation of transition metal ions capable of existing in more than one valence state.

Results and Discussion

Variation with Current and Following Electrolyte. The data derived from 40 transference runs are summarized in Tables I and II. Inspection shows that the transference numbers of a given system often vary significantly with current. High currents had to be employed with sulfuric acid because of the extreme slowness of the boundaries, and Joule heating was therefore appreciable. Moreover, this heating has most effect when the mobilities of the two ions of the leading solution possess different temperature coefficients, as happens when one of them (HSO_4^-) moves by proton jumping and the other by normal migration. From the conductances of dilute solutions of water,[14] to which the HSO_4^- ion makes by far the largest contribution, we deduce that $d \ln \lambda(HSO_4^-)/dt$ = ca. 0.035 deg^{-1}. The cationic conductances are likely to follow a modified form of Stokes' law such as[22]

$$\lambda_+ \eta^{0.7} \approx \text{constant} \qquad (4)$$

from which[23] $d \ln \lambda_+/dt$ = ca. 0.025 deg^{-1} and $d \ln T_+/dt$ = ca. −0.01 deg^{-1}. The transference number should therefore decrease as the current rises, for not only will the leading solution warm up but heat will also flow across the boundary from the hotter following solution.[24] The effect should be most marked at the center of the tube, and indeed saucer-shaped boundaries were often observed in the rising cell and (at high currents and with dilute solutions) in the falling cell. In most of the systems in which the current variation was about 0.0002 mA^{-1} or greater ($Na^+ \leftarrow Ba^{2+}$, $NH_4^+ \leftarrow Ba^{2+}$, $H_2OAc^+ \leftarrow H_2OBz^+$, but not $NH_4^+ \leftarrow H_2OAc^+$), the transference numbers did decrease with increasing current. Other factors, such as the thermal expansion of the closed electrode compartment, will have had the opposite effect; a more detailed discussion of causes is given elsewhere.[24]

Two main procedures exist for extrapolating the transference numbers to zero current (I). One is a simple T_+ vs. I plot (cf. Figure 2), the other a plot of T_+ vs. I^2 as suggested by the theory of heat conduction.[24] Although the former procedure led to results of better internal consistency, both were employed and the mean values adopted. These are the zero-current transference numbers listed in Tables I and II.

A theoretically unexpected feature of the results is the marked variation of the transference numbers of Na^+, NH_4^+, and (to a lesser extent) Ag^+, with the nature of the following electrolyte. Fortunately this variation largely disappears when the results are extrapolated to zero current (Table I and Figure 2). The effect is therefore exposed as a spurious consequence of Joule heating. Changing the concentration of a given following electrolyte by over 20% produced no significant alteration in transference number (except for the $Ag^+ \leftarrow H_2OAc^+$ system), and this testifies to adequate Kohlrausch adjustment behind the boundaries.

Volume and Solvent Corrections. Between the cathode and a point in the leading c *M* $MHSO_4$ solution the volume increase is given by

$$\Delta V = V(Ag) - \phi(AgHSO_4) + T_M\phi(MHSO_4) \qquad (5)$$

where ϕ is the apparent molar volume.[25] Numerical values of ϕ for the various solutes have been given by Flowers et al.[15] Since the concentration dependence of ϕ in sulfuric acid solutions has not been studied, and in view of the evidence that silver deposition may have been accompanied by a slight amount of solvent reduction, the ΔV values cannot be more certain than ±2 $cm^3\ F^{-1}$. The cation boundaries always moved toward the closed cathode compartment and the volume correction $c\Delta V$ was therefore[16] added to the observed transference numbers (Table III).

Evaluation of the solvent correction is more difficult, for each solution contains ionic species derived both from the solute (M^+,HSO_4^-) and from the self-dissociation of the solvent ($H_3SO_4^+$, HSO_4^-, H_3O^+, $HS_2O_7^-$). The ionic concentrations were taken from tables[8] based on cryoscopic and conductimetric data and reasoning.[26] For the calculation of the ionic conductances of $H_3SO_4^+$ and HSO_4^- a modified approach was employed which does not depend

TABLE I: Summary of Cation Transference Measurements in Sulfuric Acid at 25°

Leading soln[a]	Following soln[a]	Type	Current, mA	T_+
0.127 M Li^+	0.106 M H_2OBz^+	Falling	8.11	0.0085_5
			3.90	0.0083
			0	0.0081
0.076 M Na^+	0.048 M H_2OBz^+	Falling	8.02	0.0066
			3.88	0.0064_5
			0	0.0063_5
0.126 M Na^+	0.063 M H_2OBz^+	Falling	8.02	0.0091
			3.55	0.0089
			0	0.0088
	0.080 M H_2OBz^+	Falling	8.03	0.0092_5
			3.90	0.0090
			0	0.0088
	0.036 M Ba^{2+}	Rising	8.03	0.0073
			3.80	0.0080
			0	0.0084
	0.054 M Ba^{2+}	Rising	8.04	0.0071
			3.44	0.0081
			0	0.0086
0.194 M Na^+	0.128 M H_2OBz^+	Falling	8.34	0.0105_5
			4.00	0.0104
			0	0.0103
0.123 M K^+	0.103 M H_2OAc^+	Falling	8.2	0.0118
			6.1	0.0117
			0	0.0115
0.062 M NH_4^+	0.015 M Ba^{2+}	Rising	5.56	0.0057
			3.93	0.0060
			0	0.0065
0.111 M NH_4^+	0.026 M Ba^{2+}	Rising	6.85	0.0088
			3.84	0.0094
			0	0.0099
0.187 M NH_4^+	0.033 M Ba^{2+}	Rising	8.15	0.0115
			4.60	0.0118
			0	0.0121
0.193 M NH_4^+	0.090 M H_2OAc^+	Falling	7.31	0.0133
			5.22	0.0129
			0	0.0122
	0.120 M H_2OAc^+	Falling	7.09	0.0134
			5.22	0.0131
			0	0.0125
0.118 M H_3O^+	0.062 M H_2OBz^+	Falling	7.97	0.0101_5
			4.03	0.0104
			0	0.0106
0.090 M H_2OAc^+	0.060 M H_2OBz^+	Falling	5.53	0.0056
			3.45	0.0064
			0	0.0073

[a] All the ions were present as hydrogen sulfates. M = mol dm^{-3}.

directly on the assumption that the ratio $\mu = \lambda(H_3SO_4^+)/\lambda(HSO_4^-)$ is constant. The steps taken were as follows. (i) The ionic strength, I_s, of a particular c M $MHSO_4$ solution was calculated by the equation

$$I_s = \tfrac{1}{2}[c(M^+) + c(HSO_4^-) + c(H_3SO_4^+) + c(H_3O^+) + c(HS_2O_7^-)] \quad (6)$$

from the appropriate ionic concentrations interpolated from the tables of Flowers et al.[8] for strong base systems in sulfuric acid. The conductivity of the solution, κ_{base}, was obtained from the data of Bass et al.[7] (ii) From the published tables for strong acid systems in sulfuric acid,[8] the concentration of an $HB(HSO_4)_4$ solution was found that possesses the same ionic strength I_s. Its ionic composition was thus known, and its conductivity κ_{acid} was obtained from the literature.[7] For a more precise evaluation, allowance would have to be made for the later finding[27] that $HB(HSO_4)_4$ is not fully dissociated. (iii) The "proton-jump conductivities" κ' of both solutions[8] were then calculated by

$$\kappa'_{base} = \kappa_{base} - [c(M^+)\lambda(M^+) + c(H_3O^+)\lambda(H_3O^+) + c(HS_2O_7^-)\lambda(HS_2O_7^-)]_{base}$$

$$\kappa'_{acid} = \kappa_{acid} - [c(H_3O^+)\lambda(H_3O^+) + c(HS_2O_7^-)\lambda(HS_2O_7^-) + c(B(HSO_4)_4^-)\lambda(B(HSO_4)_4^-)]_{acid}$$

The ions inside the square brackets all move by bulk migration and a value of 1 cm^2 ohm^{-1} mol^{-1} was taken for their small ionic conductances. (iv) Values of the ionic con-

TABLE II: Cation Transference Measurements of Systems Showing Two Falling Boundaries in Sulfuric Acid at 25°

Leading soln[a]	Following soln[a]	Type	Current	T_+
0.0915 M Ag^+	0.031 M H_2OAc^+	*b*	7.49	0.0121
		c	4.96	0.0120
			0	0.0119
	0.055 M H_2OAc^+	*b*	7.51	0.0126
		c	4.73	0.0124
			0	0.0122
0.218 M Ag^+	0.128 M H_2OAc^+	*d*	8.14	0.0161
		e	4.96	0.0160
			0	0.0159
	0.020 M Ba^{2+}	*f*	8.05	0.0169
		c	4.60	0.0166
			0	0.0163
0.042 M Ba^{2+}	0.052 M H_2OBz^+	*g*	8.17	0.0049
		g	5.41	0.0048
			0	0.0047

[a] All the ions were present as hydrogen sulfates. M = mol dm^{-3}. [b] The second boundary soon caught up with the first and the two then moved together. The leading boundary was the sharper and was timed. [c] Only one boundary was seen. [d] The two boundaries, ca. 5 mm apart, were of comparable speed and strength. [e] The leading boundary was the faster and the separation between them increased. The two boundaries were of similar strength and the T_+ value was calculated from their mean velocity. [f] The following boundary soon caught up with the leading one. When the separation became small they moved at the same velocity from which T_+ was calculated. The leading boundary was the weaker one. [g] The two boundaries were close together and moved at the same speed. The leading boundary was the sharper.

ductances of $H_3SO_4^+$ and HSO_4^- at the ionic strength I_s were then obtained by solving the two simultaneous equations

$$\kappa'_{base} = [c(H_3SO_4^+)\lambda(H_3SO_4^+) + c(HSO_4^-)\lambda(HSO_4^-)]_{base}$$

$$\kappa'_{acid} = c(H_3SO_4^+)\lambda(H_3SO_4^+) + c(HSO_4^-)\lambda(HSO_4^-)]_{acid}$$

(v) It was now possible to calculate the contribution made to the conductivity of the base $MHSO_4$ solution by the solvent ions, κ_{solv}:

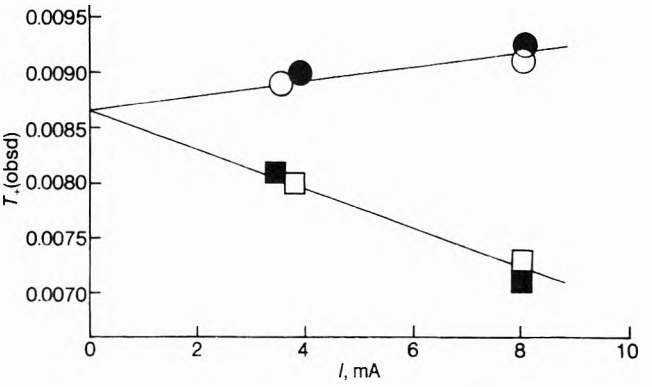

Figure 2. Extrapolation to zero current of the cation transference numbers of 0.126 *M* $NaHSO_4$ solutions measured with the following different electrolyte solutions: ○, 0.063 *M* $H_2OBzHSO_4$; ●, 0.080 *M* $H_2OBzHSO_4$; □, 0.036 *M* $Ba(HSO_4)_2$; ■, 0.054 *M* $Ba(HSO_4)_2$.

$$\kappa_{solv} = [c(H_3SO_4^+)\lambda(H_3SO_4^+) + c'(HSO_4^-)\lambda(HSO_4^-) + c(H_3O^+)\lambda(H_3O^+) + c(HS_2O_7^-)\lambda(HS_2O_7^-)]_{base}$$

where $c'(HSO_4^-)$ is the extra concentration of HSO_4^- ions arising from the self-dissociation of the solvent, i.e.

$$c'_{base}(HSO_4^-) = c_{base}(HSO_4^-) - c_{base}(M^+)$$

In the case of the solute water, an analogous $c'(H_3O^+)$ replaced $c(H_3O^+)$. The transference number solvent correction thus became[16]

$$T_+(corr) = T_+\left(1 + \frac{\kappa_{solv}}{\kappa_{base} - \kappa_{solv}}\right) \quad (7)$$

Values of I_s and the fully corrected transference numbers are listed in Table III.

Comparisons with Previous Results. The cation transference numbers obtained here are considerably smaller than the Hittorf results in the literature[10-12] by factors ranging from 4 (for K^+, Ag^+) to 10 (for Na^+). The temperature coefficient of the Hittorf numbers for $KHSO_4$[11] is also of opposite sign to that deduced above. This comparison between the two sets of data cannot be exact because they refer to different concentration ranges: the mb results cover HSO_4^- molarities from 0.06 to 0.22 *M* while the Hit-

TABLE III: Summary of Mean Zero-Current Observed and Corrected Cation Transference Numbers and Ionic Conductances

Solution	I_s, mol dm^{-3}	T_+(obsd)	T_+ with vol corr	T_+ with all corr	κ,[a] ohm^{-1} m^{-1}	λ_+, cm^2 ohm^{-1} mol^{-1}
0.127 *M* $LiHSO_4$	0.146	0.0081	0.0027	0.0030	1.71	0.36
0.076 *M* $NaHSO_4$	0.099	0.0063_5	0.0031	0.0041	1.36	0.55
0.126 *M* $NaHSO_4$	0.145	0.0086_5	0.0033	0.0037	1.73	0.45
0.194 *M* $NaHSO_4$	0.211	0.0103	0.0020	0.0021	2.22	0.23
0.123 *M* $KHSO_4$	0.142	0.0115	0.0063	0.0071_5	1.74	0.89
0.062 *M* NH_4HSO_4	0.087	0.0065	0.0039	0.0056	1.29	0.81
0.111 *M* NH_4HSO_4	0.131	0.0099	0.0052	0.0060_5	1.68	0.79
0.187 *M* NH_4HSO_4	0.204	0.0121	0.0041	0.0043	2.28	0.50
0.193 *M* NH_4HSO_4	0.210	0.0123_5	0.0041_5	0.0043	2.32	0.50
0.118 *M* H_3OHSO_4	0.127	0.0106	0.0056	0.0059	1.67	0.79
0.090 *M* $H_2OAcHSO_4$	0.111	0.0073	0.0035	0.0043	1.46[b]	0.57
0.091_5 *M* $AgHSO_4$	0.113	0.0119	0.0080	0.0099	1.48	1.29
0.218 *M* $AgHSO_4$	0.234	0.0161	0.0069	0.0072	2.42	0.77
0.042 *M* $Ba(HSO_4)_2$	0.148	0.0047	0.0011	0.0014	1.44	0.38

[a] Interpolated from the data of ref 7. [b] Extrapolated from the data of ref 6.

torf results cover 0.4–2.0 *M* for 1:1 electrolytes and 0.6–2.7 *M* for 2:1 electrolytes. For *dilute* solutions the mb data and theory[28] agree that T_+ values fall with increasing concentration, thus accentuating the differences between the two sets. In *concentrated* solutions, electrolyte conductances decrease with increasing concentration[6,8] showing that the HSO_4^- ions move more slowly due, it is believed,[6,8] to various interferences with the proton-jump mechanism. The cations might also be expected to move more slowly because the solutions generally become more viscous.[5] If, however, the cation conductances are presumed to remain constant while the anion conductances decrease as reported,[6,8] then T_+ values in the Hittorf concentration region ought to be larger than those at the highest mb concentrations by from 30 (for Ag^+) to 160% (for Li^+, Na^+) for the 1:1 salts. This would improve the agreement between the two sets of data but still leave the mb results smaller than the Hittorf ones, by factors ranging from 1.7 (for Li^+, K^+) to 4 (for NH_4^+). We believe the mb results to be the more reliable. Hittorf values, which depend on the small differences between the amounts present before and after electrolysis, are of necessity less precise and particularly so when the transference numbers in question are so tiny. More specifically, the methods of analyzing the sulfuric acid solutions in the Hittorf experiments often involved distillation or pyrolysis as well as titration or gravimetry, and small errors in any operation could have produced relatively large errors in the transference number.

Most of the moving boundary results in Table I are probably accurate to ±0.0003. The main uncertainties arise from the extrapolation to zero current and the large volume and solvent corrections. The figures in Table II for barium and silver hydrogen sulfates are bound to be suspect until the origin of the double boundaries is established. Some internal evidence suggests that the barium transference number may be somewhat too low. Since a stable falling boundary $H_2OAc^+ \leftarrow H_2OBz^+$ was observed, we can deduce from the Kohlrausch relation[16] and the known solution densities[5] that the corrected transference number for H_2OBz^+ should be at least 0.0017_5. The transference number for barium ought to be greater than this if $Ba^{2+} \leftarrow H_2OBz^+$ correctly describes one of the observed double boundaries. The silver transference numbers, on the other hand, seem anomalously large when compared with those of alkali ions of comparable radius. If indeed some of the silver was present on both sides of the boundaries that were timed, the full moving boundary equation[16] would have to be employed and a different transference number would result.

Ionic Conductances. Individual ionic conductances may be calculated from the transference numbers in Table III by combining them with the conductivities κ of the solutions. Experimental values of the latter, at the concentrations used in the transference runs, were obtained by interpolation from data in the literature.[7] Only for acetic acid solutions was it necessary to extrapolate beyond the published values,[6] and this was done by noting the close agreement between the conductances of acetic acid and of $NaHSO_4$ solutions. These κ values are listed in Table III; they are not solvent corrected. Multiplication by the volume (but not solvent) corrected transference numbers according to eq 1 leads to the molar cation conductances λ_+ in the last column of Table III.

Estimation of Limiting Transference Numbers and Ionic Conductances. The λ_+ values, and the fully corrected T_+ values, refer to solutions whose ionic strengths I_s are given in the second column of Table III. Only for one solution is I_s appreciably below 0.1 *M*, and in general the ionic strengths are higher than is normal in such an investigation. The reason lies in the extensive autoprotolysis of sulfuric acid. Not even the use of much lower solute concentrations (at which the boundaries would have become invisible) would have produced a marked decrease in I_s because of the corresponding increase in the solvent's self-dissociations: pure sulfuric acid itself possesses an ionic strength of 0.082 *M*.

Despite the fact that the ionic strengths are beyond the limits of applicability of the various Fuoss and Pitts equations,[28] attempts were made to extrapolate the data to infinitesimal ionic strength. The simplest equation for the limiting transference number T_+^0 is that of Fuoss and Onsager earlier designated[28] $(FO)_1$:

$$T_+^0 = T_+ + \frac{(1/2 - T_+)B_2\sqrt{I_s}}{\Lambda^0(1 + B\mathring{a}\sqrt{I_s})} \qquad (8)$$

where the electrophoretic parameter $B_2 = 1.947$ cm^2 ohm^{-1} mol$^{-3/2}$ dm$^{3/2}$, $B = 0.291_2$ dm$^{3/2}$ mol$^{-1/2}$ Å^{-1}, $\mathring{a}$ is the distance of closest approach between cation and anion (in angstroms), and Λ^0 the limiting molar conductance of the 1:1 electrolyte (taken as[8] 171 cm^2 ohm^{-1} mol^{-1}). The normal procedure is to vary $\mathring{a}$ until the T_+^0 values, calculated from the data points at the different concentrations, are equal within experimental error. For the three $NaHSO_4$ points this occurred at the physically meaningless $\mathring{a} = -2$ Å ($T_+^0 = 0.0063$); for the three NH_4HSO_4 points no value of $\mathring{a}$ could possibly lead to a constant T_+^0. Next, only the two points at the lowest ionic strengths were considered, and the T_+^0 values calculated from them by the limiting Debye–Hückel–Onsager equation were extrapolated against I_s to $I_s = 0$ according to the Longsworth method.[29] This gave $T_+^0 = 0.0060$ for $NaHSO_4$ and $T_+^0 = 0.0055$ for NH_4HSO_4. These results appear inconsistent, for at all finite concentrations the transference numbers for NH_4HSO_4 are considerably larger than those for $NaHSO_4$. Allowing for the experimental uncertainty of ±0.0003 in each figure gives 0.0060 ± 0.0016 and 0.0055 ± 0.0015, respectively, a 27% uncertainty in each case.

A similar story can be told for the ionic conductances, λ_+. Employing the Robinson and Stokes equation[22b]

$$\lambda_+^0 = \lambda_+ + \frac{(B_1\lambda_+^0 + 1/2 B_2)\sqrt{I_s}}{1 + B\mathring{a}\sqrt{I_s}} \qquad (9)$$

with the relaxation parameter $B_1 = 0.159_3$ dm$^{3/2}$ mol$^{-1/2}$, we find that the three sodium points give a constant λ_+^0 value (0.95 cm^2 ohm^{-1} mol^{-1}) at $\mathring{a} = -2$ Å while the three ammonium points can never give the same limiting conductance. Taking the two lower ionic strength points only, and applying the Shedlovsky procedure[30] of extrapolating λ_+^0 (calculated from (9) with $\mathring{a} = 0$) against I_s, one obtains $\lambda^0(Na^+) = 0.96 \pm 0.22$ and $\lambda^0(NH_4^+) = 1.03 \pm 0.20$, if likely error limits are taken into account. These results are also unsatisfactory. The Na^+–NH_4^+ order differs from that in the T_+ extrapolation because the molar conductances of the two salts do not obey the theory either.[8]

It was therefore decided to represent the results in two ways. The first involved only interpolation of T_+ (or λ_-) within the ionic strength region covered, using smooth curves of T_+ (or λ_+) vs. $\sqrt{I_s}$ for the three sodium and the three ammonium points as guides. The resulting values at $I_s = 0.145$ mol dm^{-3} are set out in Table IV; they do not depend on a particular theoretical conductance equation

TABLE IV: Interpolated and Extrapolated Cation Transference Numbers and Conductances

Ion	T_+	λ_+, cm² Ω⁻¹ mol⁻¹	T_+^0	$T_+^0\Lambda^0$, cm² Ω⁻¹ mol⁻¹	λ_+^0	λ_+^0(Zwanzig), cm² Ω⁻¹ mol⁻¹	
	at I_s = 0.145 *M*		calcd[a] from lowest exptl I_s			Stick	Slip
Li^+	0.0030	0.36	0.0045	0.77	0.64	0.18	0.09
Na^+	0.0037	0.45	0.0054	0.92	0.80	0.61	0.35
K^+	0.0071	0.88	0.0086	1.47	1.20	1.12	0.80
NH_4^+	0.0059	0.75	0.0068	1.16	1.06	1.25	0.99
H_3O^+	0.0057	0.74	0.0073	1.25	1.08		
H_2OAc^+	0.0040	0.49	0.0057	0.97	0.84		
Ag^{+b}	0.0097	1.22	0.0112	1.92	1.59	1.05	0.71
Ba^{2+b}	0.0014	0.39	*d*	*d*	*d*	1.75	0.99
$H_3SO_4^{+c}$					245		
HSO_4^{-c}					170[e]		

[a] From eq 8 and 9, respectively, assuming $\mathring{a}$ = 4 Å. [b] From double boundary systems. [c] From ref 8. [d] Equations 8 and 9 only apply to 1:1 electrolytes. The corresponding equations for unsymmetrical electrolytes are quite unreliable in present conditions.[22c] [e] λ_-^0.

and are useful for comparing one ion with another. Second, the points at the lowest ionic strengths were extrapolated to I_s = 0 using eq 8 and 9, respectively, with $\mathring{a}$ = 4 Å for all electrolytes. These T_+^0 and λ_+^0 values are also listed in Table IV. It is immediately apparent that the two sets of limiting data are not consistent with each other, for the $T_+^0\Lambda^0$ values (Λ^0 = 171) are between 9 and 23% greater than the λ_+^0 values. The reason is that the experimental salt conductances only fit[8] the theoretical equations with negative values of $\mathring{a}$. To attain concordance between $T_+^0\Lambda^0$ and λ_+^0, therefore, the λ_+ values should have been treated with eq 9 using an $\mathring{a}$ value intermediate between the 4 Å assumed for the transference extrapolation and the negative $\mathring{a}$ value needed to fit the salt conductances. Indeed, application of eq 9 with $\mathring{a}$ = 0 leads to much better agreement between $T_+^0\Lambda^0$ and λ_+^0. An attempt was also made to extrapolate the λ_+ values with a modification to eq 9 in which (cf. Fuoss[31]) λ_+ was replaced by $\lambda_+(1 + {}_cB_\eta c)$. Here ${}_cB_\eta$ is the viscosity *B* coefficient whose numerical values have been given elsewhere.[32] However, this affected λ_+^0 by at most 0.01_5 cm² ohm⁻¹ mol⁻¹. Flowers et al.[8] have already pointed out that only a small effect is produced by multiplying salt conductances in sulfuric acid by relative solution viscosities. It is clear that, unlike the T_+ and λ_+ results, the T_+^0 and λ_+^0 figures in Table IV should not be taken at their face values but do represent the correct sizes and sequences of the limiting properties.

The two sets of limiting ionic conductances, and the set referring to I_s = 0.145, show the usual order $K^+ > Na^+ > Li^+$. Clearly the smaller the ion, the greater the solvation, and the greater the resistance to bulk motion. Application of Stokes' law indicates that the doubly charged barium ion is even more solvated than is lithium. The NH_4^+ and H_3O^+ ions possess similar mobilities, slightly smaller than that of K^+. Comparison with the relatively huge ionic conductances for $H_3SO_4^+$ and HSO_4^- demonstrates the unfair advantage held by proton-jumping ions in such a highly viscous solvent.

The experimental molar conductances of the normally migrating ions can be tested against the predictions of the revised Zwanzig theory,[33] according to which

$$\lambda_i^0\eta = z_i^2eF/(A_v\pi r_i + A_D z_i^2 P^* r_i^{-3}) \qquad (10)$$

Here z_ie is the charge on the given ion and r_i its radius, and *F* the Faraday constant. The parameter A_v equals 6 if there is "perfect sticking" at the ion–solvent interface and 4 if there is "perfect slipping", whereas A_D equals 0.375 and 0.75, respectively. The symbol P^* is defined by

$$P^* \equiv \frac{e^2(\epsilon_0 - \epsilon_\infty)\tau}{\epsilon_0(2\epsilon_0 + 1)\eta}$$

where ϵ_0 and ϵ_∞ are respectively the low-frequency and limiting high-frequency dielectric constants, and τ is the dielectric relaxation time. For sulfuric acid[34] at 20°, ϵ_0 = 110, ϵ_∞ = 5, and $\tau = 4.8 \times 10^{-10}$ sec. We shall employ these figures as they stand although they contain considerable experimental uncertainties (because of the high electrolytic conductance of the liquid[34]) and refer to 20° rather than 25°. It follows that $P^* = 1.95 \times 10^{-30}$ cm⁴, which is not much larger than the value for ethylene glycol[35] (a liquid almost as viscous) but an order of magnitude smaller than that for a monohydric alcohol. The ionic conductances calculated with eq 10 and Pauling radii[22d] are listed in Table IV. The theory in its "stick" form is seen to be moderately successful for the singly charged ions of larger radius but fails badly for the smaller ions. This is similar to the pattern found earlier.[35] The "stick" model which implies solvation generally fits better than the "slip" version. As has recently been pointed out,[36] the Zwanzig theory cannot be improved for the small ions by allowing for the dielectric saturation around them.

Acknowledgments. We thank the Science Research Council for the award of a Research Studentship to D.P.S.

References and Notes

(1) Presented in July 1974 at the IVth International Conference on Non-aqueous Solutions in Vienna, Austria.
(2) R. J. Gillespie, *Rev. Pure Appl. Chem.*, **9**, 1 (1959); R. J. Gillespie and E. A. Robinson, *Adv. Inorg. Radiochem.*, **1**, 386 (1959).
(3) R. J. Gillespie and E. A. Robinson in "Non-Aqueous Solvent Systems", T. C. Waddington, Ed., Academic Press, London, 1965, Chapter 4.
(4) W. H. Lee in "Chemistry in Non-Aqueous Solvents", Vol. II, J. J. Lagowski, Ed., Academic Press, New York, N.Y., 1967, Chapter 3.
(5) R. J. Gillespie and S. Wasif, *J. Chem. Soc.*, 215 (1953).
(6) R. J. Gillespie and S. Wasif, *J. Chem. Soc.*, 221 (1953).
(7) S. J. Bass, R. H. Flowers, R. J. Gillespie, E. A. Robinson, and C. Solomons, *J. Chem. Soc.*, 4315 (1960).
(8) R. H. Flowers, R. J. Gillespie, E. A. Robinson, and C. Solomons, *J. Chem. Soc.*, 4327 (1960).
(9) Limiting properties refer to a state of infinitesimal ionic strength, not to

one of "infinite dilution". Diluting an infinite number of times with the solvent would in this case produce a solution of 0.082 *M* ionic strength! See M. Spiro, *Educ. Chem.*, **3**, 139 (1966).
(10) L. P. Hammett and F. A. Lowenheim, *J. Am. Chem. Soc.*, **56**, 2620 (1934).
(11) R. J. Gillespie and S. Wasif, *J. Chem. Soc.*, 209 (1953).
(12) S. Wasif, *J. Chem. Soc.*, 372 (1955).
(13) R. J. Gillespie and S. Wasif, *J. Chem. Soc.*, 204 (1953).
(14) R. J. Gillespie, J. V. Oubridge, and C. Solomons, *J. Chem. Soc.*, 1804 (1957).
(15) R. H. Flowers, R. J. Gillespie, and E. A. Robinson, *J. Chem. Soc.*, 845 (1960).
(16) M. Spiro in "Physical Methods of Chemistry, Part IIA: Electrochemical Methods" A. Weissberger and B. W. Rossiter, Ed., Interscience, New York, N.Y., 1971, Chapter 4.
(17) J. R. Gwyther, *J. Phys. E*, **5**, 979 (1972).
(18) A. J. Arvia and J. S. W. Carrozza, *Electrochim. Acta*, **11**, 1641 (1966); F. Beck, *ibid.*, **17**, 2317 (1972).
(19) R. Parsons, private communication.
(20) J. B. Gill, private communication.
(21) G. Marx, private communication.
(22) R. A. Robinson and R. H. Stokes, "Electrolyte Solutions", 2nd ed, Butterworths, London, 1959: (a) pp 307–310, (b) pp 144, 171, (c) Chapter 7, (d) p 461.
(23) N. N. Greenwood and A. Thompson, *J. Chem. Soc.*, 3474 (1959).
(24) J. R. Gwyther, S. Kumarasinghe, and M. Spiro, *J. Solution Chem.*, **3**, 659 (1974).
(25) J. R. Gwyther and M. Spiro, to be submitted for publication.
(26) R. J. Gillespie, E. A. Robinson, and C. Solomons, *J. Chem. Soc.*, 4320 (1960).
(27) J. Barr, R. J. Gillespie, and E. A. Robinson, *Can. J. Chem.*, **39**, 1266 (1961).
(28) D. P. Sidebottom and M. Spiro, *J. Chem. Soc., Faraday Trans. 1*, **69**, 1287 (1973).
(29) L. G. Longsworth, *J. Am. Chem. Soc.*, **54**, 2741 (1932).
(30) D. A. MacInnes, T. Shedlovsky, and L. G. Longsworth, *J. Am. Chem. Soc.*, **54**, 2758 (1932).
(31) R. M. Fuoss, *J. Am. Chem. Soc.*, **79**, 3301 (1957).
(32) M. Spiro, *J. Chem. Soc., Faraday Trans. 1*, **71**, 988 (1975).
(33) R. Zwanzig, *J. Chem. Phys.*, **52**, 3625 (1970).
(34) J. C. D. Brand, J. C. James, and A. Rutherford, *J. Chem. Soc.*, 2447 (1953).
(35) M. Carmo Santos and M. Spiro, *J. Phys. Chem.*, **76**, 712 (1972).
(36) R. Fernández-Prini, *J. Phys. Chem.*, **77**, 1314 (1973).

Journal of Chemical and Engineering Data

APRIL 1975, Vol. 20, No. 2

TABLE OF CONTENTS

■ Supplementary material for this paper is available separately, in photocopy or microfiche form. Ordering information is given in the paper.

From the borders of organic chemistry . . . To the borders of theoretical physics:

Inorganic Chemistry brings you a broad range of authoritative information presenting both experimental and theoretical studies in all phases of inorganic chemistry.

Each month, this rapidly growing journal brings you the data you need on synthesis and properties of new compounds, quantitative studies regarding structure, and thermodynamics of inorganic reactions.

When you've seen the 50 or more papers offered in each issue, you'll also want to look through the Notes and Correspondence sections for their concise exchange of scientific views and ideas.

To order INORGANIC CHEMISTRY today, just complete and return the form below.

. . another ACS service

Inorganic Chemistry

Inorganic Chemistry
American Chemical Society
1155 Sixteenth Street, N.W.
Washington, D.C. 20036

1975

Yes, I would like to receive INORGANIC CHEMISTRY at the one-year rate checked below:

	U.S.	*Canada*	*Latin America*	*Other Nations*
ACS Member Personal-Use One-Year Rate	☐ $18.00	☐ $22.00	☐ $22.00	☐ $22.50
Nonmember	☐ $72.00	☐ $76.00	☐ $76.00	☐ $76.50

Bill me ☐ Bill company ☐ Payment enclosed ☐

Name _____

Street _____ Home ☐ Business ☐

City _____ State _____ Zip _____

Journal subscriptions start on January '75